

博士論文

Search for new physics by a time-dependent CP
violation analysis of the decay $B \rightarrow K_S \eta \gamma$
using the Belle detector
(Belle 実験における $B \rightarrow K_S \eta \gamma$ 崩壊の時間に依
存した CP の破れの解析による新物理の探索)

東北大学理学研究科物理学専攻

中野浩至

平成 25 年

Abstract

We report the measurement of time dependent CP violation parameters in $B \rightarrow K_S \eta \gamma$ decays. The results are obtained from the final data sample that contains $772 \times 10^6 B \bar{B}$ pairs that was collected near the $\Upsilon(4S)$ resonance, with the Belle detector at the KEKB asymmetric energy e^+e^- collider. We obtain the CP violation parameters $\mathcal{S} = -1.32_{-0.81}^{+0.88}(\text{stat.}) \pm 0.36(\text{syst.})$ and $\mathcal{A} = -0.48_{-0.33}^{+0.36}(\text{stat.}) \pm 0.07(\text{syst.})$. where \mathcal{A} and \mathcal{S} represent the direct and mixing-induced CP asymmetries in $B \rightarrow K_S \eta \gamma$ decays, respectively.

Acknowledgment

First, I would like to express my great appreciation to Yamamoto-sensei for giving me such a really interesting topic. He also gave me many opportunities to participate in international school. I am also especially indebted to Ishikawa-san for giving me many advices as a supervisor. I couldn't finish my study without him. I greatly appreciate Sumisawa-san for many advices about K_S reconstruction and vertex reconstruction. I am grateful to Miyabayashi-san and Tagir-san as conveners of ICPV group and advisors for CPV measurement. Further, I am grateful to laboratory stuffs and members and secretary, Kobayashi-san. I appreciate Yamaguchi-san for first discussion of the topic. I also appreciate Yusa-san, Christian, Gagan-san for giving many useful comments as referee team of the Belle group. I also thank to Belle and KEKB group for excellent operation of the detector and accelerator. I am also grateful to Nishida-san and Belle computer system engineers for maintain super computer. Finally, I also wish to express my obligation to my family. This work was supported by JSPS KAKENHI Grant Number 23·3221.

Contents

1	Introduction	1
2	Physics motivation	3
2.1	The Standard Model	3
2.2	Powerfulness of the SM	3
2.3	Necessity for a theory beyond the SM	4
2.4	The way of searching BSM	4
2.5	$b \rightarrow s\gamma$ decay and photon's polarization	4
2.6	Polarization measurement and time dependent CP violation observation . .	5
2.7	The amount of time dependent CP Violation	6
2.8	Method of TDCPV measurement using $\Upsilon(4S)$	10
3	Experimental apparatus	11
3.1	KEKB accelerator	11
3.1.1	Linac	11
3.1.2	Storage rings	12
3.2	Belle detector	14
3.2.1	Overall	14
3.2.2	Tracking and vertex reconstruction	14
3.2.3	Particle identification	17
3.2.4	Photon detection	20
4	New K_S reconstruction method	21
4.1	Training strategy	21
4.1.1	Pre-selection	22
4.1.2	V-particle like candidate extraction	22
4.1.3	Not lambda like candidate extraction	26
4.2	performance check with MC	29
5	Selection criteria	30
5.1	Data set and event types	30
5.1.1	Monte Carlo signal generation	30
5.1.2	Monte Carlo background data	31
5.1.3	Kinds of signal candidate	31

5.1.4	2 × 7 groups of signal candidate	31
5.2	Reconstruction	33
5.2.1	Photon reconstruction	33
5.2.2	Kaon reconstruction	33
5.2.3	η reconstruction	34
5.2.4	B reconstruction	35
5.3	Background suppression	36
5.3.1	Best candidate selection	36
5.3.2	Veto of photons from $\pi^0 \eta$ decay	36
5.3.3	NeuroBayes training for continuum suppression	38
5.3.4	Peaking background and well known CPV background veto	52
5.3.5	$B \rightarrow K\pi^0\gamma$ veto	54
5.3.6	Helicity angle and $M_{K\eta}$ cut	54
5.3.7	Summary	56
6	3D fit with ΔE, M_{bc} and NB'	63
6.1	PDF shapes and components	63
6.1.1	Range	63
6.1.2	PDF shapes	63
6.1.3	Fit method	66
6.2	Spin search of $K^\pm \eta$ system	70
6.3	Invariant mass distribution of $K^\pm \eta$ system	71
6.4	Signal and background fraction of B candidate	72
6.5	Fit bias study with MC simulation	83
7	Δt distribution fit	87
7.1	PDF of Δt distribution	87
7.1.1	Possibility of wrongly tagged B meson flavor	87
7.1.2	Resolution of Δt	90
7.1.3	Contamination of BG events	95
7.1.4	PDF shape	95
7.2	Confirmation of fitter code	100
7.2.1	Life time fit	100
7.2.2	Life time fit with toy MC	100
7.2.3	Life time fit with GEANT based MC	102
7.2.4	Life time fit with real data	103
7.2.5	Linearity check with MC study	109
7.2.6	CP fit with real data $B^\pm \rightarrow K^\pm \eta \gamma$ sample	113
7.3	Fit result	114
8	Systematic error	117
8.1	Vertex reconstruction	117
8.2	Physics parameters	118
8.3	BG Δt PDF shape	119

8.4	Flavor tagging	119
8.5	Resolution function parameters	119
8.6	3D fit for signal/BG fraction	119
8.7	CPV effect from BG	119
8.8	Tag side interference	120
8.9	Possible fit bias	121
8.10	Summary	122
9	Consideration of the result	123
9.1	Checks of the analysis	123
9.1.1	Likelihood scan	123
9.1.2	2D fit for signal/BG ratio	124
9.1.3	Data instability	124
9.1.4	MC distribution	127
9.2	Consideration	128
9.2.1	Confidence interval using Feldman-Cousins method	128
9.2.2	Limit on new physics (general, $A_{\text{NP}} = 0$)	132
9.2.3	Limit on new physics (LRSM)	134
10	Conclusion	136
A	Systematic error lists	$\mathcal{A} - 1$

Chapter 1

Introduction

At the end of 19th century, Newton's laws and electro-magnetic dynamics were all of the physics. It was thought that if we know positions and momentums of all objects with infinite accuracy, we can calculate our universe's past and future uniquely, and remaining subject for physicists were solving some problems and just improving precision of physical constants. Problems were, for instance, searching unfound luminous ether which mediates electro-magnetic wave and ultraviolet catastrophe of the black body radiation. Since around the boundary between 19th and 20th century, relativity and quantum theory had been developed from these two problems. These theory destroyed our old view of the world. Now, we, living in the 21st century, understand our world as written follow. There is no absolute time and absolute space, and speed of light is always same amount in every system. Both matter and light have aspect of wave and particle, and their position and momentum cannot be measured with infinite accuracy. The universe has continued enlarging from high density and high temperature state. Generation and degeneration of the matter and anti-matter are continuously occurring in the vacuum. No one can predict our future.

The Standard model (SM) had been developed together with experiments of elementary particle physics since the discovery of electron in 1897. The SM can almost perfectly explain behavior of elementary particles. In 2012, a Higgs boson which is predicted by the SM is discovered at LHC. On the other hand, SUSY particles which should be observed before Higgs discovery have still not be seen. It seems that remaining subject for physicists are just improving precision of constants of the SM. This situation is, however, looks like as if we are on the eve of the evolution at the end of 19th century.

Although many experimental results are consistent with the SM, there are some problems. Getting idea from the wise history, these holes of the theory must be keyholes to the deeper truth. How the new knowledge will overthrow our current view of the world? Many studies for new physics beyond the SM have been done and human's knowledge border is extended day by day. As one of a these study, I carried out search for time dependent CP violation (TDCPV) of $B^0 \rightarrow K_S \eta \gamma$ mode.

In Chapter 2, physics motivation of TDCPV measurement of $B^0 \rightarrow K_S \eta \gamma$ mode is introduced. KEKB accelerator and Belle detector used for B meson production and detection of its decay are mentioned in Chapter 3. Chapter 4 presents newly developed K_S

reconstruction method with using Neural network. This new K_S finder is prepared for the study, but it can also be used for other analysis which needs K_S reconstruction. Chapter 5 explains method to extract signal from background, and then, in Chapter 6, the way of counting signal and remaining background is described. Chapter 7 deals with TDCPV search method with Δt distribution analysis and its result, while Chapter 8 discusses its systematic uncertainty. In Chapter 9, validity of the result and constraint on new physics are considered. Finally, we summarize the study in Chapter 10.

Chapter 2

Physics motivation

2.1 The Standard Model

The Standard Model (SM) is a model which can explain behavior of elementary particles under quantum mechanics, special relativity and some conservation law. 3 known basic force out of 4 can be explained by Gauge symmetry. Vector boson generated by requirement of gauge symmetry cannot have its mass. On the other hand, however, weak force's propagators, W and Z bosons, do have masses. For the sake of solving this problem, Higgs field is introduced. $U(1)_{EW}$ gauge symmetry is originated from spontaneous symmetry breaking of $U(1)_Y \times SU(2)_L$ gauge symmetry. Strong force come from $SU(3)$ symmetry. The SM has 18 parameters: 6 quark-Higgs coupling, 3 charged lepton-Higgs coupling, $U(1)$, $SU(2)$ and $SU(3)$ coupling, 4 parameters of CKM matrix, a vacuum expectation value and a Higgs mass. (If we count strong CP phase which is somehow set to be 0, it will be 19.)

2.2 Powerfulness of the SM

LEP and SLC experiment in 1990's are one of the best example of powerfulness of the SM. The SM had passed many precise measurement without contradiction. In addition, quantum correction (which considers off-shell particles effect) predicts undiscovered particle's feature very well. Experimental result of LEP and SLC at Z pole mass predicted top quark mass which was not discovered at that time. In 1995, Tevatron discovered a 6th quark which has a mass which is consistent to the prediction. Moreover, mass of the Higgs boson have been predicted around $\mathcal{O}(100 \text{ GeV})$, and ATLAS and CMS detector at LHC found unknown 126 GeV boson in 2012. Spin of this boson is measured to be 0, and it is recognized as Higgs in 2013. To recap, the Standard Model is so powerful that can explain known phenomena well. In addition, it predicted mass of top quark and Higgs as well as their existence. A Higgs boson being discovered in 2013, all 18 parameters of the SM have been measured.

2.3 Necessity for a theory beyond the SM

The Standard model (SM) is so powerful that most of its predictions are consistent with experimental result. However, it is true that there are some things which cannot be explained by the SM; it cannot explain existence of dark matter, baryon asymmetry of the universe (BAU) with CKM matrix only, hierarchy problem on Higgs mass and so on. Although various new theories which resolve these problems are suggested, they have not been checked by experimentally. SUSY, for example, with demanding R-parity conservation ensures existence of stable neutral massive particle, and it becomes a candidate for dark matter. It also solves naturalness problem. On the other hand, Left-right symmetric model which demands $SU(2)_R$ as well as $SU(2)_L$ explains dark matter as right handed heavy neutrino. In addition, both theories add new CP phase which cannot be seen in the SM, BAU might be explained, also.

We are desiring observation of a phenomenon which contradicts the SM and can be explained by theory beyond the SM (BSM).

2.4 The way of searching BSM

If we describe true Lagrangian as $\mathcal{L}_{\text{true}}$, it can be written as

$$\mathcal{L}_{\text{true}} \sim \mathcal{L}_{\text{SM}} + \frac{1}{\Lambda_{\text{NP}}} \mathcal{L}_{\text{NP,dim=5}} + \frac{1}{\Lambda_{\text{NP}}^2} \mathcal{L}_{\text{NP,dim=6}}. \quad (2.1)$$

Here, $\mathcal{L}_{\text{NP,dim=5}}$ and $\mathcal{L}_{\text{NP,dim=6}}$ are dimension 5 and 6 effective New Physics (NP) Lagrangian, respectively. Λ_{NP} is energy scale of the new physics, and we expect that there are unfound particles which have mass around Λ_{NP} . In order to solve hierarchy problem, Λ_{NP} must be around 1-100 TeV. We expect that this scale can be searched.

There are two ways to search NP. One is direct search which tries to find on-shell new particle at a energy higher than Λ_{NP} . LHC is at the forefront of this kind of search. The other is indirect search which tries to find the effect of off-shell new particle with very precise measurement. Even if we cannot reach Λ_{NP} , we can search this energy scale by measuring $\Delta\mathcal{L} = \mathcal{L}_{\text{true}} - \mathcal{L}_{\text{SM}}$.

2.5 $b \rightarrow s\gamma$ decay and photon's polarization

$b \rightarrow s\gamma$ decay is one of a probe to new physics. Flavor changing neutral current (FCNC) is prohibited in the SM. It makes easier to find deviation from the SM expectation. The SM predict that photon polarization is dominated by left handed, but some kinds of BSM theory permit not a small ratio of right handed photon emission. The reason why the SM suppresses right handed photon emission severely is W boson only interacts with V-A current. Assuming that s quark is massless, helicity of s quark from b decay must be left handed. Then, from a demand on conservation of magnitude of spin, a choice of photon's helicity is left handed only. Figure 2.1 shows these decay diagrams. Effective hamiltonian

for the decay can be written as

$$H_{\text{eff}} = -\frac{G_F}{\sqrt{2}} \mathcal{C}_{7\gamma} V_{tb} V_{ts}^* \frac{e}{4\pi^2} (m_s \bar{s}_R \sigma_{\mu\nu} P_L b_L + m_b \bar{s}_L \sigma_{\mu\nu} P_R b_R) F^{\mu\nu}. \quad (2.2)$$

It means that a ratio of amplitude between left handed photon emission and right handed one is m_b/m_s .

While right handed photon emission from $b \rightarrow s\gamma$ decay is strongly suppressed in the SM, there are some BSM theory which have a possibility of gaining ratio of right handed photon emission. For instance, Left-Right (LR) symmetry model permits a decay diagram like Fig.2.2(left), or if SUSY is true, there can be a decay diagram like Fig.2.2(middle). In addition, two Higgs doublet model (2HDM) which can be considered together with LR symmetry or SUSY allows a decay diagram like Fig.2.2(right) [1,2]. Therefore, if we have a way to measure photon polarization from $b \rightarrow s\gamma$ decay, we can examine these theories.



Figure 2.1: Diagrams of $b \rightarrow s\gamma_L$ (left) and $b \rightarrow s\gamma_R$ (right) in the SM.

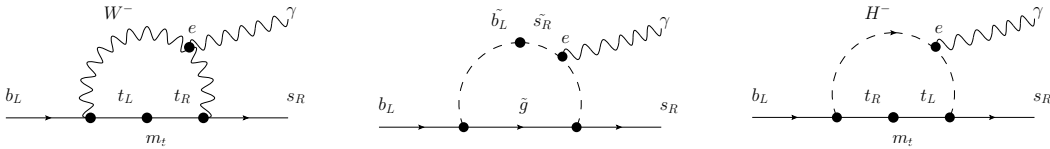


Figure 2.2: Diagrams of $b \rightarrow s\gamma_R$ in LR symmetry (left), SUSY (middle) and 2HDM (right).

2.6 Polarization measurement and time dependent CP violation observation

Measurement of time dependent CP violation (TDCPV) enables us to search photon's polarization. TDCPV is caused by quantum mechanical interference between $B^0(b\bar{d}) \rightarrow f_{CP}$ and $\bar{B}^0(b\bar{d}) \rightarrow f_{CP}$ decay channel. Here, f_{CP} is a CP eigenstate. $B^0 \rightarrow X_s^{CP} \gamma_R$ and $\bar{B}^0 \rightarrow X_s^{CP} \gamma_L$ are different final states because photon's polarization is not same. (X_s^{CP} is a CP eigenstate containing s quark.) Then, in the SM, quantum mechanical interference is strongly suppressed and thus TDCPV cannot be observed. In contrast to the SM, however, if there is a new physics which allows $B^0 \rightarrow X_s^{CP} \gamma_L$ and $\bar{B}^0 \rightarrow X_s^{CP} \gamma_R$ transitions as well as $B^0 \rightarrow X_s^{CP} \gamma_R$ and $\bar{B}^0 \rightarrow X_s^{CP} \gamma_L$, we can observe TDCPV.

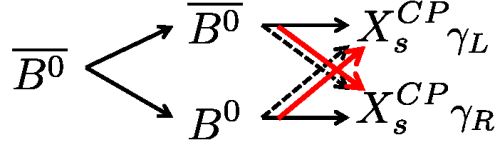


Figure 2.3: Illustration of quantum interference. Black solid lines show the SM allowed process. Black dash lines show the SM suppressed process. Red lines show interested NP process. We cannot see TDCPV only with black line, however, if there are red lines, TDCPV can be seen.

2.7 The amount of time dependent CP Violation

Defining that

$$\langle X_s^{CP} \gamma_R | H | B^0 \rangle (0) = A, \quad (2.3)$$

$$\langle X_s^{CP} \gamma_L | H | \overline{B^0} \rangle (0) = \bar{A}, \quad (2.4)$$

$$\langle X_s^{CP} \gamma_L | H | B^0 \rangle (0) = a \text{ and} \quad (2.5)$$

$$\langle X_s^{CP} \gamma_R | H | \overline{B^0} \rangle (0) = \bar{a}. \quad (2.6)$$

$$(2.7)$$

Using $e_{a,b} = e^{(-\frac{\Gamma_{a,b}}{2} - im_{a,b})t}$, B^0 and $\overline{B^0}$ at time t can be written as

$$|B^0\rangle(t) = \frac{e_a + e_b}{2} |B^0\rangle(0) + \frac{e_a - e_b}{2} \frac{q}{p} |\overline{B^0}\rangle(0) \text{ and} \quad (2.8)$$

$$|\overline{B^0}\rangle(t) = \frac{e_a + e_b}{2} |\overline{B^0}\rangle(0) + \frac{e_a - e_b}{2} \frac{p}{q} |B^0\rangle(0), \quad (2.9)$$

respectively. Here, $\Gamma_{a,b}$ and $m_{a,b}$ are decay widths and masses of $B_{a,b}$ which is Hamiltonian's eigenstate. We define that B_a is heavier than B_b , i.e.

$$\Delta m \equiv m_a - m_b > 0. \quad (2.10)$$

$$(\text{then, } q/p \sim e^{-2i\phi_1} \text{ in the SM.}) \quad (2.11)$$

Time dependent asymmetry of decay rate is

$$\text{asym} = \frac{\Gamma_{\overline{B^0} \rightarrow X_s^{CP} \gamma}(t) - \Gamma_{B^0 \rightarrow X_s^{CP} \gamma}(t)}{\Gamma_{\overline{B^0} \rightarrow X_s^{CP} \gamma}(t) + \Gamma_{B^0 \rightarrow X_s^{CP} \gamma}(t)} \quad (2.12)$$

$$= \frac{(|\text{Amp}_1|^2 + |\text{Amp}_2|^2) - (|\text{Amp}_3|^2 + |\text{Amp}_4|^2)}{(|\text{Amp}_1|^2 + |\text{Amp}_2|^2) + (|\text{Amp}_3|^2 + |\text{Amp}_4|^2)}. \quad (2.13)$$

Here, $|\text{Amp}_1|^2$ to $|\text{Amp}_4|^2$ are defined that

$$\langle X_s^{CP} \gamma_L | H | \bar{B}^0 \rangle (t) = \frac{e_a + e_b}{2} \bar{A} + \frac{e_a - e_b p}{2} \frac{p}{q} a \equiv \text{Amp}_1, \quad (2.14)$$

$$\langle X_s^{CP} \gamma_R | H | \bar{B}^0 \rangle (t) = \frac{e_a + e_b}{2} \bar{a} + \frac{e_a - e_b p}{2} \frac{p}{q} A \equiv \text{Amp}_2, \quad (2.15)$$

$$\langle X_s^{CP} \gamma_R | H | B^0 \rangle (t) = \frac{e_a + e_b}{2} A + \frac{e_a - e_b q}{2} \frac{q}{p} \bar{a} \equiv \text{Amp}_3 \text{ and} \quad (2.16)$$

$$\langle X_s^{CP} \gamma_L | H | B^0 \rangle (t) = \frac{e_a + e_b}{2} a + \frac{e_a - e_b q}{2} \frac{q}{p} \bar{A} \equiv \text{Amp}_4. \quad (2.17)$$

Their absolute values can be calculated as

$$\begin{aligned} |\text{Amp}_1|^2 &= \left(\frac{e_a + e_b}{2} \bar{A} + \frac{e_a - e_b p}{2} \frac{p}{q} a \right) \left(\frac{e_a + e_b}{2} \bar{A} + \frac{e_a - e_b p}{2} \frac{p}{q} a \right)^* \\ &= \left| \frac{e_a + e_b}{2} \bar{A} \right|^2 + \left| \frac{e_a - e_b p}{2} \frac{p}{q} a \right|^2 + 2 \text{Re} \left[\left(\frac{e_a + e_b}{2} \bar{A} \right)^* \left(\frac{e_a - e_b p}{2} \frac{p}{q} a \right) \right] \\ &= \frac{|\bar{A}|^2}{2} e^{-\Gamma t} \{1 + \cos(\Delta mt)\} + \left| \frac{p}{q} \right|^2 \frac{|a|^2}{2} e^{-\Gamma t} \{1 - \cos(\Delta mt)\} \\ &\quad + e^{-\Gamma t} \text{Re} \left[\frac{p}{q} a \bar{A}^* \left(\times \frac{\bar{A}}{A} \right) \{-i \cdot \sin(\Delta mt)\} \right] \end{aligned} \quad (2.18)$$

$$\begin{aligned} &= \frac{|\bar{A}|^2}{2} e^{-\Gamma t} \left[\left\{ 1 + \left| \frac{pa}{q\bar{A}} \right|^2 \right\} + \cos(\Delta mt) \left\{ 1 - \left| \frac{pa}{q\bar{A}} \right|^2 \right\} \right. \\ &\quad \left. + 2 \text{Im} \left[\frac{pa}{q\bar{A}} \right] \sin(\Delta mt) \right], \end{aligned} \quad (2.19)$$

$$\begin{aligned} |\text{Amp}_2|^2 &= \frac{|\bar{a}|^2}{2} e^{-\Gamma t} \left[\left\{ 1 + \left| \frac{pA}{q\bar{a}} \right|^2 \right\} + \cos(\Delta mt) \left\{ 1 - \left| \frac{pA}{q\bar{a}} \right|^2 \right\} \right. \\ &\quad \left. + 2 \text{Im} \left[\frac{pA}{q\bar{a}} \right] \sin(\Delta mt) \right], \end{aligned} \quad (2.20)$$

$$\begin{aligned} |\text{Amp}_3|^2 &= \frac{|A|^2}{2} e^{-\Gamma t} \left[\left\{ 1 + \left| \frac{q\bar{a}}{pA} \right|^2 \right\} + \cos(\Delta mt) \left\{ 1 - \left| \frac{q\bar{a}}{pA} \right|^2 \right\} \right. \\ &\quad \left. + 2 \text{Im} \left[\frac{q\bar{a}}{pA} \right] \sin(\Delta mt) \right] \text{ and} \end{aligned} \quad (2.21)$$

$$\begin{aligned} |\text{Amp}_4|^2 &= \frac{|a|^2}{2} e^{-\Gamma t} \left[\left\{ 1 + \left| \frac{q\bar{A}}{pa} \right|^2 \right\} + \cos(\Delta mt) \left\{ 1 - \left| \frac{q\bar{A}}{pa} \right|^2 \right\} \right. \\ &\quad \left. + 2 \text{Im} \left[\frac{q\bar{A}}{pa} \right] \sin(\Delta mt) \right]. \end{aligned} \quad (2.22)$$

Here, we assumed that decay widths of B_a and B_b are same,

$$\Gamma_a = \Gamma_b = \Gamma. \quad (2.23)$$

Then, decay widths of $\overline{B^0} \rightarrow X_s^{CP} \gamma$ and $B^0 \rightarrow X_s^{CP} \gamma$ are

$$\begin{aligned} \Gamma_{\overline{B^0} \rightarrow X_s^{CP} \gamma}(t) &= |\text{Amp}_1|^2 + |\text{Amp}_2|^2 \\ &= \frac{|\overline{A}|^2}{2} e^{-\Gamma t} \left[\left\{ 1 + \left| \frac{pa}{q\overline{A}} \right|^2 + \left| \frac{\overline{a}}{\overline{A}} \right|^2 + \left| \frac{pA}{q\overline{A}} \right|^2 \right\} \right. \\ &\quad \left. + \left\{ 1 - \left| \frac{pa}{q\overline{A}} \right|^2 + \left| \frac{\overline{a}}{\overline{A}} \right|^2 - \left| \frac{pA}{q\overline{A}} \right|^2 \right\} \cos(\Delta mt) \right. \\ &\quad \left. + \left\{ 2\text{Im} \left[\frac{pa}{q\overline{A}} \right] + 2 \left| \frac{\overline{a}}{\overline{A}} \right|^2 \text{Im} \left[\frac{pA}{q\overline{a}} \right] \right\} \sin(\Delta mt) \right] \\ &= \frac{\mathcal{I}}{2} e^{-\Gamma t} [1 + \mathcal{A} \cos(\Delta mt) + \mathcal{S} \sin(\Delta mt)] \end{aligned} \quad (2.24)$$

$$\begin{aligned} \Gamma_{B^0 \rightarrow X_s^{CP} \gamma}(t) &= |\text{Amp}_3|^2 + |\text{Amp}_4|^2 \\ &= \frac{|A|^2}{2} e^{-\Gamma t} \left[\left\{ 1 + \left| \frac{q\overline{a}}{pA} \right|^2 + \left| \frac{a}{A} \right|^2 + \left| \frac{q\overline{A}}{pA} \right|^2 \right\} \right. \\ &\quad \left. + \left\{ 1 - \left| \frac{q\overline{a}}{pA} \right|^2 + \left| \frac{a}{A} \right|^2 - \left| \frac{q\overline{A}}{pA} \right|^2 \right\} \cos(\Delta mt) \right. \\ &\quad \left. + \left\{ 2 \left| \frac{a}{A} \right|^2 \text{Im} \left[\frac{q\overline{A}}{pa} \right] + 2\text{Im} \left[\frac{q\overline{a}}{pA} \right] \right\} \sin(\Delta mt) \right] \\ &= \frac{|\overline{A}|^2}{2} \left| \frac{q}{p} \right|^2 e^{-\Gamma t} \left[\left\{ 1 + \left| \frac{pa}{q\overline{A}} \right|^2 + \left| \frac{\overline{a}}{\overline{A}} \right|^2 + \left| \frac{pA}{q\overline{A}} \right|^2 \right\} \right. \\ &\quad \left. - \left\{ 1 - \left| \frac{pa}{q\overline{A}} \right|^2 + \left| \frac{\overline{a}}{\overline{A}} \right|^2 - \left| \frac{pA}{q\overline{A}} \right|^2 \right\} \cos(\Delta mt) \right. \\ &\quad \left. - \left\{ 2\text{Im} \left[\frac{pa}{q\overline{A}} \right] + 2 \left| \frac{\overline{a}}{\overline{A}} \right|^2 \text{Im} \left[\frac{pA}{q\overline{a}} \right] \right\} \sin(\Delta mt) \right] \\ &= \frac{\mathcal{I}}{2} \left| \frac{q}{p} \right|^2 e^{-\Gamma t} [1 - \mathcal{A} \cos(\Delta mt) - \mathcal{S} \sin(\Delta mt)] \end{aligned} \quad (2.25)$$

Here, we defined \mathcal{I} , \mathcal{A} and \mathcal{S} as follow:

$$\mathcal{I} = |\bar{A}|^2 + \left| \frac{p}{q} a \right|^2 + |\bar{a}|^2 + \left| \frac{p}{q} A \right|^2, \quad (2.26)$$

$$\mathcal{A} = \left\{ |\bar{A}|^2 - \left| \frac{p}{q} a \right|^2 + |\bar{a}|^2 - \left| \frac{p}{q} A \right|^2 \right\} / \mathcal{I} \quad \text{and} \quad (2.27)$$

$$\mathcal{S} = \left\{ 2 |\bar{A}|^2 \text{Im} \left[\frac{pa}{q\bar{A}} \right] + 2 |\bar{a}|^2 \text{Im} \left[\frac{pA}{q\bar{a}} \right] \right\} / \mathcal{I}. \quad (2.28)$$

Be aware that these \mathcal{A} and \mathcal{S} are different from ordinary definitions. Using $|q/p| \sim 1$ from eq.(71) of HFAG results [3], time dependent asymmetry is

$$\begin{aligned} \text{asym} &= \frac{\Gamma_{\bar{B}^0 \rightarrow X_s^{CP} \gamma}(t) - \Gamma_{B^0 \rightarrow X_s^{CP} \gamma}(t)}{\Gamma_{\bar{B}^0 \rightarrow X_s^{CP} \gamma}(t) + \Gamma_{B^0 \rightarrow X_s^{CP} \gamma}(t)} \\ &= \mathcal{A} \cos(\Delta mt) + \mathcal{S} \sin(\Delta mt). \end{aligned} \quad (2.29)$$

In the SM, using eq.(2.2), we can say that

$$\begin{aligned} \langle X_s^{CP} \gamma_R | H | B^0 \rangle(0) &= A \propto m_b V_{tb}^* V_{ts}, \\ \langle X_s^{CP} \gamma_L | H | \bar{B}^0 \rangle(0) &= \bar{A} \propto m_b V_{tb} V_{ts}^*, \\ \langle X_s^{CP} \gamma_L | H | B^0 \rangle(0) &= a \propto m_s V_{tb}^* V_{ts} \quad \text{and} \\ \langle X_s^{CP} \gamma_R | H | \bar{B}^0 \rangle(0) &= \bar{a} \propto m_s V_{tb} V_{ts}^*. \end{aligned}$$

So,

$$|A| \sim |\bar{A}|, \quad (2.30)$$

$$|a| \sim |\bar{a}|, \quad (2.31)$$

$$\left| \frac{a}{A} \right| \sim \frac{m_s}{m_b} \sim 0.02 \quad \text{and} \quad (2.32)$$

$$q/p \sim e^{-2i\phi_1}. \quad (2.33)$$

Here, ϕ_1 is one of an Unitarity triangle's angle. Asymmetry predicted by the SM, asym_{SM} , can be calculated as

$$\begin{aligned} \text{asym}_{\text{SM}} &= \frac{\text{Im} \left[\frac{pa}{q\bar{A}} \right] + \frac{m_s^2}{m_b^2} \text{Im} \left[\frac{pA}{q\bar{a}} \right]}{1 + m_s^2/m_b^2} \sin(\Delta mt) \\ &= \frac{(m_s/m_b) \left\{ \sin(2\phi_1 + \delta_1) + \sin(2\phi_1 + \delta_2) \right\}}{1 + m_s^2/m_b^2} \sin(\Delta mt) \\ &\lesssim 2 \frac{m_s}{m_b} \sin(\Delta mt). \end{aligned} \quad (2.34)$$

Here, we defined that

$$\frac{a}{\bar{A}} = \frac{m_s}{m_b} e^{i\delta_1} \quad \text{and} \quad (2.35)$$

$$\frac{A}{\bar{a}} = \frac{m_b}{m_s} e^{i\delta_2}. \quad (2.36)$$

In a word, SM says that \mathcal{S} is less than 0.04. [4]'s eq.(9) says that asymmetry in the SM is

$$\text{asym}_{\text{SM}} = 2 \frac{m_s}{m_b} \sin(2\phi_1) \sin(\Delta mt). \quad (2.37)$$

The observation of significantly larger \mathcal{S} than this would be a “smoking gun” evidence of the new physics!

2.8 Method of TDCPV measurement using $\Upsilon(4S)$

Since $\Upsilon(4S)$ is spin-1 $b\bar{b}$ resonance, B meson pair state from its decay can be described as

$$|B_1^0\rangle |\bar{B}_2^0\rangle - |\bar{B}_1^0\rangle |B_2^0\rangle. \quad (2.38)$$

It means B meson has opposite flavor to its counterpart each other. If we measure flavor specific decay like $B^0 \rightarrow \ell^+ \nu X_c$, we can determine another B meson at that time is \bar{B}^0 . Then, if we define Δt as decay time difference in center of mass system, equation(2.24, 2.25) can be written as

$$\Gamma_{\bar{B}^0 \rightarrow X_s^{CP} \gamma}(\Delta t) = \frac{\mathcal{I}}{2} e^{-\Gamma|\Delta t|} [1 + \mathcal{A} \cos(\Delta m \Delta t) + \mathcal{S} \sin(\Delta m \Delta t)] \quad \text{and} \quad (2.39)$$

$$\Gamma_{B^0 \rightarrow X_s^{CP} \gamma}(\Delta t) = \frac{\mathcal{I}}{2} e^{-\Gamma|\Delta t|} [1 - \mathcal{A} \cos(\Delta m \Delta t) - \mathcal{S} \sin(\Delta m \Delta t)]. \quad (2.40)$$

Chapter 3

Experimental apparatus

3.1 KEKB accelerator

3.1.1 Linac

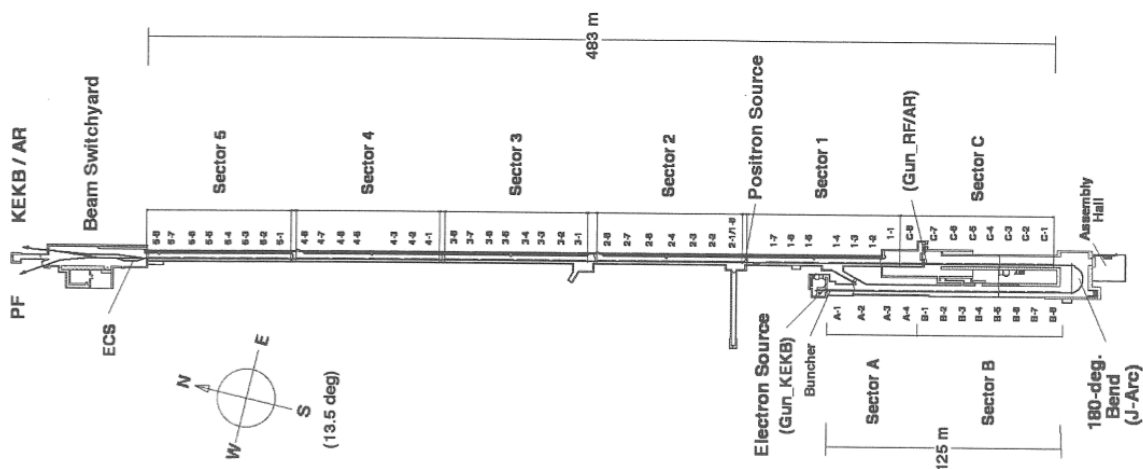


Figure 3.1: KEKB linac

Figure 3.1 shows overall of KEKB linac which has 600 m length [5]. At the beginning of the linac, electron gun emits electrons and they are accelerated. When the electrons are accelerated to 4 GeV, there is a target for positron source. Electrons and positrons are finally accelerated to 8 GeV and 3.5 GeV respectively, and injected into storage rings.

Electron source

Electrons are generated by applying 200 kV of pulse voltage to heated barium impregnated wolfram cathode. Pulse length is about 1 ns; emitted beams are shorten into 10 ps length with bunchers [6].

Positron source

Positrons are generated by colliding 4 GeV electron to wolfram target which has 14 mm thickness. In general, targets are made from Ta, W or alloy of W and Re; they have common features below.

1. They have large atomic number because cross sections of bremsstrahlung and pair creation are roughly proportional to Z^2/A .
2. They have high melting point.
3. They have enough strength to stand transformation by heating and cooling.

If the target is too thin, bremsstrahlung and pair production does not develop adequately. If the target is too thick, generated positrons are absorbed by the target. So, thickness of the target is decided in order to maximize positron efficiency, and 0.64 nC positrons are obtained from 10 nC electron injection [7].

3.1.2 Storage rings

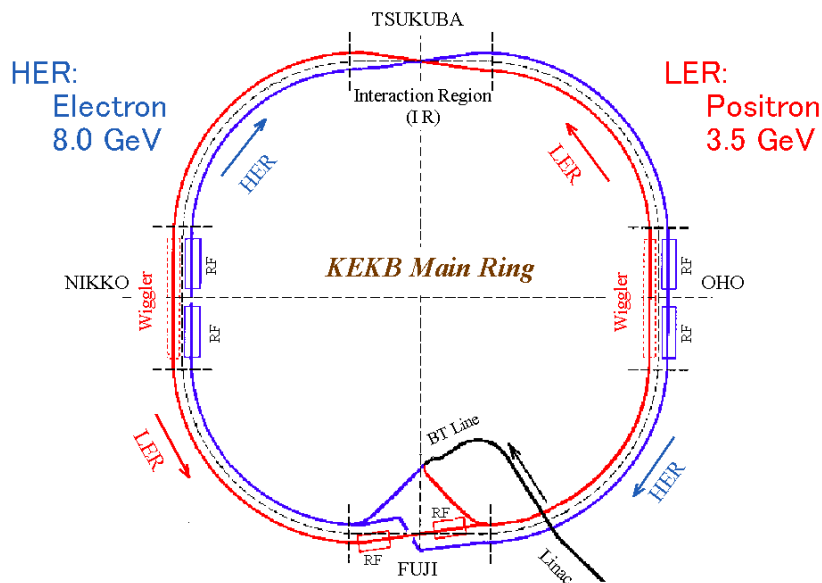


Figure 3.2: KEKB ring

Figure 3.2 shows overall of KEKB storage rings which have 3 km circumference. Electron and positron beam from injector are delivered to Higher energy ring (HER) and Lower energy ring (LER), and each of them can storage 1.2 A and 1.6 A current, respectively. Both of them are consist of 4 arc parts and 4 linear parts. As energy loss by synchrotron radiation at arc part and acceleration at RF cavity are repeated, beam quality becomes better. This phenomenon is called “damping”, and in LER, since this

damping is not enough just with arc part, there are wigglers which make beam snake its orbit. At interaction point (IP), electron and positron beam are focused an order of $\sigma_x \sim 100[\mu\text{m}]$ and $\sigma_y \sim 1[\mu\text{m}]$, crossing with an 22 mrad of angle, and B meson pairs are generated. Because they collide asymmetric energy, B meson moves; its Lorentz boost factor is $\beta\gamma \sim 0.425$. Number of B meson pair production rate per unit time can be described as

$$N = \sigma_{e^+e^- \rightarrow BB} \times \mathcal{L}. \quad (3.1)$$

Here, σ at center of mass energy $\sqrt{s} = 10.58 \text{ GeV}$ is about 1.1 nb, and luminosity record of KEKB collider is $\mathcal{L}_{\text{max}} = 21.1 \text{ nb}^{-1}\text{s}^{-1}$. Figure 3.3 shows records of integrated luminosity of KEKB and PEP-II which is also B meson factory. KEKB's luminosity is world record of electron positron collider.

Integrated luminosity of B factories

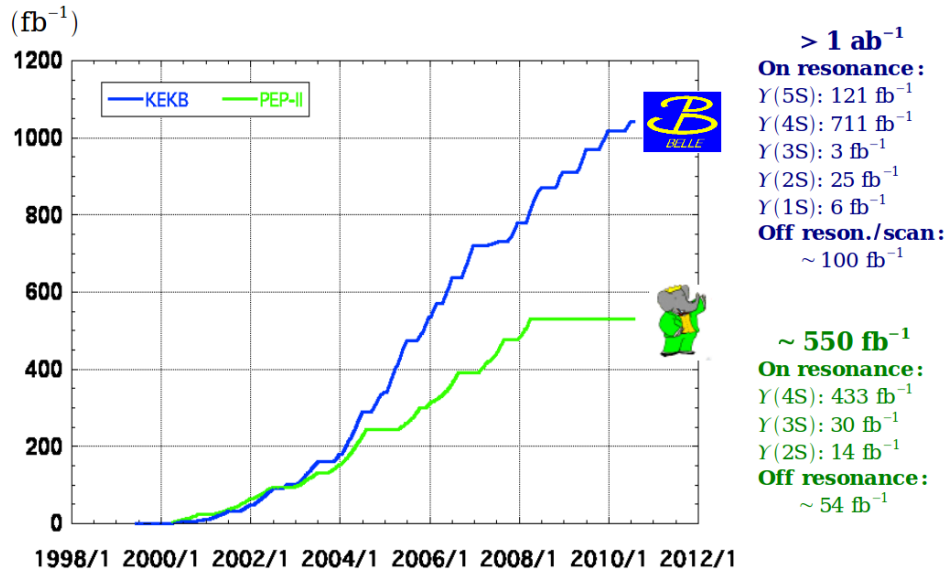


Figure 3.3: Luminosity record of KEKB and PEP-II

3.2 Belle detector

3.2.1 Overall

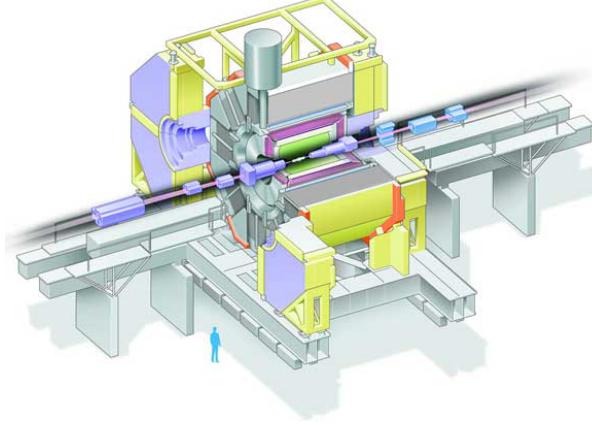


Figure 3.4: Overview of the Belle detector.

Figure 3.4 shows a overview of the Belle detector. In order to measure charged particle's track as much precise as possible, beam pipe around IP is very narrow and thin. For the sake of minimization of multiple scattering, beam pipe is made of Be which has 35 cm of radiation length. The innermost tracker is double sided silicon strip detector, and it is called "Silicon vertex detector (SVD)". Next, drift chamber covers SVD, and it is called "Central drift chamber (CDC)". These SVD and CDC are used for charged particle tracking. CDC can identify particle type from information of dE/dx . "Aerogel Cherenkov Counter (ACC)" and "Time of flight (TOF)" which cover CDC are used for particle Identification, also. If a charged particle has too high momentum, dE/dx of CDC cannot be used for particle ID. ACC and TOF measure velocity of such a kind of charged particle, and we can calculate its mass from its momentum and velocity using equation $p = \gamma mc\beta$. Outside of them, "Electro-magnetic calorimeter (ECL)" made of thallium doped CsI is placed. It has $16 X_0$ of radiation length. Next to ECL, 1.5 T superconducting solenoid follows, and outermost " K_L and muon detector (KLM)" is placed. It is made from iron and RPC sandwich. Interaction length of ECL and KLM are 0.76 and 3.92λ respectively. It is thick enough to stop K_L and distinguish with muon which passes through the detector. Following sections describe tracking, particle identification and photon detection which are specially important for this analysis.

3.2.2 Tracking and vertex reconstruction

Since we obtain Δt from Δz , vertex reconstruction is very important. Besides, accurate tracking is necessary for getting decay point and momentum vector of K_S . SVD and CDC is designed to reduce multiple-Coulomb scattering effect because momentum of particles from B meson is around ~ 1 GeV.

In phase 1 (1999-2003), 3 layers of SVD covers a solid angle of $23^\circ < \theta < 139^\circ$. Their radiuses are 30.0 mm, 45.5 mm and 60.5 mm, and their thicknesses are $300 \mu\text{m}$. Strip pitch of $r - \phi$ direction and z direction are $25 \mu\text{m}$ and $42 \mu\text{m}$. In phase 2 (2004-2010), 4 layers of SVD covers a solid angle of $17^\circ < \theta < 150^\circ$. Their radiuses are 20.0 mm, 43.5 mm, 70.0 mm and 88.0 mm. Strip pitch of $r - \phi$ direction and z direction are $50 \mu\text{m}$ ($65 \mu\text{m}$ for outermost layer) and $75 \mu\text{m}$ ($73 \mu\text{m}$ for outermost layer). The reason why pitch size of z direction is not small is there are no benefit. If a track with an angle $\theta = 45^\circ$, it makes signals along $300 \mu\text{m}$ in z direction. Multi cell hit information improves vertex reconstruction without reducing pitch size. Tracking errors for $r\phi$ and z direction using cosmic lay are shown in Fig.3.5 and 3.6 [8]. “Ghost” hits are generated by multiple hit. In order to distinguish true hit from ghost, CDC track is extrapolated to SVD volume.

Gas of CDC is consist of 50% He and 50% ethane. Its radiation length is 640 m and this is why such a low-Z gas is used. Measurement accuracy of dE/dx and spatial resolution are also considered. It covers a solid angle of $17^\circ < \theta < 150^\circ$. Spatial resolution is an order of $\sim 100 \mu\text{m}$ as shown in Fig.3.7. Momentum resolution is shown in Fig.3.8.

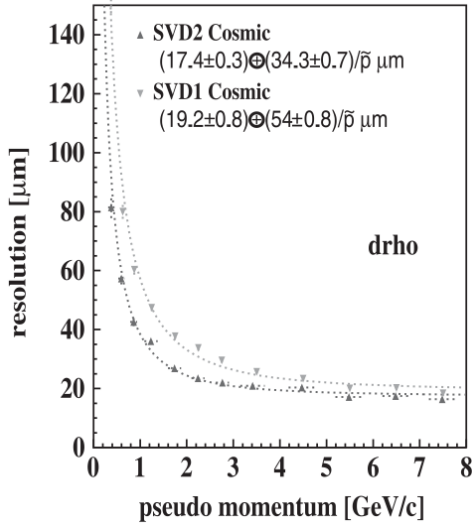


Figure 3.5: ρ resolution of SVD

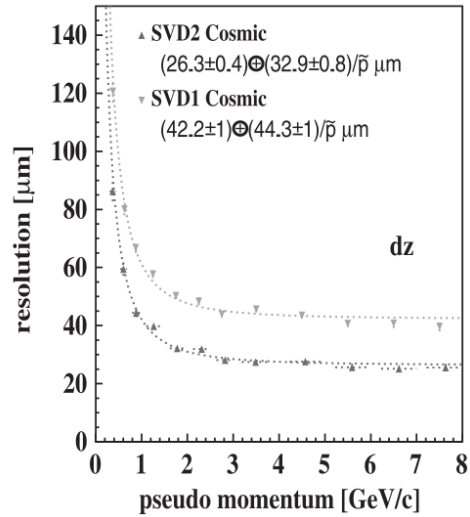


Figure 3.6: z resolution of SVD

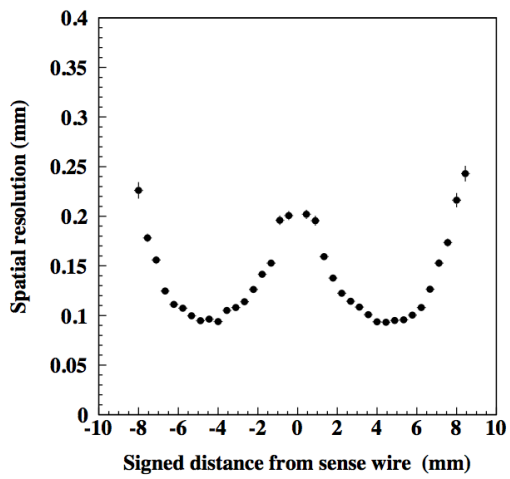


Figure 3.7: Spatial resolution of CDC

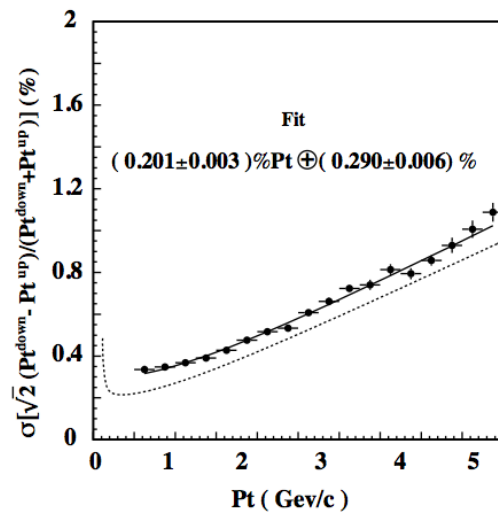


Figure 3.8: Momentum resolution of CDC

3.2.3 Particle identification

In order to reconstruct K_S or η , we have to check whether child particles are π or not. Then, particle identification plays an important role. It is also used for flavor tagging which is a must for time dependent CP violation measurement. As shown in Fig.3.9, K- π tagging is done by three sub-detectors: CDC, TOF and ACC. dE/dx distribution of CDC is shown in Fig.3.10, and it is useful for low momentum particle identification.

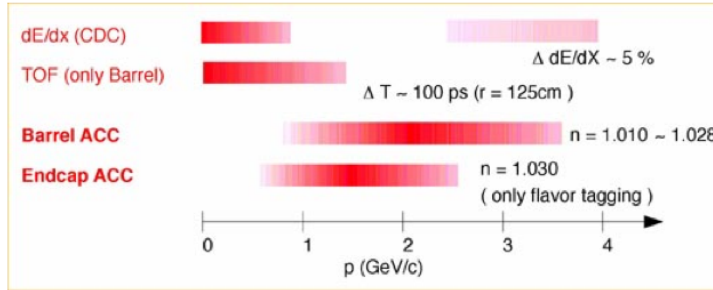


Figure 3.9: Detectors and momentum region for K- π tagging

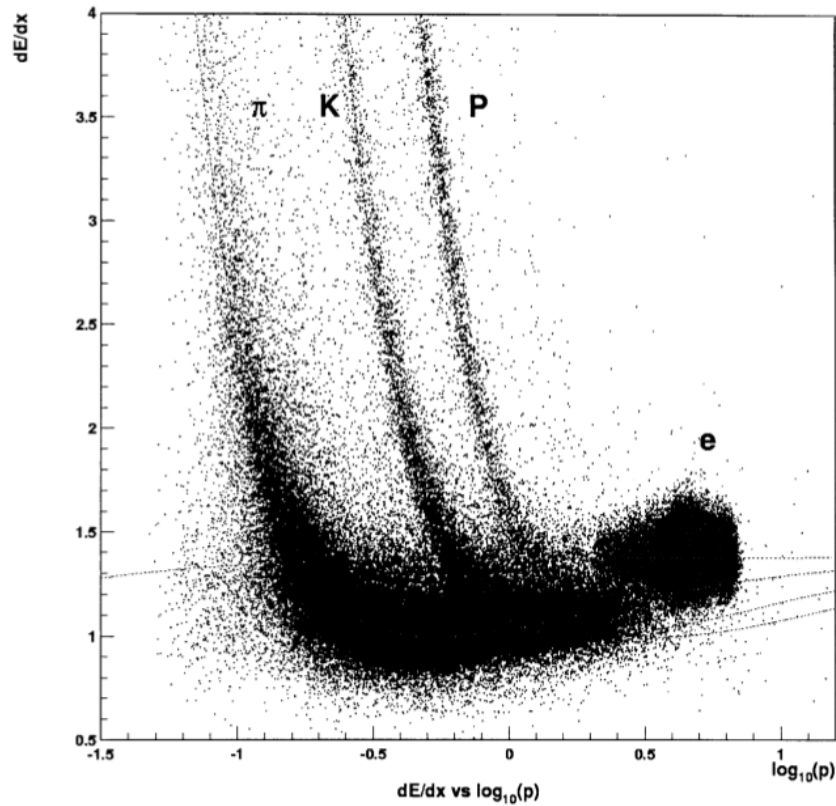


Figure 3.10: dE/dx vs. momentum [9].

TOF measures particle's time of flight from IP to the detector. It places 1.2 m from IP. For example, pion, kaon and proton need 4.0 ns, 4.3 ns and 5.1 ns if its transverse momentum is 1.2 GeV. Since time resolution of TOF is an order of ~ 0.1 ns, it can identify low momentum ($\lesssim 1.2$ GeV) charged tracks as shown in Fig.3.11.

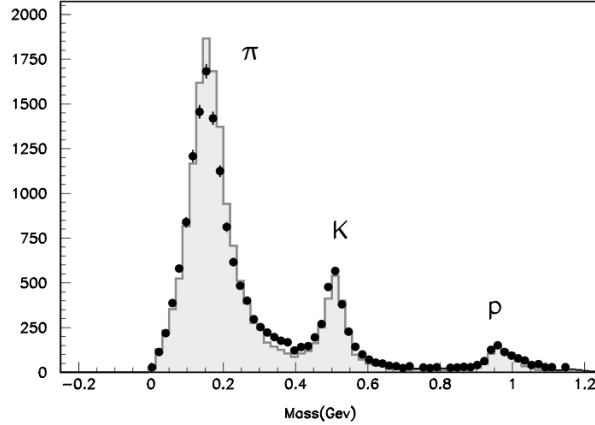


Figure 3.11: Mass distribution from TOF measurements for particle momenta below 1.2 GeV/c [9].

Aerogel is a material whose $n-1$ is an order of ~ 0.01 . Typical $n-1$ of gaseous material is an order of ~ 0.001 and liquid material is an order of ~ 0.1 . In the view of $n-1$, aerogel places middle of them, and it is useful for distinguish ~ 1 GeV charged pion and Kaon. Figure 3.12 shows position and n of ACC, and table 3.1 shows lowest momentum of K and π for Cherenkov radiation. We can distinguish K and π if the charged track's momentum is between them. Barrel ACC is used for $K-\pi$ identification whose momentum is too high to use TOF. Because backward particles tend to be slower than forward particles, n of backward ACC is smaller than forward ACC. Since there is no TOF at endcap region, ACC have to cover lower momentum region as shown in Fig.3.9. This is why endcap ACC has highest n . It is very important to identify low momentum K of $b \rightarrow c \rightarrow s$ chain for flavor tagging.

Table 3.1: n and lowest momentum of π and K for Cherenkov radiation

n	lowest p_π [GeV]	lowest p_K [GeV]
1.010	0.99	3.53
1.013	0.87	3.09
1.015	0.81	2.88
1.020	0.70	2.49
1.028	0.59	2.10
1.030	0.57	2.03

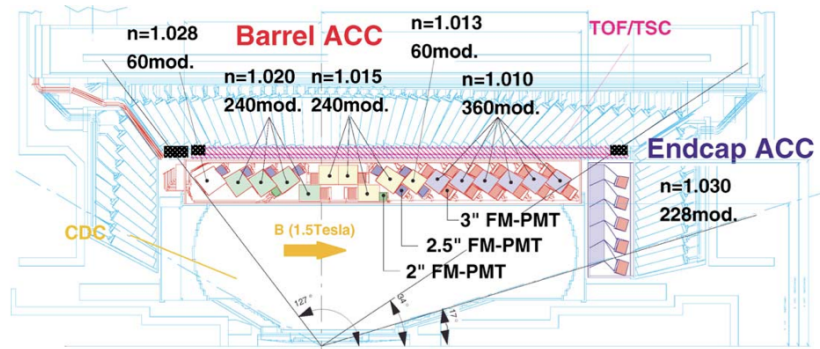


Figure 3.12: Alignment and n of ACC [9].

3.2.4 Photon detection

ECL is used for photon detection. 6624, 1152 and 960 crystals are used for barrel, forward endcap and backward endcap respectively. Its length is 30 cm and corresponds to $16.2 X_0$. In order to gain amount of photon emission and to lengthen typical wave length, Thallium is doped. Its side view is trapezoidal shape; inner side is smaller than outer side, and all crystals point to IP. Cover range and typical shape of the crystal are summarized on a table 3.2. Energy resolution of photon detection is

$$\frac{\sigma_E}{E} = \frac{0.0066(\%)}{E} \oplus \frac{1.53(\%)}{E^{1/4}} \oplus 1.18(\%) \quad (3.2)$$

for 3×3 matrix sum of crystals [9].

Table 3.2: Cover range and typical shape of the crystal of ECL

	Barrel	Forward endcap	Backward endcap
Cover range	32.2°, 128.7°	12.4°, 31.4°	130.7°, 155.1°
Inner side [cm]	5.5	4.45	5.4
Outer side [cm]	6.5	7.08	8.2

We measure low energy photons from η and π^0 decays as well as high energy prompt photon from $b \rightarrow s\gamma$ transition. As eq.(3.2) says, energy resolution of low energy photon is not good, and reconstruction efficiency is bad. Then, we have to apply a cut on photon energy in lab system.

95% of electro magnetic shower energy is deposited in a cylindrical shape whose radius is $2R_M$ [10]. Here, R_M is Moliere radius and $2R_M = 7.14$ cm for CsI. This length is roughly same to outer side of the crystals. It means that 3×3 matrix sum of energy deposit contains about 95% of photon energy. We call a ratio between this 3×3 matrix sum and 5×5 matrix sum of energy deposit as “E9/E25 (E nine over E twenty-five)”. E9/E25 of E.M. shower is close to 1 while hadronic shower takes smaller value; it can be used for photon selection.

Chapter 4

New K_S reconstruction method

We used neural network for K_S selection and achieved much better purity and efficiency than Belle's traditional method. In this chapter, detailed selection strategy and performance are described.

4.1 Training strategy

Background (BG) of K_S candidate can be divided into two groups. One is non-V particle BG: combinatorial BG, fake track and curl track. The other is V particle BG, i.e. Λ particle. Converted photon BG can be included into V particle BG, but its amount is negligible. Then, two NeuroBayes outputs are calculated: nb_vlike and nb_nolam. Former describes how the candidate is V-particle like and latter describes how the candidate is not Lambda like. K_S candidates and NeuroBayes output parameters are illustrated in Fig.4.1.

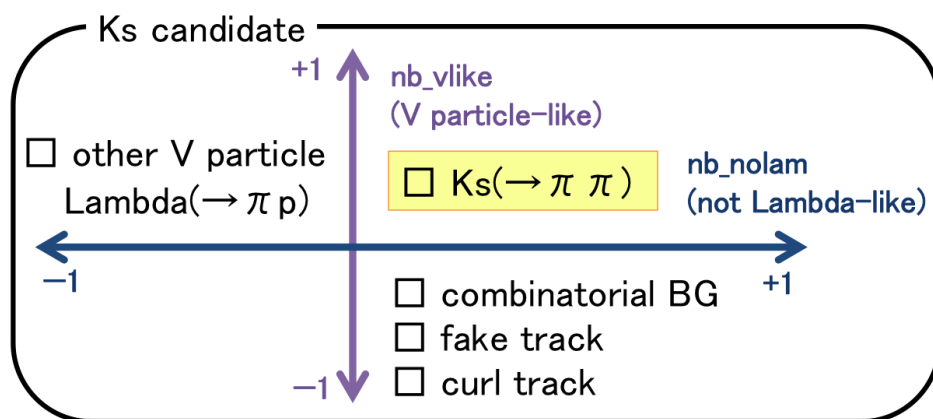


Figure 4.1: Kinds of K_S candidate and NeuroBayes outputs

4.1.1 Pre-selection

Curl track BG has no momentum, and K_S which has too small momentum is difficult to extract from curl track BG. Therefore, we decided to reject too small momentum candidate. Poorly reconstructed candidates also should be removed. Therefore, we applied pre-selection to the candidates as shown below.

- momentum is greater than 0.06 GeV
- mass difference from K_S nominal mass is less than 20 MeV
- Distance between child pions in z direction is less than 20 cm

4.1.2 V-particle like candidate extraction

For the sake of extracting V particles, Belle's traditional method uses 4 parameters: distance between two helices in z direction, flight length in x-y plane, angle between K_S momentum in K_S frame and K_S direction in lab frame, shorter distance between interaction point (IP) and child helix. They are good inputs for checking V particle feature below.

- Two child pions come from one point.
- Vertex and interaction point of a V particle are different.
- V particle's momentum has same direction with the particle's vertex.

Figure 4.2 to 4.5 show these parameter's distribution. In addition to these parameters, we used 9 parameters: K_S momentum, longer distance between IP and child helix, angle between K_S momentum in lab frame and Pion momentum in K_S frame, whether positive/negative child hit SVD or not, axial wire hit number of positive/negative child, stereo wire hit number of positive/negative child.

Longer distance between IP and child helix can also be used like shorter distance between IP and child helix. Non-V particle BGs tend to distribute around small value while signal distribute up to higher value (Fig.4.6).

If one of the K_S candidate child is different from pion, angle between K_S momentum in lab frame and Pion momentum in K_S frame has different distribution from signal (Fig.4.7).

Since some of fake track BGs have no hits in tracker detector, rest of 6 hit information of the tracker become useful variable to separate out fake track backgrounds from signal K_S events (Fig.4.8, 4.9, 4.10).

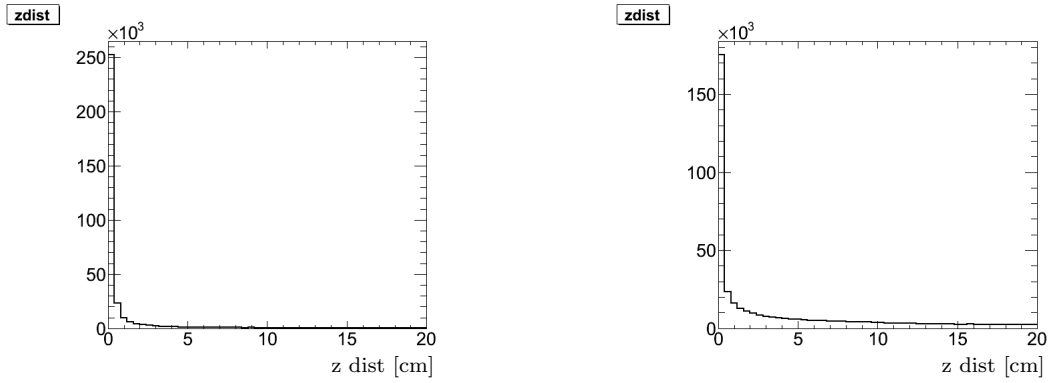


Figure 4.2: z distance of signals (left) and non-V BGs (right).

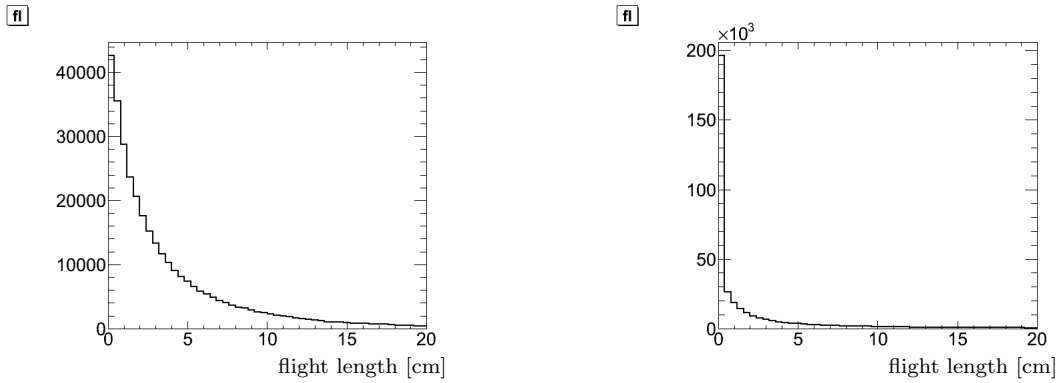


Figure 4.3: Flight length of signals (left) and non-V BGs (right).

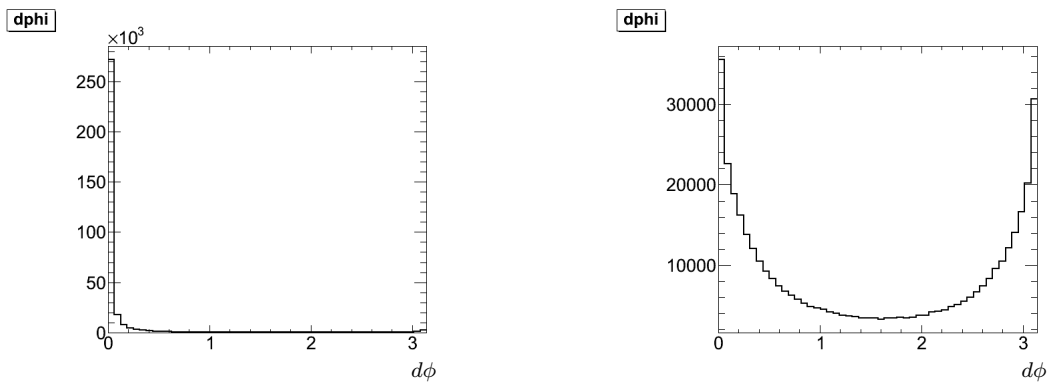


Figure 4.4: Angle bet. vertex position and momentum of signals (left) and non-V BGs (right).

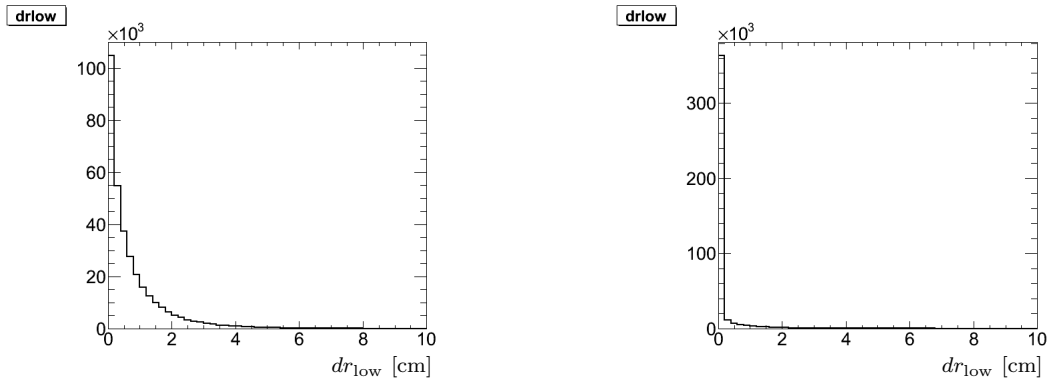


Figure 4.5: Shorter dr of signals (left) and non-V BGs (right).

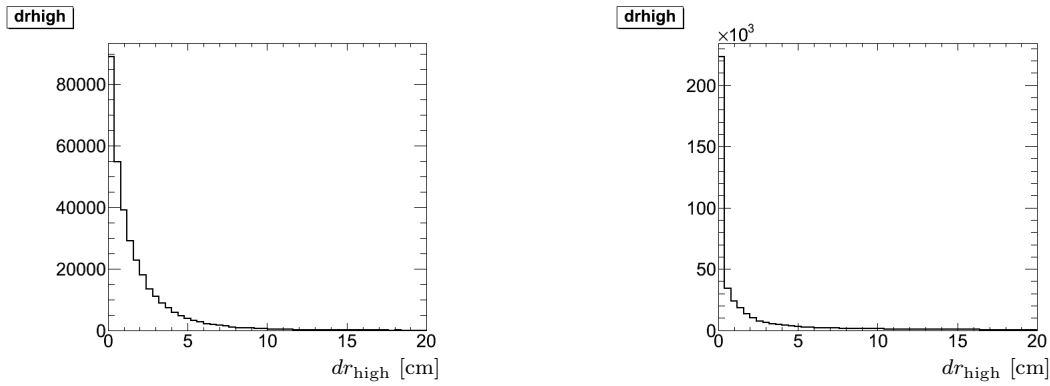


Figure 4.6: Longer dr of signals (left) and non-V BGs (right).

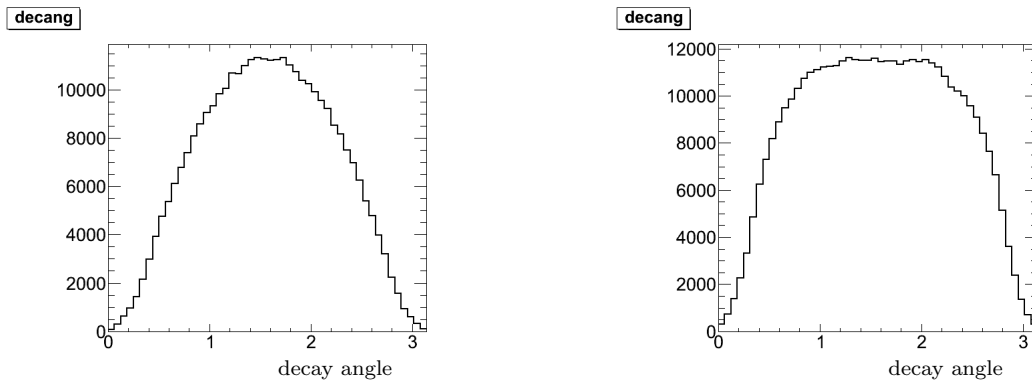


Figure 4.7: Decay angle of signals (left) and non-V BGs (right).

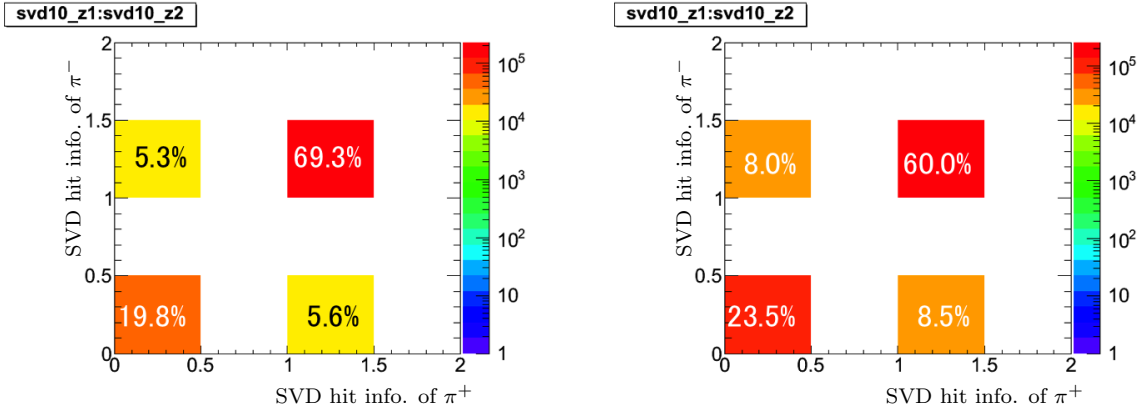


Figure 4.8: SVD hit information of signals (left) and non-V BGs (right). “0” means there’s no hit, and “1” means there’s any hit.

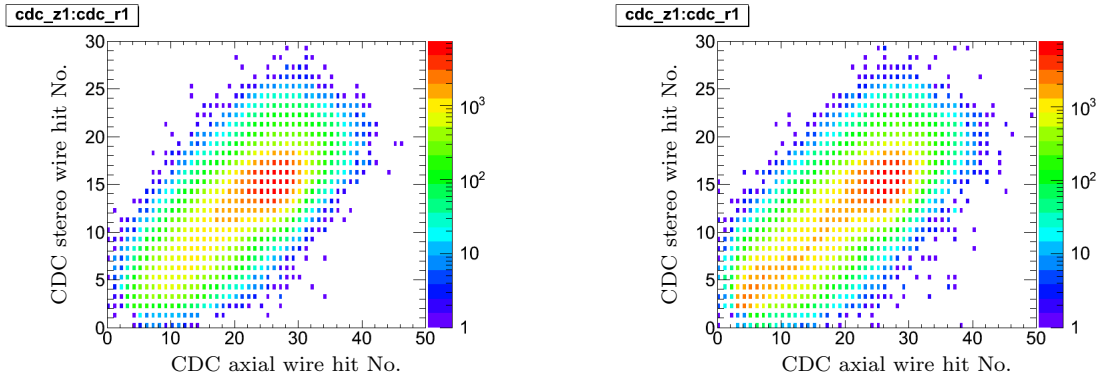


Figure 4.9: CDC hit numbers of π^+ candidate of signals (left) and non-V BGs (right).

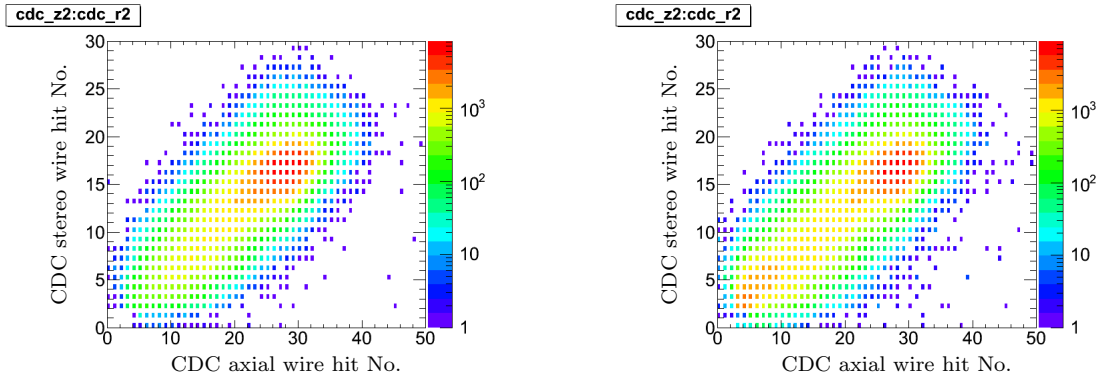


Figure 4.10: CDC hit numbers of π^- candidate of signals (left) and non-V BGs (right).

4.1.3 Not lambda like candidate extraction

In order to separate Lambda particles from signals, we used 7 parameters: binned PID likelihood ratio of π rather than proton ($\mathcal{L}_\pi/(\mathcal{L}_\pi + \mathcal{L}_p)$) value of positive/negative child, reconstructed mass with lambda hypothesis, momentum of positive/negative child, $\sin\theta$ of positive/negative child's momentum. Here, θ is an angle between particle's momentum and beam axis.

If the candidate is lambda decay event, one of the pion candidate is very proton-like (Fig.4.11). In order to suppress systematics from difference between data and MC, particle ID information is binned into 21 bins.

Lambda mass takes non-zero value if lambda particle can be reconstructed from children. 8% K_S events have non-zero value and distribute as left side of Fig.4.12. 92% lambda events have non-zero value and make a peak at lambda mass, 1.116 GeV.

Figure 4.13 to 4.15 shows last 4 parameters distribution. They do not only improve separation performance, but make discrete output smooth as well. Figure 4.16 shows performance comparison between NB output with 3 inputs and 7 inputs.

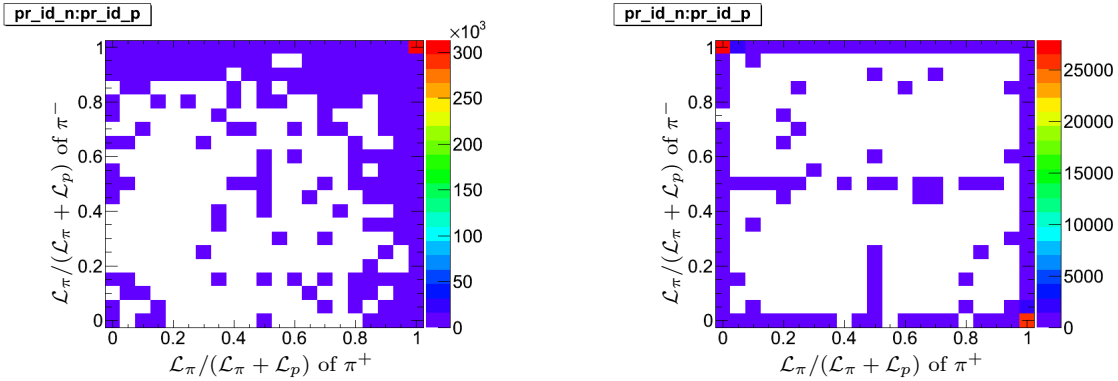


Figure 4.11: Particle ID values of signals (left) and lambda BGs (right).

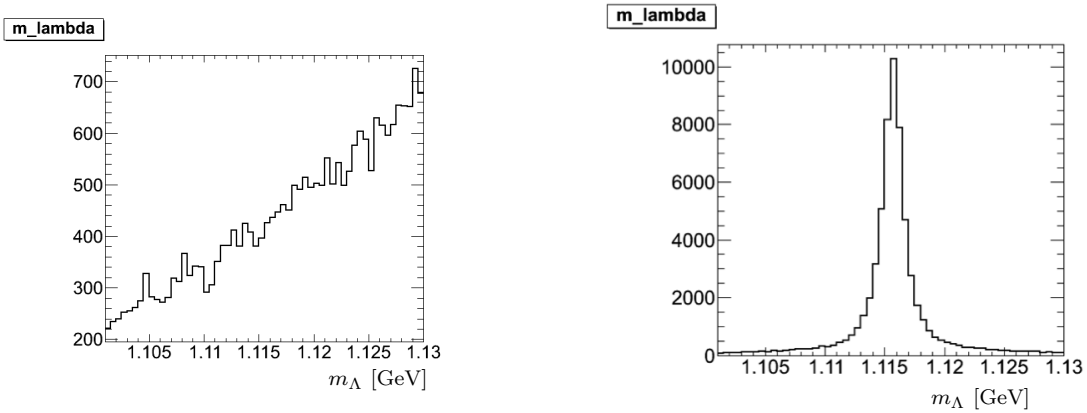


Figure 4.12: Lambda mass distribution of signals (left) and lambda BGs (right).

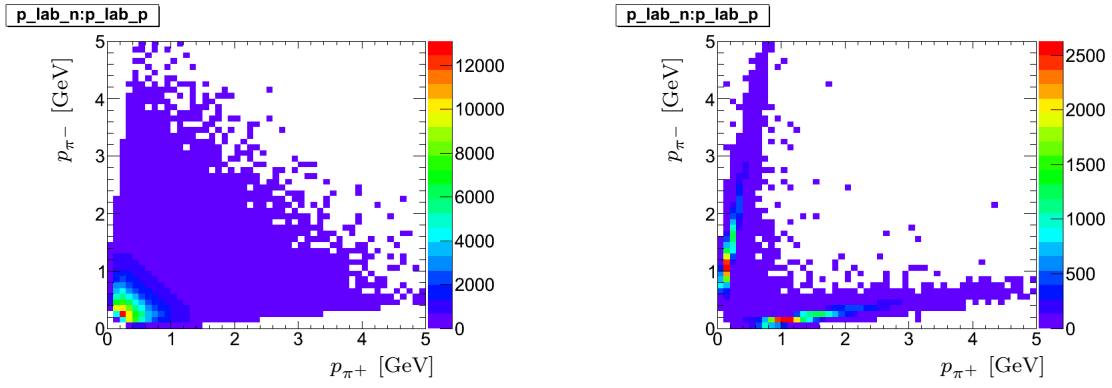


Figure 4.13: Child's momenta of signals (left) and lambda BGs (right).

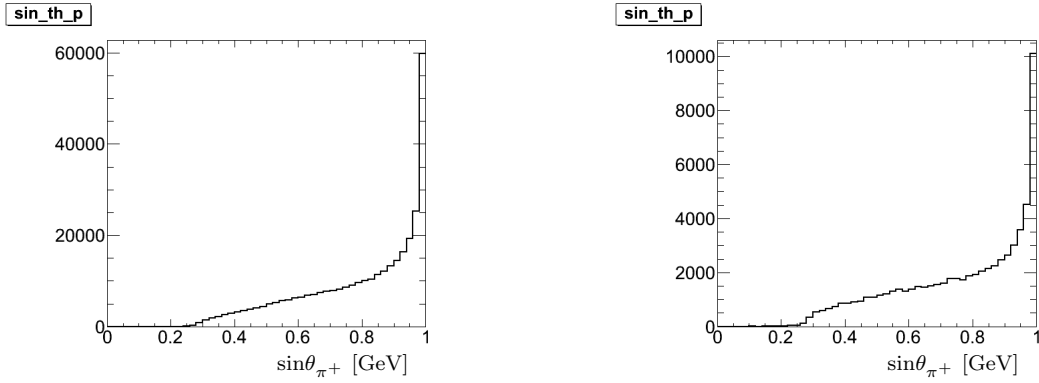


Figure 4.14: π^+ momentum direction of signals (left) and lambda BGs (right).

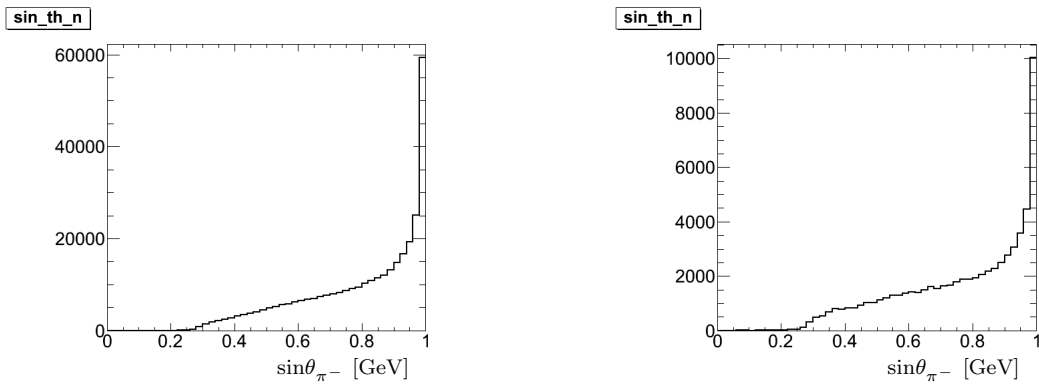


Figure 4.15: π^- momentum direction of signals (left) and lambda BGs (right).

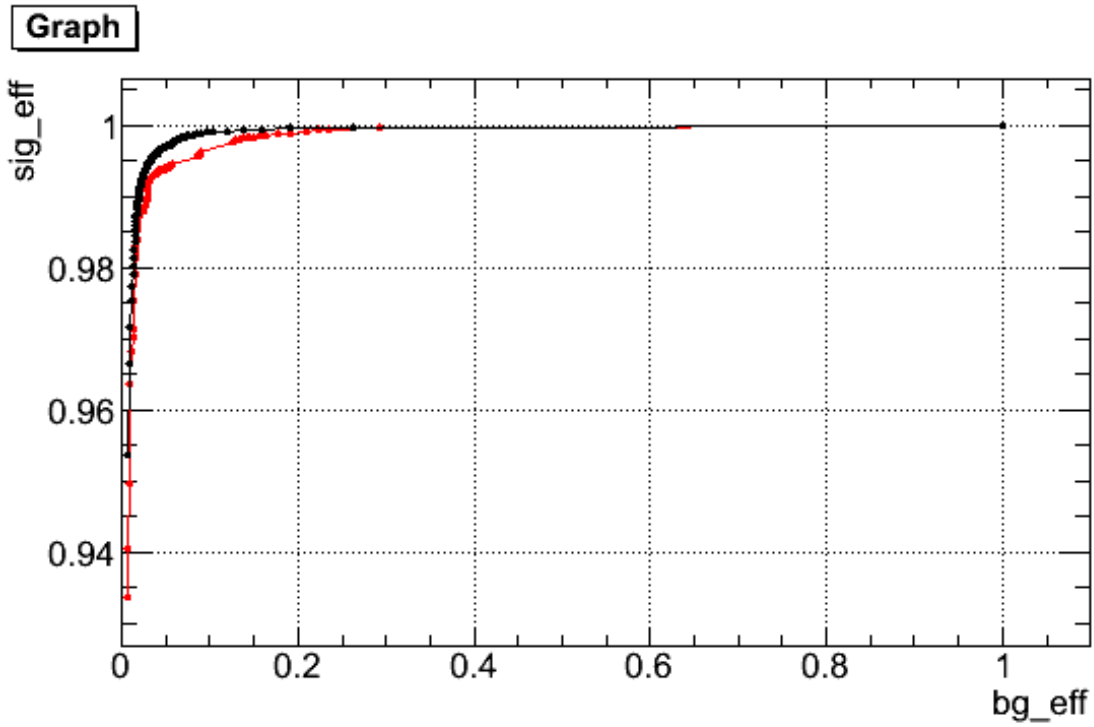


Figure 4.16: Signal efficiency vs. lambda BG efficiency. Red plot shows NB output with 3 inputs: pid values and M_{Λ} . Black plot shows NB output with 7 inputs.

4.2 performance check with MC

Figure 4.17 shows that K_S selection performance of Belle's traditional method and the new method. Horizontal axis means purity and vertical axis means efficiency. Blue cross is traditional method's result. Red curve is written by scanning nb_vlike threshold without nb_nolam cut. Black curve is written by scanning nb_vlike threshold with nb_nolam cut at -0.4. Magenta curve is written by scanning nb_vlike threshold with nb_nolam cut at +0.5.

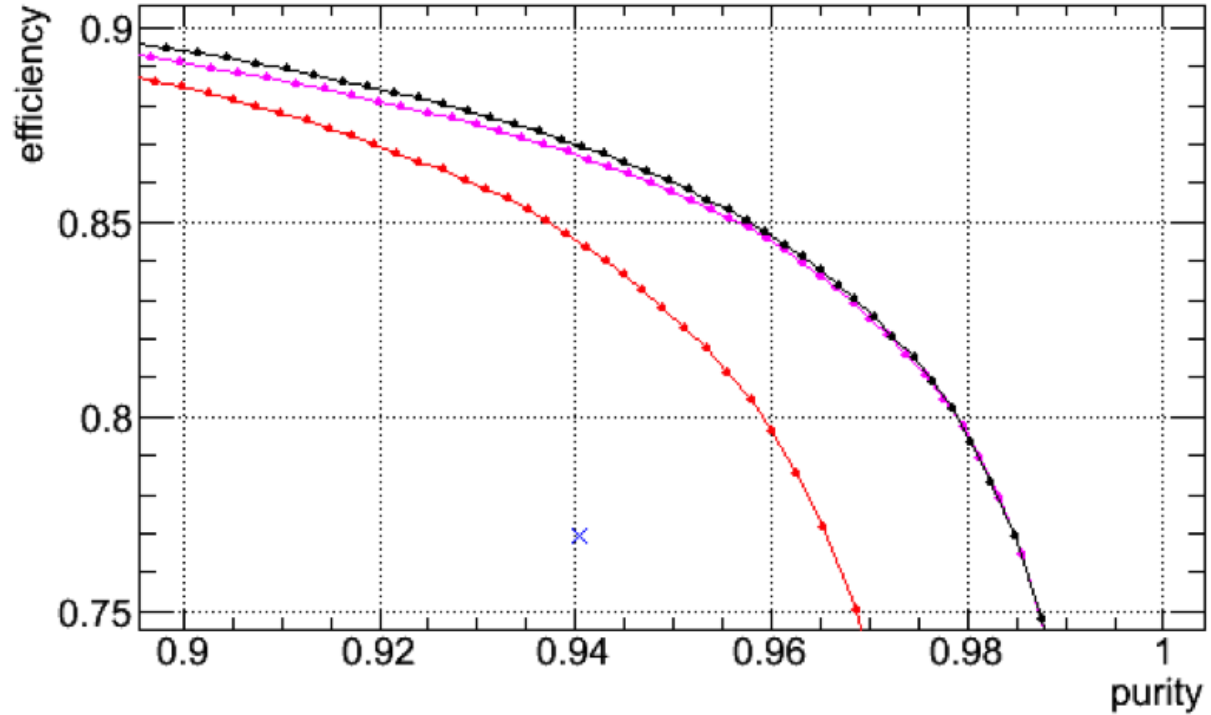


Figure 4.17: Comparison of purity vs. efficiency (MC exp# is 55). Blue cross : result of traditional method. Red curve : scanning plot of nb_vlike threshold without nb_nolam cut. Black curve : scanning plot of nb_vlike threshold with nb_nolam > -0.4. Magenta curve : scanning plot of nb_vlike threshold with nb_nolam > +0.5.

Chapter 5

Selection criteria

In this analysis, it is expected that statistics will be the main error. Selection criteria should be decided in order to obtain signal events as much as we can. However, if there are too many backgrounds, its statistical fluctuation may swallow signal excess. Therefore we have to maximize “significance” defined as

$$N_{\text{signal}}/\sqrt{N_{\text{signal}} + N_{\text{background}}}; \quad (5.1)$$

its square corresponds to effective signal events with null-background.

Selection criteria is decided using GEANT based Monte Carlo simulation. In this chapter, MC data sets and detail of selection criteria are described.

5.1 Data set and event types

5.1.1 Monte Carlo signal generation

Physics process is two body decay of b quark to s quark and photon, which have energy of $m_b/2$; photon energy is expected to be greater than ~ 2 GeV. In order to produce such situation in MC, we had B meson decay into photon and “ X_s ” which is a combined system of $K \eta$, which decays to Kaon and η . Mass distribution of X_s is decided based on BaBar’s measurement [11] and former analysis of Belle experiment [12]. Although there’s no resonance, Breit-Wigner is chosen as distribution shape in order to describe the structure (better than flat distribution). Its peak and width are set to 1.5 GeV and 0.2 GeV. Lower and upper limits are set to 1.05 GeV and 3.0 GeV respectively. Expected branching ratio of neutral and charged decays used for significance optimization are based on newest PDG (2012) value: $\mathcal{B}(B^0 \rightarrow K_S \eta \gamma) = (7.6 \pm 1.8) \times 10^{-6}$ and $\mathcal{B}(B^+ \rightarrow K^+ \eta \gamma) = (7.9 \pm 0.9) \times 10^{-6}$. Spin of X_s is assumed to be 1. X_s should have spin more than 0, because spin-0 B meson decays to spin-1 photon and X_s .

We want to estimate reconstruction efficiency as accurate as possible. On the other hand, real data amount has $\mathcal{O}(1\%)$ order error, i.e. $(771.6 \pm 10.6) \times 10^6$ B pairs. There is no meaning of estimating better than this order, we need about ten thousands of reconstructed events. Considering typical efficiency is the order of $\mathcal{O}(1\%)$, we should

generate million of events. Then, with the safety margin, we generated about 3 million signal events. It corresponds to about 500 times larger statistics than real data.

5.1.2 Monte Carlo background data

Light quark background

There are 6 streams of qq BG MC data are available. We found that qq BG of real data of charged sample is about 1.5 times higher than expected by the simulation. (This ratio is different reconstruction mode-by-mode.) This is originated from wrong PYTHIA parameter in the MC code. Therefore, we actually have 4 (=6/1.5) times larger qq BG MC data than real data. We call this type of BG as “ qq BG”.

Background from other B decay

Major $b \rightarrow cW$ decays of neutral and charged B meson are simulated. 6 times larger statistics than real data is available. We call this type of BG as “ BB BG”.

Rare B background

Rare decays like $b \rightarrow uW$, $b \rightarrow s\gamma$ or $b \rightarrow sl^+\ell^-$ of neutral and charged B meson are simulated. 50 times larger statistics than real data is available. We do not use $b \rightarrow s\gamma$ radiative decays including $B^0(\overline{B}^0) \rightarrow K^0\eta\gamma$ and $B^\pm \rightarrow K^\pm\eta\gamma$ events in this data set as we use other MC data set instead. We call this type of BG as “rare B BG”.

Radiative B background

BG from $b \rightarrow s\gamma$ radiative decays except for signal mode ($B \rightarrow K^{\pm/0}\eta\gamma$) are simulated. There are 40 times larger statistics than real data. s quarks forms $K^*(892)$ or inclusive X_s based on Kagan-Neubert model [13]. We call this type of BG as “rad B BG”.

5.1.3 Kinds of signal candidate

We divide B candidate reconstructed from signal into 2 groups. If an signal event reconstructed perfectly, we call it “perfectly reconstructed signal”. If an signal event reconstructed with only low energy photon misreconstruction from η or π^0 decay, we call it “poorly reconstructed signal”. If we misreconstruct prompt photon, kaon or charged tracks from η , it is included into “rad B BG”. Charged signal ($B \rightarrow K^\pm\eta\gamma$) BG for neutral mode reconstruction is also included into “rad B BG”, and vice versa.

5.1.4 2×7 groups of signal candidate

Reconstructed events are divided into 14 groups: two reconstructed decay types times seven flavor tagging quality bins. CP fit is done with 14 groups of Δt distributions simultaneously. Then, selection optimization have to be done to maximize quadratic sum of these 14 significances.

Two reconstructed types

We used 2 types of reconstructed mode.

- $\eta \rightarrow 2\gamma$ mode
- $\eta \rightarrow \pi^+\pi^-\pi^0$ mode

Considering low energy γ reconstruction efficiency, $\eta \rightarrow \pi^0\pi^0\pi^0$ mode and $K_S \rightarrow \pi^0\pi^0$ mode are expected to be too small statistics to see Δt distribution. 2 charged pions from η are used for vertex reconstruction of $\eta \rightarrow 3\pi$ mode, and K_S track is used for vertex reconstruction of $\eta \rightarrow 2\gamma$ mode. If we reconstruct vertex from pions from η , events which has one or two pions leaving at least two SVD hits for z direction and one SVD hit for $r-\phi$ direction are used for vertex reconstruction. We do not require such SVD hit conditions for a K_S track.

Seven flavor tagging quality bins

Probability of misreconstruction of B flavor is different for each event. This fraction is called “wrong tag fraction”. In order to avoid systematics from difference between MC and data, wrong tag fraction group is divided into 7 groups like table 5.1. The way of obtaining wrong tag fraction is written in the section 7.1.1.

Table 5.1: “qr bin” definition

bin #	condition
#0	$0.000 < (1 - 2w) \leq 0.100$
#1	$0.100 < (1 - 2w) \leq 0.250$
#2	$0.250 < (1 - 2w) \leq 0.500$
#3	$0.500 < (1 - 2w) \leq 0.625$
#4	$0.625 < (1 - 2w) \leq 0.750$
#5	$0.750 < (1 - 2w) \leq 0.875$
#6	$0.875 < (1 - 2w) \leq 1.000$

5.2 Reconstruction

5.2.1 Photon reconstruction

Since prompt photon is generated by two-body decay of $b \rightarrow s\gamma$, energy of the photon is greater than about half of b quark mass, ~ 2 GeV. Therefore, the highest energy photon is chosen as a prompt photon candidate. We require photon energy in center of mass system ($E_{\gamma(\text{c.m.})}$) is between 1.8 GeV and 3.4 GeV. A candidate whose “E9/E25 (E9 over E25)” is lower than 0.95 is discarded; if E9/E25 is close to 1, it means that shower shape in ECL cell is sharp. (For more detail, please see chapter 3.) Figure 5.1 and 5.2 shows $E_{\gamma(\text{c.m.})}$ and E9/E25 distributions of signal MC. These signal MC distributions in this section are distributions of perfectly reconstructed signals in signal region.

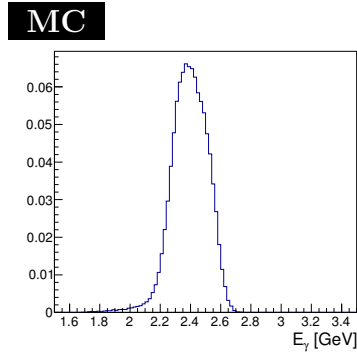


Figure 5.1: $E_{\gamma(\text{c.m.})}$ distribution of perfectly reconstructed signal in signal region

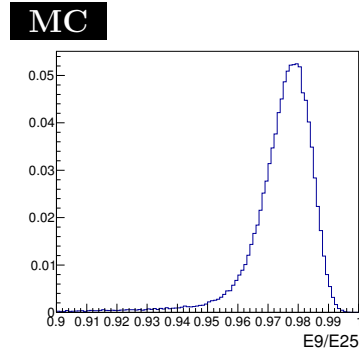


Figure 5.2: E9/E25 distribution of perfectly reconstructed signal in signal region

5.2.2 Kaon reconstruction

K_S candidate must pass following selections:

- momentum in lab frame is greater than 0.06 GeV,
- distance between two helices in z-direction is smaller than 20 cm,
- $0.470 \text{ GeV} < M_{K_S} < 0.520 \text{ GeV}$ and
- $\text{nb_vlike} > 0.4$ and $\text{nb_nolam} > -0.9$.

“nb_vlike” shows how the candidate is V-particle like. “nb_nolam” shows how the candidate is not Λ like. (For more detail, please see chapter 4.) Figure 5.3 shows $M_{K_S \rightarrow \pi^+\pi^-}$ distribution of signal MC. For K^\pm from charged decay, $B^\pm \rightarrow K^\pm \eta \gamma$, we required $\text{dr} <$

0.5 cm, $dz < 5.0$ cm and PID likelihood ratio of K rather than π is $\mathcal{L}_K/(\mathcal{L}_K + \mathcal{L}_\pi) > 0.1$.

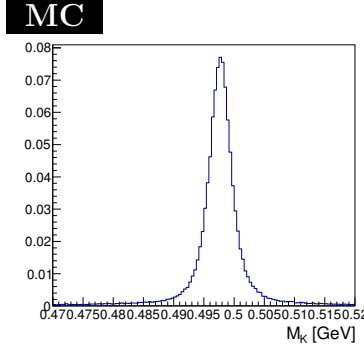


Figure 5.3: $M_{K_S \rightarrow \pi^+ \pi^-}$ distribution of perfectly reconstructed signal in signal region.

5.2.3 η reconstruction

η candidates are reconstructed from two modes: $\eta \rightarrow \gamma\gamma$ and $\eta \rightarrow \pi^+ \pi^- \pi^0$. After η selection, “mass-constrained” fit is applied to η . Mass-constrained fit adjusts child tracks within error in order to fit its detected invariant mass equals to nominal mass.

For $\eta \rightarrow \gamma\gamma$ mode, following conditions are required.

- $0.510 < M_{\eta \rightarrow \gamma\gamma} < 0.575$ [GeV].
- E_γ in lab system is greater than 0.15 GeV.

This $M_{\eta \rightarrow \gamma\gamma}$ window keeps 91% perfectly reconstructed signal in signal region. Figure 5.4 and 5.5 shows $M_{\eta \rightarrow \gamma\gamma}$ and $E_{\gamma(\text{lab})}$ distributions of signal MC. For $\eta \rightarrow \pi^+ \pi^- \pi^0$ mode, following conditions are required.

- $0.537 < M_{\pi^+ \pi^- \pi^0} < 0.556$ [GeV].
- $dr < 0.5$ cm, $dz < 5.0$ cm and $\mathcal{L}_K/(\mathcal{L}_K + \mathcal{L}_\pi) < 0.9$ for charged pion.
- $0.114 < M_{\gamma\gamma} < 0.147$ [GeV] for π^0 candidate.
- E_γ from π^0 in lab system is greater than 0.05 GeV.
- π^0 momentum in c.m. system is greater than 0.1 GeV.

This $M_{\eta \rightarrow 3\pi}$ window keeps 94% perfectly reconstructed signal in signal region. This $M_{\pi^0 \rightarrow \gamma\gamma}$ window keeps 95% perfectly reconstructed signal in signal region. Figure 5.6, 5.7 and 5.8 shows $M_{\eta \rightarrow \gamma\gamma}$ and $E_{\gamma(\text{lab})}$ distributions of signal MC.

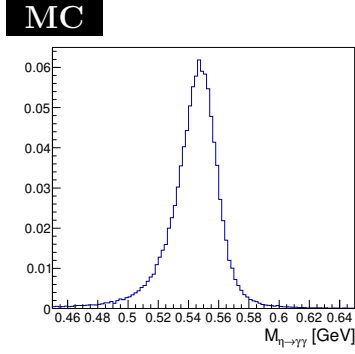


Figure 5.4: $M_{\eta \rightarrow \gamma\gamma}$ distribution of perfectly reconstructed signal in signal region.

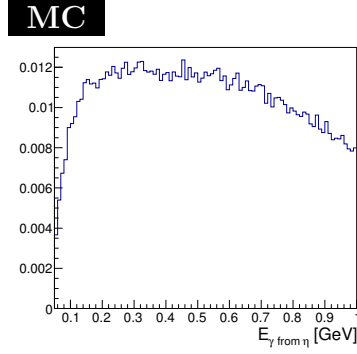


Figure 5.5: $E_{\gamma(\text{lab})}$ from η distribution of perfectly reconstructed signal in signal region.

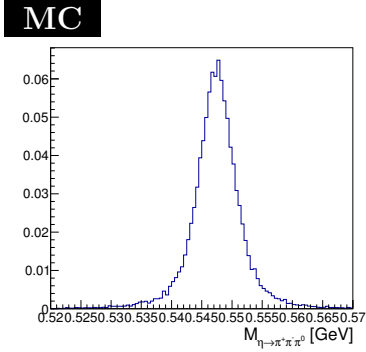


Figure 5.6: $M_{\eta \rightarrow 3\pi}$ distribution of perfectly reconstructed signal in signal region.

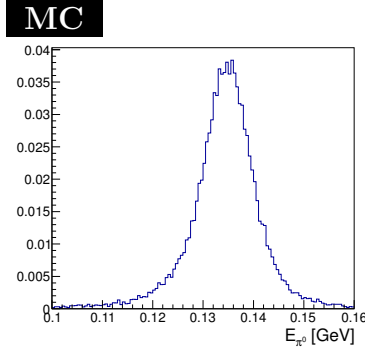


Figure 5.7: M_{π^0} distribution of perfectly reconstructed signal in signal region.

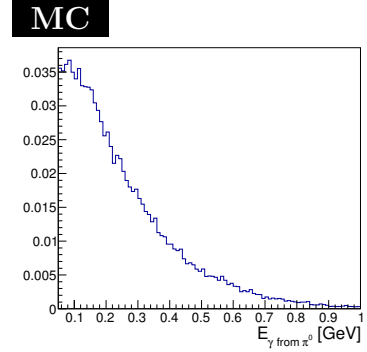


Figure 5.8: $E_{\gamma(\text{lab})}$ from π^0 distribution of perfectly reconstructed signal in signal region.

5.2.4 B reconstruction

Following conditions are required for B meson candidate: $-0.15 < \Delta E < 0.08$ [GeV] and $5.27 < M_{bc} < 5.29$ [GeV]. Here, ΔE and M_{bc} are defined as $\Delta E \equiv E_B - E_{\text{beam}}$ and $M_{bc} \equiv \sqrt{E_{\text{beam}}^2 - p_B^2}$ respectively.

5.3 Background suppression

Event numbers shown in this section is normalized to amount of real data. Normalization factor can be found at section 5.1.

5.3.1 Best candidate selection

If there are B candidates more than one, following steps are proceeded to select the best B candidate.

1. A candidate or candidates which have the smallest ΔM_η are selected.
2. A candidate which has smallest ΔM_{K_S} (for neutral mode) or better PID likelihood of charged K (for charged mode) is selected.

Here, PDG values are used for nominal mass; $M_\eta = 0.547853$ [GeV] and $M_{K_S} = 0.497614$ [GeV]. Since best γ , η and Kaon candidates are picked, single B candidate at most is selected per event.

Table 5.2: Number of signal candidate in signal region before/after Best candidate selection (BCS)

	$\eta \rightarrow 2\gamma$ mode			$\eta \rightarrow 3\pi$ mode		
	perfectly reconstructed	poorly reconstructed	misreconstructed	perfectly reconstructed	poorly reconstructed	misreconstructed
Before BCS	139.5	37.3	4.0	49.5	17.3	9.6
After BCS	103.7	19.6	2.3	37.8	7.9	3.2
efficiency	74.3%	52.5%	57.6%	76.4%	45.4%	33.6%

5.3.2 Veto of photons from π^0 η decay

Higher energy photon from $\pi^0 \rightarrow 2\gamma$ or $\eta \rightarrow 2\gamma$ decay tend to be misreconstructed as prompt photon candidate. In order to reduce these high energy gamma BG from π^0 or η decay, “ $\pi^0\eta$ veto” is carried out; it consists of following steps.

1. All lower energy gamma candidates are combined to higher energy gamma; π^0 or η candidates are reconstructed.
2. Probability of being π^0 or η child based on MC study (= “ π^0/η probability”) is calculated for each candidates with three information: reconstructed mass, energy and 3 hit region (front, barrel or end cap) of lower energy gamma.
3. Event will be discarded if it’s highest π^0 (η) probability more than 0.1 (0.2).

Table 5.3 to 5.6 show event numbers of BGs in the signal region and rejection efficiency of $\pi^0\eta$ veto to each BG. We can see that this veto is effective to qq , BB and rare B BG while not effective to radiative B BG. Signal efficiency of the veto is 81.3% and 79.6% for $\eta \rightarrow 2\gamma$ mode and $\eta \rightarrow 3\pi$ mode respectively.

Table 5.3: qq BG rejection with $\pi^0\eta$ veto

	$\eta \rightarrow 2\gamma$ mode			$\eta \rightarrow 3\pi$ mode		
	γ from π^0	γ from η	others	γ from π^0	γ from η	others
N_{qq}	5274.3	743.0	770.0	1138.0	173.8	171.8
N_{qq} with $\pi^0\eta$ veto	980.0	223.8	513.5	244.5	60.8	111.5
Fraction[%]	18.6	30.1	66.7	21.5	35.0	64.9

Table 5.4: BB BG rejection with $\pi^0\eta$ veto

	$\eta \rightarrow 2\gamma$ mode			$\eta \rightarrow 3\pi$ mode		
	γ from π^0	γ from η	others	γ from π^0	γ from η	others
N_{bb}	40.8	6.0	53.0	29.8	2.2	2.8
N_{bb} with $\pi^0\eta$ veto	11.8	3.5	39.0	6.3	1.3	2.5
Fraction[%]	29.0	58.3	73.6	21.2	61.5	88.2

Table 5.5: rare B BG rejection with $\pi^0\eta$ veto

	$\eta \rightarrow 2\gamma$ mode			$\eta \rightarrow 3\pi$ mode		
	γ from π^0	γ from η	others	γ from π^0	γ from η	others
N_{rare}	45.7	36.9	4.8	12.2	8.8	0.82
N_{rare} with $\pi^0\eta$ veto	7.2	11.3	3.4	2.8	4.5	0.56
Fraction[%]	15.8	30.5	70.6	23.1	50.7	68.3

Table 5.6: rad B BG rejection with $\pi^0\eta$ veto

	$\eta \rightarrow 2\gamma$ mode			$\eta \rightarrow 3\pi$ mode		
	γ from π^0	γ from η	others	γ from π^0	γ from η	others
N_{rad}	0.60	0.0	165.8	0	0	36.8
N_{rad} with $\pi^0\eta$ veto	0.18	0.0	127.5	0	0	27.5
Fraction[%]	29.2	-	76.9	-	-	74.7

5.3.3 NeuroBayes training for continuum suppression

MC signal and qq BG data are used for NB training to suppress continuum BG. 4 inputs are used for the training:

1. cosine of an angle between B momentum in c.m. system and z-axis ($\cos\theta_B$),
2. KSFW likelihood ratio (lr_ksfw),
3. cosine of an angle between 3rd sphericity axis of tracks from B_{rec} and B_{tag} (“v3_v3”) and
4. cosine of an angle between 1st sphericity axis of tracks from B_{tag} and z axis (“v1_z_oth”).

Distributions of these values of signal MC and qq BG MC are shown in Fig. 5.9 and 5.10. NB output distributions of signal and qq BG in fit region are shown in Fig. 5.11 and 5.12. Further description of these inputs and input candidates are written in following sections.

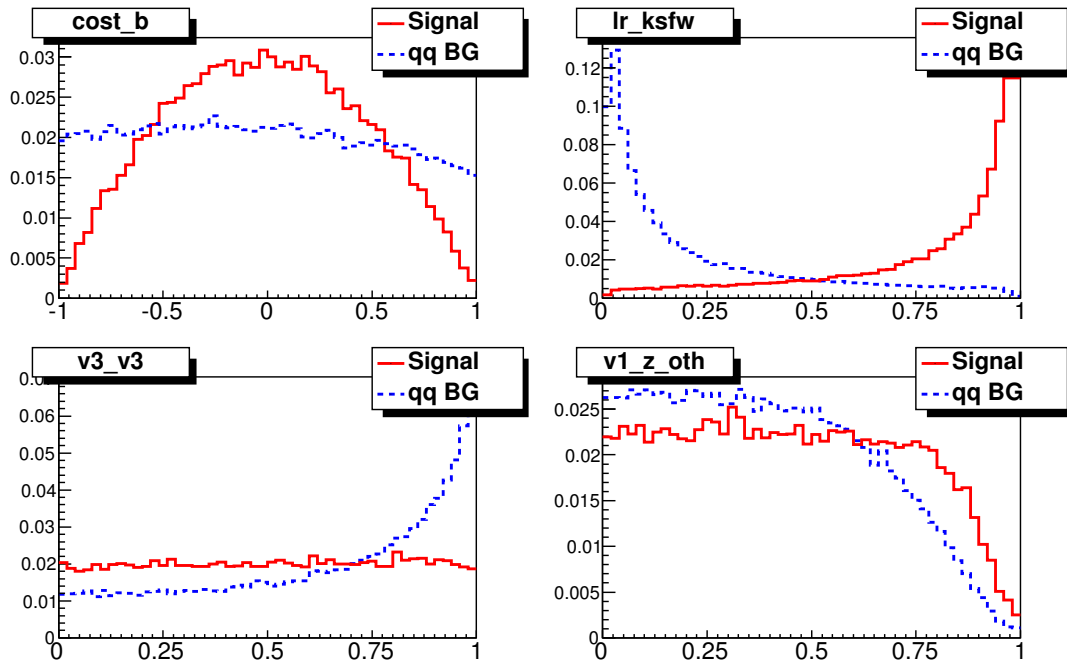


Figure 5.9: Distribution of 4 inputs for qq suppression ($\eta \rightarrow 2\gamma$ mode) Meaning of parameters are described in Tab.5.7.

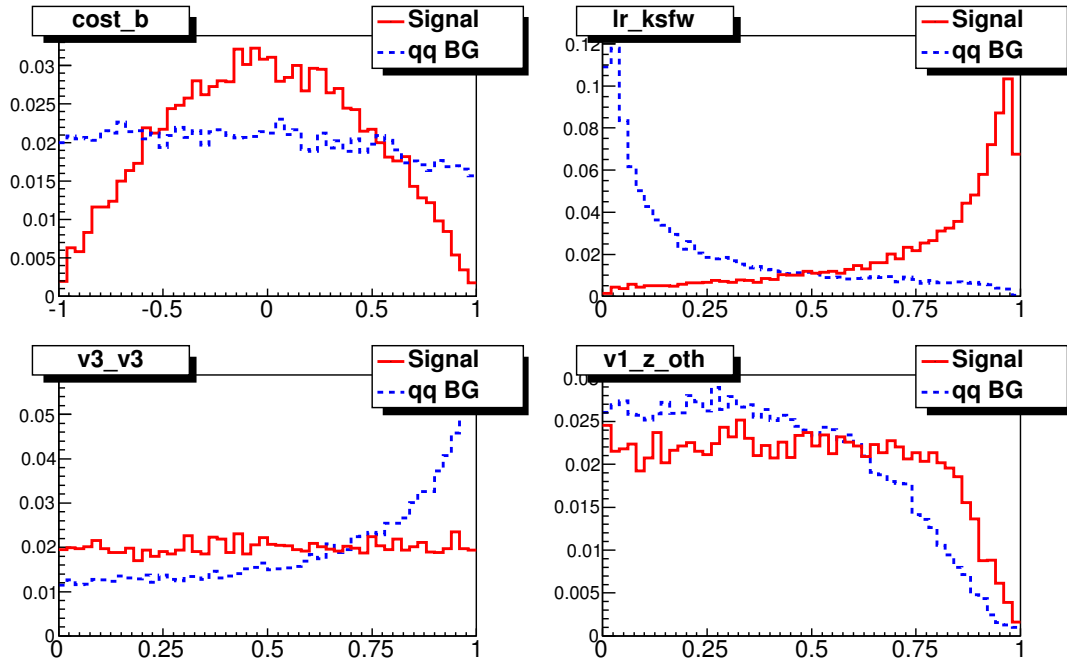


Figure 5.10: Distribution of 4 inputs for qq suppression ($\eta \rightarrow 3\pi$ mode)

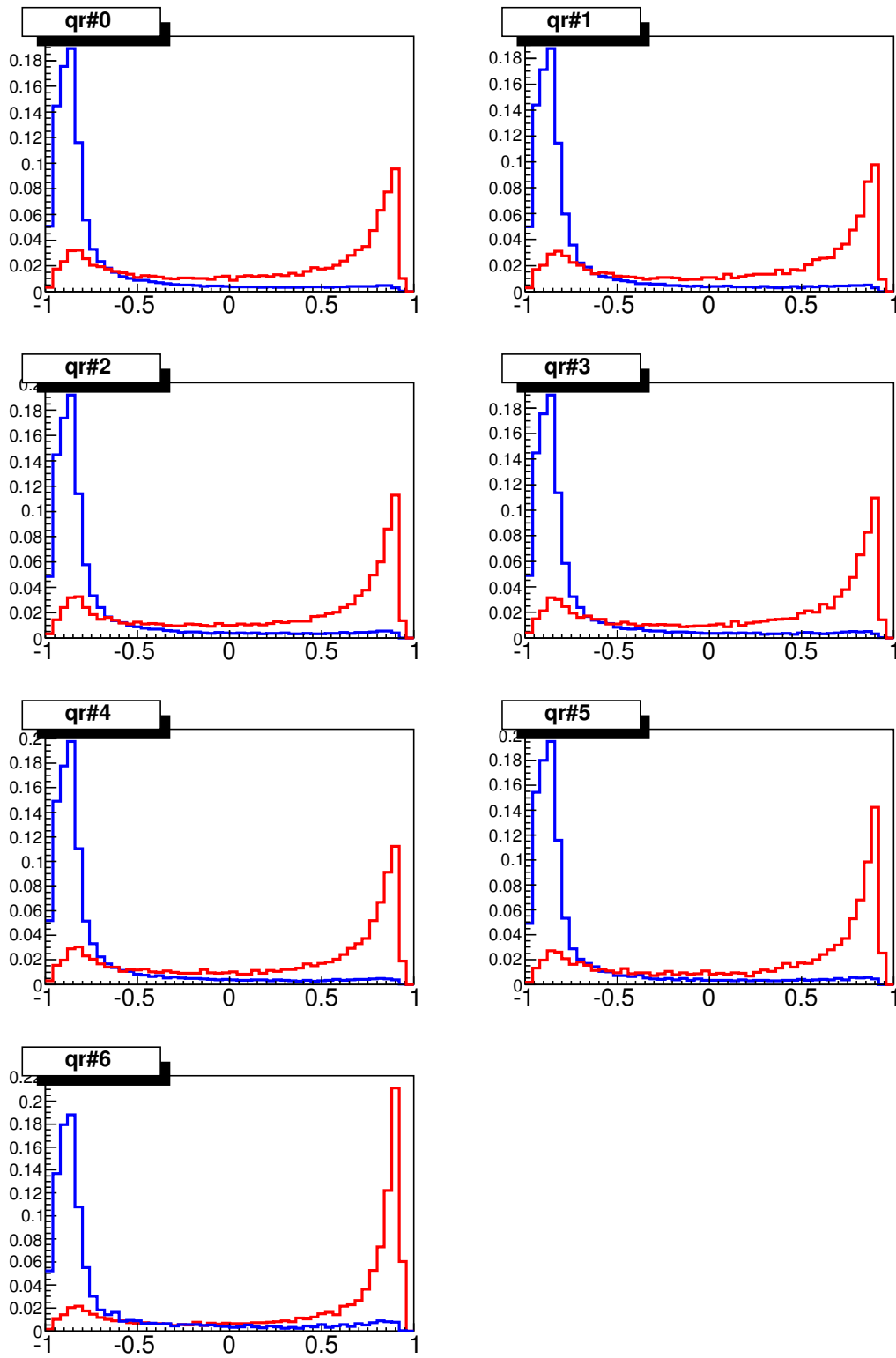


Figure 5.11: NB output distribution in fit region for each qr bin ($\eta \rightarrow 2\gamma$ mode)

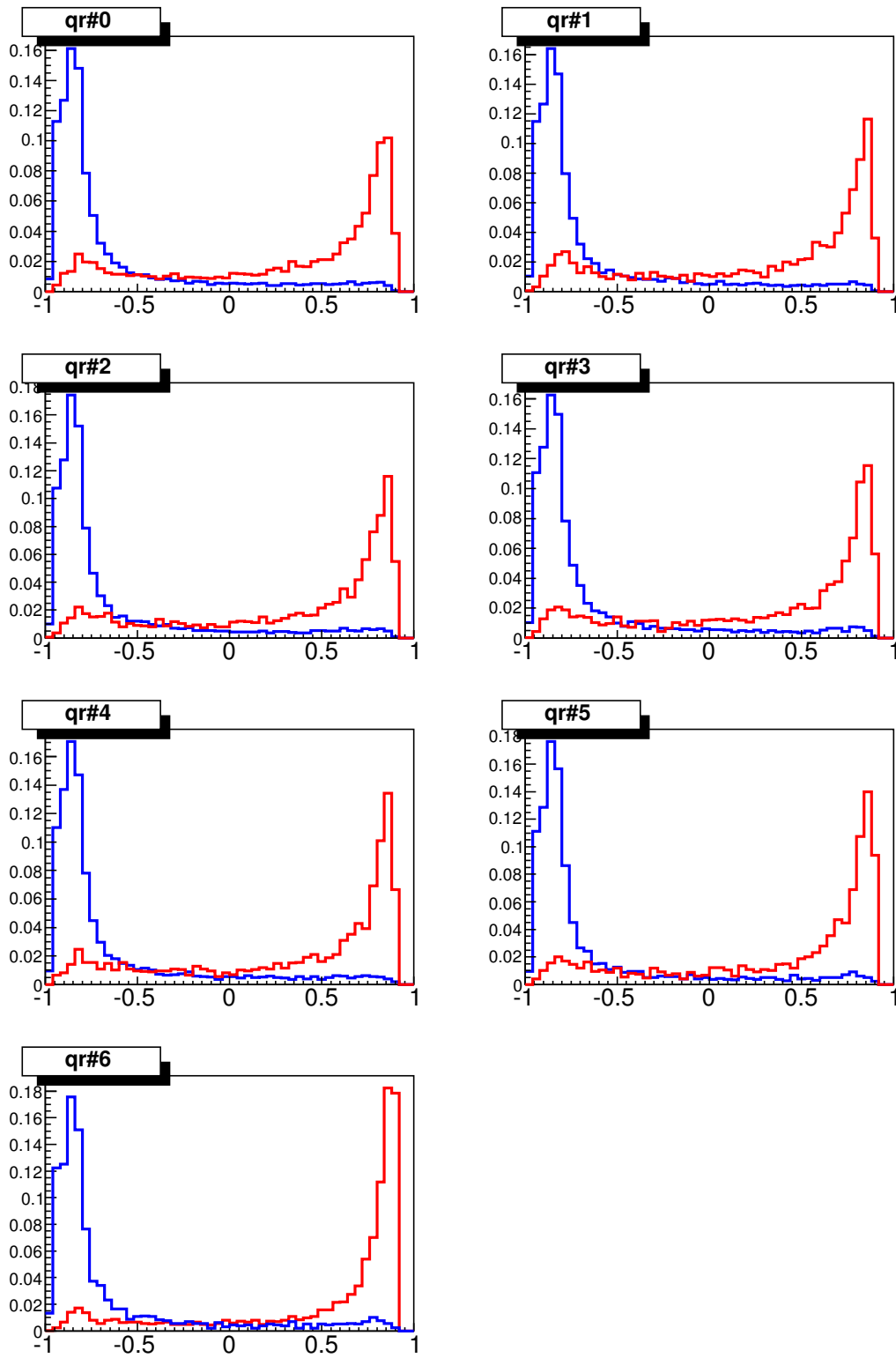


Figure 5.12: NB output distribution in fit region for each qr bin ($\eta \rightarrow 3\pi$ mode)

$\cos\theta_B$

θ_B is an angle between beam direction and momentum direction of B meson in center of mass system. B meson pair comes from $\Upsilon(4S)$ decay. Spin of $\Upsilon(4S)$ is 1, and its direction is parallel to z axis, since it is produced by electron and positron collision. Because there is no angular momentum in 2 body decay direction and B meson has no spin, spin component of decay direction is 0. Then, probability of decay direction taking θ_B is

$$|d_{1,0}^1|^2 = \frac{\sin^2\theta}{2} = \frac{1 - \cos^2\theta}{2} \quad (5.2)$$

On the other hand, if we wrongly reconstruct B from qq BG, $\cos\theta_B$ distribution becomes flat as there is no angular dependence.

lr_ksfw

Kakuno Super Fox-Wolfram moments (KSFW) based on Fox-Wolfram moments [14] is useful observable for separating signal and qq BG powerfully. “lr_ksfw” is likelihood ratio of KSFW; its distribution is fitted by Bifurcated Gaussian, and KSFW is defined as

$$\text{KSFW} \equiv \sum_i \sum_j \alpha_{ij} R_{ij}^{so} + \sum_i \beta_i R_i^{oo} + \gamma \sum_n |p_{T,n}|. \quad (5.3)$$

Since distribution of KSFW is depend on missing mass square, M_{miss}^2 , fitting and calculation of likelihood ratio is done for each seven M_{miss}^2 bins separately. M_{miss}^2 is defined as

$$\begin{aligned} M_{\text{miss}}^2 &\equiv \frac{E_{\text{miss}}}{|E_{\text{miss}}|} (E_{\text{miss}}^2 - \mathbf{p}_{\text{miss}}^2) \\ &= \frac{E_{\Upsilon(4S)} - \sum_n^{trk} E_n}{\left| E_{\Upsilon(4S)} - \sum_n^{trk} E_n \right|} \left\{ \left(E_{\Upsilon(4S)} - \sum_n^{trk} E_n \right)^2 - \left(\sum_n^{trk} (-\mathbf{p}_n) \right)^2 \right\}, \end{aligned} \quad (5.4)$$

using

$$\begin{aligned} P_{\text{miss}} &\equiv (E_{\text{miss}}, \mathbf{p}_{\text{miss}}) \\ &= (E_{\Upsilon(4S)}, 0, 0, 0) - \sum_n^{trk} (E_n, \mathbf{p}_n). \end{aligned} \quad (5.5)$$

Here, E_{beam} ($= 10.58/2$ GeV) and $E_{\Upsilon(4S)}$ ($= 10.58$ GeV) are beam energy and energy of $\Upsilon(4S)$ respectively. P_{miss} is missing momentum subtracted by all track's center of mass system momentum from momentum of $\Upsilon(4S)$. M_{miss}^2 bin are separated into 7 bins:

- $M_{\text{miss}}^2 < -0.5$ GeV (imm=0),

- $-0.5 < M_{\text{miss}}^2 < 0.3$ GeV (imm=1),
- $0.3 < M_{\text{miss}}^2 < 1.0$ GeV (imm=2),
- $1.0 < M_{\text{miss}}^2 < 2.0$ GeV (imm=3),
- $2.0 < M_{\text{miss}}^2 < 3.5$ GeV (imm=4),
- $3.5 < M_{\text{miss}}^2 < 6.0$ GeV (imm=5) and
- $6.0 < M_{\text{miss}}^2$ GeV (imm=6).

α_{ij} , β_i and γ are 11+5+1 parameter set for each M_{miss}^2 bin to separate distribution of signal and BG optimized by Fisher discriminant method.

Definition of R_{ij}^{so} in 1st term of eq.(5.3) is

$$R_{ij}^{so} = \begin{cases} \frac{1}{2(E_{\text{beam}} - \Delta E)} \sum_a^{\text{sig}} \sum_b^{\text{oth}_i} Q_a Q_b |\mathbf{p}_b| P_j(\cos\theta_{ab}) & (\text{if } j = 1, 3) \\ \frac{1}{2(E_{\text{beam}} - \Delta E)} \sum_a^{\text{sig}} \sum_b^{\text{oth}_i} |\mathbf{p}_b| P_j(\cos\theta_{ab}) & (\text{if } j = 0, 2, 4). \end{cases} \quad (5.6)$$

Here, “a” and “b” in the equation represent labels of signal-side track and other-side track respectively. So, Q_a means charge of track from signal-side track set, and Q_b means charge of track from other-side track set. $|\mathbf{p}_b|$ is magnitude of momentum of track from other-side track set. θ_{ab} is an angle between two tracks. Tracks of signal side are taken from B meson child (in this analysis, K_S , η , γ). V particles like K_S in other-side track set are taken as V particle from V particle candidate rather than two charged tracks, and remaining charged tracks are taken from charged track list and photon tracks are taken from photon candidate list. Other-side tracks are separated into 3 groups with a label “i”: “oth₀” is the set of other-side charged tracks, “oth₁” is the set of other-side neutral tracks and “oth₂” is missing momentum, P_{miss} , as shown in eq.(5.5). $P_j(x)$ is Legendre polynomial defined as

$$P_n(x) = \frac{1}{2^n n!} \frac{d^n}{dx^n} [(x^2 - 1)^n]. \quad (5.7)$$

Writing concretely, first five polynomials can be written as

$$P_0(x) = 1, \quad (5.8)$$

$$P_1(x) = x, \quad (5.9)$$

$$P_2(x) = \frac{1}{2}(3x^2 - 1), \quad (5.10)$$

$$P_3(x) = \frac{1}{2}(5x^3 - 3x) \quad \text{and} \quad (5.11)$$

$$P_4(x) = \frac{1}{8}(35x^4 - 30x^2 + 3). \quad (5.12)$$

R_{11}^{so} , R_{13}^{so} , R_{21}^{so} and R_{23}^{so} are meaningless because $Q_b = 0$. Then, 11 combination of i and j , R_{00} , R_{01} , R_{02} , R_{03} , R_{04} , R_{10} , R_{12} , R_{13} , R_{20} , R_{22} and R_{23} are used. However, because all of

child particles in this analysis (K_S, η, γ) are neutral, R_{01}^{so} and R_{03}^{so} becomes always zero. If we set R_{01}^{so} and R_{03}^{so} to zero, same KSFW distributions can be obtained with charged sample of $B^+ \rightarrow K^+ \eta \gamma$ mode. It is useful to check qq suppression performance or other performance check, we do not use these two measurements.

Definition of R_i^{oo} in 2nd term of eq.(5.3) is

$$R_i^{oo} = \begin{cases} \frac{1}{4(E_{\text{beam}} - \Delta E)^2} \sum_a^{\text{oth}} \sum_b^{\text{oth}} Q_a Q_b |\mathbf{p}_a| |\mathbf{p}_b| P_i(\cos\theta_{ab}) & (\text{if } i = 1, 3) \\ \frac{1}{4(E_{\text{beam}} - \Delta E)^2} \sum_a^{\text{oth}} \sum_b^{\text{oth}} |\mathbf{p}_a| |\mathbf{p}_b| P_i(\cos\theta_{ab}) & (\text{if } i = 0, 2, 4). \end{cases} \quad (5.13)$$

Here, definition of values are same as 1st term, but other-side track set is not separated into some groups like R_{ij}^{so} .

3rd term means scalar sum of transverse momentum of all tracks.

Figure 5.13 and 5.14 show KSFW distribution for each M_{miss}^2 bin.

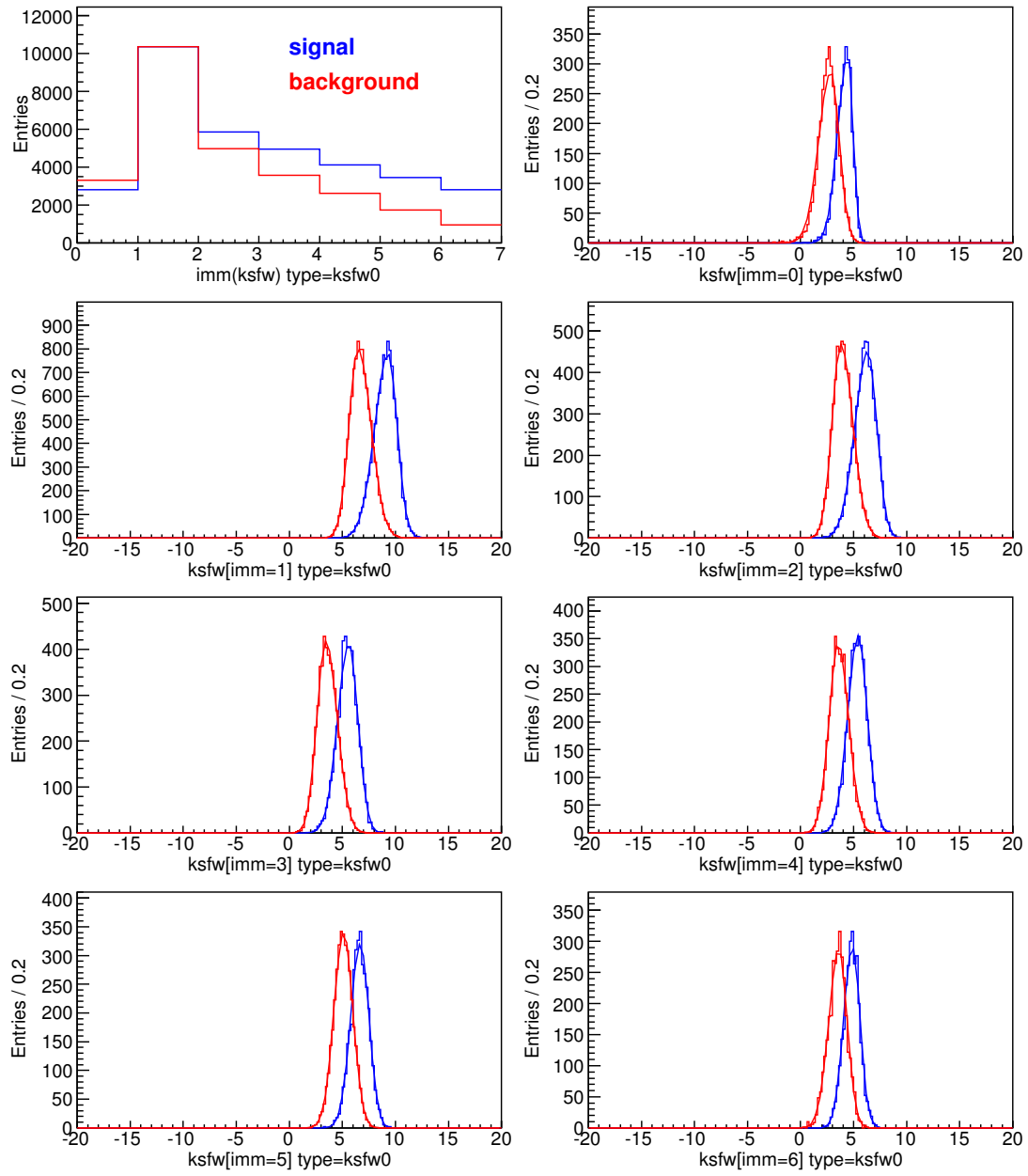


Figure 5.13: KSW distribution for each M_{miss}^2 bin ($\eta \rightarrow 2\gamma$ mode)

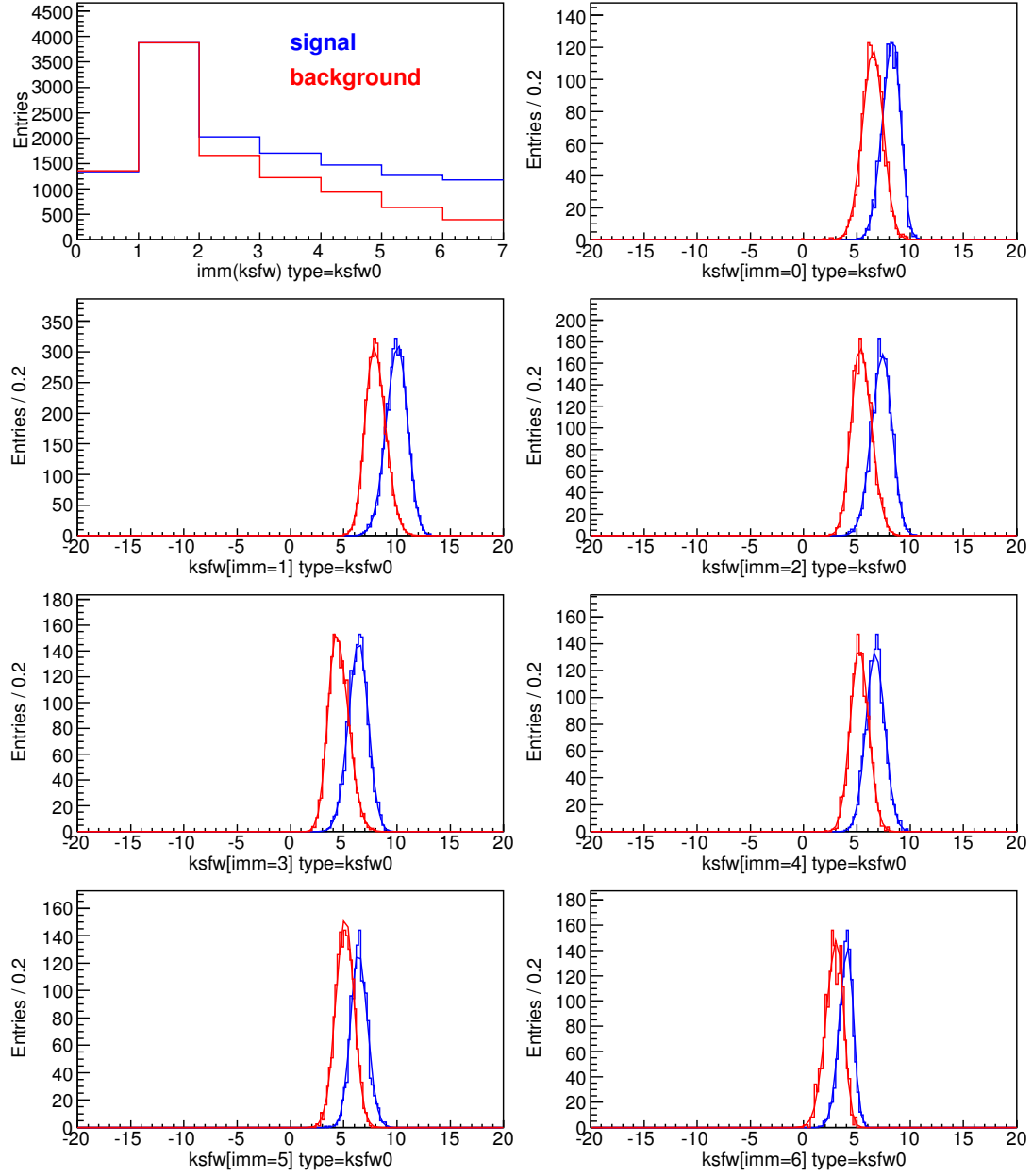


Figure 5.14: KSW distribution for each M_{miss}^2 bin ($\eta \rightarrow 3\pi$ mode)

R_2

R_2 is reduced Fox-Wolfram moment and defined as

$$R_2 = \frac{\sum_{i,j}^{\text{trk}} |p_i||p_j| P_2(\cos\theta_{ij})}{\sum_{i,j}^{\text{trk}} |p_i||p_j|}. \quad (5.14)$$

Here, $P_2(x)$ is Legendre polynomial as shown in eq.(5.7).

Sphericity vector

Sphericity tensor is 3×3 matrix, and its elements are described as

$$S_{\alpha\beta} = \frac{\sum_i^{\text{trk}} p_{i,\alpha} p_{i,\beta}}{\sum_i^{\text{trk}} |\mathbf{p}_i|^2}. \quad (5.15)$$

Here, $p_{i,\alpha}$ and $p_{i,\beta}$ are x , y or z component of momentum of i th track in center of mass system. Tracks are collected from charged track list and photon candidate list. Sphericity tensor has real positive three eigen values which satisfies that

$$\lambda_1 + \lambda_2 + \lambda_3 = 1. \quad (5.16)$$

Here, we define their label as they satisfy

$$\lambda_1 \geq \lambda_2 \geq \lambda_3. \quad (5.17)$$

These eigen values describe how the decay is spherical, flat or 2 jet like. Corresponding eigen vector to the eigen value is called 1st, 2nd or 3rd sphericity vector. Sphericity is defined as $S = \frac{3}{2}(1 - \lambda_1)$. From the definition of λ , a condition $0 \leq S \leq 1$ is derived. The more a decay shape be spherical, the more S becomes larger. Aplanarity is defined as $A = \frac{3}{2}\lambda_3$. From the definition of λ , a condition $0 \leq A \leq 1/2$ is derived. A of a plane decay shape likely to be 0, and one of a spherical decay shape tend to be 1/2.

To obtain eigen value of 3×3 matrix, we have to solve cubic equation. Thanks to the feature of this matrix, eigen values can be obtained easily and are always positive real number. Condition of matrix having eigen value λ is

$$\det [S - \lambda I] = 0. \quad (5.18)$$

Here, S is sphericity tensor, and I is 3×3 unit matrix. Because sphericity tensor satisfies that

$$S_{11} + S_{22} + S_{33} = \frac{\sum_i p_{i,x}^2 + \sum_i p_{i,y}^2 + \sum_i p_{i,z}^2}{\sum_i (p_{i,x}^2 + p_{i,y}^2 + p_{i,z}^2)} = 1 \quad (5.19)$$

and

$$S_{\alpha\beta} = S_{\beta\alpha}, \quad (5.20)$$

equation (5.18) becomes

$$\begin{aligned} & - \left\{ \lambda^3 - \lambda^2 + (S_{11}S_{22} + S_{22}S_{33} + S_{33}S_{11} - S_{12}^2 - S_{23}^2 - S_{31}^2)\lambda \right. \\ & \left. + (S_{11}S_{23}^2 + S_{22}S_{31}^2 + S_{33}S_{12}^2 - S_{11}S_{22}S_{33} - 2S_{12}S_{23}S_{31}) \right\} = 0. \end{aligned} \quad (5.21)$$

The cubic formula for $x^3 + ax^2 + bx + c = 0$ can be written as

$$\begin{cases} x_1 = -\frac{a}{3} + A_+ + A_- \\ x_2 = -\frac{a}{3} + \frac{-1 + \sqrt{3}i}{2}A_+ + \frac{-1 - \sqrt{3}i}{2}A_- \\ x_3 = -\frac{a}{3} + \frac{-1 - \sqrt{3}i}{2}A_+ + \frac{-1 + \sqrt{3}i}{2}A_- \end{cases} \quad (5.22)$$

using

$$A_{\pm} = \sqrt[3]{-q \pm \sqrt{q^2 + p^3}}, \quad (5.23)$$

$$q = \frac{c}{2} + \frac{a^3}{27} - \frac{ab}{6} \quad \text{and} \quad (5.24)$$

$$p = \frac{b}{3} - \frac{a^2}{9}. \quad (5.25)$$

Here, sphericity tensor always satisfy

$$q^2 + p^3 \leq 0. \quad (5.26)$$

Thanks to this condition, we can describe solutions more simply. If we define A_{\pm}^3 as

$$A_{\pm}^3 = re^{i\theta} = -q \pm \sqrt{q^2 + p^3}, \quad (5.27)$$

and considering eq.(5.26), (i.e. $p \leq 0$ and $|q^2| \leq |p^3|$), r and θ can be written as

$$r = \sqrt{q^2 + (-q^2 - p^3)} = \sqrt{-p^3} \quad \text{and} \quad (5.28)$$

$$\theta = \pm \arccos \left(\frac{-q}{\sqrt{-p^3}} \right). \quad (5.29)$$

Then,

$$\begin{aligned} A_{\pm} &= r^{1/3} e^{i\theta/3} = \sqrt{-p} \exp \left[\pm \frac{i}{3} \arccos \left(\frac{-q}{\sqrt{-p^3}} \right) \right] \\ &= R \pm i I \end{aligned} \quad (5.30)$$

Here,

$$R = \sqrt{-p} \cos \left[\frac{1}{3} \arccos \frac{-q}{\sqrt{-p^3}} \right] \text{ and} \quad (5.31)$$

$$I = \sqrt{-p} \sin \left[\frac{1}{3} \arccos \frac{-q}{\sqrt{-p^3}} \right]. \quad (5.32)$$

Substituting $a = -1$ and eq.(5.30) to eq.(5.22), we obtain

$$x_1 = \frac{1}{3} + 2R, \quad (5.33)$$

$$x_2 = \frac{1}{3} - R - \sqrt{3} I \text{ and} \quad (5.34)$$

$$x_3 = \frac{1}{3} - R + \sqrt{3} I \quad (5.35)$$

as solutions.

Thrust vector

An unit vector \mathbf{n} which maximizes

$$T = \frac{\sum_i^{\text{trk}} |\mathbf{n} \cdot \mathbf{p}_i|}{\sum_i^{\text{trk}} |\mathbf{p}_i|} \quad (5.36)$$

is called thrust vector, and this maximized value T is called thrust. Here, \mathbf{p}_i is momentum vector of i th track in center of mass system. Tracks are collected from charged track list and photon candidate list. Thrust vector indicates decay shape's direction. The vector's concept is roughly same to 1st sphericity vector, however, there is differences in summation term whether summation is taken as 1st power of momentum or 2nd power of one.

Correlation of these input values

We tested many values as you can see in Fig.5.15 to 5.18. Tested values are summarized on table 5.7. We avoided to use R_2 , sphericity, aplanarity and thrust because they are strongly correlated with ΔE , M_{bc} or $M_{K\eta}$. Some values which do not contribute to improvement of NB output (like "v1_v1") are not used. This is because they are highly correlated to "lr_ksfw".

Table 5.7: Meaning of variables in Fig.5.15 to 5.18

		meaning
o	cost_b	cosine of an angle between B momentum and z-axis
o	lr_ksfw	KSFW likelihood ratio
-	th_z_all	cosine of an angle between thrust vector of all tracks and z axis
-	thru_all	thrust of all tracks
-	R_2	reduced Fox-Wolfram moment
-	sphe_all	sphericity of all tracks
-	apla_all	aplanarity of all tracks
-	v1_z_all	cosine of an angle between 1st sphericity axis of tracks and z axis
o	v1_z_oth	cosine of an angle between 1st sphericity axis of B_{tag} tracks and z axis
-	v1_v1	cosine of an angle between 1st sphericity axis of B_{rec} tracks and B_{tag} tracks
-	v2_v2	cosine of an angle between 2nd sphericity axis of B_{rec} tracks and B_{tag} tracks
o	v3_v3	cosine of an angle between 3rd sphericity axis of B_{rec} tracks and B_{tag} tracks
-	thrust_a	cosine of an angle between thrust vector of B_{rec} tracks and B_{tag} tracks

Event set used for training

We used MC events as training sample data for $7 \times (11 + 5 + 1)$ coefficients of Fisher discriminant $[\alpha_{ij}, \beta_i, \gamma]_{\text{imm}}$ and neural network. 34,397 and 12,882 events of “perfectly reconstructed signal” in signal region and 63,774 and 19,106 events of qq BG in fit region (corresponds to 3 streams of the MC data) are used for training of $\eta \rightarrow 2\gamma$ decay mode and $\eta \rightarrow 3\pi$ mode, respectively. Signal MC data is additionally generated for the training.

5.3.4 Peaking background and well known CPV background veto

Some BGs from other B meson decay mode make peak in ΔE or M_{bc} distribution. Even if an amount of BG is small, BG which has CP asymmetry is seriously affects CPV measurement which is suppressed in the SM. Then, we studied such BGs expected decay mode and rejection strategy using BB , rare B and rad B BG MC data.

We found that $B \rightarrow \eta + \text{something}$ and $B \rightarrow K_S + \text{something}$ rare decay modes are one of major BG of non-radiative rare decay and can be rejected with a slight loss of signal events. Figure 5.19 and 5.20 shows $M_{\gamma K_S}$ distribution of $B \rightarrow \eta + \text{something}$ and $M_{\gamma\eta}$ distribution of $B \rightarrow K_S + \text{something}$ BG. These BGs can be removed by applying cuts on $2 [\text{GeV}] < M_{\gamma K}$ and $2 [\text{GeV}] < M_{\gamma\eta}$.

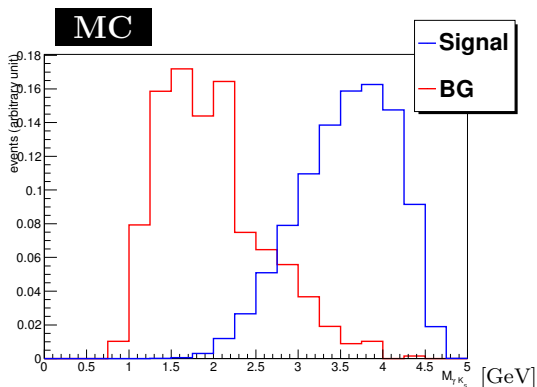


Figure 5.19: $M_{\gamma K_S}$ distributions of signal and $B \rightarrow \eta + \text{something}$ BG

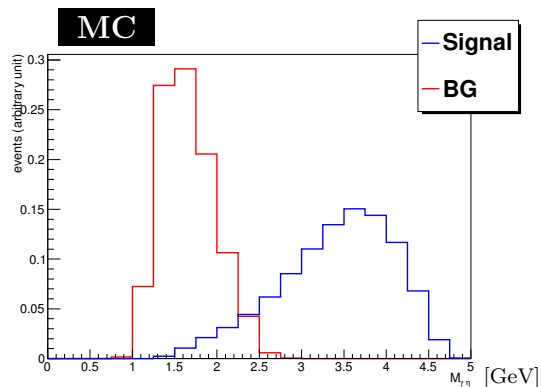


Figure 5.20: $M_{\gamma\eta}$ distributions of signal and $B \rightarrow K_S + \text{something}$ BG

We found that $B^0 \rightarrow D^0\eta/\pi^0$ and $B^0 \rightarrow J/\psi K_S$ becomes major peaking BG, which have CP asymmetry. There are 3 ways to become signal candidate for these BGs.

$B^0 \rightarrow D^0(\rightarrow K_S \eta/\pi^0)\eta$ mode

If a higher energy photon from η/π^0 which is D^0 's daughter, these final state but a slow photon can be reconstructed as $B \rightarrow K_S\eta\gamma$ mode. This event makes a peak on $K_S\eta$ invariant mass around M_{D^0} . This BG can also be rejected by $2[\text{GeV}] < M_{\gamma K}$ selection.

$B^0 \rightarrow D^0(\rightarrow K_S \eta)\eta/\pi^0(\rightarrow 2\gamma)$ mode

If a higher energy photon from η/π^0 which is B^0 's daughter, these final state but a slow photon can be reconstructed as $B \rightarrow K_S\eta\gamma$ mode. This event makes a peak on $K_S\eta$ invariant mass around M_{D^0} . Figure 5.21 and 5.22 show the distributions of high statistical exclusive MC data. Veto of $1.82 < M_{K\eta} < 1.90$ region rejects 70% of $D^0(\rightarrow K_S\eta)\eta$ BG and 81% $D^0(\rightarrow K_S\eta)\pi^0$ BG respectively.

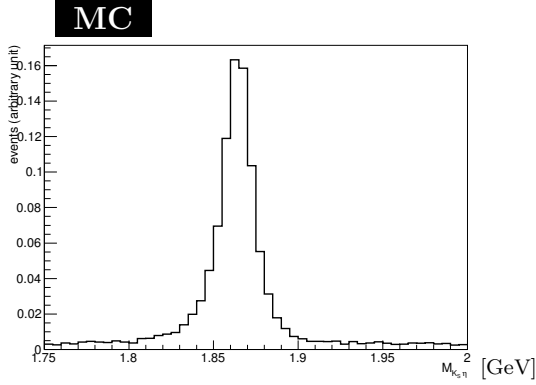


Figure 5.21: $M_{K_S\eta}$ distribution of $B \rightarrow D^0(\rightarrow K_S\eta)\eta$ BG

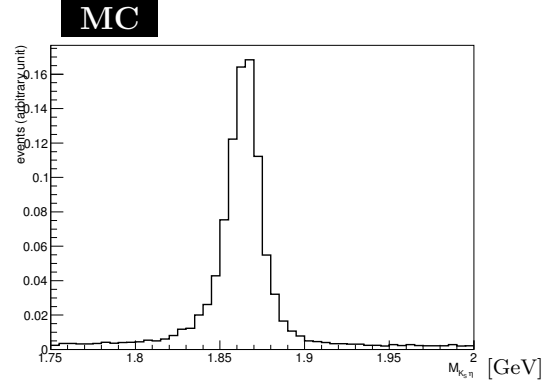


Figure 5.22: $M_{K_S\eta}$ distribution of $B \rightarrow D^0(\rightarrow K_S\eta)\pi^0$ BG

$B^0 \rightarrow J/\psi K_S$ mode

If J/ψ decays to $\gamma\eta$, these final state cannot be distinguished with $B \rightarrow K_S\eta\gamma$ mode. This event makes a peak on $\gamma\eta$ invariant mass around J/ψ . Figure 5.23 shows the distribution of high statistical exclusive MC data. Veto of $2.9 < M_{\gamma\eta} < 3.2$ [GeV] rejects 98% of $J/\psi(\rightarrow \gamma\eta)K_S$ BG.

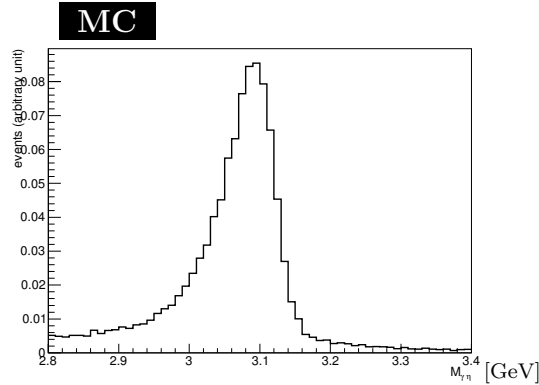


Figure 5.23: $M_{\gamma\eta}$ distribution of $B \rightarrow J/\psi(\rightarrow \gamma\eta)K_S$ BG

$B^0 \rightarrow D^{0*}\eta/\pi^0, B^0 \rightarrow J/\psi K^*$ mode?

Why don't we see peaking BG of $B^0 \rightarrow D^{0*}\eta/\pi^0$ or $B^0 \rightarrow J/\psi K^*$ modes while $B^0 \rightarrow D^0\eta/\pi^0, B^0 \rightarrow J/\psi K_S$ modes appear as peaking BG? This is because emitted pion or

photon from D^* or K^* takes energy; their distributions on ΔE are much lower than signal peak. Then, these modes are not so harmful for us.

Considering these conditions above, we applied following cuts to remove BG from B decay.

- $2[\text{GeV}] < M_{\gamma K}$
- $2[\text{GeV}] < M_{\gamma\eta} < 2.9[\text{GeV}]$ or $3.2[\text{GeV}] < M_{\gamma\eta}$
- $M_{K\eta} < 1.82[\text{GeV}]$ or $1.9[\text{GeV}] < M_{K\eta}$

5.3.5 $B \rightarrow K\pi^0\gamma$ veto

After B BG veto, still $B \rightarrow K\pi^0\gamma$ events are remaining; we rejected events which have $B \rightarrow K\pi^0\gamma$ candidate. Reconstruction conditions are shown below.

- $0.12 < M_{\pi^0} < 0.15$ [GeV]
- $1.6 < E_\gamma(\text{CM sys.}) < 3.4$ [GeV]
- $-0.20 < \Delta E < 0.10$ [GeV]
- $5.27 < M_{bc}$ [GeV]

5.3.6 Helicity angle and $M_{K\eta}$ cut

In order to explain definition of helicity angle and relationship to spin, we call $K\eta$ system as X_s . Helicity angle, θ_{hel} , is an angle between opposite direction of momentum of B in X_s system (= X_s 's motion direction in X_s 's system) and momentum of K_S in X_s system. X_s is not a spin 0 particle because X_s is generated with spin 1 photon from two body decay of spin 0 B meson. X_s has at least spin 1 component in this decay direction. Then, this non-zero spin particle decays to two spin 0 particle. Spin component of this decay direction is 0 as there's no angular momentum in the direction. Here, if we take z and n axis for X_s 's momentum direction and its decay direction, and assuming that X_s 's net spin is j , probability amplitude of taking θ_{hel} is proportional to

$$d_{1,0}^j(\theta_{\text{hel}}) = {}_z\langle j, 1|j, 0\rangle_n. \quad (5.37)$$

Assuming that $j = 1$ or $j = 2$, probability distribution of taking θ_{hel} become

$$|d_{1,0}^1(\theta_{\text{hel}})|^2 = \frac{1 - \cos^2\theta_{\text{hel}}}{2} \quad \text{and} \quad (5.38)$$

$$|d_{1,0}^2(\theta_{\text{hel}})|^2 = \frac{3}{2} (1 - \cos^2\theta_{\text{hel}}) \cos^2\theta_{\text{hel}}, \quad (5.39)$$

respectively.

We measured $\cos\theta_{\text{hel}}$ distribution of charged event and found that net spin of X_s is 1. We also measured $M_{K\eta}$ distribution of charged event and found that we cannot expect

many events at high $M_{K\eta}$ region. Detail of the measurements are described in Chapter 6, and their distributions can be seen at Fig.6.10 to 6.13.

Because of isospin symmetry, $M_{K\eta}$ and helicity angle distribution of $B^0 \rightarrow K_S\eta\gamma$ and $B^+ \rightarrow K^+\eta\gamma$ should be same. Figure 5.24 to 5.27 show background distribution of cosine of helicity angle and $M_{K\eta}$ estimated by MC. BG distributions are normalized to Belle's luminosity. Then, in order to maximize significance, we apply cuts on these values: $-0.7 < \cos\theta_{\text{hel}} < 0.9$ and $M_{K\eta} < 2.1$ GeV.

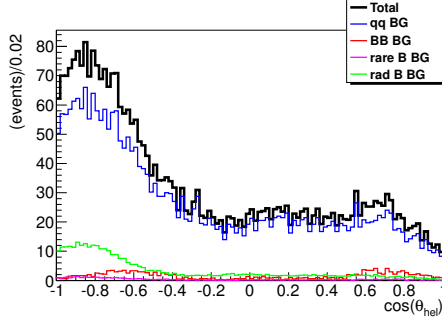


Figure 5.24: $\cos\theta_{\text{hel}}$ distribution of BG ($\eta \rightarrow 2\gamma$ mode)

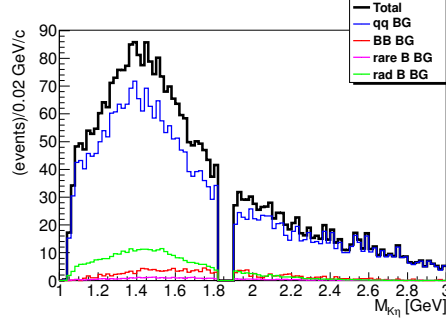


Figure 5.25: $M_{K\eta}$ distribution of BG ($\eta \rightarrow 2\gamma$ mode)

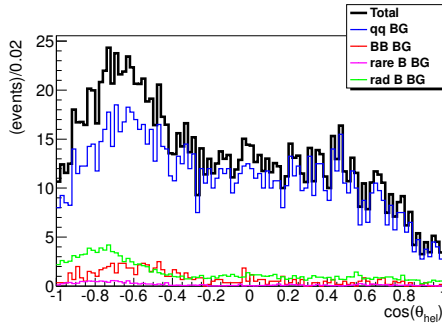


Figure 5.26: $\cos\theta_{\text{hel}}$ distribution of BG ($\eta \rightarrow 3\pi$ mode)

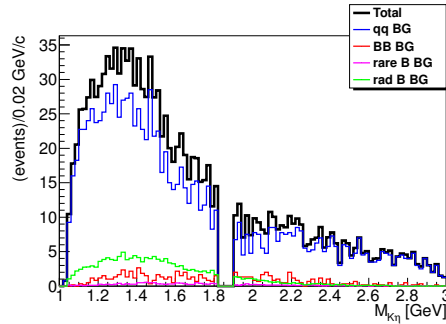


Figure 5.27: $M_{K\eta}$ distribution of BG ($\eta \rightarrow 3\pi$ mode)

5.3.7 Summary

Table 5.9 to 5.12 summarizes transition of signal and background amounts in signal box. Although NeuroBayes output is used for fit parameters, cut are applied for the table in order to show significance improvement. Threshold of the NeuroBayes output is listed on Table.5.8. Lowest threshold is -0.7 and cut at the value will be applied before 3D fit. Efficiency was obtained just divided by generated amount; no M_{X_s} correlation was considered.

Definition of efficiency ϵ in the tables are

$$\epsilon = \frac{(\text{reconstructed events})}{(\text{All } K\eta\gamma \text{ decay})} \quad (5.40)$$

Because catchable neutral kaon is one third of K^0 , $K^0 \rightarrow K_S(\sim 50\%) \rightarrow \pi^+\pi^-(\sim 70\%)$, ϵ of neutral mode is more than 3 times smaller than charged mode.

Significances in the tables are calculated from quadratic sum $\left(\sqrt{\sum x^2}\right)$ of significances of each 7 flavor tagging quality bins. From this MC study, we expect that $B^0 \rightarrow K_S\eta\gamma$ event can be seen more than 5 sigma level.

Figure 5.29 to 5.39 are showing ΔE and M_{bc} projection distributions after each cut. Signal MC contains both perfectly reconstructed and poorly reconstructed signals. Signal region cut on M_{bc} ($5.27 < M_{bc} < 5.29$ GeV/c) is applied for ΔE projection, and signal region cut on ΔE ($-0.15 < \Delta E < 0.08$ GeV) is applied for M_{bc} projection. Red line shows just after selection. Green line shows after BCS. Blue line shows after $\pi^0\eta$ veto. Magenta line shows after qq suppression. Purple line shows after $\cos\theta_{\text{hel}}$ cut. Black filled line shows after $M_{K\eta}$ cut.

Table 5.8: NeuroBayes output threshold for Table.5.9 to 5.12

qr bin #	$\eta \rightarrow 2\gamma$	$\eta \rightarrow 3\pi$
qr #0	-0.3	0.1
qr #1	-0.1	0.3
qr #2	-0.6	0.2
qr #3	-0.2	0.2
qr #4	0.1	0.3
qr #5	-0.1	-0.1
qr #6	-0.7	-0.2

Table 5.9: Transition of expected signal/BG numbers, efficiency and significance in signal box (neutral $\eta \rightarrow 2\gamma$ mode). Detail of perfectly reconstructed and poorly reconstructed signal are described in the “signal” column. Detail of major radiative BGs are also described in the “rad B” column.

$K_S\eta(\rightarrow \gamma\gamma)\gamma$ mode	Signal (perfect/poor)	qq BG	BB BG	rare B BG	rad B BG ($K_S\eta\gamma/K^\pm\eta\gamma/K_S\pi^0\gamma$)	efficiency	S
Reconstruction	176.7 (139.5/37.3)	11454.0	186.2	150.7	283.8 (4.0/1.3/159.6)	-	-
BCS	123.2 (103.7/19.6)	6787.3	99.8	87.4	169.7 (2.3/0.9/96.7)	2.1%	1.9
$\pi^0\eta$ veto	100.2 (84.3/15.9)	1717.3	54.3	21.8	130.3 (1.9/0.7/75.0)	1.7%	2.7
qq BG suppression	80.3 (68.1/12.3)	144.0	22.0	13.6	84.5 (1.4/0.5/51.0)	1.3%	4.5
CPV BG veto	68.7 (58.4/10.3)	68.8	7.3	4.9	56.4 (1.2/0.4/36.7)	1.1%	4.9
$K\pi^0\gamma$ veto	66.7 (56.9/9.9)	55.8	6.3	4.1	27.2 (1.1/0.4/11.1)	1.1%	5.4
helicity angle cut	62.5 (53.5/9.0)	32.5	4.8	2.8	14.2 (1.1/0.3/6.1)	1.0%	5.9
$M_{K\eta}$ cut	61.1 (52.3/8.8)	24.8	2.8	1.6	13.3 (1.1/0.3/5.7)	1.0%	6.1

Table 5.10: Transition of expected signal/BG numbers, efficiency and significance in signal box (neutral $\eta \rightarrow 3\pi$ mode).

$K_S\eta(\rightarrow \pi^+\pi^-\pi^0)\gamma$ mode	Signal (perfect/poor)	qq BG	BB BG	rare B BG	rad B BG ($K_S\eta\gamma/K^\pm\eta\gamma/K_S\pi^0\gamma$)	efficiency	S
Reconstruction	66.8 (49.5/17.3)	2760.3	77.5	47.6	90.3 (9.6/0.5/14.3)	-	-
BCS	45.7 (37.8/7.9)	1483.5	34.8	21.9	40.4 (3.2/0.4/5.9)	0.77%	1.5
$\pi^0\eta$ veto	36.4 (30.1/6.2)	416.8	10.2	7.9	30.3 (2.5/0.3/4.5)	0.61%	2.0
qq BG suppression	26.7 (22.5/4.3)	21.0	3.7	4.0	14.9 (1.4/0.2/1.8)	0.45%	3.3
CPV BG veto	23.3 (19.7/3.6)	15.5	0.5	1.5	9.9 (1.1/0.1/0.8)	0.39%	3.4
$K\pi^0\gamma$ veto	23.2 (19.7/3.6)	14.8	0.5	1.5	9.4 (1.1/0.1/0.5)	0.39%	3.4
helicity angle cut	22.5 (19.1/3.3)	11.0	0.5	1.2	6.3 (0.9/0.1/0.2)	0.38%	3.6
$M_{K\eta}$ cut	22.0 (18.7/3.3)	9.0	0.0	0.7	6.1 (0.9/0.1/0.2)	0.37%	3.6

Table 5.11: Transition of expected signal/BG numbers, efficiency and significance in signal box (charged $\eta \rightarrow 2\gamma$ mode)

$K^\pm \eta (\rightarrow \gamma\gamma)\gamma$ mode	Signal (perfect/poor)	qq BG	BB BG	rare B BG	rad B BG ($K^\pm \eta \gamma / K_S \eta \gamma / K^\pm \pi^0 \gamma$)	efficiency	S
Reconstruction	603.3 (480.4/122.9)	95566.5	780.5	731.4	995.1 (7.0/10.3/538.0)	-	-
BCS	434.3 (366.3/ 68.0)	56959.0	359.8	422.4	603.3 (2.9/7.4/332.4)	7.3%	2.7
$\pi^0 \eta$ veto	352.5 (297.4/ 55.1)	14320.2	195.2	104.0	459.4 (2.3/5.8/254.1)	5.9%	3.9
qq BG suppression	281.5 (239.2/ 42.3)	1090.8	74.2	65.0	298.4 (1.5/3.9/175.5)	4.7%	7.3
CPV BG veto	242.6 (206.8/ 35.8)	616.8	23.8	25.0	203.2 (1.1/3.3/128.7)	4.1%	7.9
$K \pi^0 \gamma$ veto	235.9 (201.5/ 34.4)	512.3	22.3	20.7	103.3 (1.1/3.3/ 41.3)	3.9%	8.5
helicity angle cut	221.4 (189.8/ 31.6)	316.5	15.2	15.2	55.6 (1.0/3.1/ 22.0)	3.7%	9.4
$M_{K\eta}$ cut	216.7 (185.9/ 30.9)	249.3	10.7	9.3	52.0 (1.1/3.0/ 20.8)	3.6%	9.8

 Table 5.12: Transition of expected signal/BG numbers, efficiency and significance in signal box (charged $\eta \rightarrow 3\pi$ mode)

$K^\pm \eta (\rightarrow \pi^+ \pi^- \pi^0)\gamma$ mode	Signal (perfect/poor)	qq BG	BB BG	rare B BG	rad B BG ($K^\pm \eta \gamma / K_S \eta \gamma / K^\pm \pi^0 \gamma$)	efficiency	S
Reconstruction	239.5 (179.2/60.3)	20062.2	369.3	255.1	334.8 (27.6/4.5/41.4)	-	-
BCS	173.8 (144.3/29.5)	10985.5	166.3	114.5	155.7 (9.6/3.1/17.7)	2.9%	2.3
$\pi^0 \eta$ veto	137.7 (114.7/23.0)	3076.5	53.3	36.5	116.0 (7.5/2.4/12.8)	2.3%	3.2
qq BG suppression	100.3 (84.4/15.8)	175.5	23.0	17.8	55.6 (4.0/1.3/ 4.6)	1.7%	5.5
CPV BG veto	87.3 (73.9/13.4)	124.5	7.7	7.0	39.5 (3.2/1.1/ 3.1)	1.5%	5.6
$K \pi^0 \gamma$ veto	87.2 (73.8/13.3)	122.8	7.3	6.8	37.3 (3.1/1.1/ 1.9)	1.5%	5.7
helicity angle cut	84.2 (71.7/12.5)	98.8	6.5	5.4	24.4 (2.4/1.0/ 0.8)	1.4%	5.9
$M_{K\eta}$ cut	82.6 (70.4/12.2)	74.3	2.7	3.3	22.9 (2.3/1.0/ 0.8)	1.4%	6.3

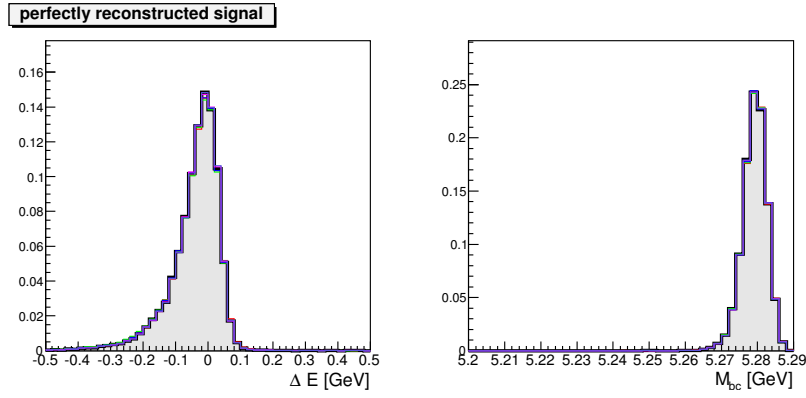


Figure 5.28: ΔE and M_{bc} distributions of perfectly reconstructed signal MC (neutral $\eta \rightarrow 2\gamma$ mode)

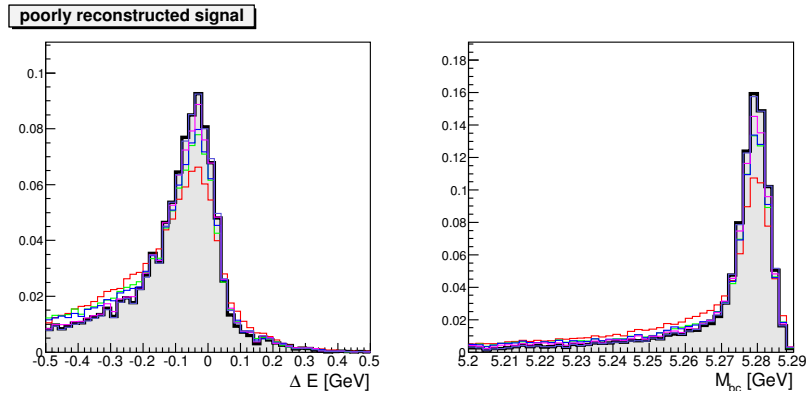


Figure 5.29: ΔE and M_{bc} distributions of poorly reconstructed signal MC (neutral $\eta \rightarrow 2\gamma$ mode)

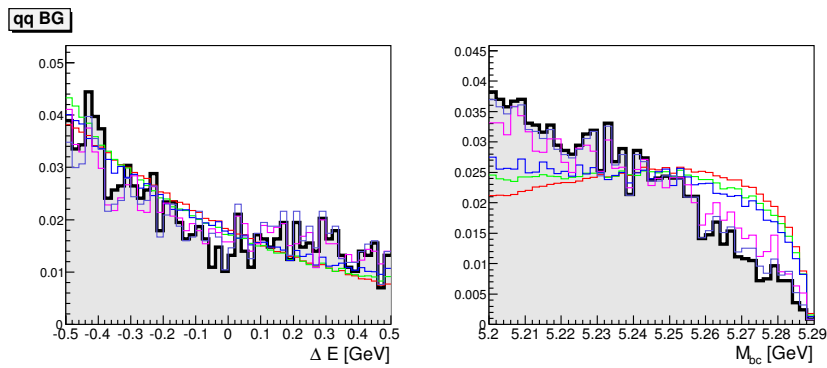


Figure 5.30: ΔE and M_{bc} distributions of qq BG MC (neutral $\eta \rightarrow 2\gamma$ mode)

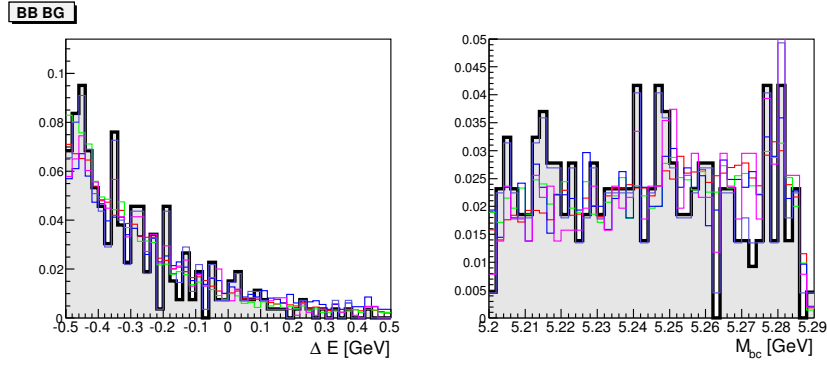


Figure 5.31: ΔE and M_{bc} distributions of BB BG MC (neutral $\eta \rightarrow 2\gamma$ mode)

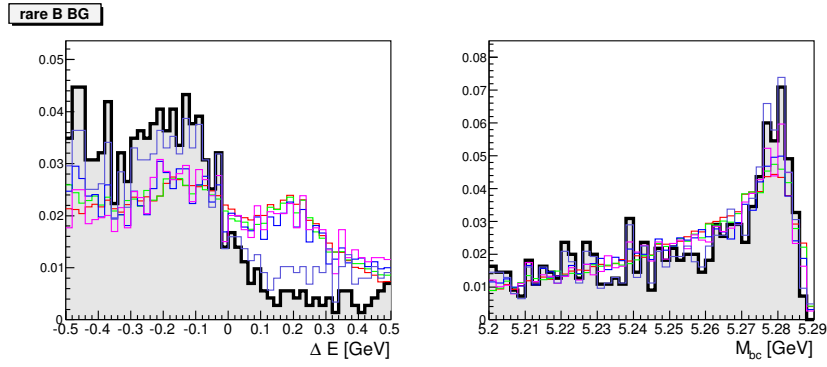


Figure 5.32: ΔE and M_{bc} distributions of rare B BG MC (neutral $\eta \rightarrow 2\gamma$ mode)

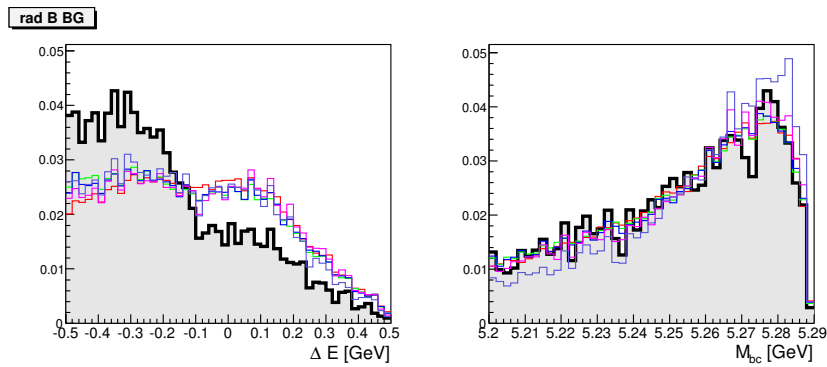


Figure 5.33: ΔE and M_{bc} distributions of rad B BG MC (neutral $\eta \rightarrow 2\gamma$ mode)

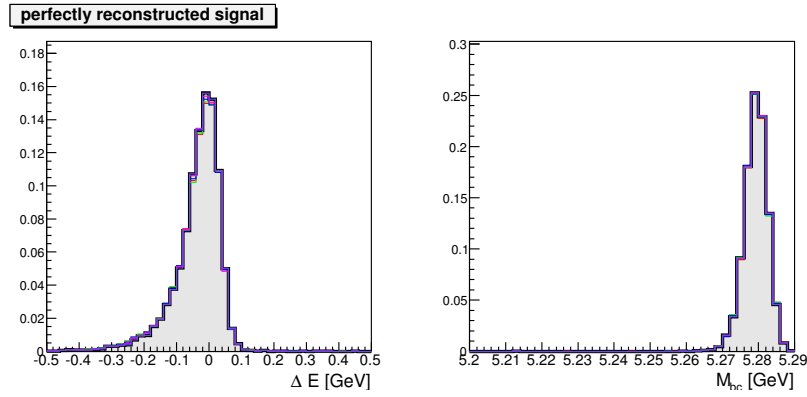


Figure 5.34: ΔE and M_{bc} distributions of perfectly reconstructed signal MC (neutral $\eta \rightarrow 3\pi$ mode)

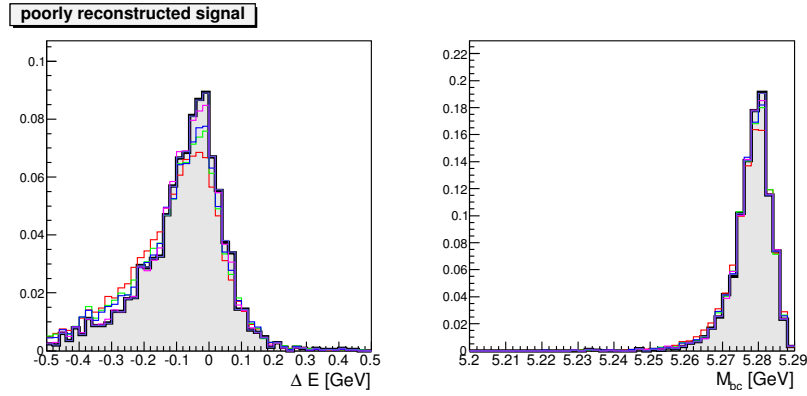


Figure 5.35: ΔE and M_{bc} distributions of poorly reconstructed signal MC (neutral $\eta \rightarrow 3\pi$ mode)

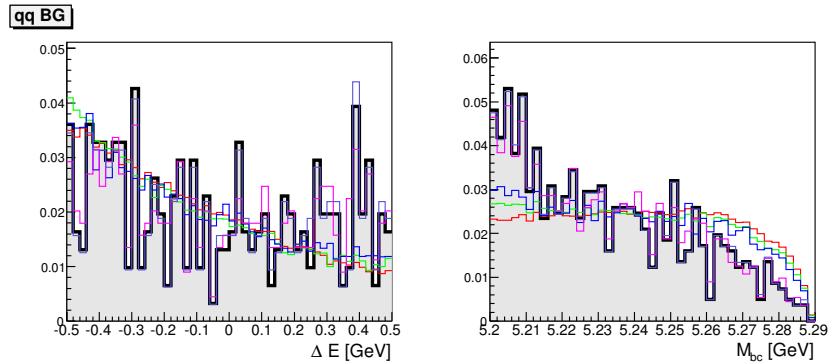


Figure 5.36: ΔE and M_{bc} distributions of qq BG MC (neutral $\eta \rightarrow 3\pi$ mode)

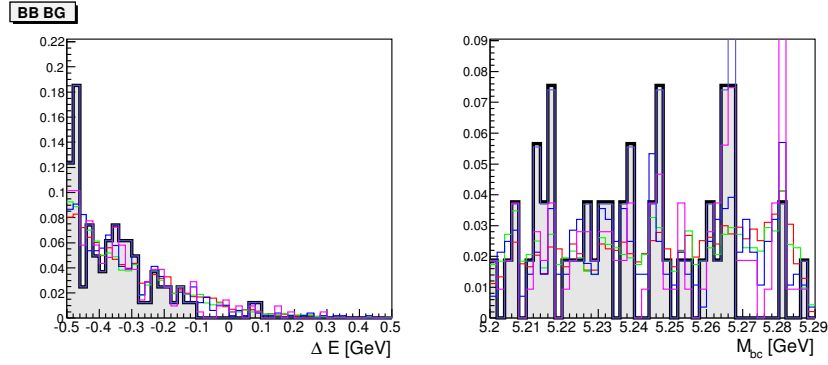


Figure 5.37: ΔE and M_{bc} distributions of BB BG MC (neutral $\eta \rightarrow 3\pi$ mode)

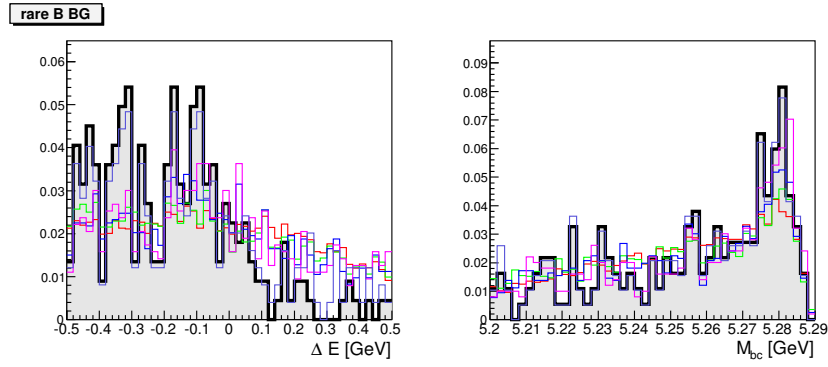


Figure 5.38: ΔE and M_{bc} distributions of rare B BG MC (neutral $\eta \rightarrow 3\pi$ mode)

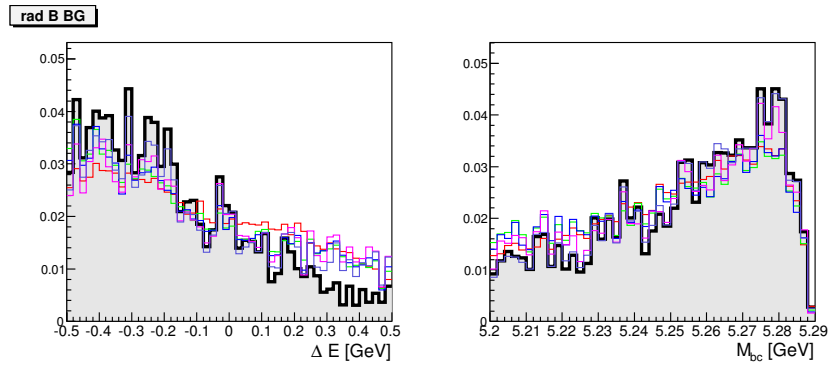


Figure 5.39: ΔE and M_{bc} distributions of rad B BG MC (neutral $\eta \rightarrow 3\pi$ mode)

Chapter 6

3D fit with ΔE , M_{bc} and NB'

6.1 PDF shapes and components

6.1.1 Range

Fit region range of ΔE is $-0.5 < \Delta E < 0.5$ GeV, $5.20 < M_{bc} < 5.29$ GeV/c for M_{bc} and $-10 < NB' < 8$ for NB' . NB' is the transferred variable of NB output for qq suppression. It is defined as

$$NB' = \log \left(\frac{NB - NB_{\text{MIN}}}{NB_{\text{MAX}} - NB} \right) \quad (6.1)$$

and forms Gaussian-like distribution which is easy to be fitted (; strictly speaking, it's not Gaussian). Here, we set $NB_{\text{MIN}} = -0.7$ and $NB_{\text{MAX}} = 0.935$ (0.915) for $\eta \rightarrow 2\gamma$ mode ($\eta \rightarrow 3\pi$ mode). Events whose $NB < NB_{\text{MIN}}$ are discarded, and we confirm that there's no event which satisfy $NB > NB_{\text{MAX}}$.

6.1.2 PDF shapes

Because of low statistics, too many fit parameter prevent fitter from converging. Fit parameters are only one N_{sig} and seven $N_{qq[\text{bin\#}]}$. Other BG amounts, PDF shape parameters and qr bin fraction of signal $f_{\text{sig}[\text{bin\#}]}$ are decided by MC study. Table 6.1 shows f_{sig} values for each decay mode. Basic policy on fixing PDF shapes are like this:

- If distributions of neutral and charged modes are same, MC data are combined.
- Basically, shape parameters are decided qr bin-by-bin, however, if statistics are not enough, some bins are combined or shape parameters are decreased.

Table 6.1: qr bin fraction of signal obtained by signal MC

	Neutral $\eta \rightarrow 2\gamma$	Neutral $\eta \rightarrow 3\pi$	Charged $\eta \rightarrow 2\gamma$	Charged $\eta \rightarrow 3\pi$
$f_{\text{sig}[0]}$ [%]	19.8	20.6	20.8	21.3
$f_{\text{sig}[1]}$ [%]	14.0	13.5	14.1	14.4
$f_{\text{sig}[2]}$ [%]	17.4	17.5	16.8	16.4
$f_{\text{sig}[3]}$ [%]	11.6	11.5	11.3	11.3
$f_{\text{sig}[4]}$ [%]	9.7	9.4	10.7	10.4
$f_{\text{sig}[5]}$ [%]	9.7	9.6	9.7	9.7
$f_{\text{sig}[6]}$ [%]	17.8	18.0	16.5	16.5

Signal PDF

Signal is consists of perfectly reconstructed and poorly reconstructed signals. Since ΔE and M_{bc} is strongly correlated as we can see in Fig.6.5, 2 dimensional histogram are used to describe $\Delta E - M_{bc}$ distribution. Its binning are 100 bins (10 [MeV/bin]) for ΔE and 90 bins (1 [MeV/bin]) for M_{bc} . In order to estimate difference of histogram PDF between MC and data, unbinned maximum likelihood fit with histogram PDF which is artificially shifted or widen have been done. Then, 2nd order polynomial is fitted into negative log likelihood distribution obtained by these fits. Here, error of each $-\log(\mathcal{L})$ is set to 0.5. We obtained minimum value of modification factor and its range whose $\Delta\log(\mathcal{L})$ is less than 0.5. This range is defined as ‘‘fudge factor’’ of the PDF. We used $B \rightarrow K^*(\rightarrow K^+\pi^-)\gamma$ mode as a control sample for the estimation. Assuming that PDF difference is mainly caused by prompt γ reconstruction, error of the $\eta \rightarrow 2\gamma$ mode and $\eta \rightarrow 3\pi$ mode are same. We set same amount of error. Figure 6.1 to 6.4 show the $-\log(\mathcal{L})$ distributions and fit result. Table 6.2 summarizes minimum point and its range of $\Delta\log(\mathcal{L}) < 0.5$. We found that fudge factor of ΔE are significantly apart from zero, while fudge factor of M_{bc} are consistent to zero within 1σ . Then, we apply correction to ΔE PDF shape.

NB' is fitted by bifurcated Gaussian for qr bin #0, 1, 2, 3 and 4, or double bifurcated Gaussian sharing peak position and right width for qr bin #5 and 6.

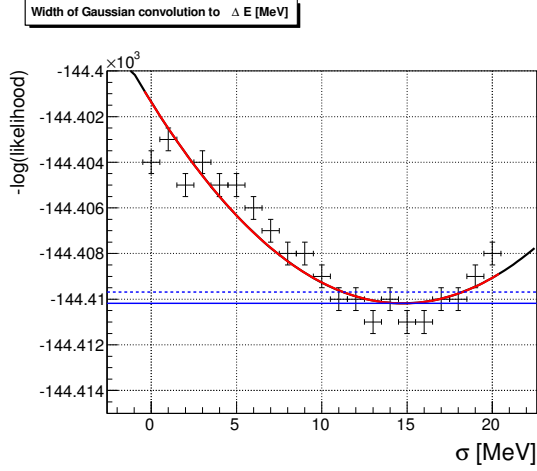


Figure 6.1: $-\log(\mathcal{L})$ distribution and fit result. Horizontal axis shows how much wide gaussian is convoluted to ΔE PDF.

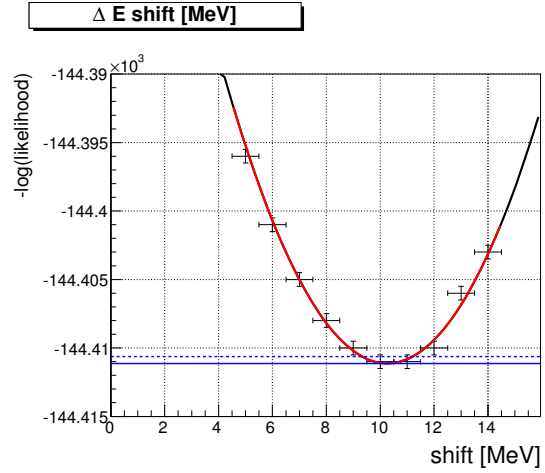


Figure 6.2: $-\log(\mathcal{L})$ distribution and fit result. Horizontal axis shows how ΔE PDF is shifted.

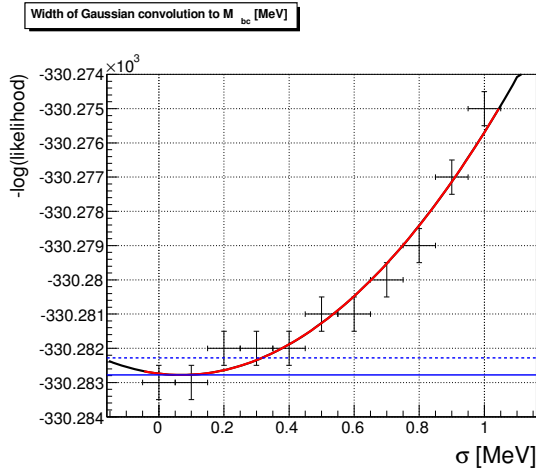


Figure 6.3: $-\log(\mathcal{L})$ distribution and fit result. Horizontal axis shows how much wide gaussian is convoluted to M_{bc} PDF.

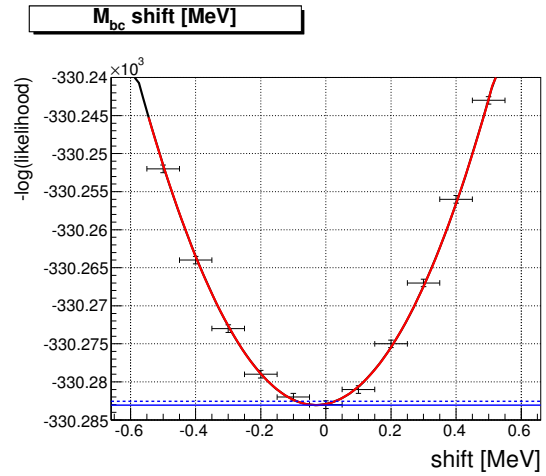


Figure 6.4: $-\log(\mathcal{L})$ distribution and fit result. Horizontal axis shows how M_{bc} PDF is shifted.

Table 6.2: Fudge factor

ΔE width	14.7 ± 3.5 [MeV]	This width of Gaussian is convoluted to histogram PDF.
ΔE shift	10.27 ± 0.93 [MeV]	Histogram PDF is shifted this amount.
M_{bc} width	0.07 ± 0.25 [MeV]	This width of Gaussian is convoluted to histogram PDF.
M_{bc} shift	-0.03 ± 0.06 [MeV]	Histogram PDF is shifted this amount.

qq BG PDF

Figure 6.6 shows correlation among 3 parameters are not so large. Then, we can describe their distributions separately (i.e. $P(\Delta E, M_{bc}, \text{NB}') = P(\Delta E) \times P(M_{bc}) \times P(\text{NB}')$). ΔE distribution is fitted by 2nd order Chebyshev, and M_{bc} distribution is fitted by Argus function. They can be written as

$$P_{\Delta E}(x) = 1 + a_1 x + a_2(2x^2 - 1) \quad (6.2)$$

$$P_{M_{bc}}(x) = x \left(1 - \left(\frac{x}{m}\right)^2\right)^P \cdot \exp \left[c \left(1 - \left(\frac{x}{m}\right)^2\right) \right] \quad (6.3)$$

Here, end point parameter m is fixed to 5.29 GeV, and parameter P is fixed to 0.5 before fit. Sum of bifurcated Gaussian and Gaussian reproduces NB' distribution well. Their peak position is different.

BB, rare B and rad B BG PDF

Figure 6.7, 6.8 and 6.9 show correlation among 3 parameters are not so large. Then, we can describe their distributions separately. BB , rare B and rad B BG PDF's ΔE distribution are described by exponential. Bifurcated Gaussian is used for their NB' fit. M_{bc} of BB BG is drawn by ARGUS function, one of rare B BG is fitted by sum of ARGUS and Gaussian, and rad B 's one is described by sum of ARGUS and Gaussian (Bifurcated Gaussian) for Neutral (Charged) mode.

Summary

Table 6.3 summarizes these discussion above. Because of the very low statistics, BB BG distribution is not obtained bin-by-bin.

6.1.3 Fit method

We used unbinned maximum likelihood method supported by **ROOFIT**. Extended fit which floats event amount is used. In order to obtain asymmetric error safely, we fitted with “**MIGRAD**” and obtained symmetric error by using “**HESSE**” with wide fit range, at first. Then, we shorten fit range to 2 or 3 σ of “**HESSE**” error. Finally, “**MIGRAD**” is applied again and asymmetric error is estimated by “**MINOS**”.

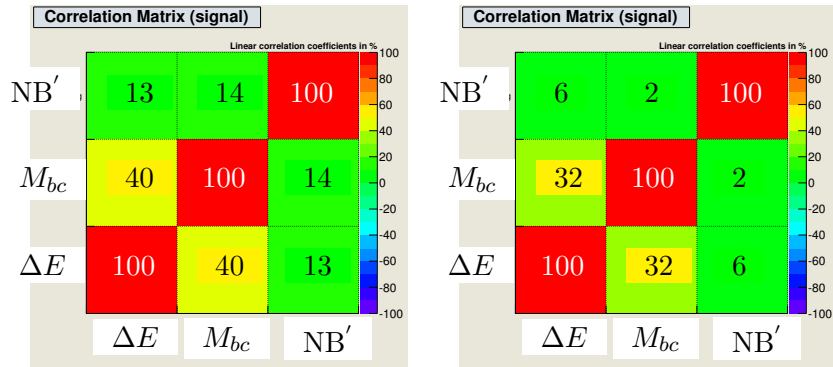


Figure 6.5: Correlation between ΔE , M_{bc} and NeuroBayes output of signal (left: $\eta \rightarrow 2\gamma$ mode. right: $\eta \rightarrow 3\pi$ mode)

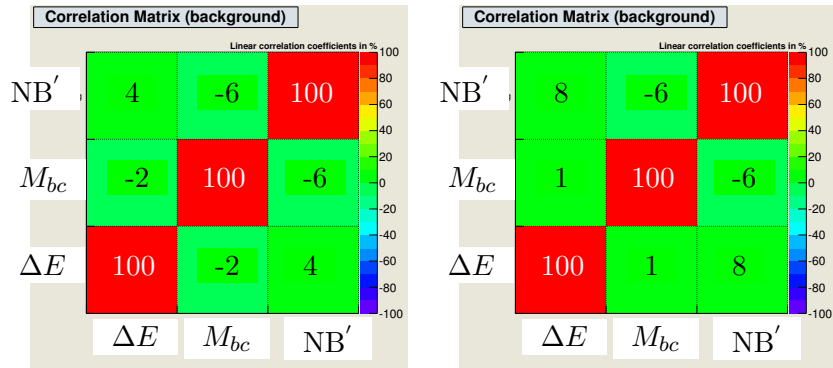


Figure 6.6: Correlation between ΔE , M_{bc} and NeuroBayes output of qq BG (left: $\eta \rightarrow 2\gamma$ mode. right: $\eta \rightarrow 3\pi$ mode)

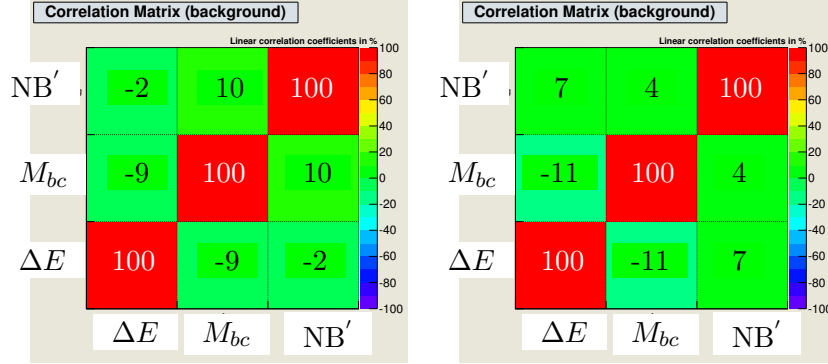


Figure 6.7: Correlation between ΔE , M_{bc} and NeuroBayes output of *BB* BG (left: $\eta \rightarrow 2\gamma$ mode. right: $\eta \rightarrow 3\pi$ mode)

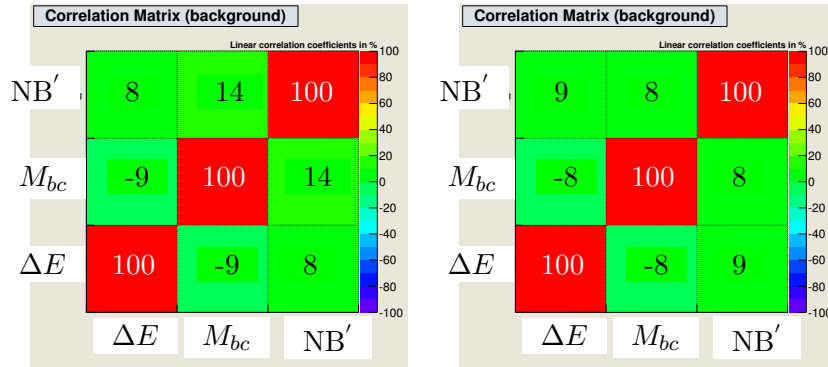


Figure 6.8: Correlation between ΔE , M_{bc} and NeuroBayes output of rare *B* BG (left: $\eta \rightarrow 2\gamma$ mode. right: $\eta \rightarrow 3\pi$ mode)

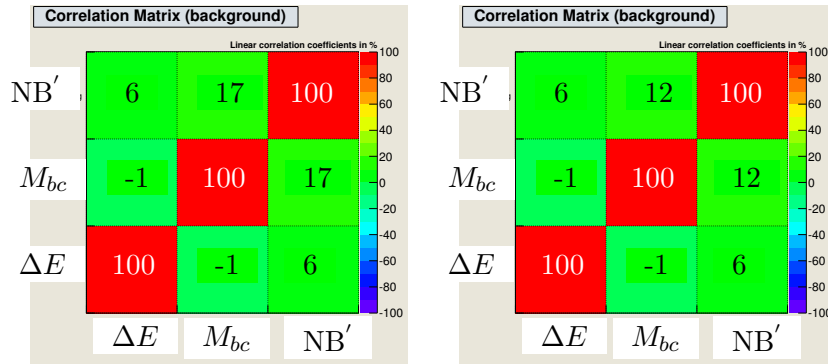


Figure 6.9: Correlation between ΔE , M_{bc} and NeuroBayes output of rad *B* BG (left: $\eta \rightarrow 2\gamma$ mode. right: $\eta \rightarrow 3\pi$ mode)

Table 6.3: Summary table of PDF shape functions

	ΔE	M_{bc}	NB'
Signal		[0/1/2/3/4/5/6] bin 2D Histogram PDF	[0/1/2/3/4] bin Bifurcated Gaussian [5/6] bin Double Bifurcated Gaussian
qq BG	[0/1/2/3/4/5/6] bin 2nd order Chebyshev Combined MC distribution	[0/1/2/3/4/5/6] bin ARGUS Combined MC distribution	[0/1/23/456] bin Bifurcated Gaussian + Gaussian Combined MC distribution
BB BG	[0123456] bin Exponential Combined MC distribution	[0123456] bin ARGUS Combined MC distribution	[0123456] bin Bifurcated Gaussian Combined MC distribution
rare B	[0/1/2/3/4/5/6] bin Exponential Combined MC distribution	[012/3456] bin ARGUS + Gaussian Combined MC distribution	[012/345/6] bin Bifurcated Gaussian Combined MC distribution
rad B	[0/1/2/3/4/5/6] bin Exponential	[0/1/2/3/4/5/6] bin ARGUS + Gaussian for B^0 ARGUS + Bifurcated Gaussian for B^+	[0/1/2/3/4/5/6] bin Bifurcated Gaussian Combined MC distribution

6.2 Spin search of $K^\pm \eta$ system

We divide $\cos\theta_{\text{hel}}$ into 10 regions and fitted for the sake of obtaining signal distribution. (θ_{hel} is defined at 5.3.6.) Since PDF of NB' easily become negative when N_{sig} is zero consistent, $\Delta E - M_{bc}$ 2D fit is used. (If PDF becomes negative, fitter doesn't converge or cannot estimate asymmetric error.) The way of fixing PDF shape is same as we discussed above, but cut on NB is applied to maximize significance. Figure 6.10 and 6.11 show helicity angle distribution of charged sample. Vertical axis shows event amount divided by reconstruction efficiency which is estimated by MC study. Eq.(5.38) and (5.39) are fitted into this distribution and obtained reduced chi square as χ^2/ndf (spin1)= 1.2 (0.6) and χ^2/ndf (spin2)= 7.5 (2.8) for $\eta \rightarrow \gamma\gamma$ ($\eta \rightarrow \pi^+\pi^-\pi^0$) mode respectively. The result says that spin of $K^\pm \eta$ system is 1 rather than 2. Considering isospin symmetry, we assumed spin of $K_S \eta$ system is 1, also.

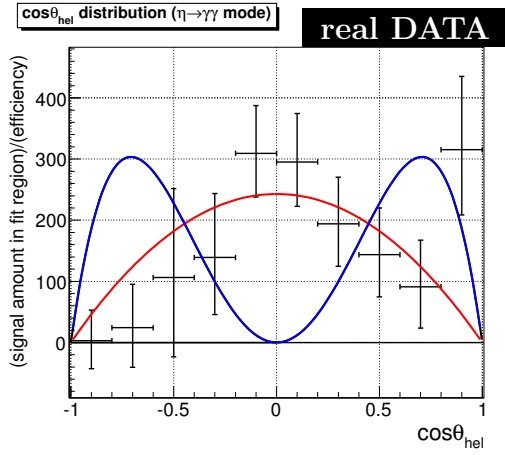


Figure 6.10: Helicity angle distribution of charged control sample and its fit result ($\eta \rightarrow \gamma\gamma$ mode)

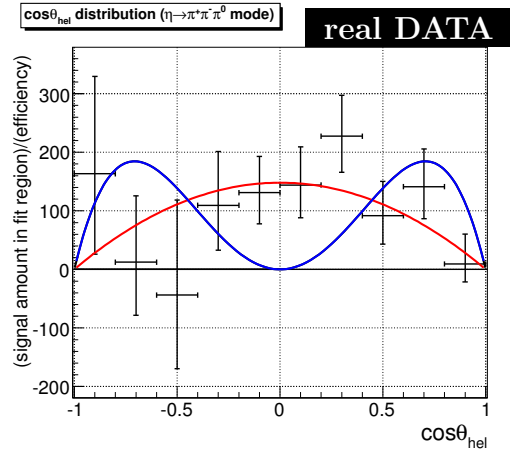


Figure 6.11: Helicity angle distribution of charged control sample and its fit result ($\eta \rightarrow \pi^+\pi^-\pi^0$ mode)

6.3 Invariant mass distribution of $K^\pm \eta$ system

We checked invariant mass distribution of $K^\pm \eta$ system. Considering isospin symmetry, distribution of invariant mass of $K_S \eta$ system should be same. Figure 6.12 and 6.13 shows invariant mass distribution of $K^\pm \eta$ system.

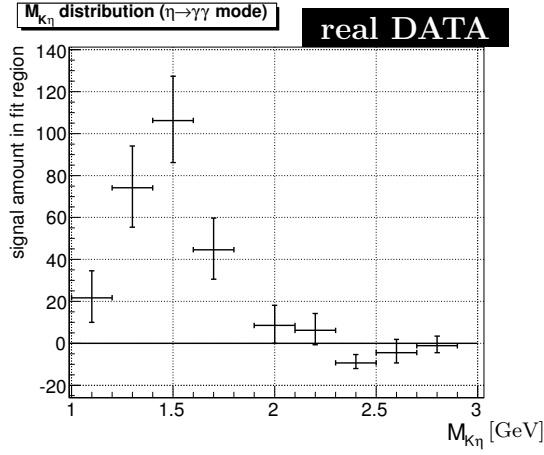


Figure 6.12: Invariant mass distribution of $K^\pm \eta$ system ($\eta \rightarrow \gamma\gamma$ mode)

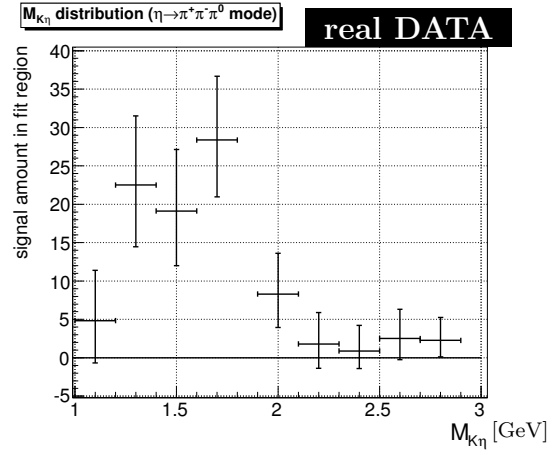


Figure 6.13: Invariant mass distribution of $K^\pm \eta$ system ($\eta \rightarrow \pi^+ \pi^- \pi^0$ mode)

6.4 Signal and background fraction of B candidate

We have to obtain signal fraction and each background fraction event by event. It is needed for Δt distribution analysis. Table 6.4 to 6.7 summarize fit result of signal and qq BG amount in fit region. Figure 6.14 to 6.22 show signal region projection of fit result to 3 axes of each qr bin. Red line is sum of all PDF. Blue line shows BG distribution. Green one describes fixed amount BG (i.e. non- qq BG) shape.

Table 6.4: Fit result of Charged mode ($\eta \rightarrow 2\gamma$ mode)

N_{sig}	$191.7^{+25.1}_{-24.0}$	$N_{qq[0]}$	$11014.3^{+107.4}_{-106.7}$
$N_{qq[1]}$	$7372.9^{+88.2}_{-87.6}$	$N_{qq[2]}$	$6869.8^{+85.9}_{-85.3}$
$N_{qq[3]}$	$3658.7^{+63.1}_{-62.5}$	$N_{qq[4]}$	$3073.7^{+57.8}_{-57.1}$
$N_{qq[5]}$	$2098.8^{+48.4}_{-47.8}$	$N_{qq[6]}$	$727.7^{+31.4}_{-30.8}$

Table 6.5: Fit result of Charged mode ($\eta \rightarrow \pi^+\pi^-\pi^0$ mode)

N_{sig}	$89.3^{+16.8}_{-15.7}$	$N_{qq[0]}$	$5359.6^{+75.1}_{-74.4}$
$N_{qq[1]}$	$3638.0^{+62.0}_{-61.4}$	$N_{qq[2]}$	$3317.8^{+59.6}_{-59.0}$
$N_{qq[3]}$	$1767.4^{+43.7}_{-43.1}$	$N_{qq[4]}$	$1439.2^{+39.6}_{-39.0}$
$N_{qq[5]}$	$959.0^{+32.5}_{-31.9}$	$N_{qq[6]}$	$334.4^{+20.5}_{-19.8}$

Table 6.6: Fit result of Neutral mode ($\eta \rightarrow 2\gamma$ mode)

N_{sig}	$69.5^{+13.4}_{-12.4}$	$N_{qq[0]}$	$1355.0^{+38.5}_{-37.8}$
$N_{qq[1]}$	$800.8^{+30.0}_{-29.3}$	$N_{qq[2]}$	$824.8^{+30.8}_{-30.1}$
$N_{qq[3]}$	$526.7^{+24.6}_{-23.9}$	$N_{qq[4]}$	$497.7^{+23.8}_{-23.1}$
$N_{qq[5]}$	$338.0^{+20.1}_{-19.4}$	$N_{qq[6]}$	$121.5^{+13.9}_{-13.2}$

Table 6.7: Fit result of Neutral mode ($\eta \rightarrow \pi^+\pi^-\pi^0$ mode)

N_{sig}	$22.4^{+7.3}_{-6.4}$	$N_{qq[0]}$	$630.9^{+26.4}_{-25.8}$
$N_{qq[1]}$	$363.4^{+20.4}_{-19.7}$	$N_{qq[2]}$	$364.8^{+20.5}_{-19.9}$
$N_{qq[3]}$	$230.6^{+16.3}_{-15.6}$	$N_{qq[4]}$	$215.9^{+15.8}_{-15.1}$
$N_{qq[5]}$	$156.7^{+13.6}_{-12.9}$	$N_{qq[6]}$	$74.9^{+10.0}_{-9.3}$

$$B^\pm \rightarrow K^\pm \eta_{(\rightarrow \gamma\gamma)} \gamma$$

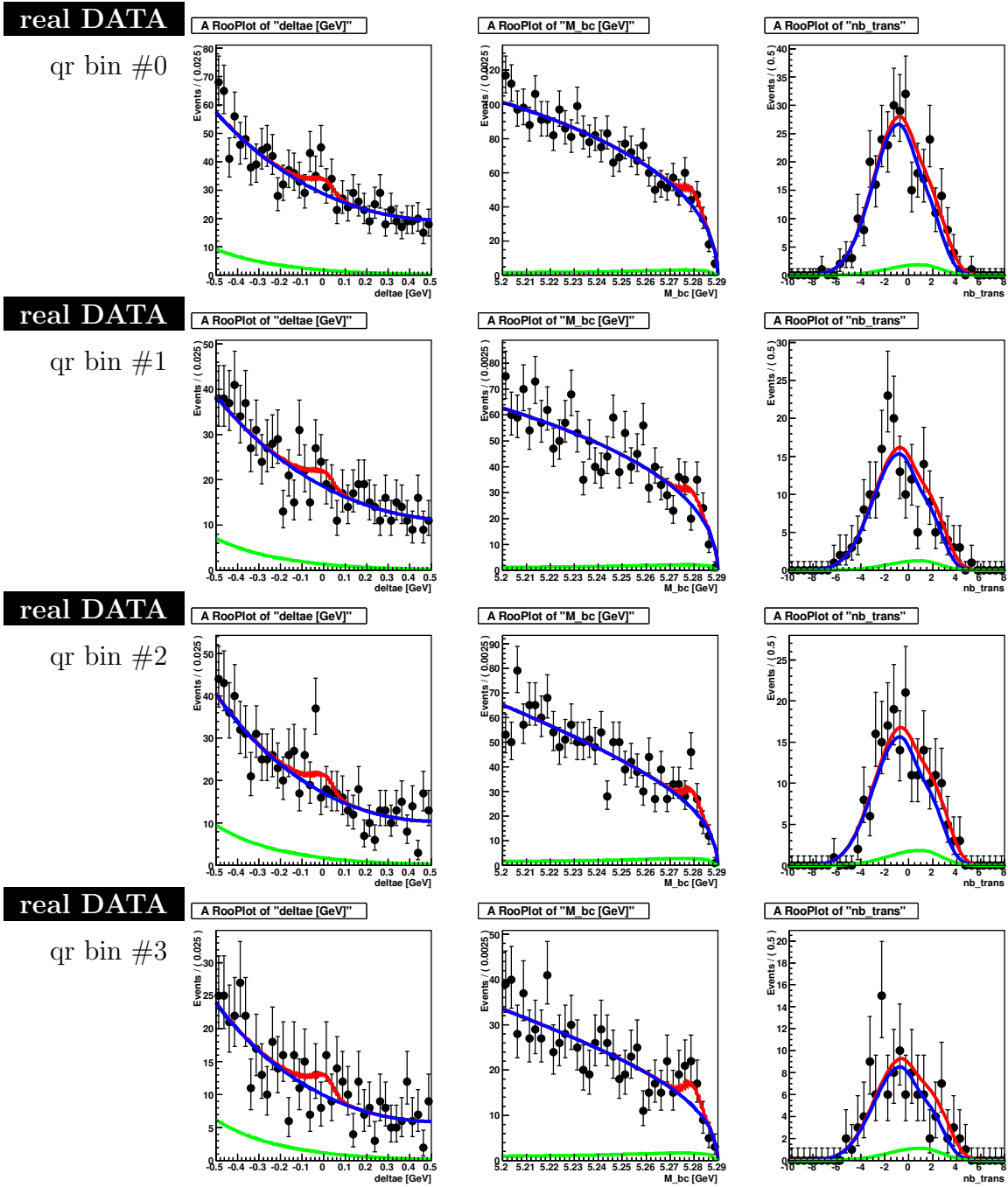


Figure 6.14: Fit result of Charged mode ($\eta \rightarrow 2\gamma$ mode, qr#0 to #3)

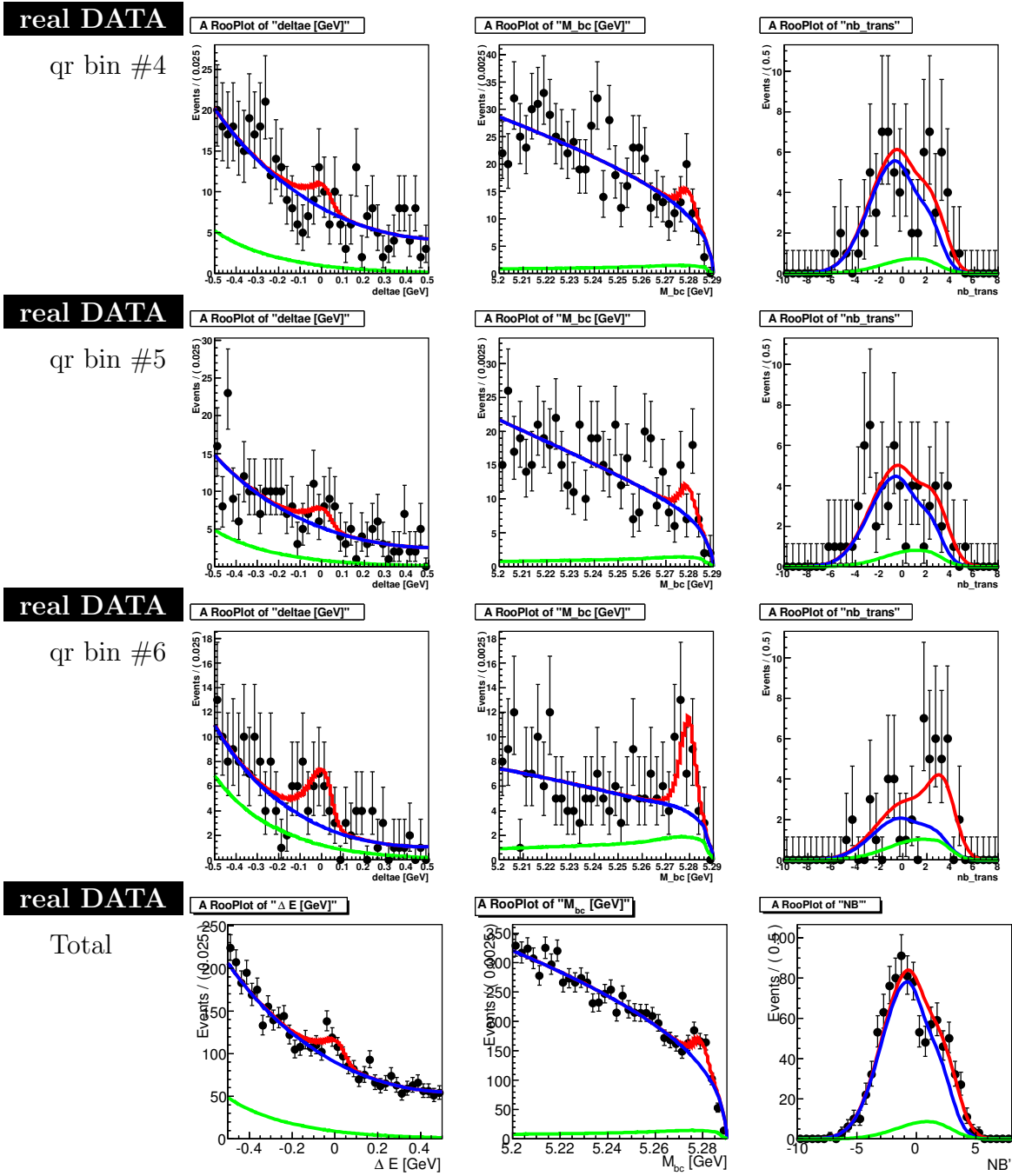


Figure 6.15: Fit result of Charged mode ($\eta \rightarrow 2\gamma$ mode, $qr\#4$ to $\#6$ and total)

$$B^\pm \rightarrow K^\pm \eta_{(\rightarrow \pi^+ \pi^- \pi^0)} \gamma$$

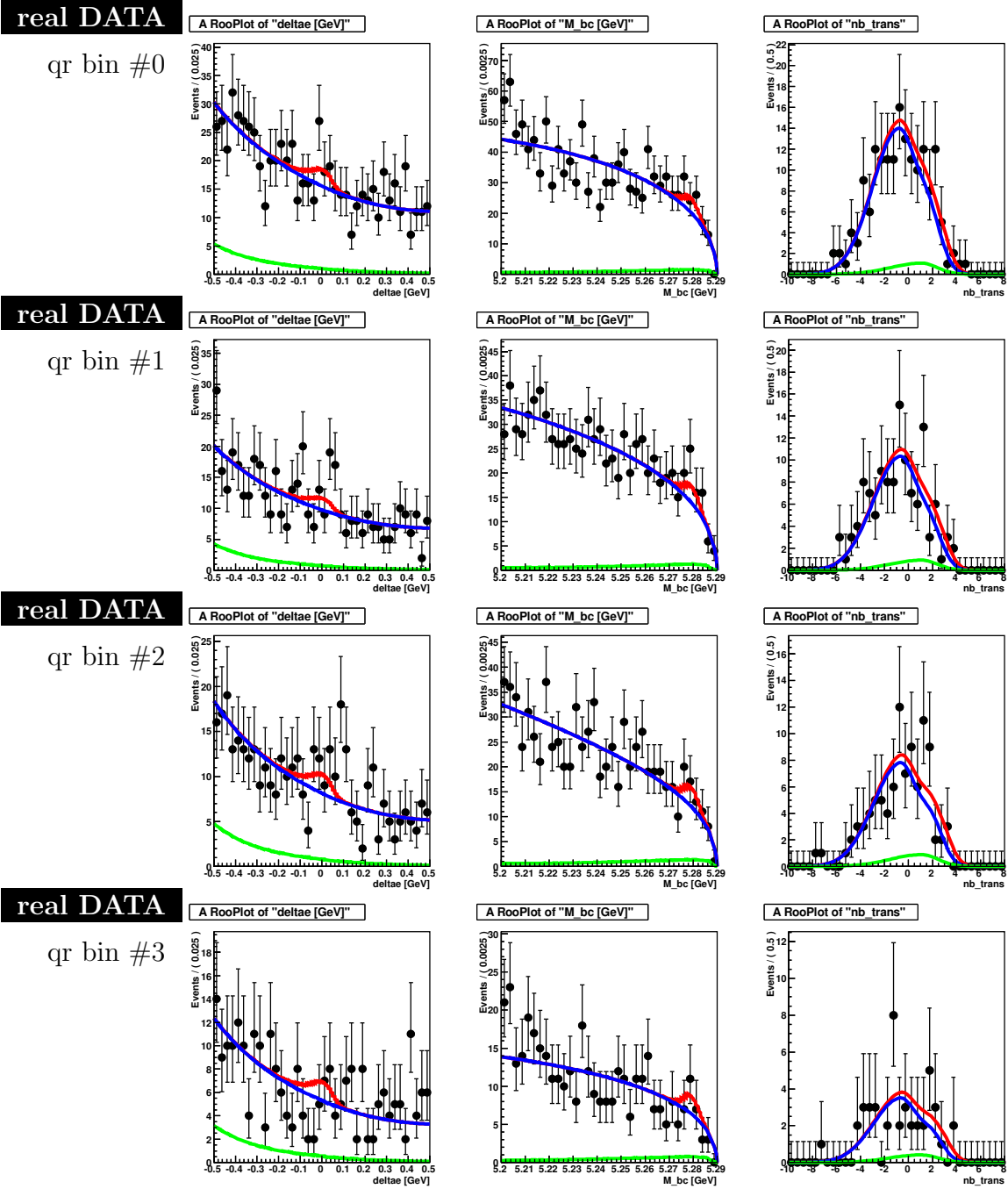


Figure 6.16: Fit result of Charged mode ($\eta \rightarrow \pi^+ \pi^- \pi^0$ mode, qr#0 to #3)

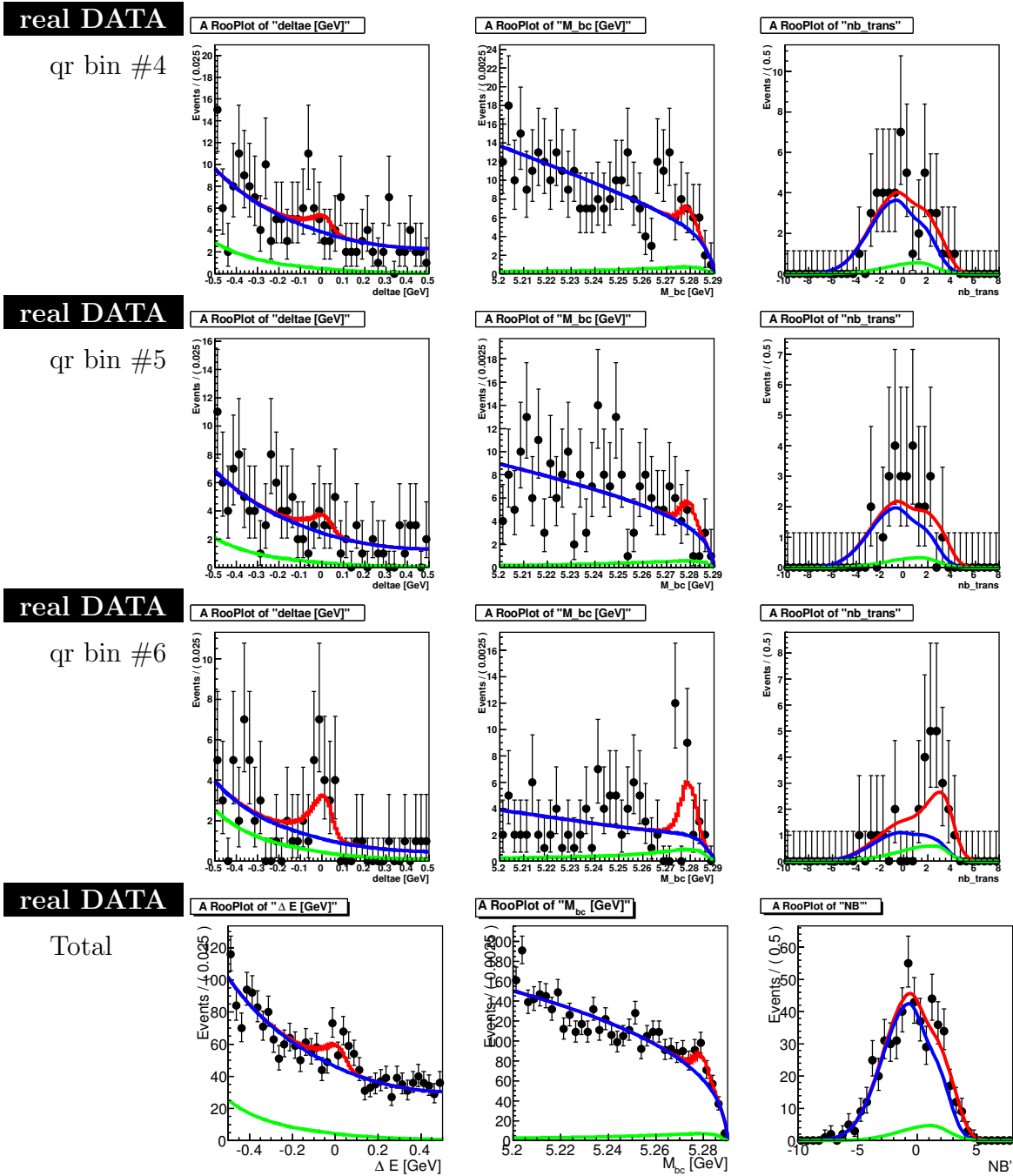


Figure 6.17: Fit result of Charged mode ($\eta \rightarrow \pi^+ \pi^- \pi^0$ mode, qr#4 to #6 and total)

Total $B^\pm \rightarrow K^\pm \eta \gamma$

real DATA

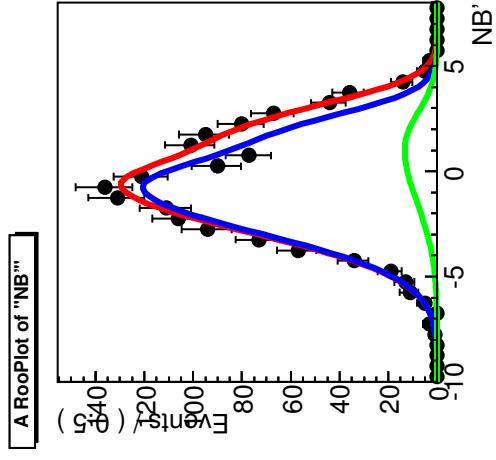
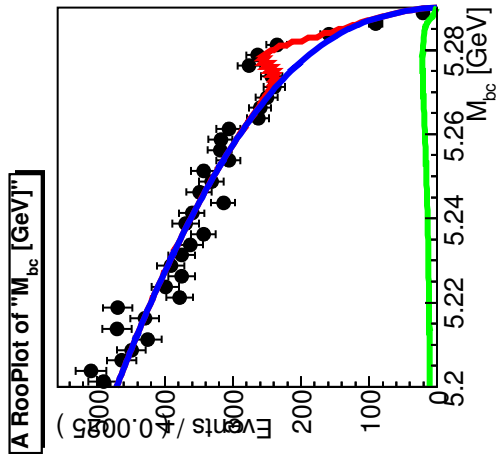
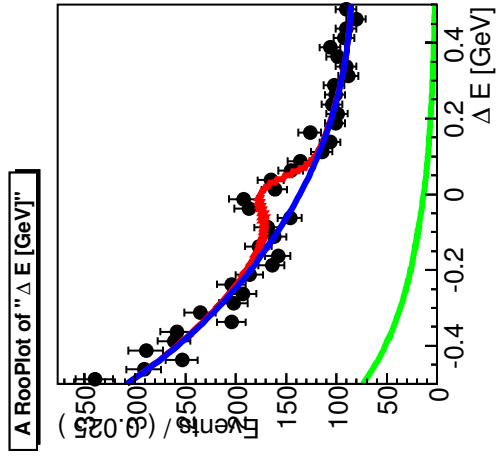


Figure 6.18: Fit result of Charged mode ($\eta \rightarrow \gamma \gamma$ mode + $\eta \rightarrow \pi^+ \pi^- \pi^0$ mode)

$$B^0 \rightarrow K_S \eta (\rightarrow \gamma\gamma) \gamma$$

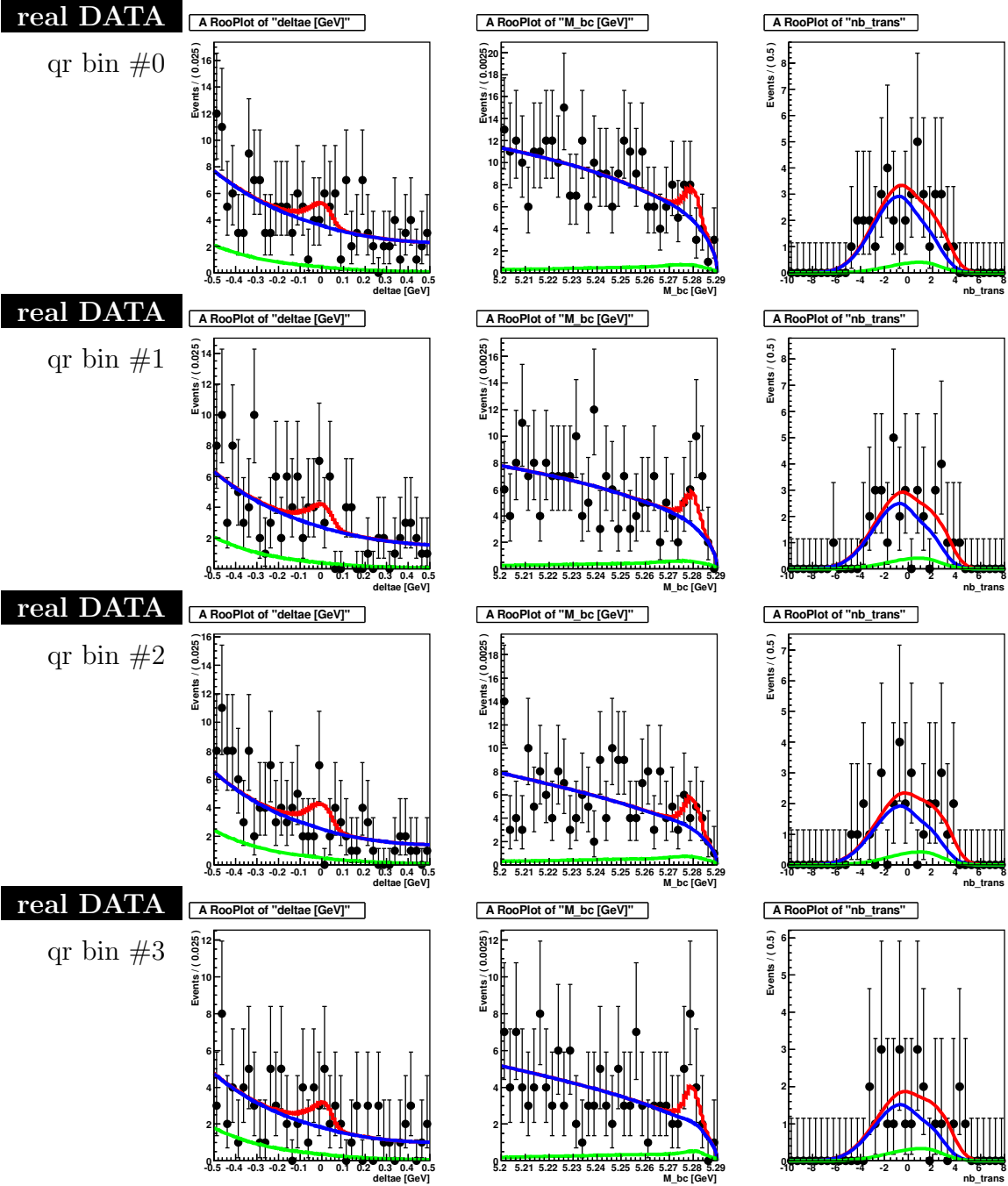


Figure 6.19: Fit result of Neutral mode ($\eta \rightarrow \gamma\gamma$ mode, $qr\#0$ to $\#3$)

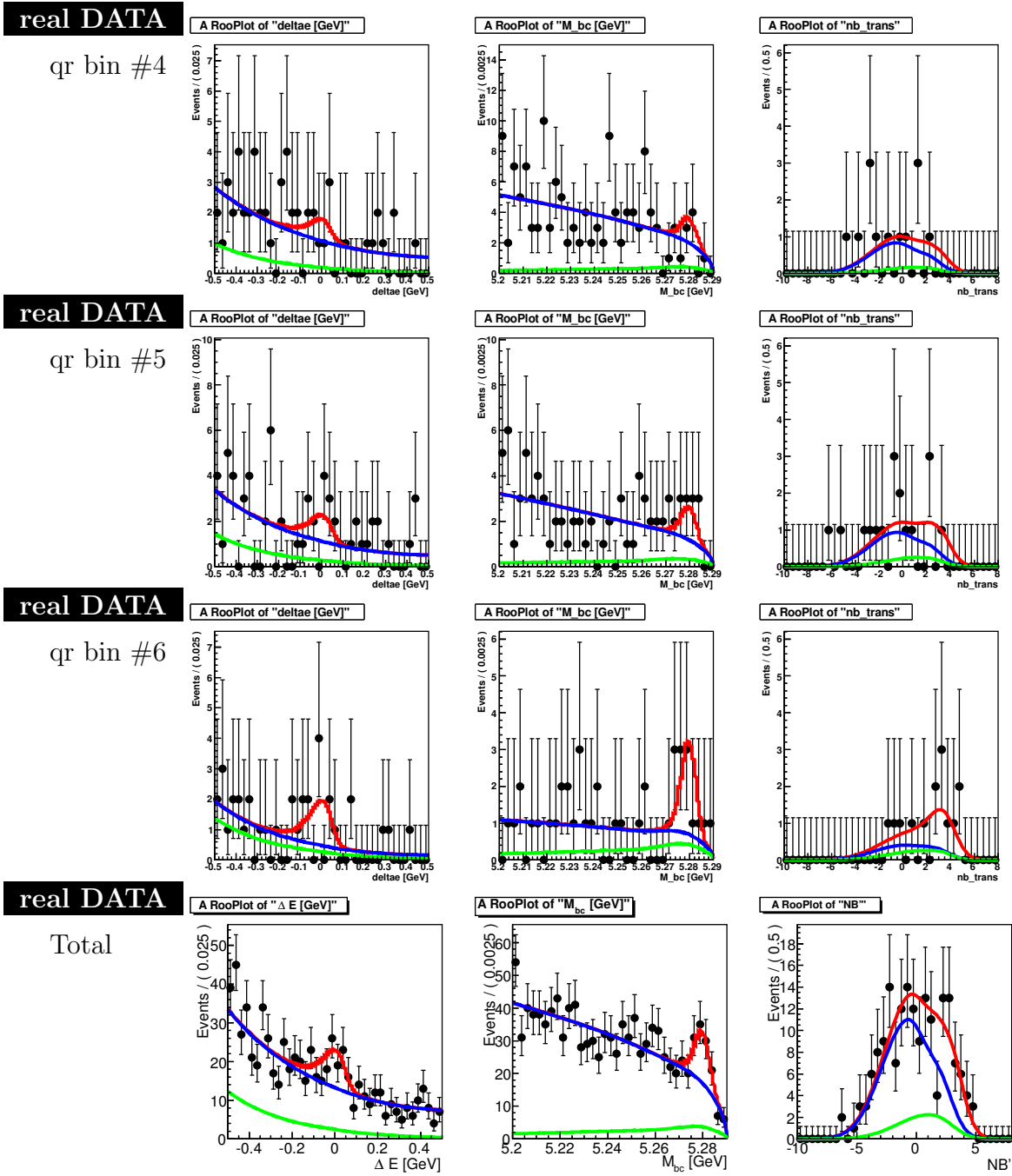


Figure 6.20: Fit result of Neutral mode ($\eta \rightarrow \gamma\gamma$ mode, qr#4 to #6 and total)

$$B^0 \rightarrow K_S \eta (\rightarrow \pi^+ \pi^- \pi^0) \gamma$$

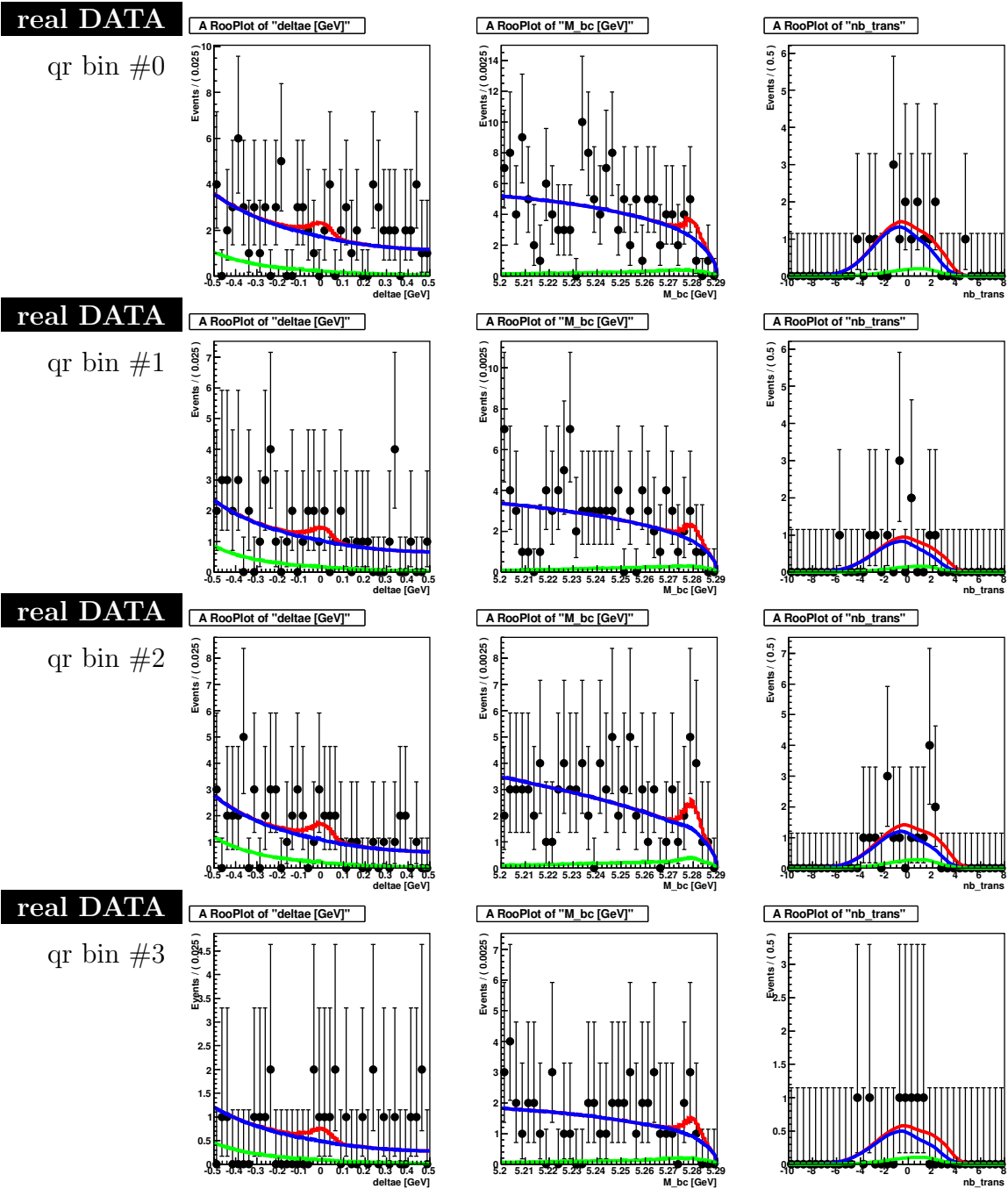


Figure 6.21: Fit result of Neutral mode ($\eta \rightarrow \pi^+ \pi^- \pi^0$ mode, qr#0 to #3)

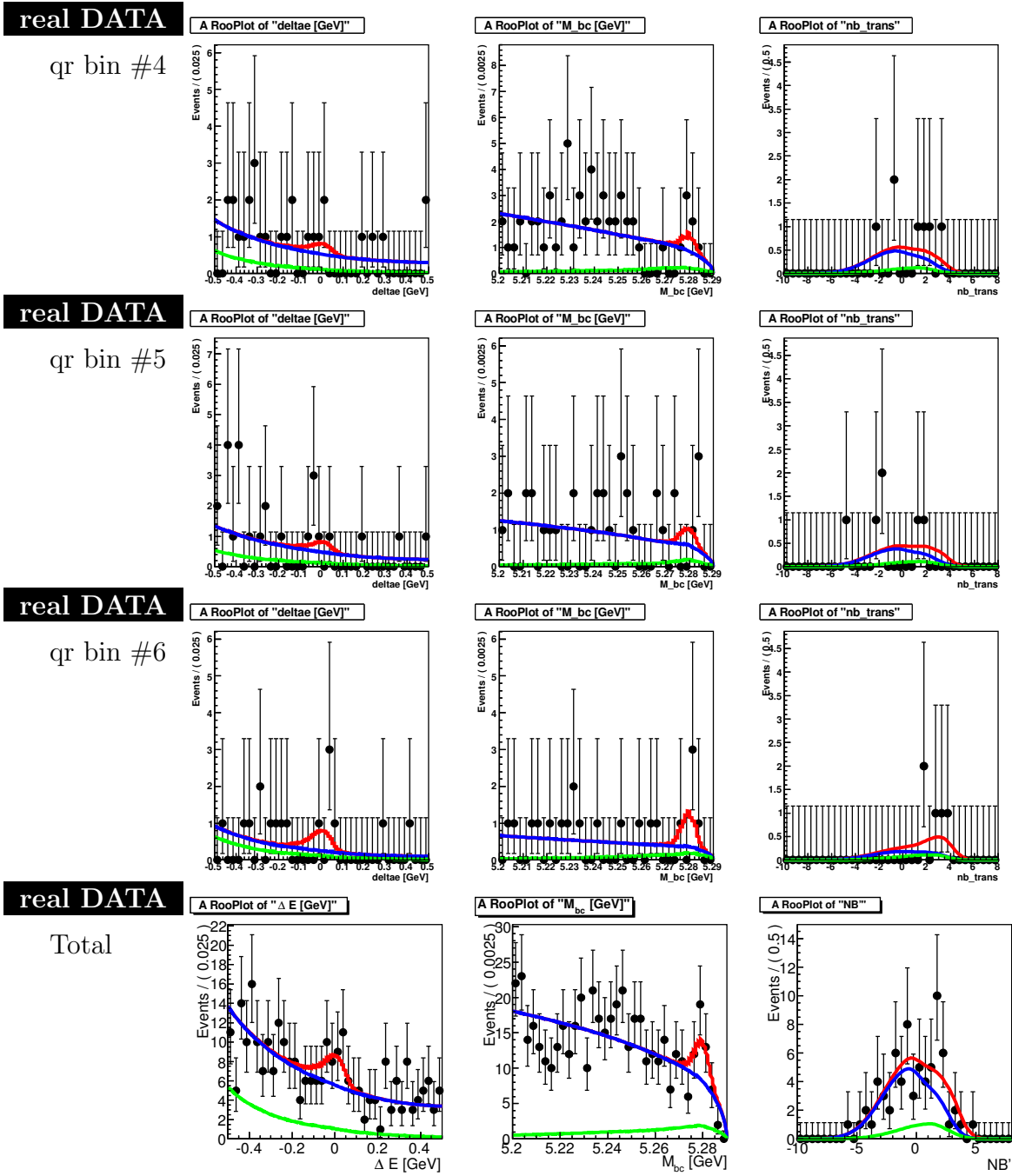


Figure 6.22: Fit result of Neutral mode ($\eta \rightarrow \pi^+ \pi^- \pi^0$ mode, qr#3 to #6)

Total $B^0 \rightarrow K_S \eta \gamma$

real DATA

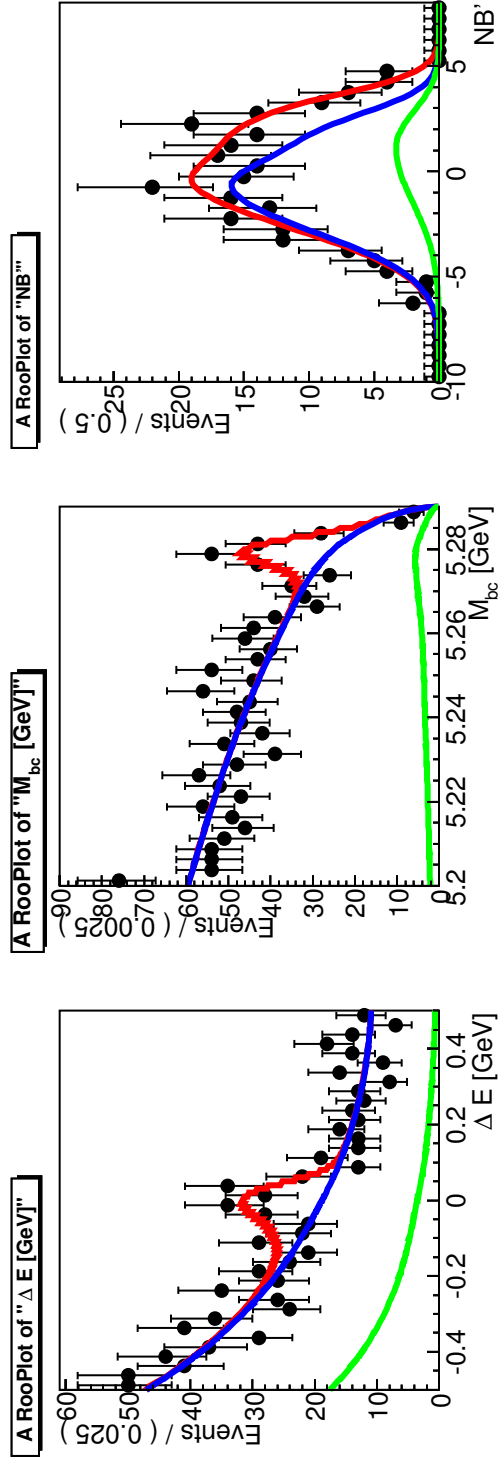


Figure 6.23: Fit result of Neutral mode ($\eta \rightarrow \gamma \gamma$ mode + $\eta \rightarrow \pi^+ \pi^- \pi^0$ mode)

6.5 Fit bias study with MC simulation

Figure. 6.24 and 6.27 are pull distribution of N_{sig} and $N_{qq[\text{bin}\#]}$ of 1000 MC fit results. Pull is defined as

$$(\text{pull}) = \frac{(\text{fit result}) - (\text{expected amount})}{(\text{fit error})}, \quad (6.4)$$

and error is asymmetric error. Event amounts are generated by poisson and distribution are generated by fit function. These distributions are fitted with Gaussian.

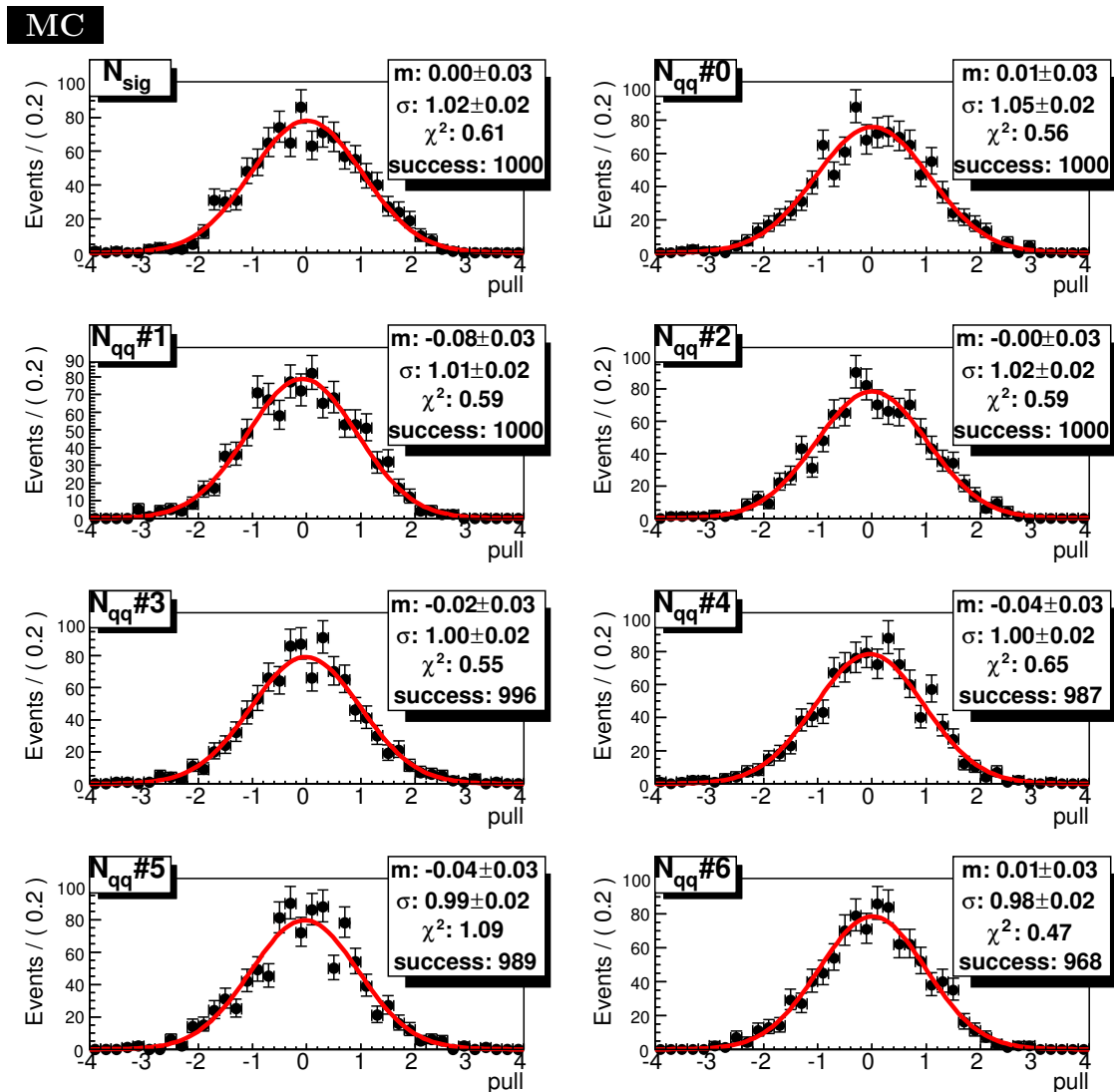


Figure 6.24: Pull distribution of N_{sig} and N_{qq} fit results of MC (neutral $\eta \rightarrow 2\gamma$ mode)

MC

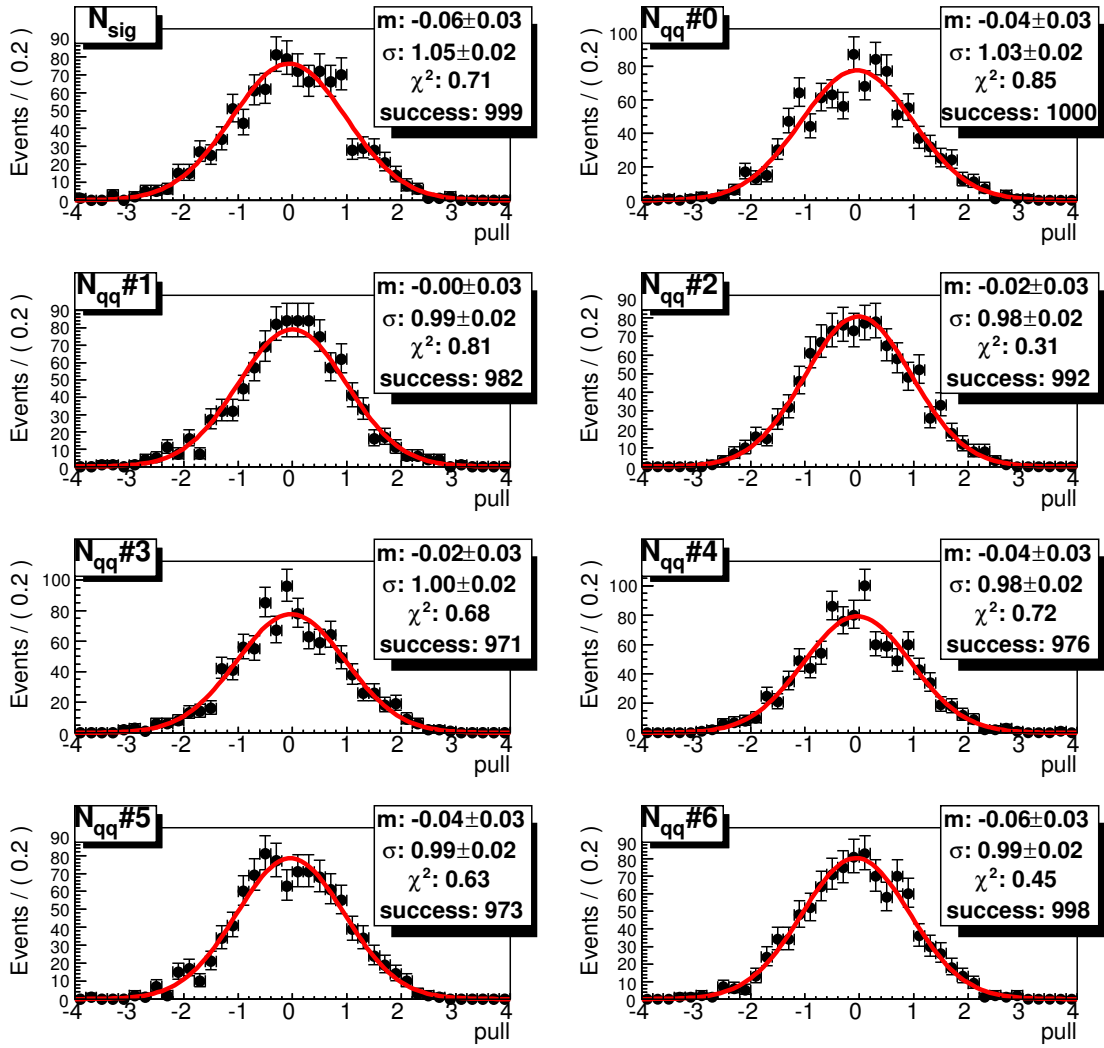


Figure 6.25: Pull distribution of N_{sig} and N_{qq} fit results of MC (neutral $\eta \rightarrow 3\pi$ mode)

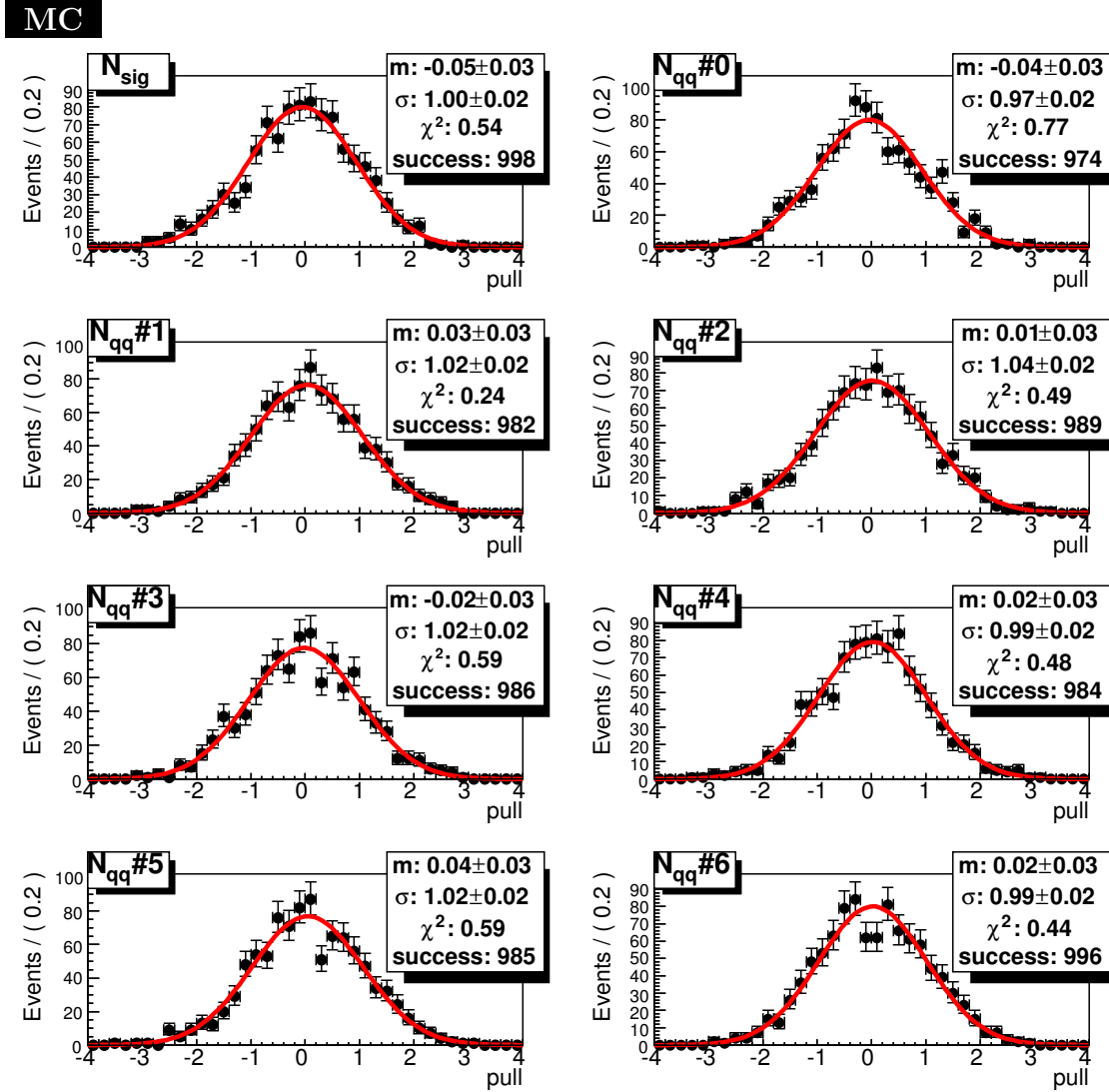


Figure 6.26: Pull distribution of N_{sig} and N_{qq} fit results of MC (charged $\eta \rightarrow 2\gamma$ mode)

MC

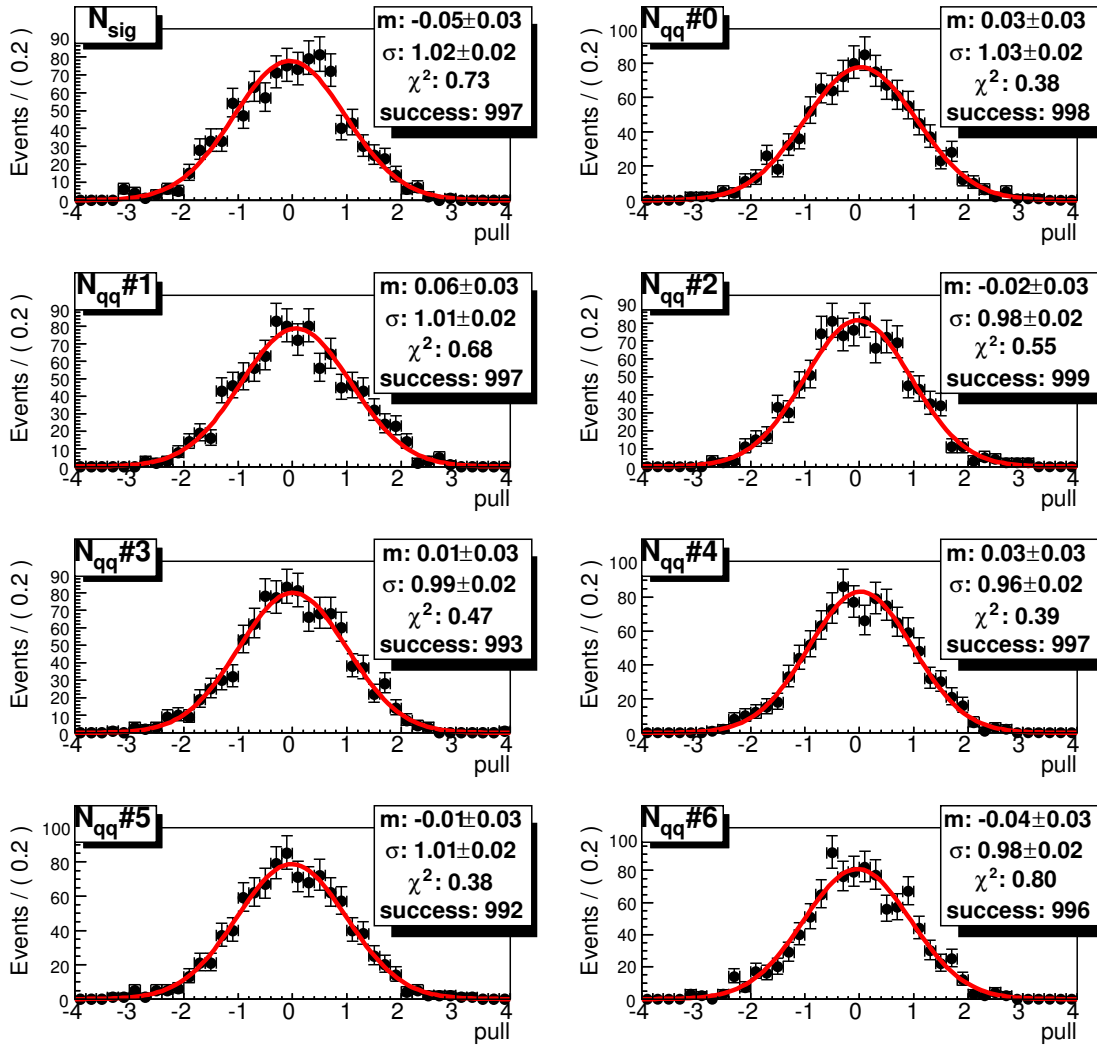


Figure 6.27: Pull distribution of N_{sig} and N_{qq} fit results of MC (charged $\eta \rightarrow 3\pi$ mode)

Chapter 7

Δt distribution fit

7.1 PDF of Δt distribution

As we discussed in Chapter 2, decay widths of $\overline{B}^0 \rightarrow X_s \gamma$ and $B^0 \rightarrow X_s \gamma$ are written as eq.(2.39 and 2.40), and we can use associated B meson with signal B to know its flavor at $\Delta t = 0$. We call a B meson which is used for reconstruction B_{rec} and a B meson used for flavor tagging B_{tag} .

When we construct realistic PDF of Δt distribution, we have to consider

- Possibility of wrongly tagged B meson flavor
- Resolution of Δt
- Contamination of BG events

These things are discussed in this section. ¹

7.1.1 Possibility of wrongly tagged B meson flavor

If we want to know about flavor of B_{rec} at $t = 0$, we have to know whether B_{tag} is B^0 or not B^0 . In order to answer this question, following particle from B_{tag} are useful:

- high energy lepton and pion from W^- of $b \rightarrow cW^-$ decays,
- non-high energy lepton and slow pion from W^+ of $b \rightarrow c \rightarrow sW^+$ decays and
- strange hadron like $\Lambda(\rightarrow p\pi^-)$, K^- from s of $b \rightarrow c \rightarrow sW^+$ decays.

We used “multi dimensional likelihood method” which estimates fraction of B^0 and \overline{B}^0 in a bin region of multi dimensional space consists of information of these tracks like charge or momentum of them. Then, flavor of B_{tag} and wrong tag fraction are obtained. Detailed discussion can be seen at elsewhere [15].

¹ If you are a member of Belle experiment, I recommend you to read BN#1326 also, because it has plenty of reference to inner document.

Let's define w_{B^0} ($w_{\overline{B^0}}$) is a probability of wrongly tagging $B_{\text{tag}} = \overline{B^0}$ (B^0) event as $B_{\text{tag}} = B^0$ ($\overline{B^0}$), i.e. $B_{\text{rec}} = B^0$ ($\overline{B^0}$) event as $B_{\text{rec}} = \overline{B^0}$ (B^0). Number of events $N_{\overline{B^0} \rightarrow X_s \gamma}$ and $N_{B^0 \rightarrow X_s \gamma}$ are

$$\begin{aligned}
N_{\overline{B^0} \rightarrow X_s \gamma}(\Delta t) &= (\text{Events from } \overline{B^0} \text{ truly}) + (\text{Contamination from } B^0) \\
&\propto e^{-|\Delta t|/\tau} \left[(1 - w_{B^0}) \{1 + (\mathcal{A} \cos(\Delta m \Delta t) + \mathcal{S} \sin(\Delta m \Delta t))\} \right. \\
&\quad \left. + w_{\overline{B^0}} \{1 - (\mathcal{A} \cos(\Delta m \Delta t) + \mathcal{S} \sin(\Delta m \Delta t))\} \right] \\
&= e^{-|\Delta t|/\tau} \left[(1 - w_{B^0} + w_{\overline{B^0}}) + (1 - w_{B^0} - w_{\overline{B^0}}) (\mathcal{A} \cos(\Delta m \Delta t) + \mathcal{S} \sin(\Delta m \Delta t)) \right] \\
&= e^{-|\Delta t|/\tau} \left[(1 - \Delta w) + (1 - 2w) \{ \mathcal{A} \cos(\Delta m \Delta t) + \mathcal{S} \sin(\Delta m \Delta t) \} \right] \quad (7.1)
\end{aligned}$$

and

$$\begin{aligned}
N_{B^0 \rightarrow X_s \gamma}(\Delta t) &= (\text{Events from } B^0 \text{ truly}) + (\text{Contamination from } \overline{B^0}) \\
&\propto e^{-|\Delta t|/\tau} \left[(1 - w_{\overline{B^0}}) \{1 - (\mathcal{A} \cos(\Delta m \Delta t) + \mathcal{S} \sin(\Delta m \Delta t))\} \right. \\
&\quad \left. + w_{B^0} \{1 + (\mathcal{A} \cos(\Delta m \Delta t) + \mathcal{S} \sin(\Delta m \Delta t))\} \right] \\
&= e^{-|\Delta t|/\tau} \left[(1 - w_{\overline{B^0}} + w_{B^0}) - (1 - w_{\overline{B^0}} - w_{B^0}) (\mathcal{A} \cos(\Delta m \Delta t) + \mathcal{S} \sin(\Delta m \Delta t)) \right] \\
&= e^{-|\Delta t|/\tau} \left[(1 + \Delta w) - (1 - 2w) \{ \mathcal{A} \cos(\Delta m \Delta t) + \mathcal{S} \sin(\Delta m \Delta t) \} \right]. \quad (7.2)
\end{aligned}$$

Here, we defined Δw and w as

$$\Delta w \equiv w_{B^0} - w_{\overline{B^0}} \quad \text{and} \quad (7.3)$$

$$w \equiv (w_{B^0} + w_{\overline{B^0}})/2. \quad (7.4)$$

If we combine eq.(7.1) and (7.2) using flavor of B_{tag} q , it can be written as

$$N(\Delta t) = e^{-|\Delta t|/\tau_B} \left[(1 - q \Delta w) + q(1 - 2w) \{ \mathcal{A} \cos(\Delta m \Delta t) + \mathcal{S} \sin(\Delta m \Delta t) \} \right]. \quad (7.5)$$

Here, $q = +1$ (-1) indicates B_{tag} is tagged as B^0 ($\overline{B^0}$) and B_{rec} is tagged as $\overline{B^0}$ (B^0) at $t = 0$. Wrong tag fraction and its differences, w and Δw used in this analysis are listed on Table.7.1 and 7.2.

Table 7.1: Wrong tag fraction and its difference between B^0 and \overline{B}^0 (MC)

	w (SVD1)	w (SVD2)	Δw (SVD1)	Δw (SVD2)
qr bin #0	0.5	0.5	0.	0.
qr bin #1	0.4208	0.4122	0.0583	0.0041
qr bin #2	0.3003	0.3078	0.0057	0.0103
qr bin #3	0.2193	0.2128	-0.0393	-0.0048
qr bin #4	0.1546	0.1499	0.0047	0.0015
qr bin #5	0.0916	0.0913	-0.0119	0.0144
qr bin #6	0.0229	0.0219	-0.0059	0.0019

Table 7.2: Wrong tag fraction and its difference between B^0 and \overline{B}^0 (real data)

	w (SVD1)	w (SVD2)	Δw (SVD1)	Δw (SVD2)
qr bin #0	0.5	0.5	0.	0.
qr bin #1	0.4189 ^{+0.0189} _{-0.0060}	0.4188 ^{+0.0041} _{-0.0036}	0.0570 ^{+0.0089} _{-0.0176}	-0.0088 ^{+0.0039} _{-0.0039}
qr bin #2	0.3299 ^{+0.0109} _{-0.0064}	0.3193 ^{+0.0032} _{-0.0028}	0.0126 ^{+0.0116} _{-0.0091}	0.0104 ^{+0.0035} _{-0.0036}
qr bin #3	0.2339 ^{+0.0282} _{-0.0077}	0.2229 ^{+0.0036} _{-0.0035}	-0.0148 ^{+0.0192} _{-0.0100}	-0.0109 ^{+0.0041} _{-0.0042}
qr bin #4	0.1706 ^{+0.0068} _{-0.0067}	0.1632 ^{+0.0033} _{-0.0042}	0.0006 ^{+0.0090} _{-0.0089}	-0.0186 ^{+0.0042} _{-0.0046}
qr bin #5	0.0998 ^{+0.0536} _{-0.0087}	0.1041 ^{+0.0032} _{-0.0037}	0.0089 ^{+0.0093} _{-0.0199}	0.0017 ^{+0.0040} _{-0.0039}
qr bin #6	0.0229 ^{+0.0043} _{-0.0065}	0.0251 ^{+0.0021} _{-0.0031}	0.0047 ^{+0.0057} _{-0.0064}	-0.0036 ^{+0.0024} _{-0.0024}

7.1.2 Resolution of Δt

In the Belle analysis, we consider four types of components.

- Detector resolution with B_{rec} vertex reconstruction ($R_{\text{det(rec)}}$).
- Detector resolution with B_{tag} vertex reconstruction ($R_{\text{det(tag)}}$).
- Contamination of non-primary tracks in B_{tag} vertexing (R_{np}).
- Caused by kinematic energy generated when $\Upsilon(4S)$ decay to B meson pairs (R_{k}).

We can describe total resolution function $R(\Delta t)$ as

$$R(\Delta t) = R_{\text{det(rec)}}(\Delta t) \otimes R_{\text{det(tag)}}(\Delta t) \otimes R_{\text{np}}(\Delta t) \otimes R_{\text{k}}(\Delta t). \quad (7.6)$$

Here, we used “ \otimes ” as convolution, i.e.

$$f(x) \otimes g(x) \equiv \int_{-\infty}^{+\infty} f(x') \cdot g(x - x') dx'. \quad (7.7)$$

Detailed discussion can be seen at elsewhere [16].

Resolution related to B_{rec}

$R_{\text{det(rec)}}$ is written as

$$R_{\text{det(rec)}}(\delta z) = (1 - f_{\text{tail}})G(\delta z; \sigma_{\text{main}}) + f_{\text{tail}}G(\delta z; \sigma_{\text{tail}}), \quad (7.8)$$

using

$$G(x; \sigma) = \frac{1}{\sqrt{2\pi}\sigma} \exp\left[-\frac{x^2}{2\sigma^2}\right]. \quad (7.9)$$

In case that vertex reconstruction is done from multiple tracks ($\eta \rightarrow 3\pi$ and both charged pions are used),

$$f_{\text{tail}} = 0 \quad \text{and} \quad (7.10)$$

$$\sigma_{\text{main}} = (s_{\text{rec},0} + s_{\text{rec},1}\xi)\sigma_z. \quad (7.11)$$

In case that vertex reconstruction is done from single track ($\eta \rightarrow 3\pi$ and only one charged pion is used),

$$\sigma_{\text{main}} = s_{\text{main}}\sigma_z \quad \text{and} \quad (7.12)$$

$$\sigma_{\text{tail}} = s_{\text{tail}}\sigma_z. \quad (7.13)$$

Here, σ_z is event by event error of the vertex reconstruction of z-component. ξ is defined as

$$\xi \equiv \frac{\chi_{\text{tracks}}^2}{\text{ndf}} \quad (7.14)$$

with

$$\chi_{\text{tracks}}^2 = \sum_i^{\text{tracks}} \delta \mathbf{h}_i^T V_i \delta \mathbf{h}_i \quad (7.15)$$

$$\text{ndf} = \begin{cases} 2n_{\text{tracks}} - 2 & (\text{using charged tracks}) \\ 3n_{\text{tracks}} - 2 & (\text{using } K_S \text{ tracks}). \end{cases} \quad (7.16)$$

Here, $\delta \mathbf{h}^T \equiv (d_\rho, \phi_0, \kappa, d_z, \tan \lambda)$ is helix parameter list, and V_i is an inverse matrix of the i -th track's error matrix. Be aware that this definition is different from [16]'s one (eq.(1)). It is said that ξ defined as above has less decay mode dependence than [16]'s.

In case that vertex reconstruction is done by single K_S track ($\eta \rightarrow 2\gamma$ and K_S is used for vertexing), $\text{ndf} = 1$ and ξ can be used for σ_{main} calculation. Same formula to eq.(7.11) is used. If each pion's innermost SVD hit layer is different, σ_{main} have to be widen from eq.(7.11) as

$$\sigma_{\text{main}} \rightarrow \begin{cases} \sigma_{\text{main}} \times S_{\text{dia},0} & (\text{if } l_{\text{flight}} < 2[\text{cm}]) \\ \sigma_{\text{main}} \times S_{\text{dia},0} \{1 + S_{\text{dia},1} (l_{\text{flight}} - 2[\text{cm}])\} & (\text{if } l_{\text{flight}} \geq 2[\text{cm}]). \end{cases} \quad (7.17)$$

Here, l_{flight} is flight length of the K_S . Parameter sets discussed above are listed on Table.7.3 and 7.4.

Table 7.3: dt resolution parameters for $R_{\text{det(rec)}}$ (MC study)

param.	SVD1	SVD2
For multi track $R_{\text{det(rec)}}$		
$S_{\text{rec},0}$	0.9626	0.9271
$S_{\text{rec},1}$	0.1986	0.2104
For single track $R_{\text{det(rec)}}$		
$S_{\text{rec},\text{main}}$	1.1098	1.0530
$S_{\text{rec},\text{tail}}$	-	4.3206
$f_{\text{rec},\text{tail}}$	0.0000	0.0707
For $R_{\text{det(rec)}}$ using K_S		
$S_{\text{rec},0}$	0.9698	0.9403
$S_{\text{rec},1}$	0.0833	0.0728
$S_{\text{dia},0}$	1.1517	1.3341
$S_{\text{dia},1}$	0.3213	0.0

Table 7.4: dt resolution parameters for $R_{\text{det(rec)}}$ (real data)

param.	SVD1	SVD2
For multi track $R_{\text{det(rec)}}$		
$S_{\text{rec},0}$	$0.705^{+0.171}_{-0.107}$	$0.808^{+0.279}_{-0.148}$
$S_{\text{rec},1}$	$0.212^{+0.043}_{-0.047}$	$0.233^{+0.069}_{-0.059}$
For single track $R_{\text{det(rec)}}$		
$S_{\text{rec},\text{main}}$	$0.980^{+0.278}_{-0.036}$	$1.015^{+0.441}_{-0.039}$
$S_{\text{rec},\text{tail}}$	-	$3.663^{+3.617}_{-0.391}$
$f_{\text{rec},\text{tail}}$	0.0	$0.111^{+0.015}_{-0.039}$
For $R_{\text{det(rec)}}$ using K_S		
$S_{\text{rec},0}$	$1.398^{+0.320}_{-0.396}$	$0.999^{+0.279}_{-0.168}$
$S_{\text{rec},1}$	$0.032^{+0.128}_{-0.032}$	$0.075^{+0.070}_{-0.053}$
$S_{\text{dia},0}$	$1.142^{+0.319}_{-0.679}$	$1.133^{+0.197}_{-0.114}$
$S_{\text{dia},1}$	$0.321^{+0.040}_{-0.037}$	0.0

Resolution related to B_{tag}

Definition of $R_{\text{det(tag)}}$ is same as $R_{\text{det(rec)}}$. However, it is different that the way to select tracks which can be used for vertex reconstruction. All tracks but used for B_{rec} reconstruction are used for vertexing. They also include non-primary tracks like D which makes

vertex resolution worse. For the sake of excluding these non-primary tracks, tracks which increase vertexing χ^2 are rejected up to the χ^2 become smaller than 20. Here, since high energy lepton is likely to be generated by $b \rightarrow cW, W \rightarrow l\nu$ chain, it is not rejected exceptionally. This lepton is called as ‘‘tag lepton’’ because it is effective for B meson flavor tagging. As this cut cannot remove all of non-primary tracks, resolution of tag side B vertex is expressed as a convolution of $R_{\text{det}(\text{tag})}$ and R_{np} .

$$R_{\text{det}(\text{tag})} \otimes R_{\text{np}} = R_{\text{det}(\text{tag}),\text{main}} \otimes R_{\text{np},\text{main}} + R_{\text{det}(\text{tag}),\text{tail}} \otimes R_{\text{np},\text{tail}} \quad (7.18)$$

Here,

$$R_{\text{det}(\text{tag}),\text{main}} = (1 - f_{\text{tail}}) G(\delta z; \sigma_{\text{main}}) \quad (7.19)$$

$$R_{\text{det}(\text{tag}),\text{tail}} = f_{\text{tail}} G(\delta z; \sigma_{\text{tail}}) \quad (7.20)$$

$$R_{\text{np},\text{main}/\text{tail}} = f_{\delta} \delta(\delta z) + (1 - f_{\delta}) \{ f_p E_p(\delta z; \tau_{\text{np}}^p) + (1 - f) E_n(\delta z; \tau_{\text{np}}^n) \} \\ \text{(for single track)} \quad (7.21)$$

$$R_{\text{np},\text{main}/\text{tail}} = (1 - f_n) \{ f_d \delta(\delta z) + (1 - f_d) E_p(\delta z; \tau_{\text{np}}^p) \} + f_n E_n(\delta z; \tau_{\text{np}}^n) \\ \text{(for multiple track)} \quad (7.22)$$

$$f_d = f_d^0 + f_d^{1s} \sigma'_z + f_d^{1h} \xi' + f_d^{1sh} \sigma'_z \xi' \quad (7.23)$$

$$\sigma'_z = \begin{cases} \sigma_z & \text{(if } \sigma_z < 0.75 \text{ [ps])} \\ 0.75 \text{ [ps]} & \text{(if } \sigma_z \geq 0.75 \text{ [ps])} \end{cases} \quad (7.24)$$

$$\xi' = \begin{cases} \xi & \text{(if } \xi < 0.35) \\ 0.35 & \text{(if } \xi \geq 0.35) \end{cases} \quad (7.25)$$

and

$$E_p(x; \tau) = \begin{cases} \frac{1}{\tau} \exp\left[-\frac{x}{\tau}\right] & \text{(if } x > 0) \\ 0 & \text{(if } x \leq 0) \end{cases} \quad (7.26)$$

$$E_n(x; \tau) = \begin{cases} 0 & \text{(if } x > 0) \\ \frac{1}{\tau} \exp\left[+\frac{x}{\tau}\right] & \text{(if } x \leq 0) \end{cases} \quad (7.27)$$

$$\tau_{\text{np}}^{p,n} = S_{\text{np}} \tau_{p,n}^0 \\ \text{(for single track)} \quad (7.28)$$

$$\tau_{\text{np}}^{p,n} = S_{\text{np}} (\tau_{p,n}^0 + \tau_{p,n}^{1s} \sigma_z + \tau_{p,n}^{1h} \xi + \tau_{p,n}^{1sh} \sigma_z \xi) \\ \text{(for multiple track)} \quad (7.29)$$

f_{δ} , f_d , f_p and $\tau_{p,n}^{0,1}$ are divided into two groups whether vertex is reconstructed by single track or multiple tracks. Moreover, f_{δ} and f_d are divided into two groups whether tracks contains tag lepton or not. This is because tag lepton is exempt from χ^2 cut, and thus, it has larger possibility of coming from non-primary particle. Parameter sets discussed above are listed on Table.7.5 and 7.6.

Table 7.5: dt resolution parameters for $R_{\text{det}(\text{tag})}$ and R_{np} (MC study)

param.	SVD1	SVD2
For multi track $R_{\text{det}(\text{tag})}$		
$S_{\text{tag},0}$	0.7291	0.8211
$S_{\text{tag},1}$	0.1719	0.1408
For single track $R_{\text{det}(\text{tag})}$		
$S_{\text{tag},\text{main}}$	1.1098	1.0530
$S_{\text{tag},\text{tail}}$	-	4.3206
$f_{\text{tag},\text{tail}}$	0.0000	0.0707
For single track R_{np}		
S_{np}	1.0000	1.0000
f_{δ} w/ taglep sgl	0.7817	0.7738
f_{δ} w/o taglep sgl	1.0000	1.0000
f_p	0.8186	0.8013
τ_p^0	1.8477	1.6260
τ_n^0	2.0411	0.9181
For multi track R_{np}		
S_{np}	1.0000	1.0000
f_d^0 w/ taglep mul	0.4664	0.5601
f_d^0 w/o taglep mul	0.6372	0.7507
f_d^{1s}	0.2706	0.1569
f_d^{1h}	-0.2204	-0.2021
f_d^{1sh}	0.2228	0.2324
f_n	0.1233	0.1224
τ_p^0	-0.0052	0.0387
τ_p^{1s}	0.7168	0.7653
τ_p^{1h}	-0.0297	-0.0263
τ_p^{1sh}	0.2515	0.3215
τ_n^0	0.0452	0.0829
τ_n^{1s}	0.5152	0.5343
τ_n^{1h}	-0.0783	-0.0301
τ_n^{1sh}	0.4305	0.3899

Table 7.6: dt resolution parameters for $R_{\text{det}(\text{tag})}$ and R_{np} (real data)

param.	SVD1	SVD2
For multi track $R_{\text{det}(\text{tag})}$		
$S_{\text{tag},0}$	$0.484^{+0.282}_{-0.073}$	$0.644^{+0.386}_{-0.072}$
$S_{\text{tag},1}$	$0.237^{+0.037}_{-0.056}$	$0.229^{+0.027}_{-0.052}$
For single track $R_{\text{det}(\text{tag})}$		
$S_{\text{tag},\text{main}}$	$0.980^{+0.278}_{-0.036}$	$1.015^{+0.441}_{-0.039}$
$S_{\text{tag},\text{tail}}$	-	$3.663^{+3.617}_{-0.391}$
$f_{\text{tag},\text{tail}}$	0.000	$0.111^{+0.015}_{-0.039}$
For single track R_{np}		
S_{np}	$1.057^{+0.117}_{-0.163}$	$1.014^{+0.075}_{-0.164}$
f_{δ} w/ taglep sgl	$0.7817^{+0.0103}_{-0.0108}$	$0.7738^{+0.0082}_{-0.0086}$
f_{δ} w/o taglep sgl	1.000	1.000
f_p	$0.8186^{+0.0173}_{-0.0185}$	$0.8013^{+0.0172}_{-0.0177}$
τ_p^0	$1.8477^{+0.0851}_{-0.0806}$	$1.6260^{+0.0500}_{-0.0489}$
τ_n^0	$2.0411^{+0.2773}_{-0.2432}$	$0.9181^{+0.0846}_{-0.0782}$
For multi track R_{np}		
S_{np}	$1.057^{+0.117}_{-0.163}$	$1.014^{+0.075}_{-0.164}$
f_d^0 w/ taglep mul	$0.4664^{+0.0401}_{-0.0411}$	$0.5601^{+0.0129}_{-0.0125}$
f_d^0 w/o taglep mul	$0.6372^{+0.0399}_{-0.0408}$	$0.7507^{+0.0129}_{-0.0126}$
f_d^{1s}	$0.2706^{+0.0704}_{-0.0703}$	$0.1569^{+0.0279}_{-0.0291}$
f_d^{1h}	$-0.2204^{+0.0158}_{-0.0153}$	$-0.2021^{+0.0047}_{-0.0048}$
f_d^{1sh}	$0.2228^{+0.0292}_{-0.0300}$	$0.2324^{+0.0119}_{-0.0115}$
f_n	$0.1233^{+0.0073}_{-0.0073}$	$0.1224^{+0.0026}_{-0.0026}$
τ_p^0	$-0.0052^{+0.0154}_{-0.0154}$	$0.0387^{+0.0056}_{-0.0054}$
τ_p^{1s}	$0.7168^{+0.0388}_{-0.0386}$	$0.7653^{+0.0202}_{-0.0205}$
τ_p^{1h}	$-0.0297^{+0.0054}_{-0.0053}$	$-0.0263^{+0.0017}_{-0.0017}$
τ_p^{1sh}	$0.2515^{+0.0144}_{-0.0144}$	$0.3215^{+0.0072}_{-0.0071}$
τ_n^0	$0.0452^{+0.0270}_{-0.0268}$	$0.0829^{+0.0093}_{-0.0093}$
τ_n^{1s}	$0.5152^{+0.0638}_{-0.0626}$	$0.5343^{+0.0311}_{-0.0309}$
τ_n^{1h}	$-0.0783^{+0.0132}_{-0.0131}$	$-0.0301^{+0.0043}_{-0.0043}$
τ_n^{1sh}	$0.4305^{+0.0344}_{-0.0332}$	$0.3899^{+0.0159}_{-0.0157}$

Resolution caused by kinematic assumption

R_k can be written as

$$R_k(x) = \begin{cases} E_p \left(x - \left\{ \left(\frac{E_B}{m_B} - 1 \right) \Delta t_{\text{true}} + \frac{p_B \cos \theta_B}{\beta_\Upsilon m_B} |\Delta t_{\text{true}}| \right\}; \right. \\ \quad \left. \left| \frac{p_B \cos \theta_B}{\beta_\Upsilon m_B} \right| \tau_B \right) & (\text{if } \cos \theta_B > 0) \\ \delta \left(x - \left(\frac{E_B}{m_B} - 1 \right) \Delta t_{\text{true}} \right) & (\text{if } \cos \theta_B = 0) \\ E_n \left(x - \left\{ \left(\frac{E_B}{m_B} - 1 \right) \Delta t_{\text{true}} + \frac{p_B \cos \theta_B}{\beta_\Upsilon m_B} |\Delta t_{\text{true}}| \right\}; \right. \\ \quad \left. \left| \frac{p_B \cos \theta_B}{\beta_\Upsilon m_B} \right| \tau_B \right) & (\text{if } \cos \theta_B < 0), \end{cases}$$

and there is no parameter dependent on SVD version or number of tracks used for vertex reconstruction. E_p and E_n are defined at eq.(7.26) and (7.27). β_Υ is the velocity of the $\Upsilon(4S)$. E_B and p_B are the B meson's energy and momentum in center of mass system, respectively. The values of them are listed on Table.7.7.

Table 7.7: Useful values for R_k

param.	values	
β_Υ	~ 0.391	$(E_{e^-} - E_{e^+}) / (E_{e^-} + E_{e^+})$
E_B	~ 5.292 [GeV]	$m_{\Upsilon(4S)} / 2$
p_B	~ 0.340 [GeV]	$\sqrt{E_B^2 - m_B^2}$

Quality requirements of vertex reconstruction

For Δt distribution analysis, we use only good quality events. Following conditions are required:

- $\xi < 50$ (7.30)

- $\begin{cases} \sigma_z < 500[\mu\text{m}] & (\text{for single charged or } K_S \text{ track}) \\ \sigma_z < 200[\mu\text{m}] & (\text{for multiple charged track}) \end{cases}$ (7.31)

- $|\Delta t| < 70[\text{ps}]$. (7.32)

7.1.3 Contamination of BG events

In addition to signal events, we have to consider about background events. We calculated signal and BG fraction event-by-event with $\Delta E - M_{bc} - NB'$ 3D fit. (Further description is written in Chapter 6.) Each event component is added and weighted by this fraction. Then, Δt PDF can be written as

$$P(\Delta t, q) = (1 - f_{ol})\{f_{sig}P_{sig}(\Delta t, q) + f_{qq}P_{qq}(\Delta t) + f_{bb}P_{bb}(\Delta t) + f_{rare}P_{rare}(\Delta t)\} + f_{ol}P_{ol}(\Delta t). \quad (7.33)$$

Here, $f_{sig} + f_{qq} + f_{bb} + f_{rare} = 1$.

7.1.4 PDF shape

Signal PDF

As we discussed above, signal PDF can be written as convolution of eq.(7.5) and (7.6),

$$P_{sig}(\Delta t) = R(\Delta t) \otimes \left[e^{-\Delta t/\tau_B} \left[(1 - q\Delta w) + q(1 - 2w) \{ \mathcal{A}\cos(\Delta m\Delta t) + \mathcal{S}\sin(\Delta m\Delta t) \} \right] \right]. \quad (7.34)$$

qq BG PDF

P_{qq} shape can be decided by fit on ‘‘sideband region’’ which is dominated by qq BG events. Sideband region is following region as shown in Fig.7.1 to 7.4. It can be described as

$$5.20 < M_{bc}[\text{GeV}] < 5.29 \quad (7.35)$$

$$M_{bc}[\text{GeV}] < 5.245 + \frac{0.045}{0.5}\Delta E[\text{GeV}] \quad (7.36)$$

$$-0.5 < \Delta E[\text{GeV}] < 0.5. \quad (7.37)$$

About 95% of events in this region are expected to be qq BGs and the number of expected events are listed in Table. 7.8 to 7.11. When we apply Δt distribution fit, we assume there are only qq BG events, i.e. $f_{qq} = 1$ and $f_{sig} = f_{bb} = f_{rare} = 0$.

Because of the low statistics, we do not confirm whether fit results of sideband region and signal region are consistent using MC simulation. In addition, because too many fit parameter prevent fit from converging, we reduced fit parameters from Belle’s standard fit, eq.(27) of [16]. We added following conditions to it.

$$f_{\delta}^{\text{multi}} = f_{\delta}^{\text{single}} (= f_{\delta}) \quad (7.38)$$

$$f_{\text{tail}}^{\text{multi}} = f_{\text{tail}}^{\text{single}} (= f_{\text{tail}}) \quad (7.39)$$

$$\sigma_{\text{tail}}^{\text{multi}} = \sigma_{\text{tail}}^{\text{single}} (= \sigma_{\text{tail}}) \quad (7.40)$$

$$\sigma_{\text{main}}^{\text{multi}} = \sigma_{\text{main}}^{\text{single}} (= \sigma_{\text{main}}) \quad (7.41)$$

$$\mu_{\delta} = \mu_{\text{life}} (= \mu) \quad (7.42)$$

$$(7.43)$$

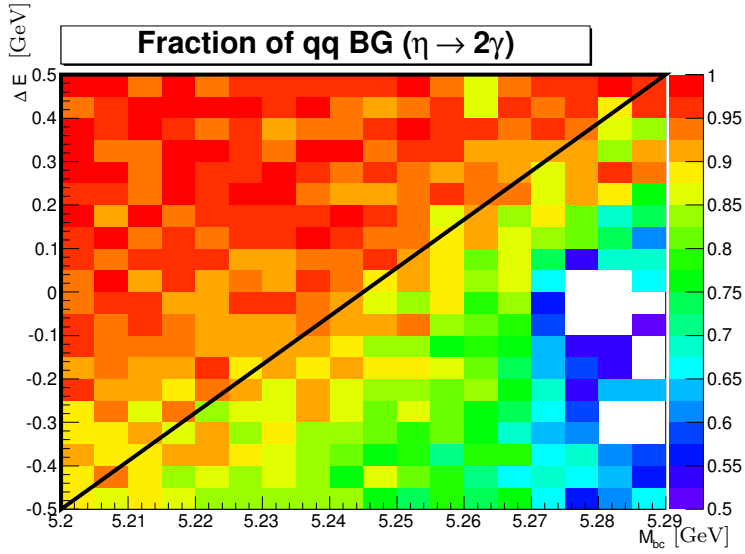


Table 7.8: qq BG fraction in sideband region (neutral $\eta \rightarrow 2\gamma$ mode)

<i>qq</i> BG	1618.0
Signal	2.2
<i>BB</i> BG	50.0
rare <i>B</i> BG	5.4
rad <i>B</i> BG	43.1
Fraction	94%

Figure 7.1: qq BG fraction expected by MC (neutral $\eta \rightarrow 2\gamma$ mode). Enclosed area by black bold line is sideband region.

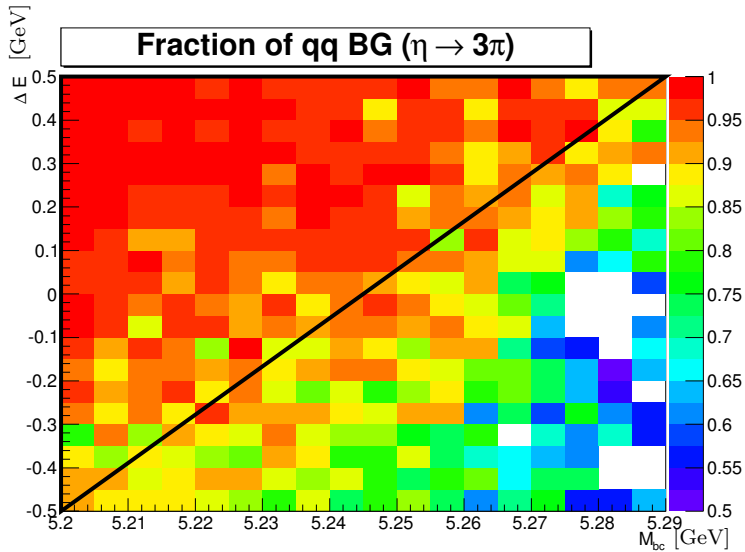


Table 7.9: qq BG fraction in sideband region (neutral $\eta \rightarrow 3\pi$ mode)

<i>qq</i> BG	848.8
Signal	0.1
<i>BB</i> BG	12.7
rare <i>B</i> BG	2.8
rad <i>B</i> BG	30.2
Fraction	95%

Figure 7.2: qq BG fraction expected by MC (neutral $\eta \rightarrow 3\pi$ mode)

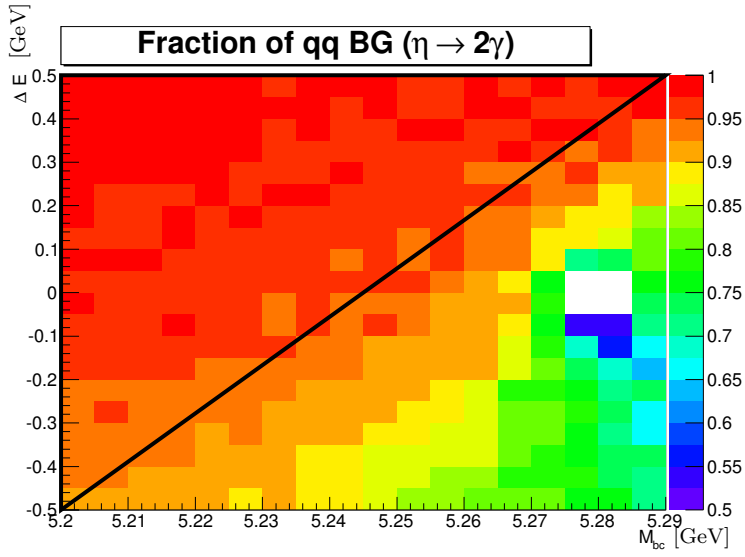


Table 7.10: qq BG fraction in sideband region (charged $\eta \rightarrow 2\gamma$ mode)

qq BG	12185.5
Signal	7.7
BB BG	246.3
rare B BG	27.3
rad B BG	184.7
Fraction	96%

Figure 7.3: qq BG fraction expected by MC (charged $\eta \rightarrow 2\gamma$ mode)

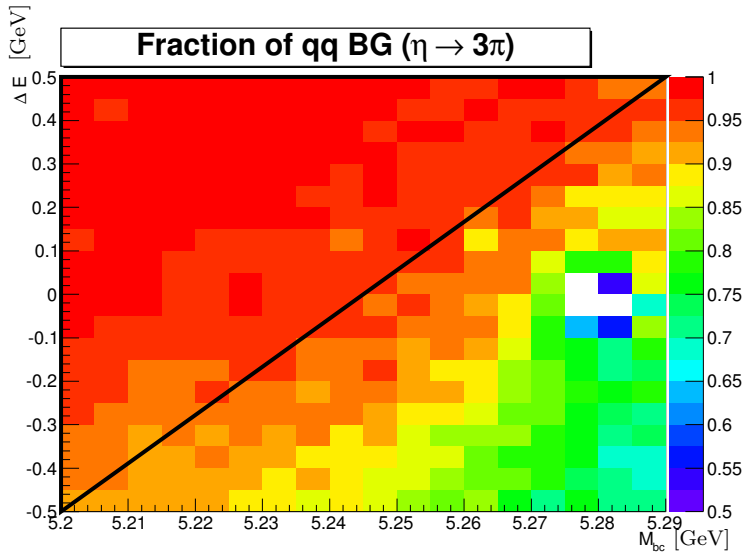


Table 7.11: qq BG fraction in sideband region (charged $\eta \rightarrow 3\pi$ mode)

qq BG	5811.0
Signal	0.6
BB BG	54.2
rare B BG	13.8
rad B BG	119.9
Fraction	97%

Figure 7.4: qq BG fraction expected by MC (charged $\eta \rightarrow 3\pi$ mode)

Then, $P_{qq}(\Delta t)$ becomes

$$P_{qq}(\Delta t) = R_{qq}(\Delta t) \otimes \left[f_\delta \cdot \delta(\Delta t - \mu) + (1 - f_\delta) \frac{1}{2\tau_{bg}} \exp \left[-\frac{|\Delta t - \mu|}{\tau_{bg}} \right] \right]. \quad (7.44)$$

Here, R_{qq} is different from R used in other PDFs. It is defined as

$$R_{qq}(\Delta t) = (1 - f_{tail}) \frac{1}{\sqrt{2\pi}\sigma_{\text{main}}\sqrt{\sigma_{\text{rec}}^2 + \sigma_{\text{tag}}^2}} \exp \left[-\frac{\Delta t^2}{2\sigma_{\text{main}}^2(\sigma_{\text{rec}}^2 + \sigma_{\text{tag}}^2)} \right] + f_{tail} \frac{1}{\sqrt{2\pi}\sigma_{\text{tail}}\sqrt{\sigma_{\text{rec}}^2 + \sigma_{\text{tag}}^2}} \exp \left[-\frac{\Delta t^2}{2\sigma_{\text{tail}}^2(\sigma_{\text{rec}}^2 + \sigma_{\text{tag}}^2)} \right]. \quad (7.45)$$

σ_{rec} and σ_{tag} are errors of vertex reconstruction of B_{rec} and B_{tag} .

***BB*, rare *B* and rad *B* BG PDF**

BB, rare *B* and rad *B* BG PDFs are prepared from fitting $P_{\text{bb/rare/rad}}$ to distribution of GEANT based MC in fit region. $P_{\text{bb/rare/rad}}$ are defined as

$$P_{\text{bb/rare/rad}}(\Delta t) = R(\Delta t) \otimes \left[\exp \left[-\frac{\Delta t}{\tau_{\text{eff}}} \right] \right]. \quad (7.46)$$

τ_{bb} , τ_{rare} and τ_{rad} are listed on Tab.7.12. Their amounts N_{BB} , N_{rare} and N_{rad} are also fixed to expected value from GEANT based MC.

Table 7.12: effective life of *BB* BG, rare *B* and rad *B* BG decided by MC study

effective life [ps] (neutral mode)	τ_{bb}	τ_{rare}	τ_{rad}
$\eta \rightarrow 2\gamma$ mode	$1.33^{+0.08}_{-0.07}$	$1.35^{+0.07}_{-0.07}$	$1.35^{+0.03}_{-0.03}$
$\eta \rightarrow 3\pi$ mode	$0.86^{+0.08}_{-0.08}$	$1.13^{+0.08}_{-0.07}$	$1.19^{+0.03}_{-0.03}$
effective life [ps] (charged mode)	τ_{bb}	τ_{rare}	τ_{rad}
$\eta \rightarrow 2\gamma$ mode	$1.20^{+0.03}_{-0.03}$	$1.37^{+0.03}_{-0.03}$	$1.38^{+0.01}_{-0.01}$
$\eta \rightarrow 3\pi$ mode	$0.90^{+0.04}_{-0.04}$	$1.20^{+0.04}_{-0.03}$	$1.12^{+0.01}_{-0.01}$

Outlier

Remaining long tail after considering resolution function $R(\Delta t)$ is treated as ‘‘outlier’’. PDF shape is single Gaussian with zero mean, witch fraction and width are Belle’s official one. Parameter sets for P_{ol} are summarized on Table. 7.13 and 7.14.

$$P_{\text{ol}}(\Delta t) = \exp \left[-\frac{\Delta t^2}{2\sigma_{\text{ol}}^2} \right] \quad (7.47)$$

Table 7.13: dt resolution parameters for outlier PDF (MC)

parameters	SVD1	SVD2
σ_{ol} [ps]	33.19	30.63
f_{ol} (If ntrk_tag=1)	0.0378	0.0223
f_{ol} (If ntrk_tag>1)	2.15×10^{-4}	8.84×10^{-5}

Table 7.14: dt resolution parameters for outlier PDF (real data)

parameters	SVD1	SVD2
σ_{ol} [ps]	$43.70^{+14.97}_{-4.85}$	$33.53^{+5.58}_{-9.22}$
f_{ol} (If ntrk_tag=1)	$0.0370^{+0.0065}_{-0.0108}$	$0.0273^{+0.0020}_{-0.0047}$
f_{ol} (If ntrk_tag>1)	$1.14^{+0.57}_{-0.68} \times 10^{-4}$	$1.53^{+1.02}_{-0.72} \times 10^{-4}$

7.2 Confirmation of fitter code

7.2.1 Life time fit

Taking summation of $q = +1$ nad $q = -1$, eq.(7.34) becomes

$$P_{sig}(\Delta t) = R(\Delta t) \otimes \left[e^{-\Delta t/\tau_B} \right]. \quad (7.48)$$

Other PDFs do not change since they are not dependent on q . Taking τ_B as a fit parameter and checking whether fit result is consistent to world average are good way to confirmation of the fitter code. If a resolution function is too wide, τ_B becomes shorter than real, and if the function is too narrow, τ_B becomes longer. Therefore, this fit is effective to check validity of the resolution function.

7.2.2 Life time fit with toy MC

Figure 7.5 to 7.7 shows pull distribution of 1000 times toy MC fit study. Toy MC is random number generator which use PDF from GEANT based simulation; it does not simulate detector process. When we make toy MC data, we assumed that PDF shape (including resolution function parameters) is correct. We can see significant negative biases which is smaller than statistical error. Small signal statistics is one of origin of these negative biases. Let me think about maximum likelihood fit with only one event. Assuming that the observable is t_1 , likelihood can be written as

$$\mathcal{L} = \frac{1}{\tau} \exp \left[-\frac{t_1}{\tau} \right]. \quad (7.49)$$

Its derivation becomes

$$\frac{\partial \mathcal{L}}{\partial \tau} = \frac{1}{\tau^2} \left(\frac{t_1}{\tau} - 1 \right) \exp \left[-\frac{t_1}{\tau} \right], \quad (7.50)$$

and

$$\frac{\partial \mathcal{L}}{\partial \tau} > 0 \quad (\text{when } \tau < t_1) \quad (7.51)$$

$$\frac{\partial \mathcal{L}}{\partial \tau} = 0 \quad (\text{when } \tau = t_1) \quad (7.52)$$

$$\frac{\partial \mathcal{L}}{\partial \tau} < 0 \quad (\text{when } \tau > t_1). \quad (7.53)$$

It means fit result of τ becomes t_1 . Probability of t_1 being longer and shorter than true life are e (Napier's constant) and $1 - e$ respectively. (Obviously $1 - e > e$.) This is why life time fit result with low statistics has negative biases. Figure 7.8 to 7.10 shows pull distribution of 1000 times toy MC fit study with 10 times higher signal amount. We can see that negative bias disappears.

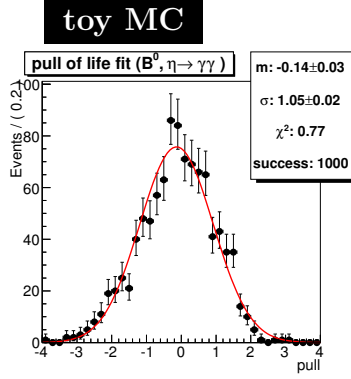


Figure 7.5: Pull distribution of life time fit with toy MC (neutral $\eta \rightarrow 2\gamma$ mode)

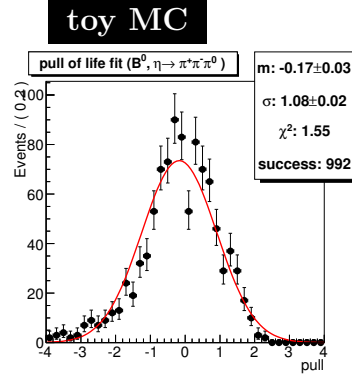


Figure 7.6: Pull distribution of life time fit with toy MC (neutral $\eta \rightarrow 3\pi$ mode)

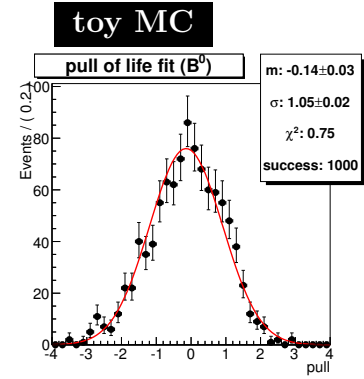


Figure 7.7: Pull distribution of life time fit with toy MC (total neutral mode)

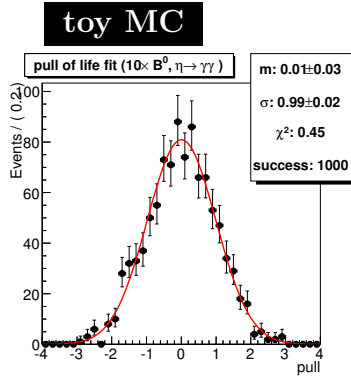


Figure 7.8: Pull distribution of life time fit with toy MC (neutral $\eta \rightarrow 2\gamma$ mode, 10 times higher N_{sig})

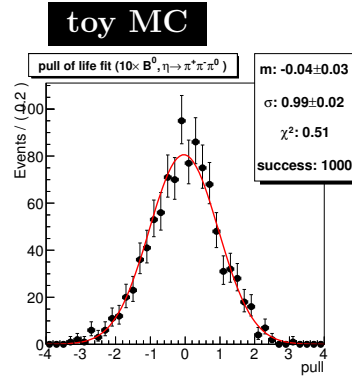


Figure 7.9: Pull distribution of life time fit with toy MC (neutral $\eta \rightarrow 3\pi$ mode, 10 times higher N_{sig})

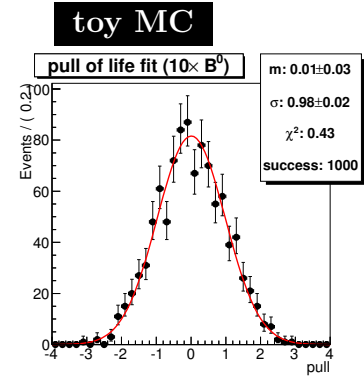


Figure 7.10: Pull distribution of life time fit with toy MC (total neutral mode, 10 times higher N_{sig})

7.2.3 Life time fit with GEANT based MC

If we want to check whether resolution function does work well, confirmation with toy MC study only is not sufficient. Figure 7.11 to 7.13 shows pull distribution of 500 times signal only GEANT based MC fit study. We executed fit with $f_{\text{sig}} = 1$. We compared signal only toy MC fit study as shown in Fig. 7.14 to 7.16. There are some discrepancies; this indicates that there may be some positive biases which is destructive to negative bias seen in toy MC. However, these differences are much smaller than statistical error. It is difficult to take into account all correlations between input variables used for life time fit by toy MC generator. This could cause such disagreement.

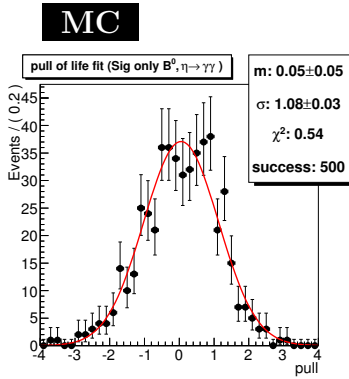


Figure 7.11: Pull distribution of life time fit with GEANT based signal MC (neutral $\eta \rightarrow 2\gamma$ mode, with signal only data)

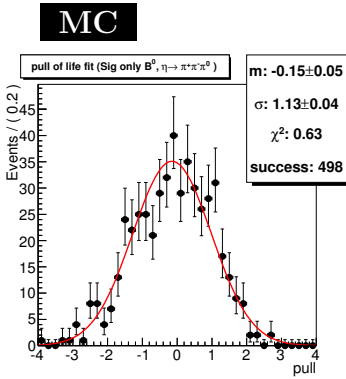


Figure 7.12: Pull distribution of life time fit with GEANT based signal MC (neutral $\eta \rightarrow 3\pi$ mode, with signal only data)

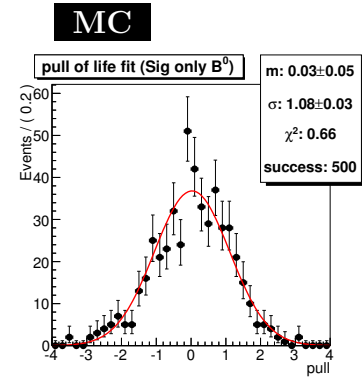


Figure 7.13: Pull distribution of life time fit with GEANT based signal MC (total neutral mode, with signal only data)

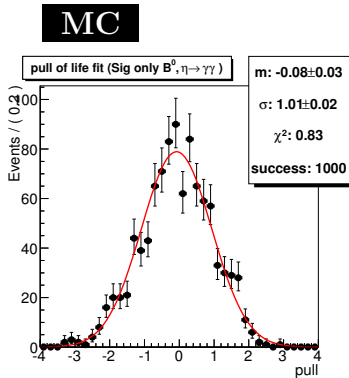


Figure 7.14: Pull distribution of life time fit with toy MC (neutral $\eta \rightarrow 2\gamma$ mode, with signal only data)

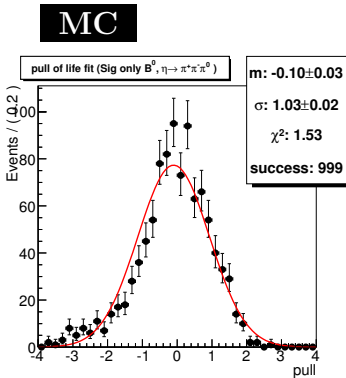


Figure 7.15: Pull distribution of life time fit with toy MC (neutral $\eta \rightarrow 3\pi$ mode, with signal only data)

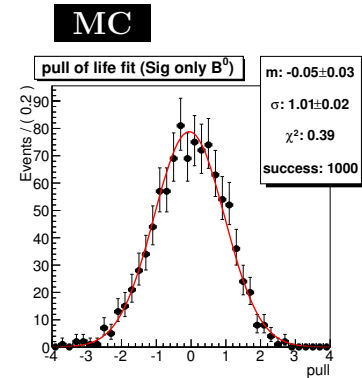


Figure 7.16: Pull distribution of life time fit with toy signal MC (total neutral mode, with signal only data)

7.2.4 Life time fit with real data

$B^\pm \rightarrow K^\pm \eta \gamma$ sample

Vertex of $\eta \rightarrow 2\gamma$ mode is reconstructed by a charged kaon track. Vertex of $\eta \rightarrow 3\pi$ mode is reconstructed by two (or one) charged pions. These life time fit can check Δt analysis using charged tracks.

Table 7.15 shows fit result of sideband fit. Table 7.16 shows fit result of life time fit. Figure 7.17 and 7.18 show Δt distributions of $\eta \rightarrow 2\gamma$ mode and $\eta \rightarrow 3\pi$ mode, respectively. Blue crosses show data. Dashed lines show BG distributions. Solid lines show Signal + BG distributions.

Table 7.15: Result of sideband fit (charged mode)

charged mode	$\eta \rightarrow 2\gamma$ mode	$\eta \rightarrow 3\pi$ mode
f_δ	$1.370^{+0.075}_{-0.071}$	$0.735^{+0.115}_{-0.093}$
f_{tail}	$-0.0167^{+0.0085}_{-0.0085}$	$-0.008^{+0.014}_{-0.014}$
σ_{main}	$1.165^{+0.017}_{-0.017}$	$1.119^{+0.030}_{-0.030}$
σ_{tail}	$23.2^{+1.7}_{-1.5}$	$4.53^{+0.86}_{-0.45}$
μ	$0.0402^{+0.0025}_{-0.0024}$	$0.085^{+0.021}_{-0.024}$
τ_{qq}	$0.692^{+0.020}_{-0.021}$	$0.516^{+0.063}_{-0.072}$

Table 7.16: Fit result of life time (charged mode)

	results	pull
$\eta \rightarrow 2\gamma$ mode	$1.97^{+0.31}_{-0.27}$	+1.2
$\eta \rightarrow 3\pi$ mode	$2.31^{+0.45}_{-0.38}$	+1.8
all	$2.10^{+0.25}_{-0.22}$	+2.1

real DATA

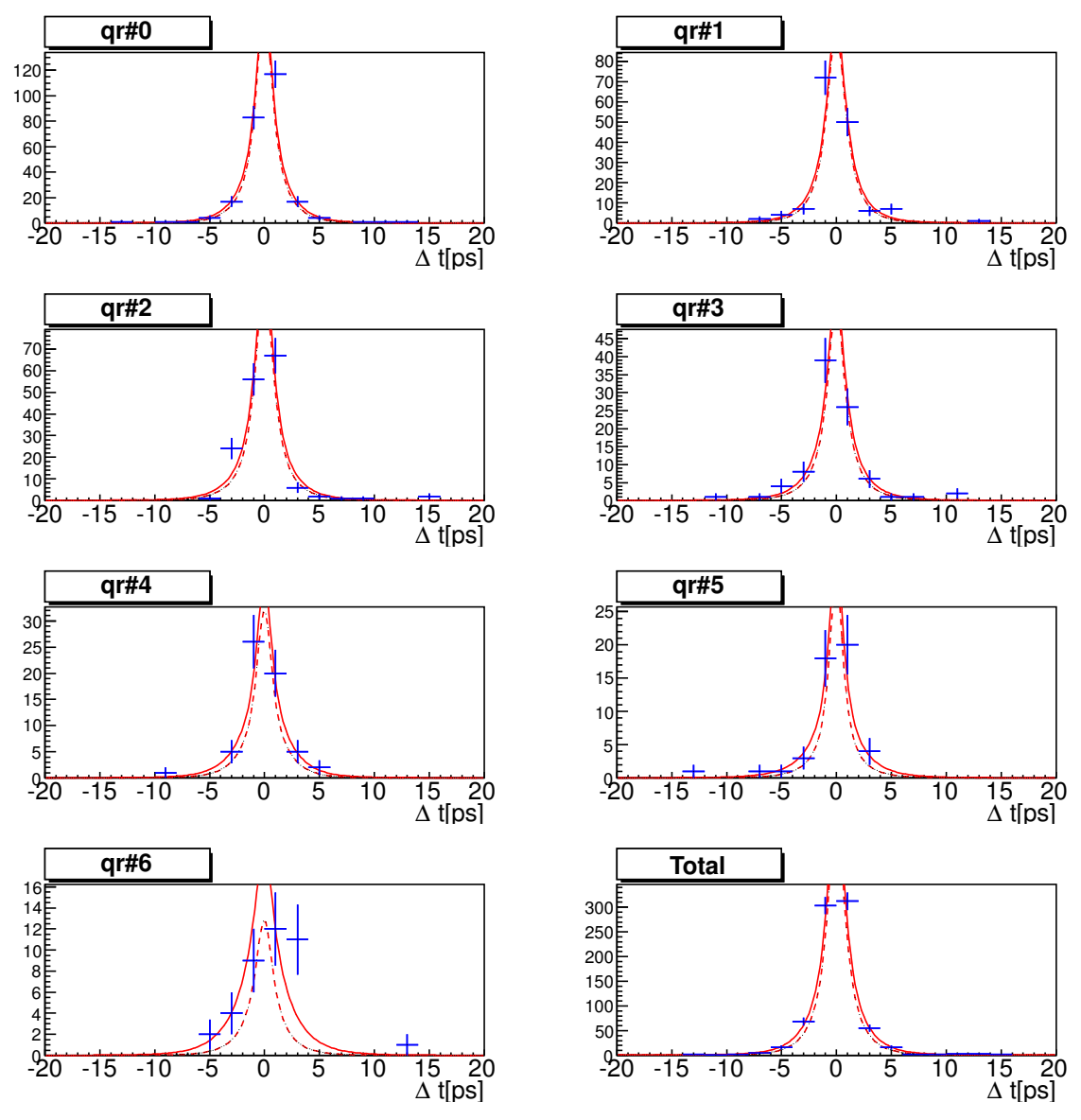


Figure 7.17: Life time fit result of charged $\eta \rightarrow 2\gamma$ mode

real DATA

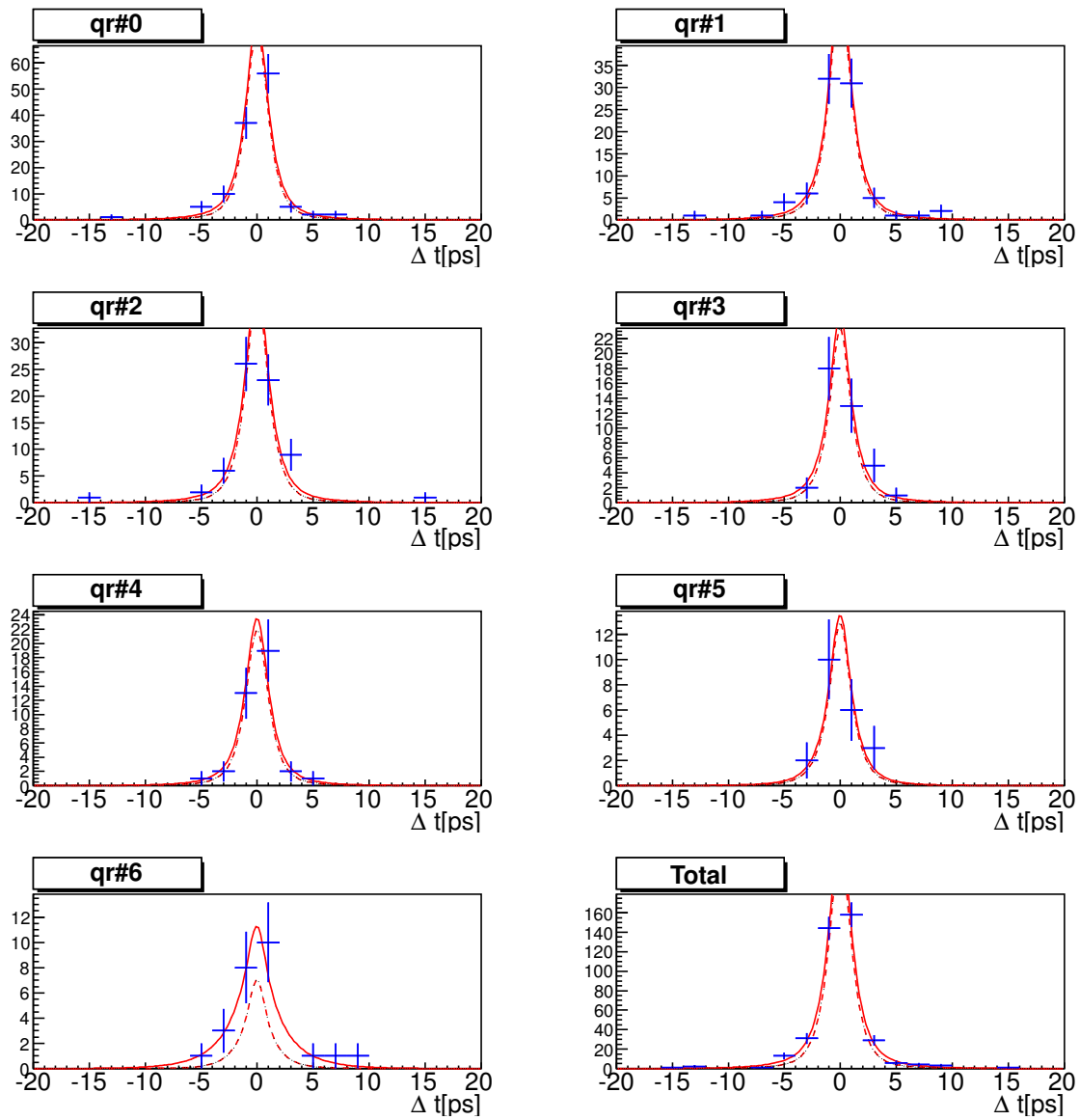


Figure 7.18: Life time fit result of charged $\eta \rightarrow 3\pi$ mode

$$B^0 \rightarrow K_S \eta \gamma$$

Table 7.17 shows fit result of sideband fit. Table 7.18 shows fit result of life time fit. Figure 7.19 and 7.20 show Δt distributions of $\eta \rightarrow 2\gamma$ mode and $\eta \rightarrow 3\pi$ mode, respectively. Fit results are consistent to world average within error. From these three fit results, we can say that the fitter code works well.

Table 7.17: Result of sideband fit (neutral mode)

neutral mode	$\eta \rightarrow 2\gamma$ mode	$\eta \rightarrow 3\pi$ mode
f_δ	$1.32^{+0.19}_{-0.16}$	$1.58^{+0.38}_{-0.34}$
f_{tail}	$0.044^{+0.043}_{-0.043}$	$0.065^{+0.042}_{-0.042}$
σ_{main}	$1.205^{+0.067}_{-0.067}$	$1.203^{+0.074}_{-0.076}$
σ_{tail}	$9.4^{+1.8}_{-1.3}$	$4.6^{+1.5}_{-0.9}$
μ	$0.036^{+0.011}_{-0.009}$	$0.069^{+0.047}_{-0.035}$
τ_{qq}	$0.512^{+0.091}_{-0.099}$	$0.74^{+0.11}_{-0.11}$

Table 7.18: Fit result of life time (neutral mode)

	results	pull
$\eta \rightarrow 2\gamma$ mode	$0.87^{+0.50}_{-0.45}$	-1.3
$\eta \rightarrow 3\pi$ mode	$1.81^{+0.71}_{-0.50}$	+0.6
all	$1.37^{+0.38}_{-0.33}$	-0.4

real DATA

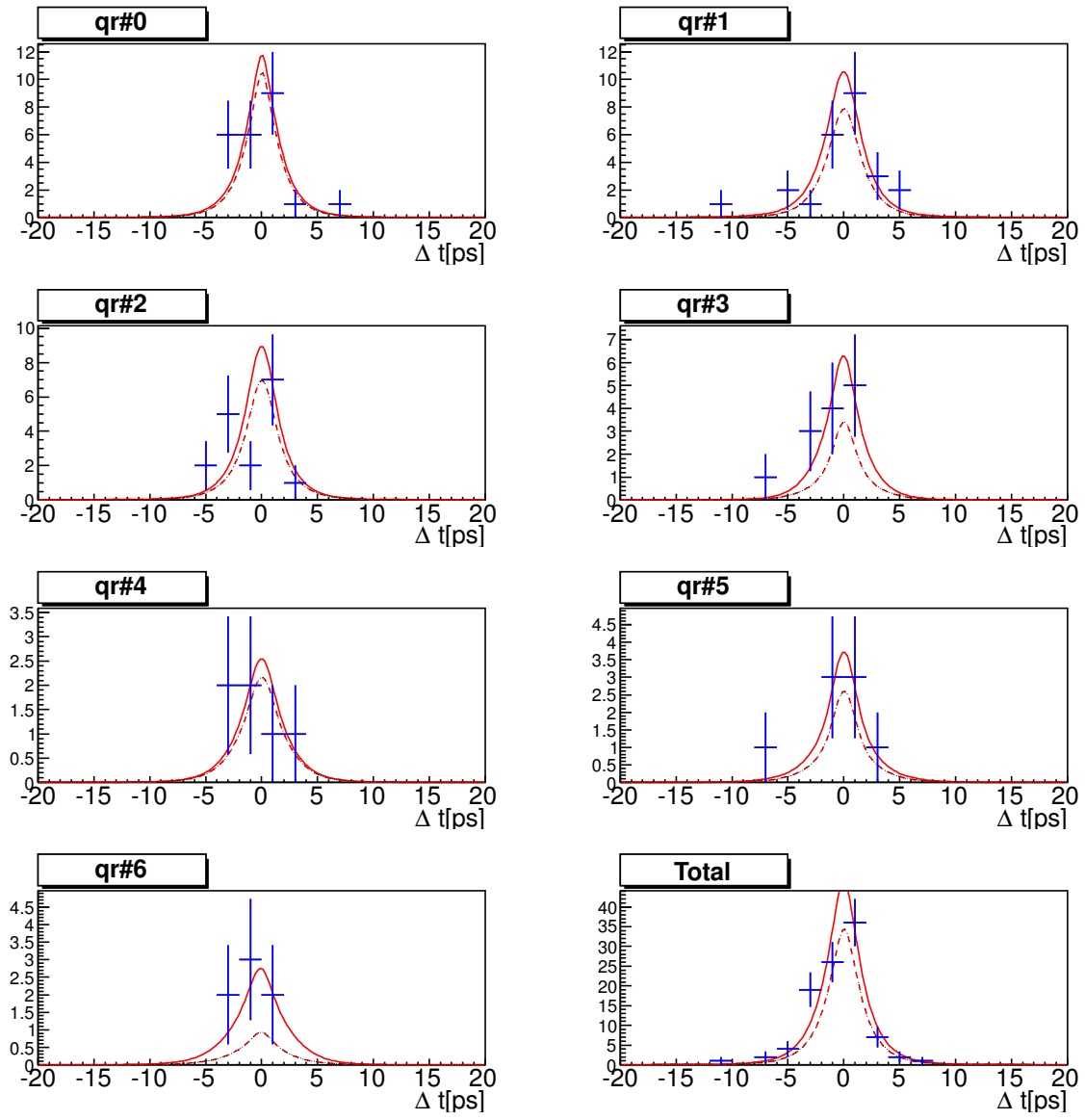


Figure 7.19: Life time fit result of neutral $\eta \rightarrow 2\gamma$ mode

real DATA

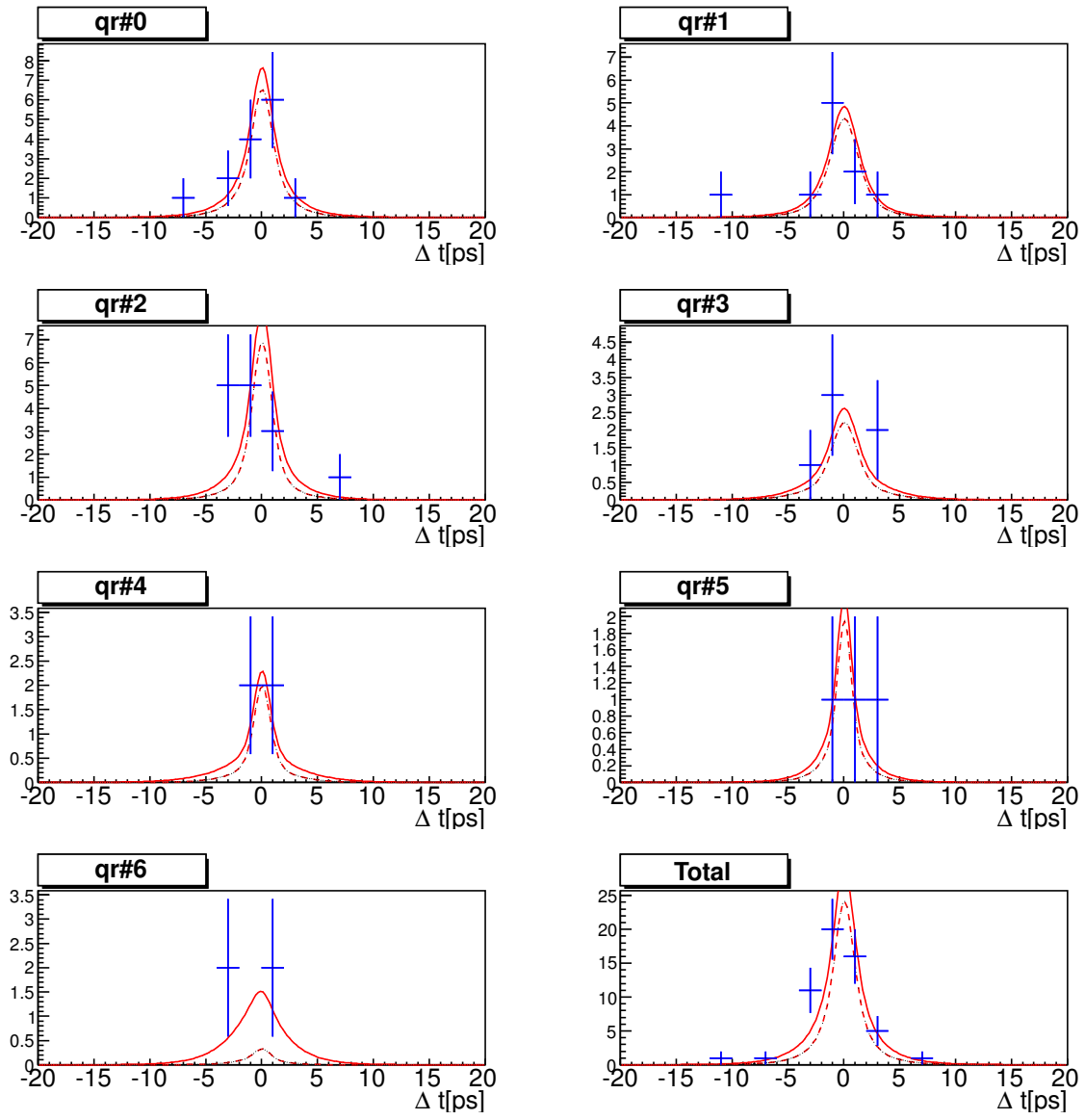


Figure 7.20: Life time fit result of neutral $\eta \rightarrow 3\pi$ mode

7.2.5 Linearity check with MC study

Figure 7.21 to 7.26 shows linearity check result with 4,500 GEANT based signal + toy MC BG result.

- \mathcal{S} is varied from -1.0 to 1.0 while \mathcal{A} is set to 0.
- \mathcal{A} is varied from -1.0 to 1.0 while \mathcal{S} is set to 0.

Means and their errors of the plot are calculated by

$$m = \frac{\sum_i^N m_i}{N} \quad (7.54)$$

$$\sigma = \frac{1}{\sqrt{\sum (1/\sigma_i)^2}}. \quad (7.55)$$

Fit result with a 1st order polynomial $f(x) = p_1x + p_0$ shows there are some biases. This bias will be included to systematic error.

Figure 7.27 shows expected error distribution with 4,500 GEANT based signal + toy MC BG result. Input $(\mathcal{S}, \mathcal{A})$ is $(0, 0)$. Mean of error is 0.59 and 0.34 for \mathcal{S} and \mathcal{A} , respectively. Since vertexing-failed events can also be used for \mathcal{A} estimation, error of \mathcal{A} is smaller than that of \mathcal{S} .

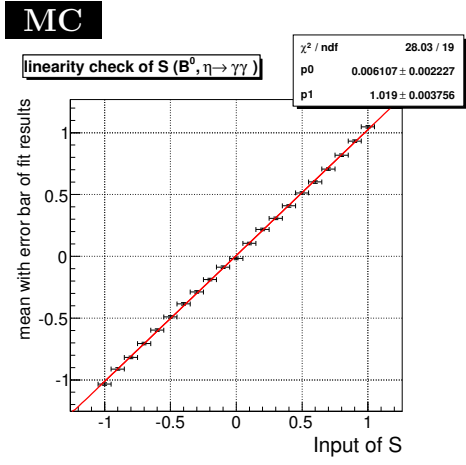


Figure 7.21: Linearity check of \mathcal{S} ($\eta \rightarrow 2\gamma$ mode)

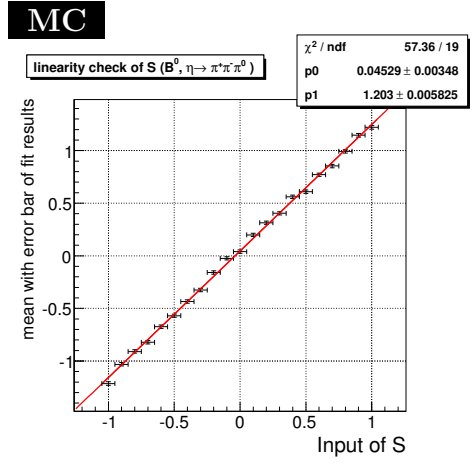


Figure 7.22: Linearity check of \mathcal{S} ($\eta \rightarrow 3\pi$ mode)

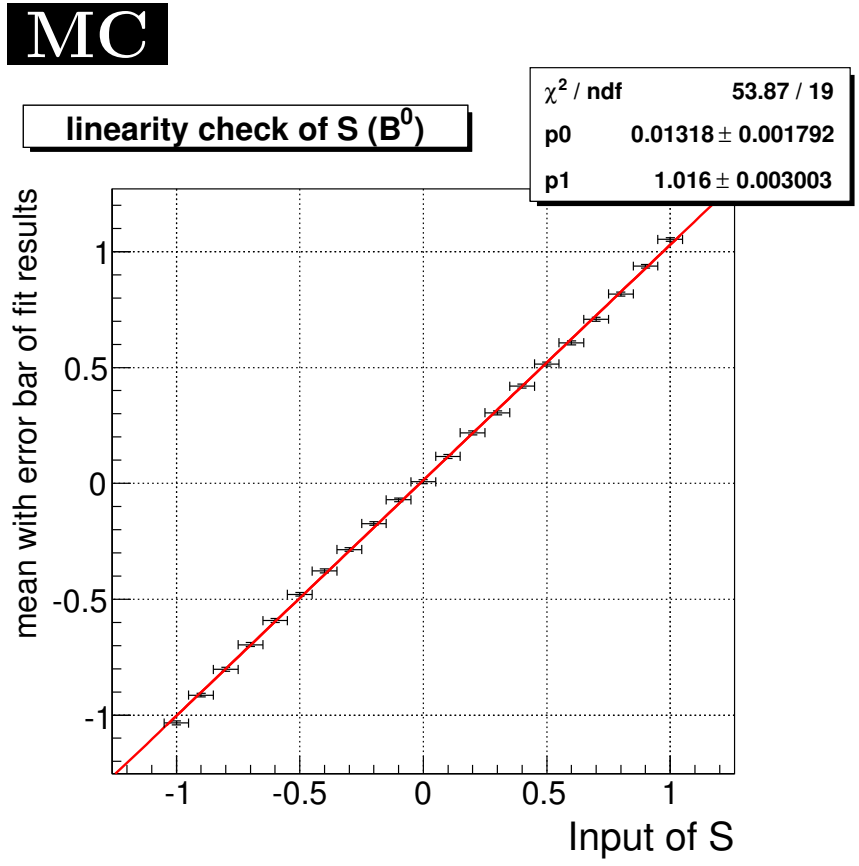


Figure 7.23: Linearity check of \mathcal{S} (with total event)

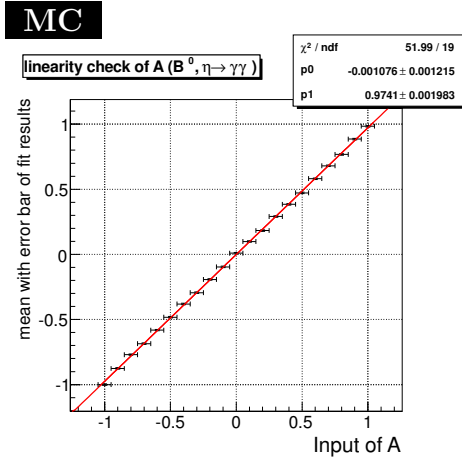


Figure 7.24: Linearity check of \mathcal{A} ($\eta \rightarrow 2\gamma$ mode)

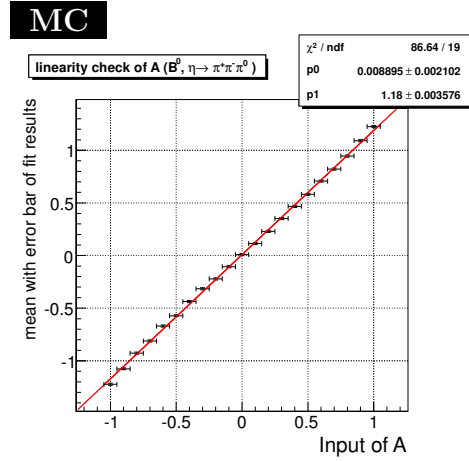


Figure 7.25: Linearity check of \mathcal{A} ($\eta \rightarrow 3\pi$ mode)

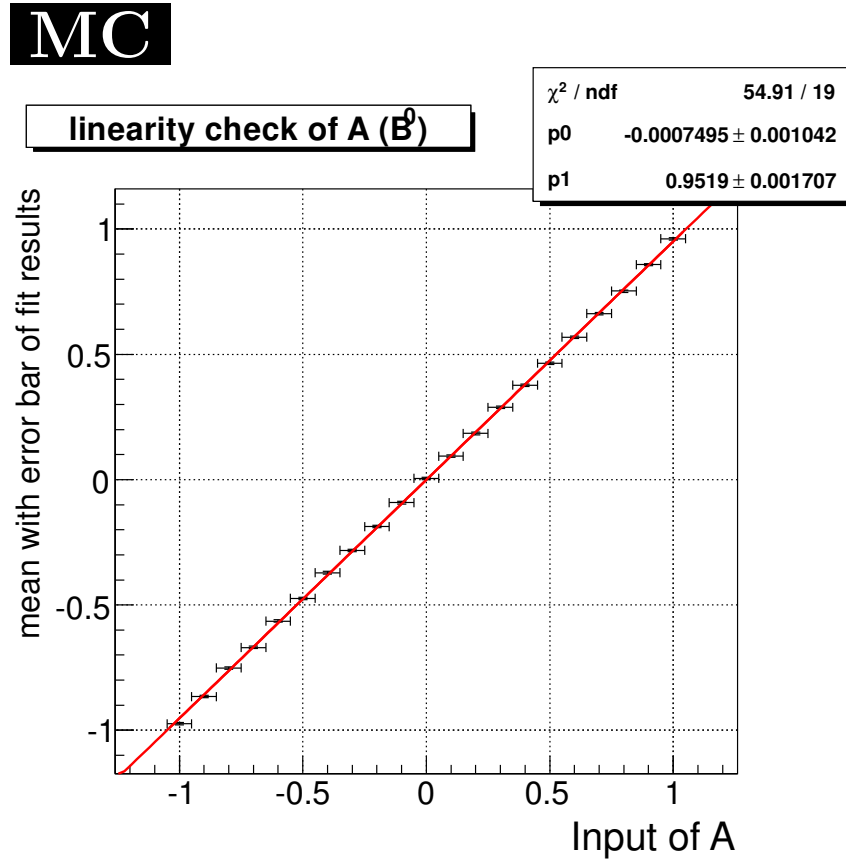


Figure 7.26: Linearity check of \mathcal{A} (with total event)

MC

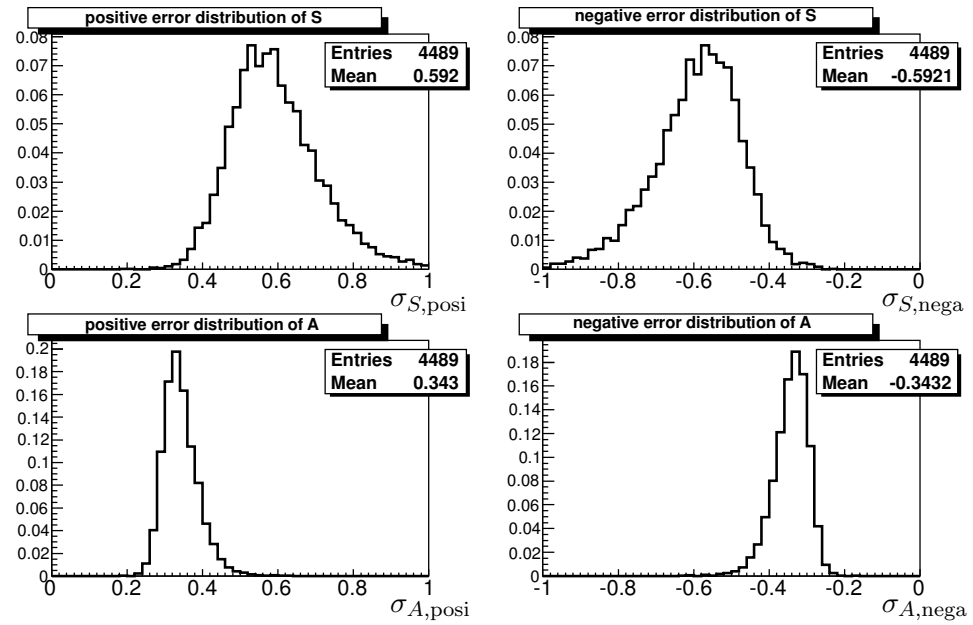


Figure 7.27: Distributions of expected error of CP fit (with total event)

7.2.6 CP fit with real data $B^\pm \rightarrow K^\pm \eta \gamma$ sample

We applied CP fitter code to $B^\pm \rightarrow K^\pm \eta \gamma$ mode. Table 7.19 shows fit result. Figure 7.28 shows Δt distribution and raw asymmetry of $qr > 0.5$ events. The result of \mathcal{S} is consistent to 0 within statistical error as expected.

Table 7.19: Result of CP fitter check with charged mode.

	S	A
$\eta \rightarrow 2\gamma$ mode	$0.01^{+0.35}_{-0.35}$	$0.06^{+0.29}_{-0.29}$
$\eta \rightarrow 3\pi$ mode	$-0.17^{+0.66}_{-0.59}$	$0.24^{+0.34}_{-0.36}$
all	$-0.04^{+0.31}_{-0.31}$	$0.13^{+0.22}_{-0.22}$

$B^0 \rightarrow K^\pm \eta \gamma$
real data

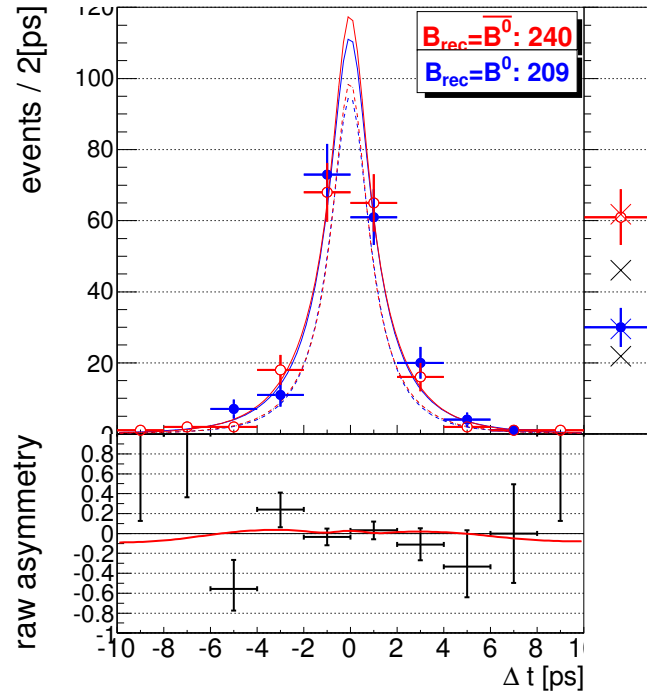


Figure 7.28: Δt distribution and raw asymmetry of charged mode (total, $qr > 0.5$). Red (Blue) plot shows distribution of $B_{\text{rec}} = \bar{B}^0 (B^0)$ events. Solid lines show total PDF. Dashed lines show BG PDF. Left plot describe events which have no Δt information. Colored crosses show total PDF and black crosses show BG PDF.

7.3 Fit result

We applied CP fitter code to $B^0 \rightarrow K_S \eta \gamma$ mode. Table 7.20 shows fit result. Figure 7.29 shows Δt distribution and raw asymmetry of $qr > 0.5$ events. Figure 7.30 and 7.31 are Δt distributions for each η decay mode and each qr bins. Fit result is out of physical boundary.

Table 7.20: Fit result of time dependent CP asymmetry. Error is MINOS error.

	S	A
$\eta \rightarrow 2\gamma$ mode	$-0.23^{+1.28}_{-1.20}$	$-0.31^{+0.46}_{-0.43}$
$\eta \rightarrow 3\pi$ mode	$-3.15^{+1.44}_{-1.15}$	$-1.10^{+0.79}_{-0.69}$
all	$-1.32^{+0.88}_{-0.81}$	$-0.48^{+0.36}_{-0.33}$

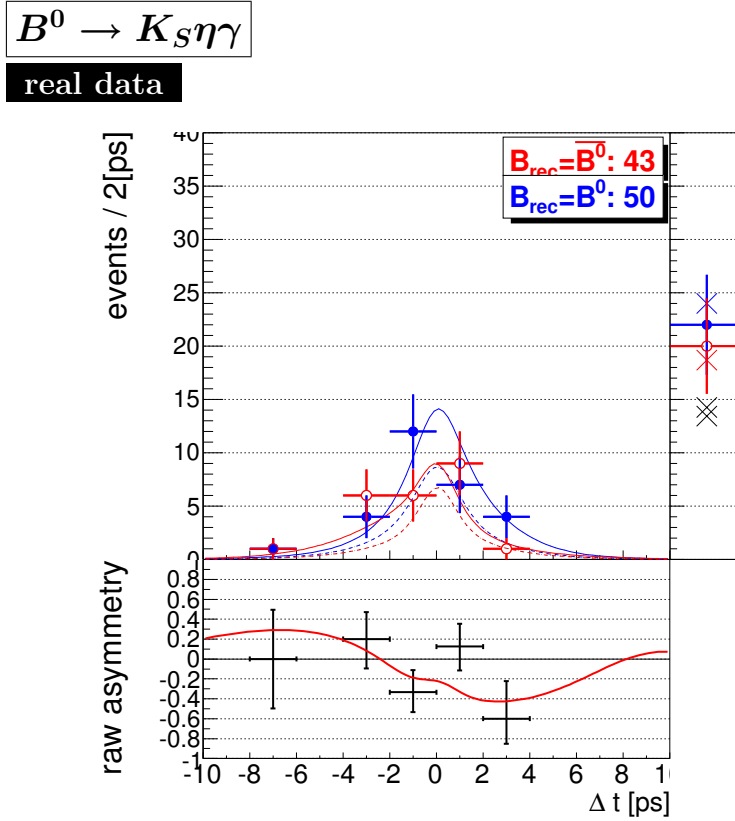


Figure 7.29: Δt distribution and raw asymmetry of neutral mode (total, $qr > 0.5$). Red (Blue) plot shows distribution of $B_{\text{rec}} = \bar{B}^0 (B^0)$ events. Solid lines show total PDF. Dashed lines show BG PDF. Left plot describe events which have no Δt information. Colored crosses show total PDF and black crosses show BG PDF.

real data

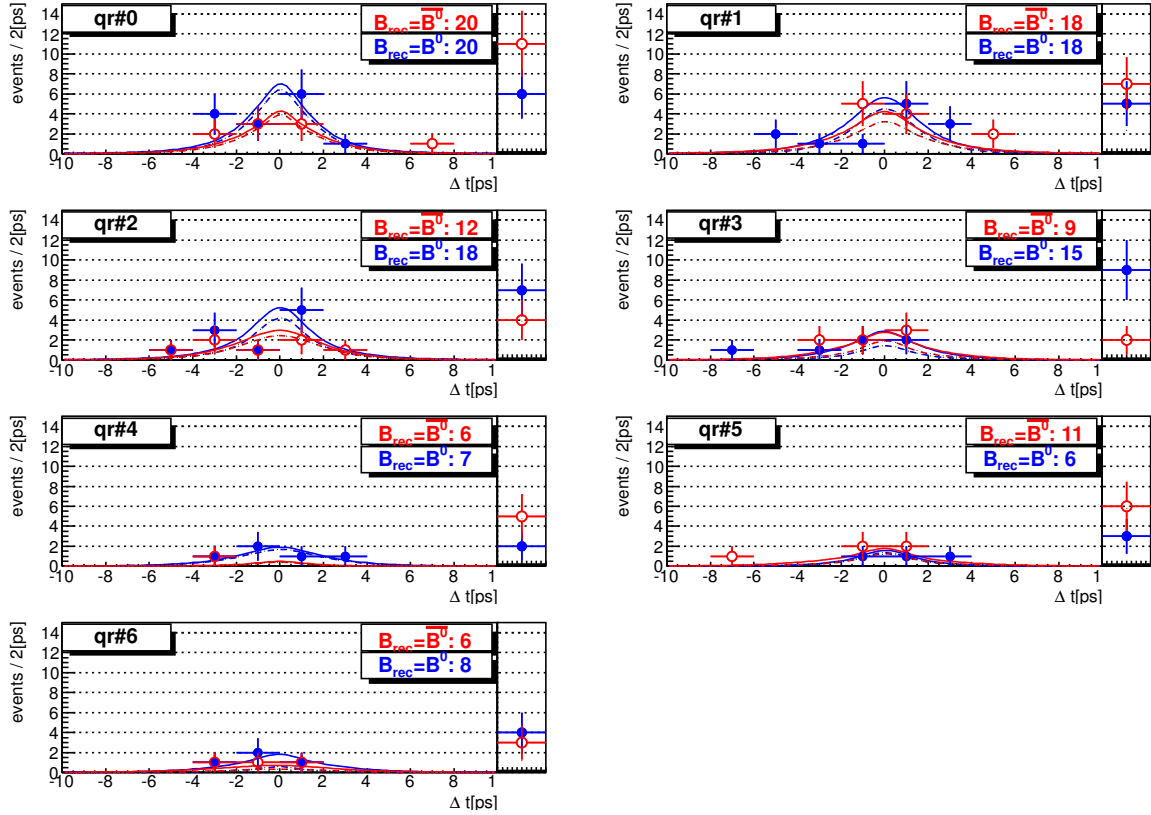


Figure 7.30: Tag quality bin-by-bin Δt distributions of neutral mode ($\eta \rightarrow 2\gamma$). Red (Blue) plot shows distribution of $B_{\text{rec}} = \overline{B^0}$ (B^0) events. Solid lines show total PDF. Dashed lines show BG PDF. Left plot describe events which have no Δt information.

real data

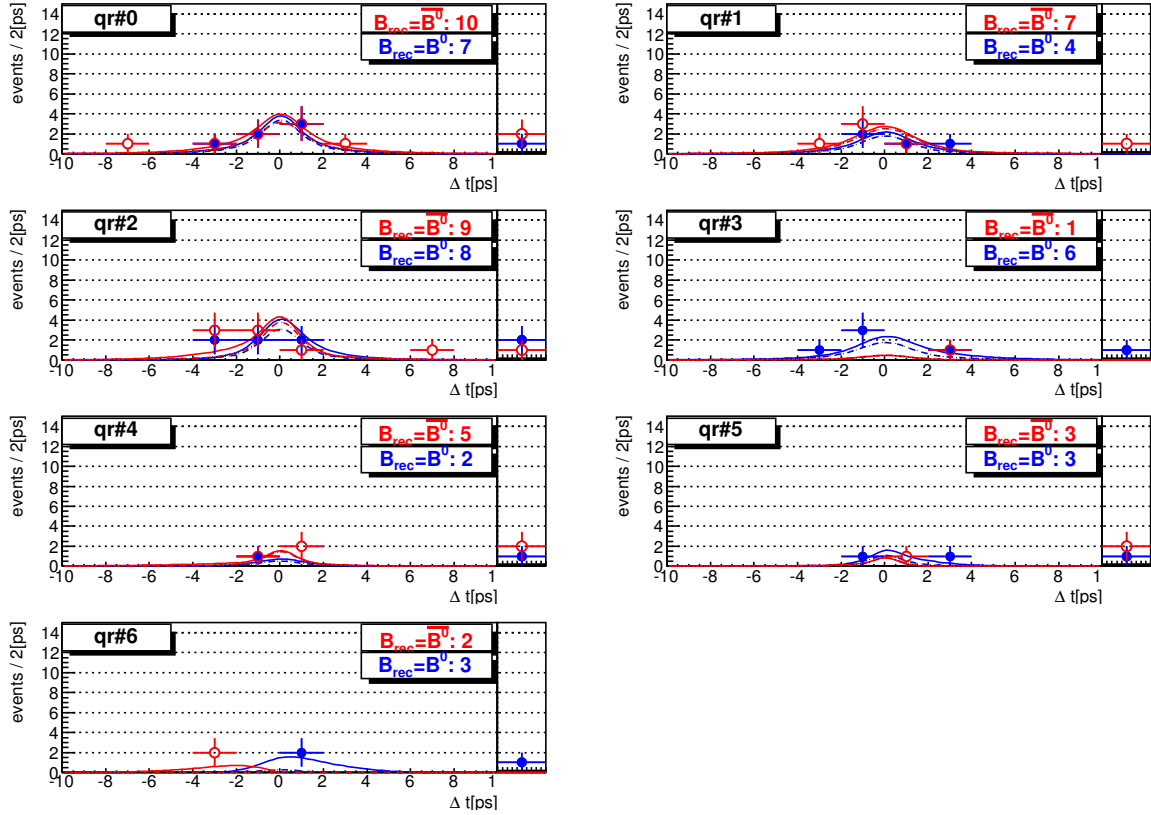


Figure 7.31: Tag quality bin-by-bin Δt distributions of neutral mode ($\eta \rightarrow 3\pi$). Red (Blue) plot shows distribution of $B_{\text{rec}} = \overline{B}^0$ (B^0) events. Solid lines show total PDF. Dashed lines show BG PDF. Left plot describe events which have no Δt information.

Chapter 8

Systematic error

In order to estimate systematics, all values used for fit are varied and change of fit results are estimated. Variable which is set by MC study is varied by $\pm 2\sigma$, and variable which is set by real data is varied by $\pm 1\sigma$.

8.1 Vertex reconstruction

Various parameters for vertex reconstruction are varied. The results are summarized on Tab.8.2, and details are described as following.

IP profile

To obtain vertex from single track, reconstruction from interaction point (IP) profile is applied. This value was changed by a factor of 2 and the difference of the result is set as systematics.

Tag side track selection

As we mentioned at 7.1.2, all tracks which is not used for B_{rec} reconstruction become candidate of B_{tag} tracks. Here, selections $dr < 500[\mu\text{m}]$, $\sigma_z < 500[\mu\text{m}]$ are applied. dr is impactparameter of the track and σ_z is tracking error along beam direction. We varied these value by $\pm 10\%$ and obtained systematic error.

Scale error

In the Belle experiment, error of trajectory of charged track is corrected by using cosmic ray information. Correction function is dependent on track's momentum, and it tunes an error of pull to be 1. Vertex quality is characterized by the error and it affects resolution function. Then, we have to consider systematics of the correction function. The method to obtain its error is "using Belle's own physics parameters". Considering a bias from the scaling error cause difference of τ_B and Δm from PDG value, we use physics parameters measured by Belle's data and take a difference between nominal result. Parameters for $\eta \rightarrow 3\pi$ mode are obtained from control sample of $B \rightarrow D^+\pi^-, D^{*+}\pi^-, D^{*+}\rho^-$, and ones for $\eta \rightarrow 2\gamma$ mode are obtained from control sample of $B \rightarrow J/\psi K_S$. The values are summarized on a Tab.8.1.

Quality requirement selection

Cut parameter of quality requirements as shown in eq.(7.30, 7.31, 7.32) are varied. These systematics are dominant source of the category.

Table 8.1: Physics parameters for systematics estimation of scale error.

	For $\eta \rightarrow 3\pi$ mode	For $\eta \rightarrow 2\gamma$ mode
τ_B	1.5161 ± 0.0079 [ps]	1.5256 ± 0.0262 [ps]
Δm	0.5159 ± 0.0050 [1/ps]	0.4926 ± 0.0334 [1/ps]

Δz bias and SVD misalignment

Bias from $\Delta z (= z_{\text{rec}} - z_{\text{tag}})$ measurement and SVD misalignment is also considered. It is known that $\Delta z_{\text{measured}} - \Delta z_{\text{true}} \neq 0$. Main reason is relative misalignment of SVD-CDC. Assuming that these values are mode independent, we used values obtained by $J/\psi K_S$ study which is Belle's golden mode .

Table 8.2: Systematic error list of vertex reconstruction.

Source	params.	ΔS	ΔA
IP profile	$21\mu\text{m} \rightarrow 11/41\mu\text{m}$	+0.02219/-0.00000	+0.00433/-0.00112
dr of B_{tag} 's track selection	$500\mu\text{m} \pm 10\%$	+0.00000/-0.00328	+0.00000/-0.00141
σ_z of B_{tag} 's track selection	$500\mu\text{m} \pm 10\%$	+0.00373/-0.01711	+0.00070/-0.00537
Scale error	Use Tab.8.1's parameters	± 0.000372	± 0.004143
$ \Delta t $ fit range	$70[\text{ps}] \rightarrow 40/100[\text{ps}]$	+0.00000/-0.00000	+0.00000/-0.00000
χ^2/ndf cut (rec side)	$50 \rightarrow 25/100$	+0.00000/-0.00961	+0.01009/-0.01887
χ^2/ndf cut (tag side)	$50 \rightarrow 25/100$	+0.00000/-0.00000	+0.00000/-0.00000
σ_z cut (rec side)	$\pm 100[\mu\text{m}]$	+0.23041/-0.00000	+0.00715/-0.00007
σ_z cut (tag side)	$\pm 100[\mu\text{m}]$	+0.00000/-0.15364	+0.00000/-0.00432
Δz bias	from $B \rightarrow J/\psi K_S$ analysis	+0.00000/-0.00392	+0.00000/-0.00498
SVD misalignment	from $B \rightarrow J/\psi K_S$ analysis	+0.00240/-0.00240	+0.00410/-0.00410
Total		+0.23152/-0.15499	+0.01435/-0.02158

8.2 Physics parameters

In this analysis, $\tau_B = 1.519 \pm 0.007[\text{ps}]$ and $\Delta m = (0.507 \pm 0.004) \times 10^{12}[\hbar/\text{s}]$ from newest PDG values are used. Systematic error from these value are obtained.

Table 8.3: Systematic error list of physics parameters.

params.		ΔS	ΔA
τ_B	$\pm 1\sigma$	+0.00281/-0.00285	+0.00051/-0.00051
Δm	$\pm 1\sigma$	+0.00221/-0.00220	+0.00153/-0.00153
Total		+0.00358/-0.00360	+0.00162/-0.00161

8.3 BG Δt PDF shape

Parameters which describe BG Δt PDF shape shown in Tab.7.17 and 7.12 are varied. Total error amount is $\Delta\mathcal{S} = \pm 0.051$ and $\Delta\mathcal{A} = \pm 0.006$. Detail table is shown in Tab.A.1.

8.4 Flavor tagging

w and Δw used in eq.(7.1) and (7.2) are varied. Their values are shown in Tab.7.2. Total error amount is $\Delta\mathcal{S} = \pm 0.015$ and $\Delta\mathcal{A} = \pm 0.019$. Detail table is shown in Tab.A.2.

8.5 Resolution function parameters

Parameters shown in Tab.7.4, 7.6 and 7.14 are varied. Total error amount is $\Delta\mathcal{S} = \pm 0.257$ and $\Delta\mathcal{A} = \pm 0.049$. $S_{\text{rec},0}$ and $S_{\text{rec},1}$ for K_S vertexing are dominant source. Detail tables are shown in Tab.A.3 and A.4.

8.6 3D fit for signal/BG fraction

We moved all PDF parameters which fixed by MC study and obtained systematics. Detail tables are shown in Tab.A.5, A.6, A.7, A.8 and A.9. Total error amount is $\Delta\mathcal{S} = \pm 0.096$ and $\Delta\mathcal{A} = \pm 0.024$. Main source is amount of radiative B BG. Radiative B source is divided into 5 groups; s and d quark system, s and u quark system, $K_S\eta\gamma$, $K^\pm\eta\gamma$ and others. Each expected amount of them is moved by $\pm 100\%$ except for $K^*\gamma$ decay in “others” because branching ratio of this mode is measured well.

8.7 CPV effect from BG

Since we search CPV which is suppressed in the SM, we have to be careful about the SM CPV effect from B BG. Although main peaking BGs are rejected exclusively as we discussed in Chapter 5, 40% (33%) of BB BG and 87% (74%) of rare B BG of $\eta \rightarrow 2\gamma$ ($\eta \rightarrow 3\pi$) mode are CP eigenstate. We estimate systematics with setting \mathcal{S} or \mathcal{A} of the BGs to ± 1 . Table 8.4 shows the result of the study, and error amount is $\Delta\mathcal{S} = \pm 0.024$ and $\Delta\mathcal{A} = \pm 0.022$. Actual CPV parameters are less than 1, and various final states effect destructively. This value is very conservative, however, it is not dominant error.

Table 8.4: Systematic error of BG CPV

	params.	$\Delta\mathcal{S}$	$\Delta\mathcal{A}$
BB BG	$\mathcal{S} = 0 \rightarrow \pm 1$	± 0.01809	± 0.00369
	$\mathcal{A} = 0 \rightarrow \pm 1$	± 0.00464	± 0.01656
rare B BG	$\mathcal{S} = 0 \rightarrow \pm 1$	± 0.01451	± 0.00400
	$\mathcal{A} = 0 \rightarrow \pm 1$	± 0.00139	± 0.01350
Total		± 0.02369	± 0.02205

8.8 Tag side interference

Although we neglect CPV effect from tag side B , there is a little effect actually. We call it ‘‘tag side interference (TSI)’’. PDF of Δt distribution can be written as

$$P = e^{-|\Delta t|/\tau} [R + q\{\mathcal{C} \cdot \cos(\Delta m \Delta t) + \mathcal{S} \cdot \sin(\Delta m \Delta t)\}]. \quad (8.1)$$

If we neglect TSI, \mathcal{R} , \mathcal{C} and \mathcal{S} are

$$\mathcal{R} = \frac{1 + |\lambda|^2}{2}, \quad (8.2)$$

$$\mathcal{C} = -q \frac{1 - |\lambda|^2}{2} \quad \text{and} \quad (8.3)$$

$$\mathcal{S} = +q \text{Im}[\lambda], \quad (8.4)$$

respectively. When we consider TSI effect, we have to add

$$\Delta\mathcal{R} = -2r' \text{Re}[\lambda] \cdot \cos(2\phi_1 + \phi_3 - q \delta'), \quad (8.5)$$

$$\Delta\mathcal{C} = +2r' \text{Im}[\lambda] \cdot \sin(2\phi_1 + \phi_3 - q \delta') \quad \text{and} \quad (8.6)$$

$$\Delta\mathcal{S} = +r'(1 - |\lambda|^2) \cdot \sin(2\phi_1 + \phi_3 - q \delta'). \quad (8.7)$$

This analysis uses two final states ($X_s \gamma_L$ and $X_s \gamma_R$), so, TSI term of \mathcal{R} , \mathcal{C} and \mathcal{S} are

$$\Delta\mathcal{R} = \frac{1}{2} \left\{ -2r' \text{Re}[\lambda_L] \cos(2\phi_1 + \phi_3 - q\delta') - |\lambda_L|^2 \times 2r' \text{Re}[\lambda_R] \cos(2\phi_1 + \phi_3 - q\delta') \right\} \quad (8.8)$$

$$\Delta\mathcal{C} = \frac{1}{2} \left\{ +2r' \text{Im}[\lambda_L] \sin(2\phi_1 + \phi_3 - q\delta') + |\lambda_L|^2 \times 2r' \text{Im}[\lambda_R] \sin(2\phi_1 + \phi_3 - q\delta') \right\} \quad (8.9)$$

$$\Delta\mathcal{S} = \frac{1}{2} \left\{ +r'(1 - |\lambda_L|^2) \sin(2\phi_1 + \phi_3 - q\delta') + |\lambda_L|^2 \times r'(1 - |\lambda_R|^2) \sin(2\phi_1 + \phi_3 - q\delta') \right\} \quad (8.10)$$

Here, using $|\lambda_R| = A_{b \rightarrow s\gamma} / A_{\bar{b} \rightarrow \bar{s}\gamma} = 1/|\lambda_L|$,

$$\Delta\mathcal{R} = -2r' \text{Re}[\lambda_L] \cos(2\phi_1 + \phi_3 - q \delta') \quad (8.11)$$

$$\Delta\mathcal{C} = +2r' \text{Im}[\lambda_L] \sin(2\phi_1 + \phi_3 - q \delta') \quad (8.12)$$

$$\Delta\mathcal{S} = 0 \quad (8.13)$$

In the SM, since $|\lambda_L| = m_s/m_b$, TSI effect is negligible. However, we estimate maximum TSI effect with setting $|\lambda_L| = 1$. We take larger value of $\text{Re}[\lambda_L] = 1$ case and $\text{Im}[\lambda_L] = 1$ case as an error. Table 8.5 shows the result of the estimation, and error amount is $\Delta\mathcal{S} = \pm 0.006$ and $\Delta\mathcal{A} = \pm 0.010$.

Here, we used the values of

$$2r' \sin(2\phi_1 + \phi_3 + \delta') = +0.0096 \pm 0.0073 \quad (8.14)$$

$$2r' \sin(2\phi_1 + \phi_3 - \delta') = -0.0067 \pm 0.0073 \quad (8.15)$$

$$2\phi_1 = 2 \times (21.5_{-0.7}^{+0.8})^\circ \quad (8.16)$$

$$\phi_3 = (68.0_{-8.5}^{+8.0})^\circ \quad (8.17)$$

for MC generation. $2r' \sin(2\phi_1 + \phi_3 \pm \delta')$ can be measured by flavor specific $B \rightarrow D^* l \nu$ decay. $2\phi_1$ and ϕ_3 are taken from newest HFAG and CKM fitter values, respectively.

Table 8.5: Systematic error of tag side interference.

params.		$\Delta\mathcal{S}$	$\Delta\mathcal{A}$
λ	$\text{Re}[\lambda] = 1$	± 0.00070	± 0.01010
	$\text{Im}[\lambda] = 1$	± 0.00620	± 0.00711
Larger value		± 0.00620	± 0.01010

8.9 Possible fit bias

We generated MC data corresponding 4500 experiments with $(\mathcal{S}, \mathcal{A}) = (-0.940, -0.340)$ which places on the physical boundary and between origin and fit result. We take a differences of fit result between mean of MC study and input value, and we set $\Delta\mathcal{S} = \pm 0.0155$, $\Delta\mathcal{A} = \pm 0.0153$ for systematic error. $\mathcal{S}_{\text{mean}}/\mathcal{S}_{\text{true}} = 1.017$ and $\mathcal{A}_{\text{mean}}/\mathcal{A}_{\text{true}} = 0.956$ are consistent to the bias obtained at linearity check (section 7.2.5).

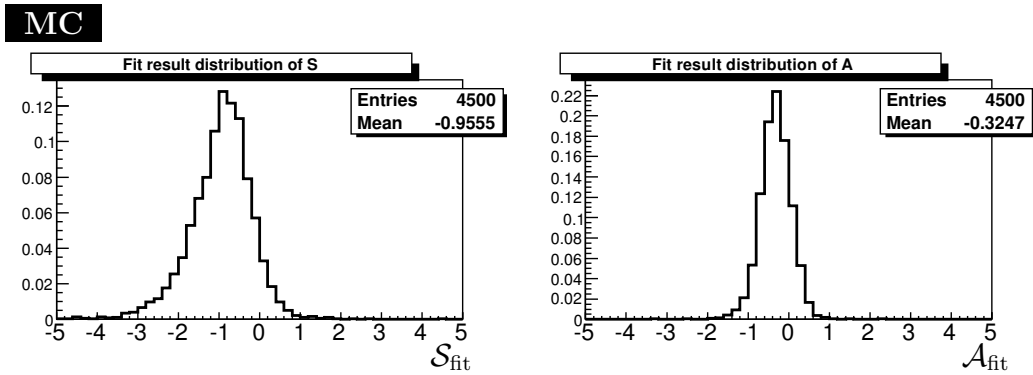


Figure 8.1: Fit result distribution with $(\mathcal{S}_{\text{true}}, \mathcal{A}_{\text{true}}) = (-0.940, -0.340)$.

8.10 Summary

Table 8.6 summarizes systematic error discussed in this chapter. Total systematic error is obtained by root sum square (RSS) of each component. Main components are vertexing and resolution parameter. Resolution parameters affect event-by-event Δt PDF shape, while systematics of vertex reconstruction is mainly come from quality requirement cut which affects event number. They seems to be not correlated, and RSS method is valid to obtain total amount.

Table 8.6: Systematic errors of \mathcal{S} and \mathcal{A} .

Source	S	A
Resolution parameters	± 0.25695	± 0.04912
Vertex reconstruction	± 0.23152	± 0.02158
BG Δt PDF shape	± 0.05114	± 0.00627
Flavor tagging	± 0.01504	± 0.01915
Physics parameters	± 0.00360	± 0.00162
PDF shape of 3D fit	± 0.09638	± 0.02355
CPV from BG	± 0.02369	± 0.02205
Possible fit bias	± 0.01550	± 0.01530
Tag side interference	± 0.00620	± 0.01010
Total	± 0.36415	± 0.06829

Chapter 9

Consideration of the result

9.1 Checks of the analysis

9.1.1 Likelihood scan

Figure 9.1 shows FCN value of scanning \mathcal{S} while fixing \mathcal{A} . Figure 9.2 shows FCN value of scanning \mathcal{A} while fixing \mathcal{S} . These plots show that the fit result is not a local minima.

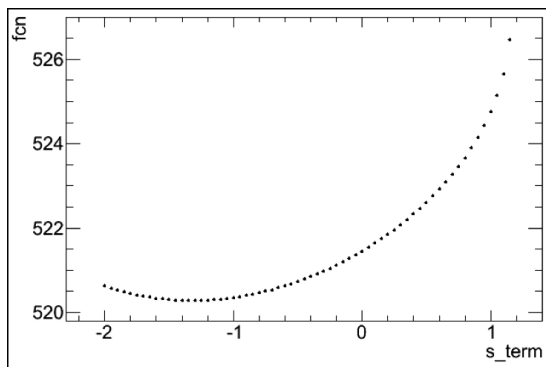


Figure 9.1: Plot of fcn vs. \mathcal{S} while \mathcal{A} is fixed to -0.479.

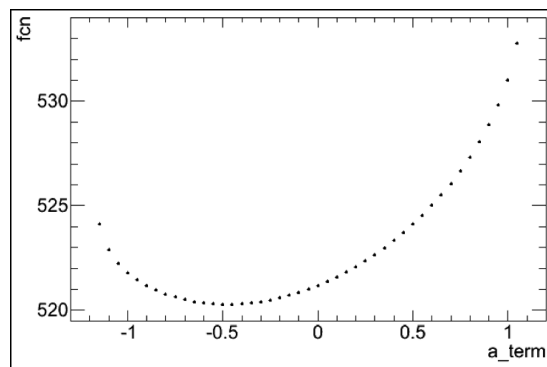


Figure 9.2: Plot of fcn vs. \mathcal{A} while \mathcal{S} is fixed to -1.323.

9.1.2 2D fit for signal/BG ratio

2D fit was used for signal/BG fraction estimation rather than 3D fit. Obtained results are summarized on Tab.9.1. They are consistent with the result obtained using 3D fit.

Table 9.1: Fit result of time dependent CP asymmetry with 2D fit.

	S	A
$\eta \rightarrow 2\gamma$ mode	$+0.11^{+1.37}_{-1.36}$	$-0.01^{+0.52}_{-0.51}$
$\eta \rightarrow 3\pi$ mode	$-6.75^{+2.21}_{-1.60}$	$-0.94^{+0.95}_{-0.91}$
all	$-1.57^{+1.00}_{-0.94}$	$-0.24^{+0.42}_{-0.40}$

9.1.3 Data instability

Low statistics result can be changed a lot by only one event. Instability of the data is checked by removing one event by one event. Since there are 244 events in the signal region, 244 results are obtained. Figure 9.3 and 9.5 shows \mathcal{S} and \mathcal{A} distribution with 3D fit. Figure 9.4 and 9.6 shows \mathcal{S} and \mathcal{A} distribution with 2D fit. We can see that some events has large weight with the result. Information of effective events are summarized on Tab.9.2. We can see that the result is dependent on small amount events which have common aspects: high signal fraction, high qr bin number and $|\Delta t|$ is about 3 ps. Especially qr bin #6 is dominated by signal.

Because of the instability, systematic error from vertex quality cut is one of dominant error. In addition, it can also explain why systematic error from BG event (Δt shape and CPV effect from BG) is not dominant.

Table 9.2: Example of events which have large weight.

reject No.	decay mode	$\Delta\mathcal{S}$	$\Delta\mathcal{A}$	$\Delta t[\text{ps}]$	qr #	f_{sig} (3D fit)
8	2γ	-0.06	-0.10	-0.31	5	0.84
67	2γ	-0.40	-0.28	1.43	6	0.94
97	2γ	-0.26	+0.07	-3.73	6	0.84
134	2γ	-0.16	+0.02	-2.56	2	0.79
140	2γ	+0.16	0.00	-3.51	3	0.75
151	2γ	-0.18	+0.07	-0.95	6	0.74
161	2γ	-0.48	0.00	-3.69	3	0.86
177	3π	+0.35	+0.02	-3.52	6	0.94
227	3π	-0.27	+0.02	-1.65	5	0.30
240	3π	+0.17	-0.08	-2.33	6	0.97

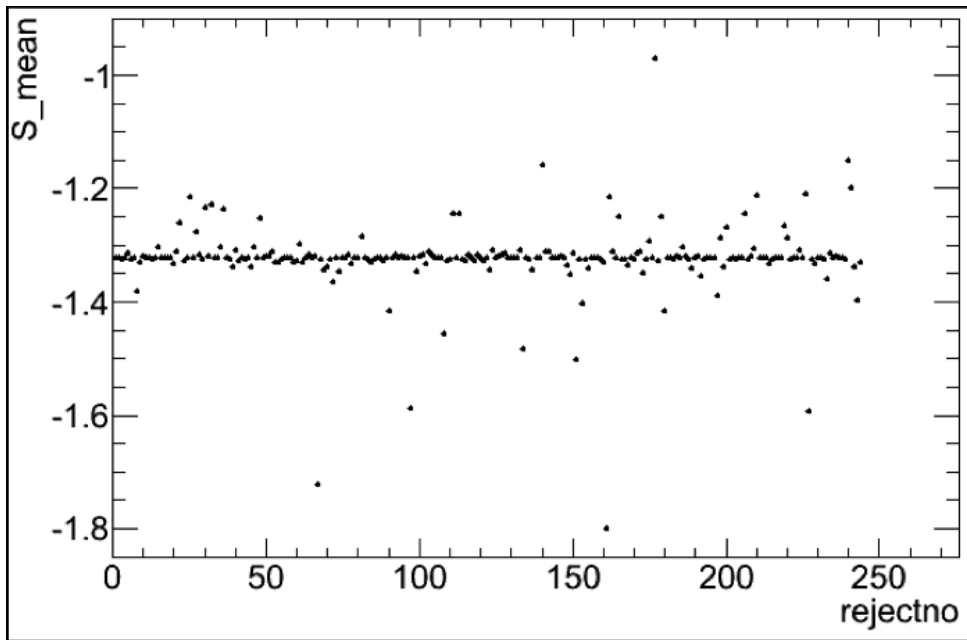


Figure 9.3: “One event-removed result” distribution of \mathcal{S} with 3D fit

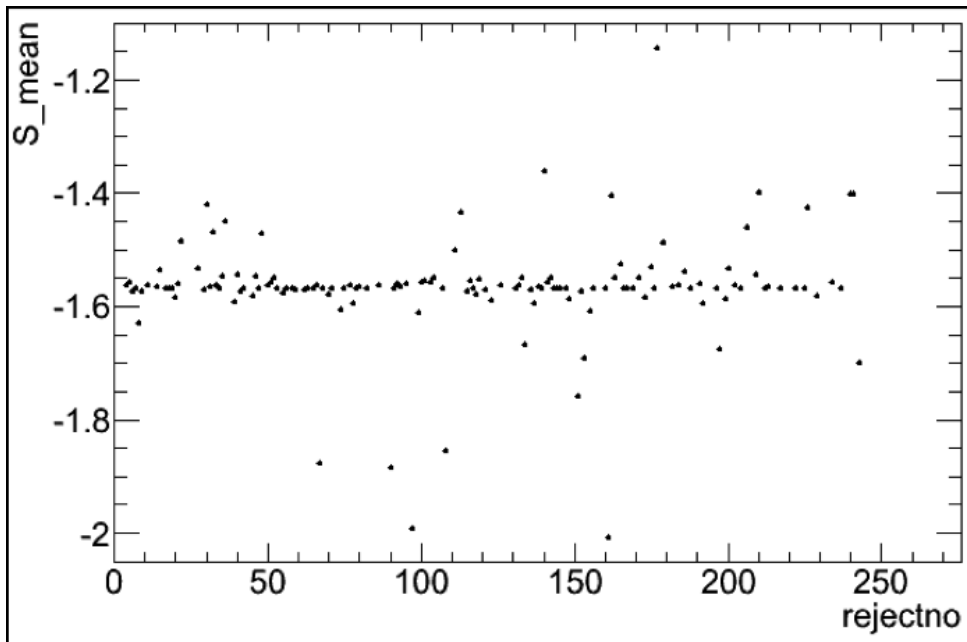


Figure 9.4: “One event-removed result” distribution of \mathcal{S} with 2D fit

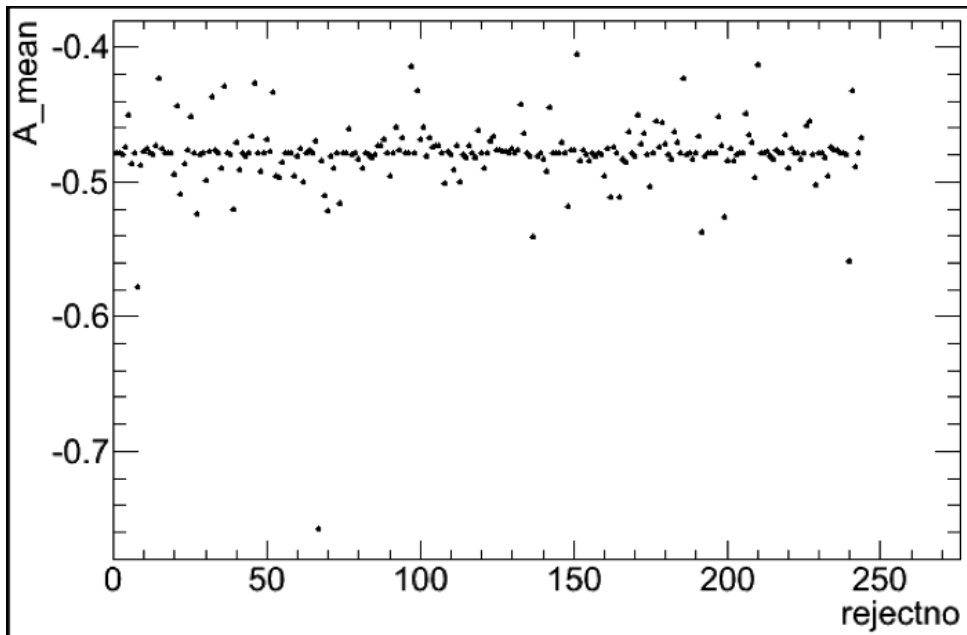


Figure 9.5: “One event-removed result” distribution of \mathcal{A} with 3D fit

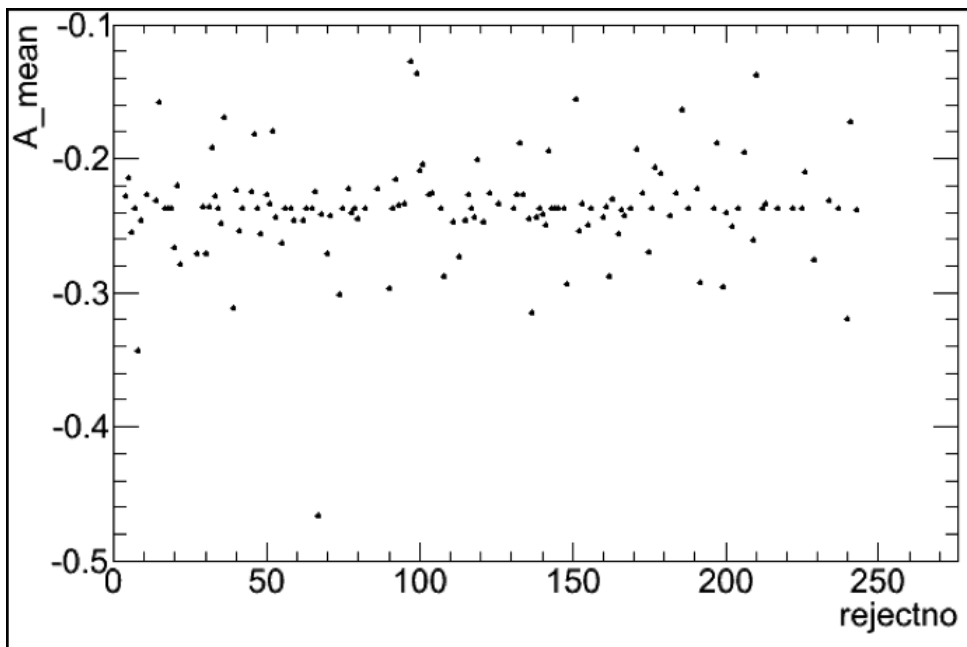


Figure 9.6: “One event-removed result” distribution of \mathcal{A} with 2D fit

9.1.4 MC distribution

Figure 9.7 and 9.8 are showing 30,000 fit result distribution generated by MC when $(\mathcal{S}_{\text{true}}, \mathcal{A}_{\text{true}}) = (0, 0)$. 11.6 % of the results are out of physical boundary. 7.5 % of the results are out of an ellipse which has same \mathcal{S}/\mathcal{A} ratio to mean of fit error, and passes the result, $(-1.323, -0.479)$.

Figure 9.9 and 9.10 are showing 30,000 fit result distribution generated by MC when $(\mathcal{S}_{\text{true}}, \mathcal{A}_{\text{true}}) = (-0.940, -0.340)$. The input places between origin and fit result, and satisfies that $\mathcal{S}^2 + \mathcal{A}^2 = 1$. 57.8 % of the results are out of physical boundary. 35.6 % of the results are out of an ellipse which has same \mathcal{S}/\mathcal{A} ratio to mean of fit error, and passes the result, $(-1.323, -0.479)$.

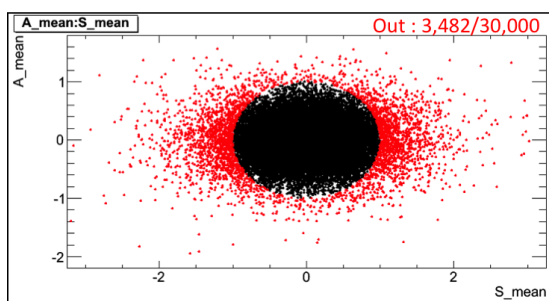


Figure 9.7: Distribution of MC fit result with $(\mathcal{S}, \mathcal{A}) = (0, 0)$. Red plots are results which satisfy $\mathcal{S}^2 + \mathcal{A}^2 > 1$.

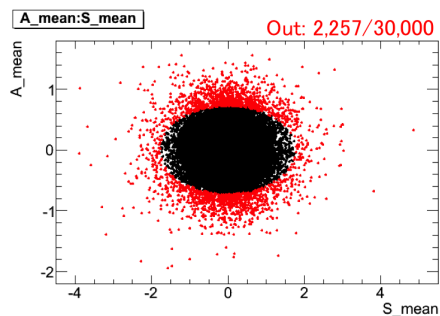


Figure 9.8: Distribution of MC fit result with $(\mathcal{S}, \mathcal{A}) = (0, 0)$. Red plots are results which satisfy $(\mathcal{S}/0.845)^2 + (\mathcal{A}/0.345)^2 > (1.323/0.845)^2 + (0.479/0.345)^2$.

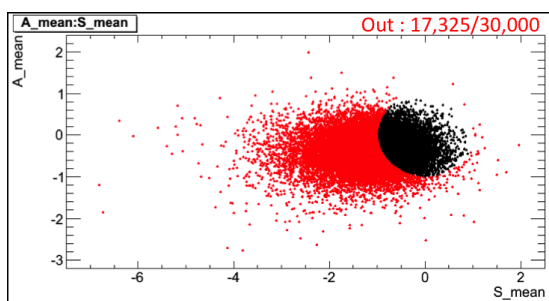


Figure 9.9: Distribution of MC fit result with $(\mathcal{S}, \mathcal{A}) = (-0.940, -0.340)$. Red plots are results which satisfy $\mathcal{S}^2 + \mathcal{A}^2 > 1$.

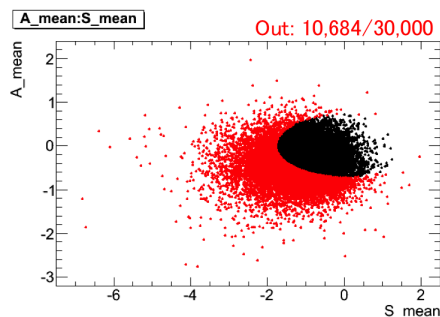


Figure 9.10: Distribution of MC fit result with $(\mathcal{S}, \mathcal{A}) = (-0.940, -0.340)$. Red plots are results which satisfy $(\mathcal{S}/0.845)^2 + (\mathcal{A}/0.345)^2 > (1.323/0.845)^2 + (0.479/0.345)^2$.

9.2 Consideration

9.2.1 Confidence interval using Feldman-Cousins method

Here, we estimate the statistical power of our measurement from the confidence interval using Feldman-Cousins method.

In a physical boundary, \mathcal{S} and \mathcal{A} are scanned with a step of 0.25. 4,500 CP fit results are generated at each 49 points by MC simulation. Then, 2D distributions of $(\mathcal{S}_{\text{result}}, \mathcal{A}_{\text{result}})$ are fitted by double 2D Gaussian which consists of 9 parameters:

$$P(\mathcal{S}_{\text{result}}, \mathcal{A}_{\text{result}} | \mathcal{S}_{\text{true}}, \mathcal{A}_{\text{true}}) = f \cdot G(m_{A1}, \sigma_{A1}) \cdot G(m_{S1}, \sigma_{S1}) + (1 - f) \cdot G(m_{A2}, \sigma_{A2}) \cdot G(m_{S2}, \sigma_{S2}). \quad (9.1)$$

Fit result of $(\mathcal{S}, \mathcal{A}) = (0.0, 0.0), (-1.0, 0.0)$ and $(-0.5, -0.5)$ are shown in Fig.9.11. They show the function can describe the distributions well.

The 9 parameters used for the function are fitted by polynomials of $\mathcal{S}_{\text{true}}$ and $\mathcal{A}_{\text{true}}$. Fit result of them are shown in Fig.9.12 to 9.20. They are described as following.

$$f = c_1 + c_2 (\mathcal{S}_{\text{true}}^2 + \mathcal{A}_{\text{true}}^2) \quad (9.2)$$

$$m_{S1} = c_3 \mathcal{S}_{\text{true}} \quad (9.3)$$

$$m_{S2} = c_4 \mathcal{S}_{\text{true}} \quad (9.4)$$

$$m_{A1} = c_5 \mathcal{S}_{\text{true}} \quad (9.5)$$

$$m_{A2} = c_6 \mathcal{S}_{\text{true}} \quad (9.6)$$

$$\sigma_{S1} = c_7 + c_8 (\mathcal{S}_{\text{true}}^2 + \mathcal{A}_{\text{true}}^2) \quad (9.7)$$

$$\sigma_{S2} = C_S \times \sigma_{S1} = c_9 \times \sigma_{S1} \quad (9.8)$$

$$\sigma_{A1} = c_{10} + c_{11} \mathcal{A}_{\text{true}}^2 \quad (9.9)$$

$$\sigma_{A2} = C_A \times \sigma_{S1} = (c_{12} + c_{13} \mathcal{A}_{\text{true}}^2) \times \sigma_{A1} \quad (9.10)$$

Figure 9.21 shows confidence level interval. Confidence level ($\equiv \alpha$) is defined as

$$\alpha(\mathcal{S}_{\text{true}}, \mathcal{A}_{\text{true}}) = \int_{\Omega} d\mathcal{S}d\mathcal{A} P(\mathcal{S}, \mathcal{A} | \mathcal{S}_{\text{true}}, \mathcal{A}_{\text{true}}). \quad (9.11)$$

Here, Ω is a region which satisfies

$$LR(\mathcal{S}, \mathcal{A} | \mathcal{S}_{\text{true}}, \mathcal{A}_{\text{true}}) \geq LR(-1.32, -0.48 | \mathcal{S}_{\text{true}}, \mathcal{A}_{\text{true}}). \quad (9.12)$$

$LR(\mathcal{S}, \mathcal{A} | \mathcal{S}_{\text{true}}, \mathcal{A}_{\text{true}})$ in the function is defined as

$$LR(\mathcal{S}, \mathcal{A} | \mathcal{S}_{\text{true}}, \mathcal{A}_{\text{true}}) = P(\mathcal{S}, \mathcal{A} | \mathcal{S}_{\text{true}}, \mathcal{A}_{\text{true}}) / P(\mathcal{S}, \mathcal{A} | \mathcal{S}_{\text{best}}, \mathcal{A}_{\text{best}}). \quad (9.13)$$

Here, $(\mathcal{S}_{\text{best}}, \mathcal{A}_{\text{best}})$ are the input set which gives maximum P for $(\mathcal{S}, \mathcal{A})$ within physical boundary, $\mathcal{S}^2 + \mathcal{A}^2 \leq 1$.

This plot says that the result is 0 consistent within 2 sigma.

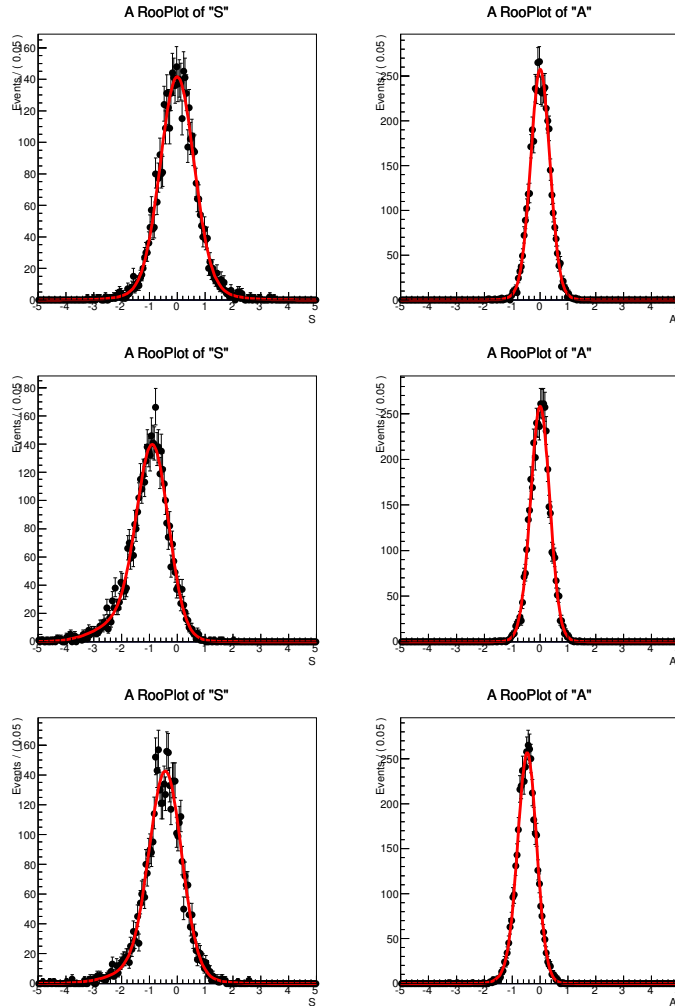


Figure 9.11: Double 2D Gaussian fit to $(\mathcal{S}_{\text{result}}, \mathcal{A}_{\text{result}})$ distribution. Red lines show fitted function. Black points show MC result distribution. (Top) $(\mathcal{S}_{\text{true}}, \mathcal{A}_{\text{true}})$ is set to $(0.0, 0.0)$. (Middle) $(\mathcal{S}_{\text{true}}, \mathcal{A}_{\text{true}})$ is set to $(-1.0, 0.0)$. (Bottom) $(\mathcal{S}_{\text{true}}, \mathcal{A}_{\text{true}})$ is set to $(-0.5, -0.5)$.

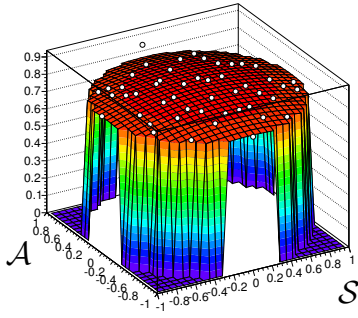


Figure 9.12:
2D fit result of f .

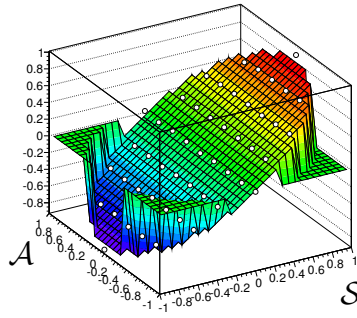


Figure 9.13:
2D fit result of m_{S1} .

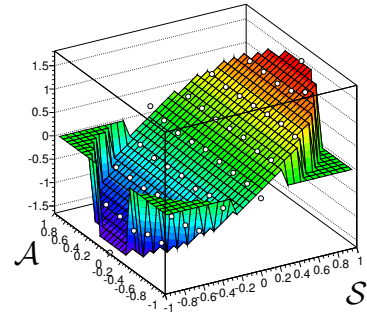


Figure 9.14:
2D fit result of m_{S2} .

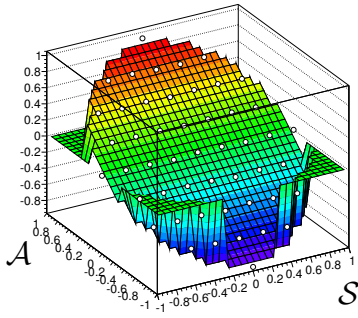


Figure 9.15:
2D fit result of m_{A1} .

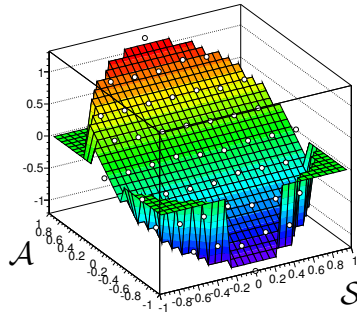


Figure 9.16:
2D fit result of m_{A2} .

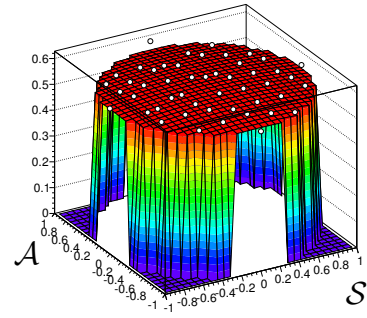


Figure 9.17:
2D fit result of σ_{S1} .

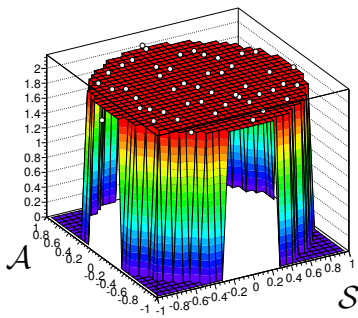


Figure 9.18:
2D fit result of C_S .

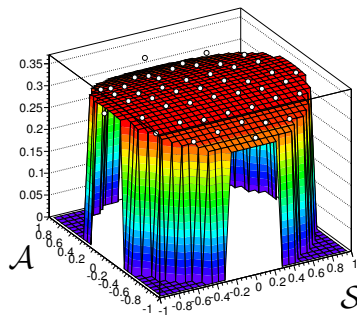


Figure 9.19:
2D fit result of σ_{A1} .

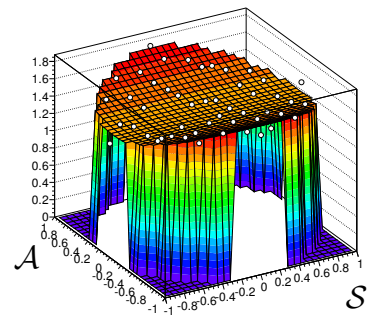


Figure 9.20:
2D fit result of C_A .

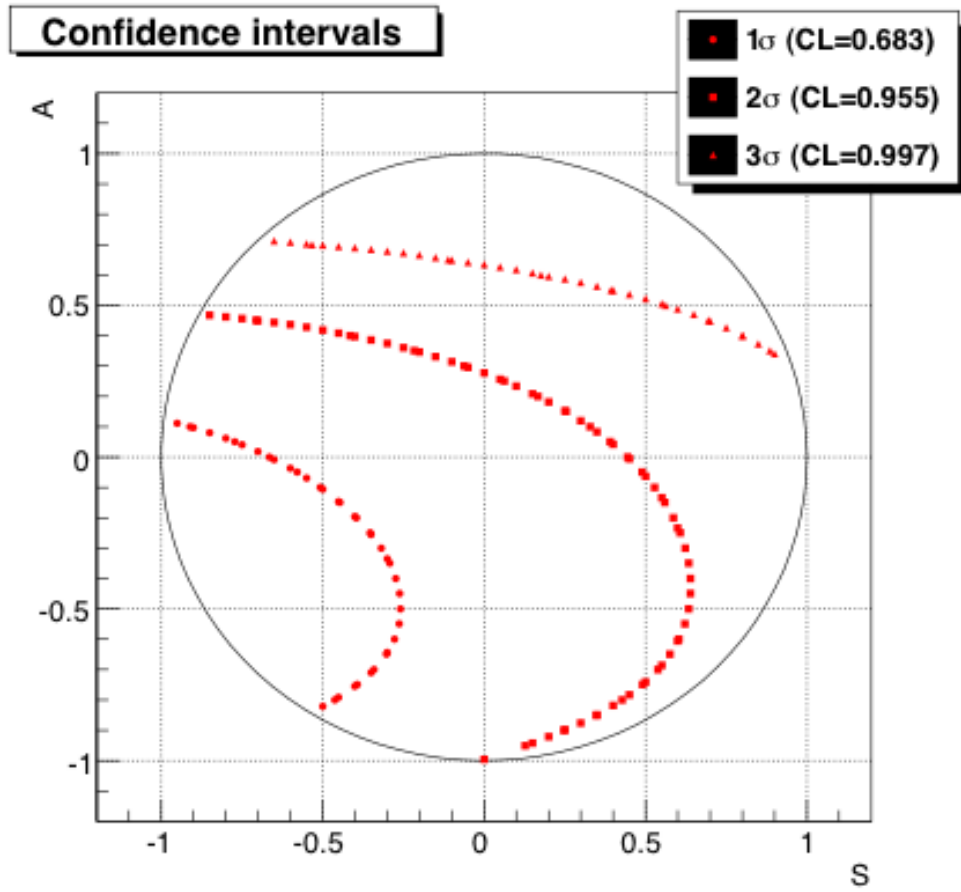


Figure 9.21: Confidence intervals.

9.2.2 Limit on new physics (general, $A_{\text{NP}} = 0$)

Assuming that new physics does not contribute to $B\bar{B}$ oscillation (i.e. $p/q = e^{2i\phi_1}$), $A = \bar{A}^*$, and $a = \bar{a}^*$, eq.(2.28) can be written as

$$\mathcal{S} = \frac{2|a/\bar{A}|}{1 + |a/\bar{A}|^2} \sin \left(2\phi_1 + \arg \left[\frac{a}{\bar{A}} \right] \right) \quad (9.14)$$

Mixing-induced CP asymmetry \mathcal{S} can be described one complex number, a/\bar{A} . Figure 9.22 shows that \mathcal{S} distribution in a/\bar{A} space. Obtained result of \mathcal{S} can make constraint on this space. In addition, let's assume that there's no contribution to A from new physics and neglect effect on a from the SM.

$$A = A_{\text{SM}} \quad (9.15)$$

$$a = a_{\text{NP}} \quad (9.16)$$

Then, a/\bar{A} space can be constrained by a ratio of $\text{BR}(b \rightarrow s\gamma)$ between theory and experiment,

$$\frac{\text{BR}_{\text{experiment}}(b \rightarrow s\gamma)}{\text{BR}_{\text{theory}}(b \rightarrow s\gamma)} = 1 + \left| \frac{a_{\text{NP}}}{A_{\text{SM}}} \right|^2. \quad (9.17)$$

Here, we used $\text{BR}_{\text{experiment}} = (3.55 \pm 0.26) \times 10^{-4}$ [3], $\text{BR}_{\text{theory}} = (3.15 \pm 0.23) \times 10^{-4}$ [17]. Figure 9.23 shows that the constraint with the result.

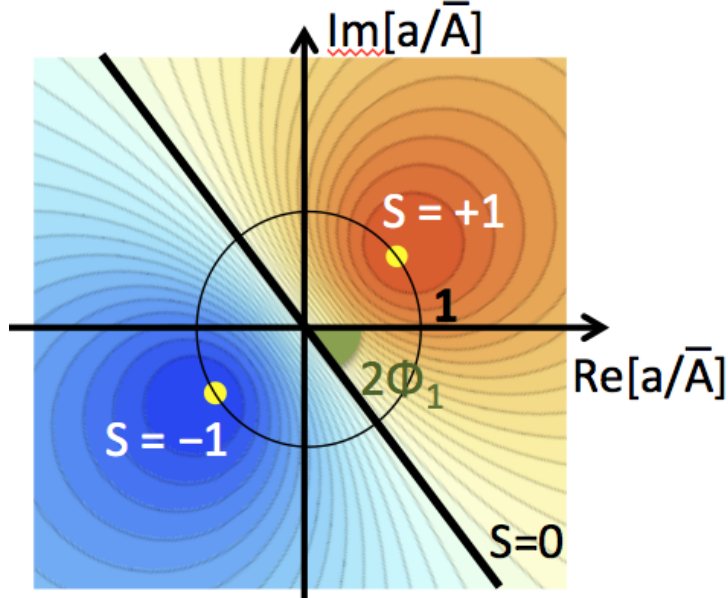


Figure 9.22: Illustration of eq.(9.14)

Limit contour

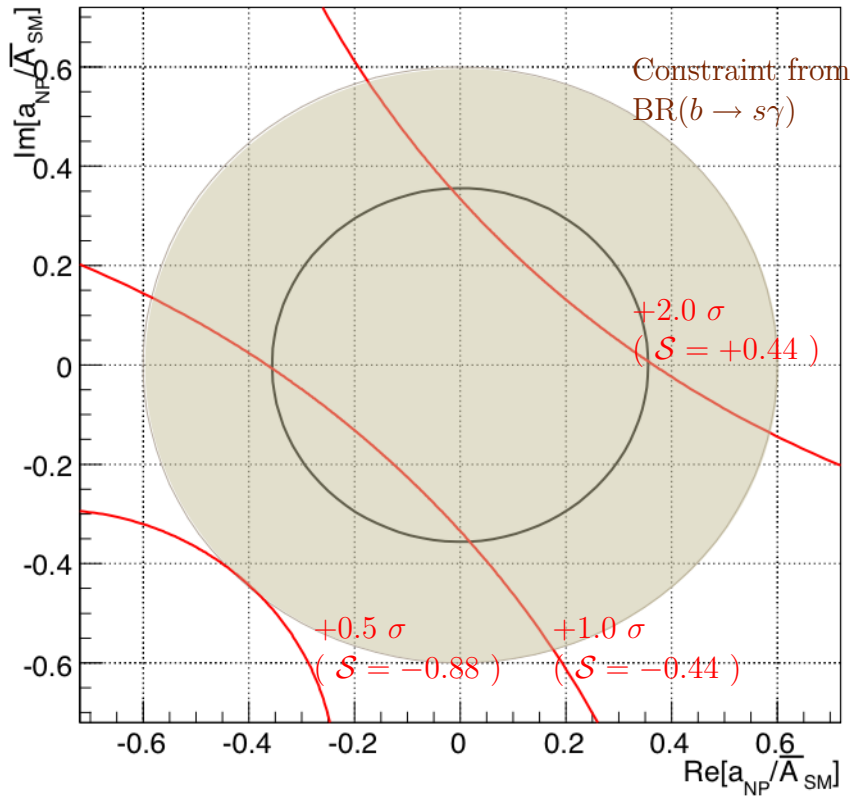


Figure 9.23: Limit on a_{NP}/\bar{A}_{SM} space. Red lines show 0.5 , 1.0 and 2.0σ contour from the result. Brown filled circle shows 2σ constraint from a ratio of $\text{BR}(b \rightarrow s\gamma)$ between theory and experiment (S), and Black line shows mean.

9.2.3 Limit on new physics (LRSM)

This time, we consider more realistic case, $A_{\text{NP}} \neq 0$. Following discussion is based on Left-Right symmetric model (LRSM) [18]. In a LRSM, W_1^\pm boson can couple to right-handed fermion as well as left-handed one. W_1^\pm is mixture state of W_R which couples to right-handed fermion and W_L which couples to left-handed fermion. Magnitude of $b \rightarrow s\gamma$ amplitude is depend on mixing angle ζ . Feynman diagram of the $b \rightarrow s\gamma_L$ and $b \rightarrow s\gamma_R$ can be written as Fig.9.24. Amplitudes of the diagram of $b \rightarrow s\gamma_L$ and $b \rightarrow s\gamma_R$ are proportional to $m_t G_F V_{tb,R} V_{ts,L}^*$ and $m_t G_F V_{tb,L} V_{ts,R}^*$, respectively. Here, $V_{CKM,R}$ is right-handed CKM matrix. The reason why $b \rightarrow s\gamma$ mode is sensitive to the model is enhancement from m_t .

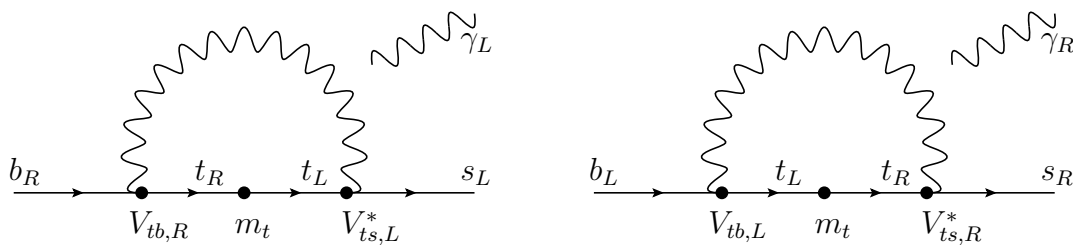


Figure 9.24: Diagrams of $b \rightarrow s\gamma_L$ (left) and $b \rightarrow s\gamma_R$ (right) in LR symmetry.

Now, assuming that $V_{CKM,R} = V_{CKM,L}$,

$$A = A_{\text{SM}} + A_{\text{NP}}, \quad (9.18)$$

$$a = a_{\text{NP}} \text{ and} \quad (9.19)$$

$$|A_{\text{NP}}| = |a_{\text{NP}}|. \quad (9.20)$$

Here, there is a solution which satisfies that

$$|A_{\text{SM}} + A_{\text{NP}}|^2 + |a_{\text{NP}}|^2 = |A_{\text{SM}}|^2. \quad (9.21)$$

Such a $(A_{\text{NP}}, a_{\text{NP}})$ set is not excluded by $\text{BR}(b \rightarrow s\gamma)$ measurement. In addition, \mathcal{S} can have large values between -0.2 and $+0.9$ as shown in Fig.9.25 (quoted from Fig.4(a) of [18]). However, recent direct search of W_2^\pm by ATLAS experiment sets a constraint of $m_{W_2} > 1.84$ [TeV]. From eq.(3) of [18], strong constraint on ζ is set.

$$\zeta \leq \frac{M_{W_1}^2}{M_{W_2}^2} < 1.9 \times 10^{-3} \quad (9.22)$$

Here, $M_{W_1} = 80$ [GeV]. Since strong constraint is applied already, study of $b \rightarrow s\gamma$ TDCPV seems to be meaningless. However, if we think about the case of

$$V_{ts,R} \gg V_{ts,L} (\sim 0.04), \quad (9.23)$$

a_{NP} can be large while ζ is small. Then, unexplored area is still remaining, and the area can be searched by $b \rightarrow s\gamma$ TDCPV.

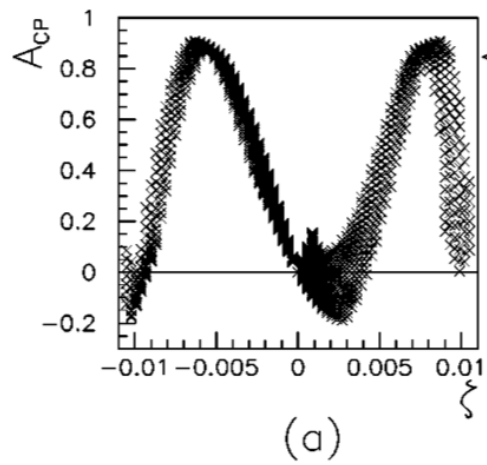


Figure 9.25: Possible \mathcal{S} in LRSM [18]. A_{CP} of vertical axis means TDCPV parameter of \mathcal{S} . Horizontal axis is mixing angle of W_L and W_R .

Chapter 10

Conclusion

We obtain the CP violation parameters

$$\mathcal{S} = -1.32_{-0.81}^{+0.88}(\text{stat.}) \pm 0.36(\text{syst.}) \text{ and} \quad (10.1)$$

$$\mathcal{A} = -0.48_{-0.33}^{+0.36}(\text{stat.}) \pm 0.07(\text{syst.}). \quad (10.2)$$

We cannot see significant deviation from zero, which is predicted by the SM. It is used for making constraint on new physics.

Appendix A

Systematic error lists

Here are details of systematic error lists discussed in Chap.8.

Table A.1: Systematic error list of BG Δt PDF shape

Source	params.		$\Delta\mathcal{S}$	$\Delta\mathcal{A}$
<i>qq</i> BG PDF shape (2γ mode)	τ_{qq}	$\pm 1\sigma$	+0.01734/-0.01692	+0.00266/-0.00231
	μ_{both}	$\pm 1\sigma$	+0.00286/-0.00279	+0.00043/-0.00047
	s_{main}	$\pm 1\sigma$	+0.00075/-0.00142	+0.00062/-0.00051
	s_{tail}	$\pm 1\sigma$	+0.00203/-0.00168	+0.00036/-0.00033
	f_{main}	$\pm 1\sigma$	+0.00399/-0.00442	+0.00024/-0.00024
	f_{delta}	$\pm 1\sigma$	+0.01358/-0.01293	+0.00386/-0.00383
<i>qq</i> BG PDF shape (3π mode)	τ_{qq}	$\pm 1\sigma$	+0.00394/-0.00000	+0.00048/-0.00043
	μ_{both}	$\pm 1\sigma$	+0.00962/-0.00998	+0.00031/-0.00019
	s_{main}	$\pm 1\sigma$	+0.00000/-0.00295	+0.00150/-0.00159
	s_{tail}	$\pm 1\sigma$	+0.00888/-0.00518	+0.00088/-0.00038
	f_{main}	$\pm 1\sigma$	+0.00971/-0.01219	+0.00107/-0.00082
	f_{delta}	$\pm 1\sigma$	+0.04255/-0.03242	+0.00331/-0.00386
<i>BB</i> BG PDF shape (2γ mode)	τ_{bb}	$\pm 2\sigma$	+0.00214/-0.00216	+0.00032/-0.00029
<i>BB</i> BG PDF shape (3π mode)	τ_{bb}	$\pm 2\sigma$	+0.00095/-0.00071	+0.00006/-0.00006
rare <i>B</i> BG PDF shape (2γ mode)	τ_{rare}	$\pm 2\sigma$	+0.00052/-0.00052	+0.00003/-0.00002
rare <i>B</i> BG PDF shape (3π mode)	τ_{rare}	$\pm 2\sigma$	+0.00012/-0.00003	+0.00004/-0.00004
rad <i>B</i> BG PDF shape (2γ mode)	τ_{rad}	$\pm 2\sigma$	+0.00210/-0.00207	+0.00020/-0.00017
rad <i>B</i> BG PDF shape (3π mode)	τ_{rad}	$\pm 2\sigma$	+0.00061/-0.00040	+0.00026/-0.00026
Total			+0.05114/-0.04278	+0.00619/-0.00627

Table A.2: Systematic error list of flavor tagging

	params.		$\Delta\mathcal{S}$	$\Delta\mathcal{A}$
wrong tag fraction (SVD1)	$w[1]$	$\pm 1\sigma$	+0.00060/-0.00018	+0.00016/-0.00047
	$w[2]$	$\pm 1\sigma$	+0.00056/-0.00080	+0.00028/-0.00015
	$w[3]$	$\pm 1\sigma$	+0.01096/-0.00293	+0.00247/-0.00909
	$w[4]$	$\pm 1\sigma$	+0.00001/-0.00001	+0.00032/-0.00031
	$w[5]$	$\pm 1\sigma$	+0.00028/-0.00073	+0.00278/-0.01618
	$w[6]$	$\pm 1\sigma$	+0.00154/-0.00225	+0.00090/-0.00133
wrong tag fraction (SVD2)	$w[1]$	$\pm 1\sigma$	+0.00152/-0.00128	+0.00002/-0.00000
	$w[2]$	$\pm 1\sigma$	+0.00223/-0.00249	+0.00029/-0.00025
	$w[3]$	$\pm 1\sigma$	+0.00800/-0.00832	+0.00187/-0.00178
	$w[4]$	$\pm 1\sigma$	+0.00010/-0.00007	+0.00246/-0.00194
	$w[5]$	$\pm 1\sigma$	+0.00162/-0.00137	+0.00077/-0.00065
	$w[6]$	$\pm 1\sigma$	+0.00415/-0.00277	+0.00170/-0.00114
difference of w (SVD1)	$\Delta w[1]$	$\pm 1\sigma$	+0.00004/-0.00009	+0.00009/-0.00018
	$\Delta w[2]$	$\pm 1\sigma$	+0.00034/-0.00043	+0.00042/-0.00033
	$\Delta w[3]$	$\pm 1\sigma$	+0.00078/-0.00153	+0.00132/-0.00067
	$\Delta w[4]$	$\pm 1\sigma$	+0.00000/-0.00000	+0.00003/-0.00003
	$\Delta w[5]$	$\pm 1\sigma$	+0.00095/-0.00198	+0.00113/-0.00235
	$\Delta w[6]$	$\pm 1\sigma$	+0.00068/-0.00061	+0.00033/-0.00037
difference of w (SVD2)	$\Delta w[1]$	$\pm 1\sigma$	+0.00009/-0.00009	+0.00032/-0.00032
	$\Delta w[2]$	$\pm 1\sigma$	+0.00162/-0.00157	+0.00028/-0.00029
	$\Delta w[3]$	$\pm 1\sigma$	+0.00257/-0.00254	+0.00058/-0.00059
	$\Delta w[4]$	$\pm 1\sigma$	+0.00012/-0.00013	+0.00078/-0.00085
	$\Delta w[5]$	$\pm 1\sigma$	+0.00065/-0.00066	+0.00066/-0.00065
	$\Delta w[6]$	$\pm 1\sigma$	+0.00036/-0.00034	+0.00193/-0.00187
Total			+0.01504/-0.01085	+0.00604/-0.01915

Table A.3: Systematic error list of resolution function parameters (SVD1)

params.		$\Delta\mathcal{S}$	$\Delta\mathcal{A}$
$S_{\text{rec},0}$	$\pm 1\sigma$	+0.00058/-0.00050	+0.00114/-0.00061
$S_{\text{rec},1}$	$\pm 1\sigma$	+0.00099/-0.00106	+0.00024/-0.00026
$S_{\text{rec/tag},\text{main}}$	$\pm 1\sigma$	+0.00119/-0.00023	+0.00101/-0.00729
$S_{\text{rec/tag},\text{tail}}$	$\pm 1\sigma$	+0.00000/-0.00000	+0.00000/-0.00000
$f_{\text{rec/tag},\text{tail}}$	$\pm 1\sigma$	+0.00000/-0.00000	+0.00000/-0.00000
$S_{\text{rec},0}$ for K_S	$\pm 1\sigma$	+0.02889/-0.03744	+0.00346/-0.00366
$S_{\text{rec},1}$ for K_S	$\pm 1\sigma$	+0.03644/-0.01065	+0.00000/-0.00088
$S_{\text{dia},0}$	$\pm 1\sigma$	+0.01430/-0.03726	+0.00075/-0.00208
$S_{\text{dia},1}$	$\pm 2\sigma$	+0.00353/-0.00339	+0.00019/-0.00023
$S_{\text{tag},0}$	$\pm 1\sigma$	+0.00113/-0.00011	+0.00004/-0.00011
$S_{\text{tag},1}$	$\pm 1\sigma$	+0.00239/-0.00171	+0.00021/-0.00025
S_{np}	$\pm 1\sigma$	+0.00283/-0.00184	+0.00079/-0.00085
f_{δ} w/ taglep sgl	$\pm 2\sigma$	+0.00166/-0.00156	+0.00004/-0.00003
f_p	$\pm 2\sigma$	+0.00186/-0.00198	+0.00038/-0.00040
τ_p^0	$\pm 2\sigma$	+0.00000/-0.00010	+0.00013/-0.00015
τ_n^0	$\pm 2\sigma$	+0.00012/-0.00000	+0.00012/-0.00006
f_d w/ taglep mul	$\pm 2\sigma$	+0.00417/-0.00304	+0.00085/-0.00074
f_d w/o taglep mul	$\pm 2\sigma$	+0.00055/-0.00055	+0.00067/-0.00067
f_d^{1s}	$\pm 2\sigma$	+0.00435/-0.00400	+0.00105/-0.00102
f_d^{1h}	$\pm 2\sigma$	+0.00157/-0.00000	+0.00088/-0.00079
f_d^{1sh}	$\pm 2\sigma$	+0.00287/-0.00211	+0.00067/-0.00059
f_n	$\pm 2\sigma$	+0.00039/-0.00039	+0.00046/-0.00046
τ_p^0	$\pm 2\sigma$	+0.00097/-0.00075	+0.00129/-0.00122
τ_p^{1s}	$\pm 2\sigma$	+0.00027/-0.00021	+0.00088/-0.00086
τ_p^{1h}	$\pm 2\sigma$	+0.00422/-0.00375	+0.00101/-0.00084
τ_p^{1sh}	$\pm 2\sigma$	+0.00335/-0.00309	+0.00062/-0.00052
τ_n^0	$\pm 2\sigma$	+0.00061/-0.00054	+0.00026/-0.00024
τ_n^{1s}	$\pm 2\sigma$	+0.00038/-0.00029	+0.00027/-0.00025
τ_n^{1h}	$\pm 2\sigma$	+0.00014/-0.00032	+0.00005/-0.00005
τ_n^{1sh}	$\pm 2\sigma$	+0.00001/-0.00004	+0.00012/-0.00012
σ_{ol}	$\pm 1\sigma$	+0.00003/-0.00002	+0.00005/-0.00003
$f_{ol}(\text{ntrk_asc}=1)$	$\pm 1\sigma$	+0.00008/-0.00013	+0.00027/-0.00044
$f_{ol}(\text{ntrk_asc}>1)$	$\pm 1\sigma$	+0.00000/-0.00000	+0.00000/-0.00000

Table A.4: Systematic error list of resolution function parameters (SVD2)

params.		$\Delta\mathcal{S}$	$\Delta\mathcal{A}$
$S_{\text{rec},0}$	$\pm 1\sigma$	+0.01771/-0.00915	+0.00214/-0.00352
$S_{\text{rec},1}$	$\pm 1\sigma$	+0.00168/-0.00000	+0.00827/-0.00800
$S_{\text{rec/tag},\text{main}}$	$\pm 1\sigma$	+0.00462/-0.03763	+0.00284/-0.00022
$S_{\text{rec/tag},\text{tail}}$	$\pm 1\sigma$	+0.00231/-0.03308	+0.00021/-0.00245
$f_{\text{rec/tag},\text{tail}}$	$\pm 1\sigma$	+0.00540/-0.00212	+0.00003/-0.00007
$S_{\text{rec},0}K_S$	$\pm 1\sigma$	+0.12220/-0.18512	+0.02451/-0.03682
$S_{\text{rec},1}K_S$	$\pm 1\sigma$	+0.21434/-0.10432	+0.01606/-0.01472
$S_{\text{dia},0}$	$\pm 1\sigma$	+0.05185/-0.07180	+0.01794/-0.02603
$S_{\text{tag},0}$	$\pm 1\sigma$	+0.00249/-0.01769	+0.00020/-0.00010
$S_{\text{tag},1}$	$\pm 1\sigma$	+0.01444/-0.02709	+0.00280/-0.00576
S_{np}	$\pm 1\sigma$	+0.03894/-0.01618	+0.00129/-0.00314
f_{δ} w/ taglep sgl	$\pm 2\sigma$	+0.01076/-0.01078	+0.00117/-0.00115
f_p	$\pm 2\sigma$	+0.00601/-0.00567	+0.00071/-0.00066
τ_p^0	$\pm 2\sigma$	+0.01037/-0.00971	+0.00086/-0.00077
τ_n^0	$\pm 2\sigma$	+0.00035/-0.00034	+0.00001/-0.00001
f_d w/ taglep mul	$\pm 2\sigma$	+0.00461/-0.00440	+0.00088/-0.00089
f_d w/o taglep mul	$\pm 2\sigma$	+0.00114/-0.00102	+0.00178/-0.00182
f_d^{1s}	$\pm 2\sigma$	+0.00594/-0.00590	+0.00219/-0.00204
f_d^{1h}	$\pm 2\sigma$	+0.00084/-0.00081	+0.00348/-0.00337
f_d^{1sh}	$\pm 2\sigma$	+0.00053/-0.00056	+0.00322/-0.00334
f_n	$\pm 2\sigma$	+0.00209/-0.00206	+0.00072/-0.00072
τ_p^0	$\pm 2\sigma$	+0.00308/-0.00314	+0.00048/-0.00048
τ_p^{1s}	$\pm 2\sigma$	+0.00450/-0.00435	+0.00049/-0.00050
τ_p^{1h}	$\pm 2\sigma$	+0.00042/-0.00045	+0.00101/-0.00109
τ_p^{1sh}	$\pm 2\sigma$	+0.00079/-0.00983	+0.00138/-0.00145
τ_n^0	$\pm 2\sigma$	+0.00050/-0.00051	+0.00018/-0.00018
τ_n^{1s}	$\pm 2\sigma$	+0.00084/-0.00081	+0.00020/-0.00019
τ_n^{1h}	$\pm 2\sigma$	+0.00070/-0.00079	+0.00009/-0.00008
τ_n^{1sh}	$\pm 2\sigma$	+0.00110/-0.00122	+0.00010/-0.00008
σ_{ol}	$\pm 1\sigma$	+0.00048/-0.00146	+0.00001/-0.00002
$f_{ol}(\text{ntrk_asc}=1)$	$\pm 1\sigma$	+0.00061/-0.00027	+0.00018/-0.00041
$f_{ol}(\text{ntrk_asc}>1)$	$\pm 1\sigma$	+0.00001/-0.00001	+0.00001/-0.00002
Total		+0.25695/-0.23357	+0.03574/-0.04912

Table A.5: Systematic error list of 3D fit for signal/BG fraction (amount of fixed BG).

	params.		$\Delta\mathcal{S}$	$\Delta\mathcal{A}$
Signal	f_{sig}		+0.00932/-0.01108	+0.00604/-0.00459
BB BG	N_{bb}	$\pm 100\%$	+0.01569/-0.01479	+0.01006/-0.00904
rare B BG	N_{rare}	$\pm 100\%$	+0.00962/-0.00957	+0.00231/-0.00227
rad B BG	$N_{rad}(sd \text{ system})$	$\pm 100\%$	+0.06247/-0.05908	+0.01085/-0.00921
	$N_{rad}(su \text{ system})$	$\pm 100\%$	+0.05515/-0.05184	+0.00782/-0.00681
	$N_{rad}(K_S\eta\gamma)$	$\pm 100\%$	+0.00110/-0.00238	+0.00309/-0.00273
	$N_{rad}(K^\pm\eta\gamma)$	$\pm 100\%$	+0.00075/-0.00070	+0.00219/-0.00203
	$N_{rad}(\text{others})$	$\pm 100\%$	+0.01098/-0.01088	+0.00204/-0.00198

Table A.6: Systematic error list of 3D fit for signal/BG fraction (2γ mode, qr bin #1-3).

	PDF	$\Delta\mathcal{S}$	$\Delta\mathcal{A}$
Signal	$(\Delta E - M_{bc})$	+0.00230/-0.00351	+0.00064/-0.00061
	(NB')	+0.00040/-0.00035	+0.00015/-0.00013
qq BG	(ΔE)	+0.00008/-0.00008	+0.00006/-0.00006
	(M_{bc})	+0.00019/-0.00019	+0.00008/-0.00008
BB BG	(NB')	+0.00045/-0.00045	+0.00045/-0.00045
	(ΔE)	+0.00001/-0.00001	+0.00000/-0.00000
rare B BG	(M_{bc})	+0.00001/-0.00001	+0.00001/-0.00001
	(NB')	+0.00001/-0.00001	+0.00004/-0.00004
rad B BG	(ΔE)	+0.00000/-0.00000	+0.00001/-0.00001
	(M_{bc})	+0.00001/-0.00001	+0.00001/-0.00001
	(NB')	+0.00001/-0.00001	+0.00002/-0.00002
	(ΔE)	+0.00006/-0.00006	+0.00008/-0.00008
	(M_{bc})	+0.00015/-0.00015	+0.00023/-0.00023
	(NB')	+0.00010/-0.00011	+0.00038/-0.00036
Signal	$(\Delta E - M_{bc})$	+0.00569/-0.00438	+0.00064/-0.00035
	(NB')	+0.00136/-0.00150	+0.00037/-0.00038
qq BG	(ΔE)	+0.00085/-0.00082	+0.00007/-0.00007
	(M_{bc})	+0.00112/-0.00112	+0.00011/-0.00011
BB BG	(NB')	+0.00187/-0.00187	+0.00042/-0.00042
	(ΔE)	+0.00017/-0.00017	+0.00001/-0.00001
rare B BG	(M_{bc})	+0.00016/-0.00017	+0.00001/-0.00001
	(NB')	+0.00027/-0.00028	+0.00002/-0.00002
rad B BG	(ΔE)	+0.00009/-0.00009	+0.00001/-0.00001
	(M_{bc})	+0.00007/-0.00007	+0.00001/-0.00001
	(NB')	+0.00013/-0.00013	+0.00001/-0.00001
	(ΔE)	+0.00116/-0.00118	+0.00004/-0.00005
	(M_{bc})	+0.00149/-0.00138	+0.00023/-0.00031
	(NB')	+0.00115/-0.00115	+0.00012/-0.00011
Signal	$(\Delta E - M_{bc})$	+0.01639/-0.00627	+0.00324/-0.00058
	(NB')	+0.00228/-0.00250	+0.00183/-0.00189
qq BG	(ΔE)	+0.00058/-0.00054	+0.00026/-0.00027
	(M_{bc})	+0.00089/-0.00085	+0.00050/-0.00050
BB BG	(NB')	+0.00099/-0.00100	+0.00085/-0.00087
	(ΔE)	+0.00015/-0.00015	+0.00001/-0.00001
rare B BG	(M_{bc})	+0.00027/-0.00028	+0.00000/-0.00000
	(NB')	+0.00048/-0.00049	+0.00012/-0.00013
rad B BG	(ΔE)	+0.00019/-0.00018	+0.00002/-0.00002
	(M_{bc})	+0.00029/-0.00029	+0.00007/-0.00007
	(NB')	+0.00040/-0.00040	+0.00011/-0.00011
	(ΔE)	+0.00129/-0.00121	+0.00001/-0.00000
	(M_{bc})	+0.00468/-0.00420	+0.00094/-0.00104
	(NB')	+0.00606/-0.00626	+0.00057/-0.00057

Table A.7: Systematic error list of 3D fit for signal/BG fraction (2γ mode, qr bin #4-6).

	PDF	$\Delta\mathcal{S}$	$\Delta\mathcal{A}$
Signal	$(\Delta E - M_{bc})$	+0.00129/-0.00338	+0.00037/-0.00243
	(NB')	+0.00119/-0.00126	+0.00220/-0.00219
qq BG	(ΔE)	+0.00033/-0.00033	+0.00003/-0.00004
	(M_{bc})	+0.00072/-0.00071	+0.00005/-0.00006
BB BG	(NB')	+0.00030/-0.00033	+0.00089/-0.00091
	(ΔE)	+0.00006/-0.00006	+0.00002/-0.00002
rare B BG	(M_{bc})	+0.00013/-0.00013	+0.00004/-0.00005
	(NB')	+0.00004/-0.00004	+0.00005/-0.00005
rad B BG	(ΔE)	+0.00005/-0.00005	+0.00002/-0.00002
	(M_{bc})	+0.00007/-0.00007	+0.00003/-0.00003
rad B BG	(NB')	+0.00002/-0.00002	+0.00002/-0.00002
	(ΔE)	+0.00036/-0.00038	+0.00019/-0.00018
rad B BG	(M_{bc})	+0.00124/-0.00137	+0.00062/-0.00056
	(NB')	+0.00012/-0.00011	+0.00029/-0.00032
Signal	$(\Delta E - M_{bc})$	+0.00472/-0.00790	+0.00159/-0.00413
	(NB')	+0.00345/-0.00293	+0.00618/-0.00584
qq BG	(ΔE)	+0.00162/-0.00167	+0.00206/-0.00195
	(M_{bc})	+0.00209/-0.00199	+0.00323/-0.00322
BB BG	(NB')	+0.00168/-0.00163	+0.00147/-0.00135
	(ΔE)	+0.00021/-0.00021	+0.00015/-0.00015
rare B BG	(M_{bc})	+0.00023/-0.00022	+0.00023/-0.00023
	(NB')	+0.00016/-0.00016	+0.00009/-0.00009
rare B BG	(ΔE)	+0.00012/-0.00011	+0.00014/-0.00013
	(M_{bc})	+0.00008/-0.00008	+0.00017/-0.00017
rad B BG	(NB')	+0.00006/-0.00006	+0.00003/-0.00003
	(ΔE)	+0.00091/-0.00087	+0.00113/-0.00110
rad B BG	(M_{bc})	+0.00122/-0.00131	+0.00338/-0.00306
	(NB')	+0.00041/-0.00041	+0.00025/-0.00024
Signal	$(\Delta E - M_{bc})$	+0.00602/-0.00493	+0.00434/-0.00521
	(NB')	+0.00231/-0.00231	+0.00145/-0.00141
qq BG	(ΔE)	+0.00169/-0.00158	+0.00095/-0.00086
	(M_{bc})	+0.00237/-0.00239	+0.00142/-0.00136
BB BG	(NB')	+0.00057/-0.00055	+0.00037/-0.00036
	(ΔE)	+0.00024/-0.00024	+0.00005/-0.00005
rare B BG	(M_{bc})	+0.00030/-0.00031	+0.00010/-0.00010
	(NB')	+0.00022/-0.00021	+0.00012/-0.00012
rare B BG	(ΔE)	+0.00046/-0.00048	+0.00002/-0.00002
	(M_{bc})	+0.00042/-0.00040	+0.00013/-0.00015
rad B BG	(NB')	+0.00037/-0.00037	+0.00027/-0.00025
	(ΔE)	+0.00047/-0.00047	+0.00016/-0.00017
rad B BG	(M_{bc})	+0.00845/-0.00693	+0.00393/-0.00363
	(NB')	+0.00320/-0.00334	+0.00141/-0.00140

Table A.8: Systematic error list of 3D fit for signal/BG fraction (3π mode, qr bin #1-3).

	PDF	$\Delta\mathcal{S}$	$\Delta\mathcal{A}$
Signal	$(\Delta E - M_{bc})$	+0.00033/-0.00204	+0.00025/-0.00084
	(NB')	+0.00056/-0.00054	+0.00024/-0.00024
qq BG	(ΔE)	+0.00015/-0.00015	+0.00007/-0.00006
	(M_{bc})	+0.00024/-0.00023	+0.00011/-0.00010
BB BG	(NB')	+0.00019/-0.00019	+0.00008/-0.00008
	(ΔE)	+0.00006/-0.00005	+0.00002/-0.00002
rare B BG	(M_{bc})	+0.00004/-0.00004	+0.00001/-0.00002
	(NB')	+0.00002/-0.00002	+0.00000/-0.00000
rad B BG	(ΔE)	+0.00003/-0.00003	+0.00001/-0.00001
	(M_{bc})	+0.00004/-0.00004	+0.00001/-0.00001
	(NB')	+0.00001/-0.00001	+0.00000/-0.00000
	(ΔE)	+0.00022/-0.00023	+0.00006/-0.00005
	(M_{bc})	+0.00037/-0.00092	+0.00024/-0.00010
	(NB')	+0.00019/-0.00019	+0.00003/-0.00003
Signal	$(\Delta E - M_{bc})$	+0.00166/-0.00809	+0.00151/-0.00018
	(NB')	+0.00391/-0.00415	+0.00032/-0.00030
qq BG	(ΔE)	+0.00047/-0.00045	+0.00005/-0.00005
	(M_{bc})	+0.00108/-0.00106	+0.00009/-0.00010
BB BG	(NB')	+0.00127/-0.00124	+0.00010/-0.00010
	(ΔE)	+0.00015/-0.00016	+0.00002/-0.00002
rare B BG	(M_{bc})	+0.00017/-0.00017	+0.00001/-0.00001
	(NB')	+0.00011/-0.00012	+0.00001/-0.00001
rad B BG	(ΔE)	+0.00005/-0.00004	+0.00001/-0.00001
	(M_{bc})	+0.00014/-0.00014	+0.00001/-0.00001
	(NB')	+0.00001/-0.00001	+0.00000/-0.00000
	(ΔE)	+0.00074/-0.00062	+0.00006/-0.00006
	(M_{bc})	+0.00368/-0.00310	+0.00020/-0.00016
	(NB')	+0.00089/-0.00092	+0.00010/-0.00011
Signal	$(\Delta E - M_{bc})$	+0.00246/-0.00399	+0.00280/-0.00132
	(NB')	+0.00579/-0.00535	+0.00266/-0.00249
qq BG	(ΔE)	+0.00045/-0.00043	+0.00067/-0.00072
	(M_{bc})	+0.00041/-0.00041	+0.00106/-0.00108
BB BG	(NB')	+0.00166/-0.00165	+0.00018/-0.00019
	(ΔE)	+0.00010/-0.00010	+0.00002/-0.00002
rare B BG	(M_{bc})	+0.00006/-0.00006	+0.00002/-0.00002
	(NB')	+0.00008/-0.00008	+0.00002/-0.00002
rad B BG	(ΔE)	+0.00005/-0.00005	+0.00001/-0.00001
	(M_{bc})	+0.00007/-0.00007	+0.00003/-0.00004
	(NB')	+0.00006/-0.00007	+0.00002/-0.00002
	(ΔE)	+0.00056/-0.00054	+0.00012/-0.00012
	(M_{bc})	+0.00143/-0.00140	+0.00053/-0.00059
	(NB')	+0.00058/-0.00060	+0.00013/-0.00014

Table A.9: Systematic error list of 3D fit for signal/BG fraction (3π mode, qr bin #4-6).

	PDF	$\Delta\mathcal{S}$	$\Delta\mathcal{A}$
Signal	$(\Delta E - M_{bc})$	+0.00083/-0.00126	+0.00062/-0.00164
	(NB')	+0.00080/-0.00080	+0.00251/-0.00246
qq BG	(ΔE)	+0.00050/-0.00048	+0.00101/-0.00097
	(M_{bc})	+0.00075/-0.00076	+0.00174/-0.00176
BB BG	(NB')	+0.00129/-0.00128	+0.00325/-0.00324
	(ΔE)	+0.00005/-0.00005	+0.00011/-0.00012
rare B BG	(M_{bc})	+0.00003/-0.00003	+0.00009/-0.00009
	(NB')	+0.00004/-0.00003	+0.00009/-0.00009
rad B BG	(ΔE)	+0.00003/-0.00003	+0.00008/-0.00008
	(M_{bc})	+0.00004/-0.00004	+0.00009/-0.00009
rad B BG	(NB')	+0.00003/-0.00002	+0.00006/-0.00006
	(ΔE)	+0.00030/-0.00029	+0.00070/-0.00067
rad B BG	(M_{bc})	+0.00089/-0.00078	+0.00230/-0.00201
	(NB')	+0.00026/-0.00025	+0.00064/-0.00062
Signal	$(\Delta E - M_{bc})$	+0.01105/-0.01495	+0.00375/-0.00384
	(NB')	+0.02737/-0.03158	+0.00118/-0.00090
qq BG	(ΔE)	+0.00443/-0.00415	+0.00418/-0.00419
	(M_{bc})	+0.00789/-0.00783	+0.00070/-0.00061
BB BG	(NB')	+0.00494/-0.00501	+0.00090/-0.00091
	(ΔE)	+0.00021/-0.00022	+0.00007/-0.00006
rare B BG	(M_{bc})	+0.00018/-0.00019	+0.00005/-0.00005
	(NB')	+0.00019/-0.00018	+0.00001/-0.00002
rare B BG	(ΔE)	+0.00015/-0.00013	+0.00006/-0.00006
	(M_{bc})	+0.00030/-0.00028	+0.00006/-0.00007
rad B BG	(NB')	+0.00022/-0.00020	+0.00002/-0.00002
	(ΔE)	+0.00170/-0.00143	+0.00067/-0.00072
rad B BG	(M_{bc})	+0.00812/-0.00828	+0.00178/-0.00194
	(NB')	+0.00280/-0.00272	+0.00019/-0.00020
Signal	$(\Delta E - M_{bc})$	+0.00143/-0.00357	+0.00061/-0.00187
	(NB')	+0.00145/-0.00139	+0.00074/-0.00072
qq BG	(ΔE)	+0.00239/-0.00262	+0.00109/-0.00119
	(M_{bc})	+0.00355/-0.00338	+0.00165/-0.00156
BB BG	(NB')	+0.00208/-0.00205	+0.00095/-0.00093
	(ΔE)	+0.00032/-0.00025	+0.00014/-0.00012
rare B BG	(M_{bc})	+0.00022/-0.00017	+0.00009/-0.00008
	(NB')	+0.00014/-0.00008	+0.00006/-0.00004
rare B BG	(ΔE)	+0.00030/-0.00025	+0.00011/-0.00010
	(M_{bc})	+0.00034/-0.00027	+0.00011/-0.00009
rad B BG	(NB')	+0.00019/-0.00014	+0.00010/-0.00008
	(ΔE)	+0.00239/-0.00230	+0.00091/-0.00088
rad B BG	(M_{bc})	+0.00529/-0.00244	+0.00192/-0.00089
	(NB')	+0.00061/-0.00054	+0.00029/-0.00027
Total		+0.09638/-0.09335	+0.02355/-0.02197

Bibliography

- [1] Kazuo Fujikawa, K.S. Babu, and Atsushi Yamada. Constraints on left-right symmetric models from the process $b \rightarrow s\gamma$. *Phys. Lett. B*, 333:196, (1994).
- [2] F. Gabbiani, E. Gabrielli, A. Masiero, and L. Silvestrini. A complete analysis of FCNC and CP constraints in general SUSY extensions of the standard model. *Nucl. Phys. B*, 477:321, (1996).
- [3] Heavy Flavor Averaging Group. Averages of b -hadron, c -hadron, and τ -lepton properties. arXiv:arXiv:1207.1158[hep-ex], (2013).
- [4] David Atwood, Michael Gronau, and Amarjit Soni. Mixing-induced CP Asymmetries in Radiative B Decays in and beyond the Standard Model. arXiv:hep-ph/9704272v1, (1997).
- [5] Ogawa Yujiro. *Outline of electron linear collider*. (2002). [Japanese].
- [6] Kamitani Takuya. *Upgrade of KEKB injector linac for SuperKEKB*. (2010). [Japanese].
- [7] Kamitani Takuya. *Positron source*. (2002). [Japanese].
- [8] H. Aihara et al. Belle svd2 vertex detector. *Nucl. Instr. Meth. A*, 568:269–273, (2004).
- [9] A. Abashian et al. Belle svd2 vertex detector. *Nucl. Instr. Meth. A*, 479:117–232, (2002).
- [10] C. Grupen and B. Shwartz. *Particle Detectors Second Edition*. (2008).
- [11] B. Aubert. Branching Fractions and CP-Violating Asymmetries in Radiative B Decays to eta K gamma. *Phys. Rev. D*, 79:01102, (2009).
- [12] S. Nishida. Observation of $B^+ \rightarrow K^+\eta\gamma$. *Phys.Lett.B*, 610:23, (2005).
- [13] Alexander L. Kagan and Matthias Neubert. QCD Anatomy of $B \rightarrow X_s\gamma$ Decays. arXiv:hep-ph/9805303, (1998).
- [14] G. C. Fox and S. Wolfram. Observables for the Analysis of Event Shapes in e^+e^- Annihilation and Other Processes. *Phys. Rev. Lett.*, 41:1581, (1978).

- [15] H. Kakuno et al. Neutral B Flavor Tagging for the Measurement of Mixing-induced CP Violation at Belle. arXiv:hep-ex/0403022v1, (2004).
- [16] H. Aihara. Proper-time resolution function for measurement of time evolution of B mesons at the KEK B-Factory. *Nucl. Instr. Meth. A*, 533:370–386, (2004).
- [17] et al M. Misiak. arXiv:hep-ph/0609232, (2006).
- [18] C. S. Kim and Yeong Gyun Kim. $b \rightarrow s\gamma$ decays in the left-right symmetric model. *Phys. Rev. D*, 61:054008, (2000).